A Multi-resonance Thickness-Shear Mode (MTSM) Measurement Technique for Quantitative Characterization of Biological Interfacial Processes

A Thesis

Submitted to the Faculty

of

Drexel University

by

Ertan Ergezen

in partial fulfillment of the

requirements for the degree

of

Doctor of Philosophy

February 2010

Dedications

This thesis is dedicated to my parents, my brother and sister for their understandings and unconditional supports and to my girlfriend for her continuous encouragement.

Acknowledgments

I wish to express my gratitude to everyone who has provided me with advices, feedback, corrections, and criticism. I would like to contribute this page to acknowledge them who made my Ph.D. thesis a reality. I must single out Dr. Ryszard M. Lec who has advised, supported, and encouraged me as an academic advisor.

I would like to want to thank Dr. David Wootton, Department of Mechanical Engineering, Cooper Union University, and Dr. Afshin Daryoush, Electrical and Computer Engineering Department, Drexel University, for their thoughtful advises. I am again grateful to Dr. Peter A. Lewin, Dr. Kenneth Barbee, School of Biomedical Engineering, Science and Health Systems, Drexel University, for their academic and technical guidance, and Dr. Steven Wrenn, Department of Biochemical Engineering, Drexel University, for advising in the area of interfacial processes.

I also appreciate to all members of Biosensor Laboratory, especially Dr. Johann Desa and Dr. Qiliang Zhang, Matias Hochman and Robert Hart who have been best Mentors as good all time friends, and most of all, I am deeply indebted to my family and my girlfriend for their unconditional support and patient throughout my studies.

Table of Contents

LIST OF FIGURES……..ix

LIST OF TABLES ……....xx

ABSTRACT……..xxiv

1 INTRODUCTION.....1

1.1 Motivation of the Thesis 1

1.1.1 Biological interfacial processes 1

1.1.2 Current techniques to study biological interfacial processes; their strengths and limitations 2

1.1.3 Theme of the thesis.....4

1.2 Organization of the Thesis 6

2 BACKGROUND.....9

2.1 General features of multi-resonance thickness shear mode (MTSM) sensor operating under viscoelastic loading 9

2.2 Previous works with MTSM sensor for quantification of multi-layer biological interfaces 10

2.3 Structure of the MTSM/genetic algorithm (GA) technique 14

2.4 Structure of the MTSM/GA measurement system.....15

2.5 Overview of genetic algorithm technique 16

2.5.1 General structure of a genetic algorithm.....18

3 OBJECTIVES 20

4 THEORETICAL ANALYSIS OF THE MTSM TECHNIQUE 23

4.1 Modeling of a MTSM sensor with a viscoelastic load.....24

4.1.1 Modeling of a non-piezoelectric layer.....25

4.1.2 Modeling of a piezoelectric layer 27

4.1.3 Combination of piezoelectric and non-piezoelectric layers.....29

4.2 Definition of parameters characterizing MTSM sensor response 30

4.3 Validation of the MTSM theoretical approach: simulation and experiment of a MTSM loaded with Newtonian liquids.....31

4.4 Summary and Conclusions.....34

5 THEORETICAL FOUNDATION OF THE MTSM/GA TECHNIQUE FOR SINGLE LAYER VISCOELASTIC SYSTEMS 35

5.1 Problem Definition.....35

5.2 Outline of Chapter 5 39

5.3 Structure of the MTSM/GA technique....40
5.3.1 Inputs to the MTSM/GA technique....41
5.3.2 Internal functions and outputs of the MTSM/GA technique....45
5.3.3 Integration of sub-spacing method to the MTSM/GA technique....47
5.3.4 Integration of a zooming method with the MTSM/GA technique....51
5.4 Optimization of the MTSM/GA's parameters....52
5.5 Stability of the MTSM/GA Technique....54
5.6 Multiple solutions obtained by the MTSM/GA technique....54
5.7 Analysis of the effect of the experimental error on the MTSM/GA technique....55
5.8 Effect of quality factor on the MTSM/GA technique....57
5.9 Theoretical validation of the GA/MTM technique for single-layer viscoelastic systems....65
5.9.1 Analysis of the MTSM/GA technique for single layer viscoelastic systems to at 5 MHZ....67
5.9.2 Analysis of the MTSM/GA technique for single layer viscoelastic systems to at 15 MHZ....74
5.9.3 Analysis of the MTSM/GA technique for single layer viscoelastic systems at 25 MHz....81
5.9.4 Analysis of the MTSM/GA technique for single layer viscoelastic systems at 35 MHz....89
5.10 Summary and Conclusions....94
6 EXPERIMENTAL VALIDATION OF THE MTSM/GA TECHNIQUE FOR SINGLE LAYER VISCOELASTIC SYSTEMS....96
6.1 Development of a MTSM sensor measurement system....96
6.2 Validation of the MTSM/GA technique using Newtonian liquids....98
6.2.1 Determination of deionized water properties....98
6.2.2 Determination of 10 % glycerin/DI water solution properties....101
6.2.3 Determination of 20% glycerin/DI water solution's properties....102
6.3 Validation of the MTSM/GA technique using SU8-2002 polymer layer....104
6.3.1 Materials and Methods....105
6.3.2 Determination of mechanical and geometrical properties of SU8-2002 layer of 1.95 μm thickness....107
6.3.3 Determination of mechanical and geometrical properties of SU8-2002 layer of 0.770 μm thickness....110
6.4 Analysis of mechanical and geometrical properties of SU8-2002 layers with different thicknesses....112

6.5 Validation of the MTSM/GA technique using collagen type-I layer deposited on the MTSM sensor surface 114
6.5.1 Materials and Methods 115
6.5.2 Results and Discussions....116
6.5.3 Time evolution of the properties during collagen evaporation process....123
6.6 Discussions on experimental validation of the MTSM/GA technique for single-layer viscoelastic systems....126
6.7 Summary and Conclusions....131
7 THEORETICAL FOUNDATION OF THE MTSM/GA TECHNIQUE FOR TWO-LAYER VISCOELASTIC SYSTEMS 132
7.1 Problem Definition....132
7.2 Outline of Chapter 7....135
7.3 Structure of the MTSM/GA technique for determination of properties of two-layer viscoelastic system 135
7.3.1 Integration of sub-spacing method to the MTSM/GA technique for two-layer viscoelastic systems 137
7.3.2 Integration of zooming technique into the MTSM/GA technique for two-layer viscoelastic systems 138
7.4 The effect of accurate estimation of the thickness and density values on the MTSM/GA technique....140
7.5 Effect of the error between experimental and theoretical results on the MTSM/GA technique 145
7.6 Effect of the quality factor on the MTSM/GA technique for two-layer viscoelastic systems 148
7.6.1 Effect of quality factor on the MTSM/GA technique for two-layer viscoelastic layers at 5 MHz 149
7.6.2 Effect of quality factor on the MTSM/GA technique for two-layer viscoelastic layers at 15 MHz 151
7.6.3 Effect of quality factor on the MTSM/GA technique for two-layer viscoelastic layers at 25 MHz 152
7.6.4 Effect of Quality Factor on the MTSM/GA technique for two-layer viscoelastic systems at 35 MHz....154
7.7 Analysis of the MTSM sensor response to a polymer deposition process for the theoretical validation of the GA/MTM technique for two-layer viscoelastic systems 155
7.7.1 Analysis of the MTSM/GA technique for two-layer viscoelastic systems to deposition process at 5 MHZ....156
7.7.2 Analysis of the MTSM/GA technique for two-layer viscoelastic systems to deposition process at 15 MHZ....165

7.7.3 Analysis of the MTSM/GA technique for two-layer viscoelastic systems to deposition process at 25 MHZ 171

7.7.4 Analysis of the MTSM/GA technique for two-layer viscoelastic systems to deposition process at 35 MHZ 176

7.8 Summary and conclusions 182

8 EXPERIMENTAL VALIDATION OF THE MTSM/GA TECHNIQUE FOR TWO-LAYER VISCOELASTIC SYSTEMS 183

8.1 Validation of the MTSM/GA technique with single-layer viscoelastic system modeled as two-layer viscoelastic system 184

8.2 Validation of the MTSM/GA technique with two-layer system combination of SU8-2002 viscoelastic layer and semi-infinite Newtonian medium 186

8.3 Validation of the MTSM/GA technique by using two-layer viscoelastic system with known properties 188

8.3.1 Two-layer viscoelastic system consists of 2 μm SU8-2002 layer as first layer and 400 nm and 200 nm thick collagen layers as second layer 188

8.3.2 Two-layer viscoelastic system consists of 0.770 μm SU8 layer as first layer and 300 nm and 100 nm thick collagen layers as second layer 194

8.4 Discussions on experimental validation of the MTSM/GA technique for two-layer viscoelastic systems 198

8.5 Summary and Conclusions 204

9 APPLICATION OF THE MTSM/GA TECHNIQUE FOR DETERMINATION OF MECHANICAL AND GEOMETRTICAL PROPERTIES OF BIOLOGICAL INTERFACIAL PROCESSES 206

9.1 Determination of properties of antibody adhesion on the MTSM sensor's gold surface 206

9.2 Determination of viscoelastic properties of bovine aortic endothelial cells (BAEC) attached on gelatin coated MTSM sensor surface 210

9.2.1 Material and methods 211

9.2.2 Characterization of the MTSM sensor readings 214

9.2.3 Determination of the mechanical properties of DMEM loaded on the MTSM sensor 215

9.2.4 Determination of the mechanical properties of gelatin layer coated on the MTSM sensor 216

9.2.5 Determination of the mechanical properties of cells attached on the gelatin coated MTSM sensor 217

9.2.6 Discussions 220

9.3 Summary and Conclusions 222

10 CONCLUSIONS AND FUTURE WORK 223

10.1 Conclusions 223

10.2 Future work 224
11 REFERENCES……225
APPENDIX 1. Genetic Algorithms……...…..……...237
APPENDIX 2. Calculation of quality factor……..……246
APPENDIX 3. Acoustic shear wave in a MTSM sensor and transmission line model…….248
APPENDIX 4. MatLab program codes for the simulations……..268
APPENDIX 5. List of Tables…….312

List of Figures

Figure 2-1 Figure2.1 Physical model of the MTSM sensor: depth of penetration for (a) fundamental and (b) harmonic resonance frequencies 9

Figure 2-2 (a) Multi-layered biological process (b) Multi-harmonic operation of MTSM (c) Application of multi-harmonic operation of MTSM.....10

Figure 2-3 The general structure of the MTSM/GA technique combining the MTSM measurement technique and the GA-based data analysis technique.....14

Figure 2-4 General structure of the MTSM/GA measurement system 16

Figure 2-5 Flow chart of genetic algorithm 18

Figure 4-1 Multi-layer biological process. (Example: Bacillus anthracis (BA) spores-antibody interactions). Figure is not to scale. 24

Figure 4-2 Multi-layer biological acoustic structure consisting of piezoelectric and non-piezoelectric layers 24

Figure 4-3 Finite thickness non-piezoelectric acoustic medium 25

Figure 4-4 Equivalent circuit of a finite thickness acoustic line 26

Figure 4-5 Mason model equivalent circuit of a finite thickness piezoelectric layer possesses two mechanical ports and one electrical port 28

Figure 4-6 Representation of multi-layer biological process in transmission line model29

Figure 4-7 A typical magnitude vs. frequency response characteristic and the associated resonance harmonics for the MTSM sensor, spanning a wide frequency range (5 MHz to 35 MHz) 30

Figure 4-8 Magnitude (a) and phase (b) response of MTSM sensor in the vicinity of fundamental frequency (shown at 5 MHz). α_R = maximum magnitude in air, f_R = resonance frequency in air, α_R^I = maximum magnitude when loaded, f_R^I = resonance frequency in when loaded, α_{AR} = minimum magnitude in air, f_{AR} = anti-resonance frequency in air, α_{AR}^I = minimum magnitude when loaded, f_{AR}^I = anti-resonance frequency when loaded, P_R = phase at maximum magnitude in air, P_R^I = phase at maximum magnitude when loaded, P_M^I = minimum phase when loaded, P_{AR} = phase at maximum magnitude in air, P_{AR}^I = phase at maximum magnitude when loaded 31

Figure 4-9 Change in (a) resonance frequency, (b) maximum magnitude, (c) minimum phase (d) frequency at minimum phase, (e) phase at resonance frequency, (f) minimum magnitude and (g) anti-resonance frequency under the loading of DI water, 10% glycerin and 20% glycerin/DI water solutions. 32

Figure 5-1 Single-layer biological viscoelastic layer loaded on the MTSM sensor 35

Figure 5-2 Modified Butterworth-Van Dyke equivalent circuit of loaded MTSM sensor 36

Figure 5-3 The MTSM/GA technique has three main parts: inputs, internal parameters and functions of GA and outputs 39

Figure 5-4 Inputs and outputs of the MTSM/GA technique 40

Figure 5-5 Experimental set-up for theoretical testing of the MTSM/GA technique 46

Figure 5-6 The physical model for a viscoelastic layer loaded on MTSM sensor surface. a) viscoelastic layer in air b) viscoelastic layer in deionized water (DI water) ... 47

Figure 5-7 The results obtained by the MTSM/GA technique after 100 runs for a) thickness b) stiffness c) viscosity, and d) density values. 50

Figure 5-8 Zooming technique applied to each variable a) thickness, b) stiffness, c) viscosity, d)density 52

Figure 5-9 Stability of the MTSM/GA technique after 10 runs 54

Figure 5-10 Influence of experimental error in (a) resonance frequency and (b) maximum magnitude on the MTSM/GA technique for single-layer viscoelastic systems at 5 MHz 56

Figure 5-11 Influence of experimental error in (a) resonance frequency and (b) maximum magnitude on the MTSM/GA technique for single-layer viscoelastic systems at 15 MHz 57

Figure 5-12 Hypothetical two layer system to investigate the effect of quality factor on the MTSM/GA technique for single layer viscoelastic systems 59

Figure 5-13 Influence of quality factor on the MTSM sensor's (a) magnitude and (b) phase responses at 5 MHz (single-viscoelastic layers) 59

Figure 5-14 Effect of the quality factor on the MTSM/GA technique single-viscoelastic layers at 5 MHz 60

Figure 5-15 Influence of quality factor on the MTSM sensor's (a) magnitude and (b) phase responses at 15 MHz (single-viscoelastic layers) 61

Figure 5-16 (a) Effect of quality factor on the MTSM/GA technique's error at 15 MHz (b) Change in maximum magnitude vs. the MTSM/GA technique's error at 15 MHz (single-viscoelastic layers) 61

Figure 5-17 Influence of quality factor on the MTSM sensor's (a) magnitude and (b) phase responses at 25 MHz (single-viscoelastic layers) 62

Figure 5-18 Maximum magnitude vs. the error in MTSM/GA technique for single layer viscoelastic systems at 25 MHz 62

Figure 5-19 Influence of quality factor on the MTSM sensor's (a) magnitude and (b) phase responses at 35 MHz (case: single-viscoelastic layers) 63

Figure 5-20 (a) Change in the maximum magnitude and resonance frequency (b) Effect of the quality factor on the MTSM/GA technique's error at 35 MHz (case: single-viscoelastic layers) 63

Figure 5-21 Influence of quality factor on the MTSM sensor's (a) magnitude and (b) phase responses at 15 MHz, when the MTSM sensor is optimized for operation at 15 MHz (case: single-viscoelastic layers) 64

Figure 5-22 Four stages of a typical evaporation-induced deposition process of a biological film.....65

Figure 5-23 Change in the magnitude (a) and (b) phase responses of the MTSM sensor during evaporation process. (c) Change in the maximum magnitude and resonance frequency by time at 5 MHz. (case: single-viscoelastic layers).....67

Figure 5-24. Effect of the changes in the single viscoelastic layer viscosity and stiffness on the MTSM magnitude (a) and resonance frequency (b) response (relative changes in resonance frequency and absolute values of attenuation in dB) at 5 MHz in Stage I.....68

Figure 5-25 Effect of the changes in the single viscoelastic layer viscosity and stiffness on the MTSM magnitude (a) and resonance frequency (b) response (relative changes in resonance frequency and absolute values of attenuation in dB) at 5 MHz in Stage II. 70

Figure 5-26 Effect of the changes in the single viscoelastic layer viscosity and stiffness on the MTSM magnitude (a) and resonance frequency (b) response (relative changes in resonance frequency and absolute values of attenuation in dB) at 5 MHz in Stage III. 72

Figure 5-27 Effect of the changes in the single viscoelastic layer viscosity and stiffness on the MTSM magnitude (a) and resonance frequency (b) response (relative changes in resonance frequency and absolute values of attenuation in dB) at 5 MHz in Stage IV.....73

Figure 5-28 Change in magnitude (a) and phase (b) responses of the MTSM sensor during evaporation process. (c) Change in maximum magnitude and resonance frequency by time at 15 MHz. (case: single viscoelastic layer) 75

Figure 5-29 Effect of the changes in the single viscoelastic layer viscosity and stiffness on the MTSM magnitude (a) and resonance frequency (b) response (relative changes in resonance frequency and absolute values of attenuation in dB) at 15 MHz in Stage I.....76

Figure 5-30 Effect of the changes in the single viscoelastic layer viscosity and stiffness on the MTSM magnitude (a) and resonance frequency (b) response (relative changes in resonance frequency and absolute values of attenuation in dB) at 15 MHz in Stage II. 77

Figure 5-31 Effect of the changes in the single viscoelastic layer viscosity and stiffness on the MTSM magnitude (a) and resonance frequency (b) response (relative changes in resonance frequency and absolute values of attenuation in dB) at 15 MHz in Stage III. 79

Figure 5-32 Effect of the changes in the single viscoelastic layer viscosity and stiffness to MTSM magnitude (a) and resonance frequency (b) response (relative changes in resonance frequency and absolute values of attenuation in dB) at 15 MHz in Stage IV. 80

Figure 5-33 Change in magnitude (a) and phase (b) responses of the MTSM sensor during evaporation process. (c) Change in maximum magnitude and resonance frequency by time at 25 MHz. (case: single-layer viscoelastic system).....82

Figure 5-34 Effect of the changes in the single viscoelastic layer viscosity and stiffness on the MTSM magnitude (a) and resonance frequency (b) response (relative changes in resonance frequency and absolute values of attenuation in dB) at 25 MHz in Stage I. 83

Figure 5-35 Effect of the changes in the single viscoelastic layer viscosity and stiffness on the MTSM magnitude (a) and resonance frequency (b) response (relative changes in resonance frequency and absolute values of attenuation in dB) at 25 MHz in Stage II. 84

Figure 5-36 Hypothetical one-layer viscoelastic layers with difference column heights (h_f) a) $h_f = \delta/4$, b) $h_f = \delta/2$, c) $h_f = 3\delta/4$, and d) $h_f = \delta$ e) $h_f = 4\delta/3$ f) $h_f = 2\delta$ 85

Figure 5-37 MTSM sensor's acoustic response and penetration depth relationship at 25 MHz 85

Figure 5-38 Effect of the changes in the single viscoelastic layer viscosity and stiffness to MTSM magnitude (a) and resonance frequency (b) response (relative changes in resonance frequency and absolute values of attenuation in dB) at 25 MHz in Stage III. 87

Figure 5-39 Effect of the changes in the single viscoelastic layer viscosity and stiffness on the MTSM magnitude (a) and resonance frequency (b) response (relative changes in resonance frequency and absolute values of attenuation in dB) at 25 MHz in Stage IV. 88

Figure 5-40 Change in magnitude (a) and phase (b) responses of MTSM sensor during evaporation process. (c) Change in maximum magnitude and resonance frequency by time at 35 MHz. 89

Figure 5-41 Effect of the changes in the single viscoelastic layer viscosity and stiffness to MTSM magnitude (a) and resonance frequency (b) response (relative changes in resonance frequency and absolute values of attenuation in dB) at 35 MHz in Stage I. 90

Figure 5-42 Effect of the changes in the single viscoelastic layer viscosity and stiffness on the MTSM magnitude (a) and resonance frequency (b) response (relative changes in resonance frequency and absolute values of attenuation in dB) at 35 MHz in Stage II. 91

Figure 5-43 Effect of the changes in the single viscoelastic layer viscosity and stiffness to MTSM magnitude (a) and resonance frequency (b) response (relative changes in resonance frequency and absolute values of attenuation in dB) at 35 MHz in Stage III. 92

Figure 5-44 Effect of the changes in the single viscoelastic layer viscosity and stiffness to MTSM magnitude (a) and resonance frequency (b) response (relative changes in resonance frequency and absolute values of attenuation in dB) at 35 MHz in Stage IV. 93

Figure 6-1 (a) MTSM sensor network analyzer based electronics measurement system 97

Figure 6-2 Theoretical and experimental resonance frequency (a) and maximum magnitude change (b) of the MTSM sensor loaded with DI water at 15 MHz, 25 MHz and 35 MHz. 100

Figure 6-3 Theoretical and experimental resonance frequency (a) and maximum magnitude change (b) of MTSM sensor loaded with 10% glycerin/DI water at 15 MHz, 25 MHz and 35 MHz. 101

Figure 6-4 Theoretical and experimental resonance frequency (a) and maximum magnitude change (b) of the MTSM sensor loaded with 20 % glycerin/DI water at 15 MHz, 25 MHz and 35 MHz. 103

Figure 6-5 a) Thickness measurements from optical profilometer sample A. SU8-2000 solution sample B. 1:1 dilution of SU8-2002 and cyclopentanone b) Surface topography of SU8 layer obtained by AFM. 106

Figure 6-6 Variations in the thickness of SU8-2002 polymer layer coated on the MTSM sensor surface....107

Figure 6-7 Relative changes in resonance frequency and the maximum magnitude under 2 μm thick SU8-2002 layer at 5 MHz, 15 MHz, 25 MHz and 35 MHz. (error bars are smaller than symbols when not visible)....108

Figure 6-8 Determined $G^{'}$ and $G^{''}$ values of SU8-2002 layer using the MTSM/GA technique at 5, 15, 25 and 35 MHz and comparison with theoretical results 110

Figure 6-9 Relative changes in (a) the resonance frequency and (b) the maximum magnitude under 0.77 μm thick SU8 layer at 5 MHz, 15 MHz, 25 MHz and 35 MHz. 111

Figure 6-10 Determined $G^{'}$ and $G^{''}$ values of SU8 layer using the MTSM/GA at 5 MHz, 15 MHz, 25 MHz and 35 MHz and comparison with theoretical results 112

Figure 6-11 Change in the resonance frequency and maximum magnitude with thickness change for SU8-2002 layers 113

Figure 6-12 Storage (a) and loss (b) modulus determined by the MTSM/GA technique for different thickness of SU8 layer....113

Figure 6-13 The surface profiles of collagen polymer layers coated on the MTSM sensor surface (a) 400 nm and (b) 140 nm. (N=10)....116

Figure 6-14 Relative changes in maximum magnitude and resonance frequency in the harmonic resonance frequencies of the MTSM with collagen sample as a function of time. (a) and (b) 400 nm, (c) and (d) 140 nm....117

Figure 6-15 The step analysis (a) of 400 nm thick collagen layer for thickness measurement and surface topography image (b) roughness measurement.....118

Figure 6-16 Determined G' and G" values of 400 nm of collagen layer using MTSM/GA technique at 5 MHz, 15 MHz, 25 MHz and 35 MHz and comparison with theoretical values 120

Figure 6-17 The step analysis (a) of 140 nm thick collagen layer for thickness measurement and surface topography image (b) for roughness measurement..120

Figure 6-18 Determined $G^{'}$ and $G^{''}$ values of 140 nm thick collagen layer using the MTSM/GA technique at 5, 15, 25 and 35 MHz and comparison with theoretical results....121

Figure 6-19 Relative changes in (a) resonance frequency and (b) maximum magnitude of the MTSM sensor loaded with 100 μl of collagen samples. 122

Figure 6-20 Storage (a) and loss (b) modulus values for different thickness of collagen layer 123

Figure 6-21 Theoretical changes in the (a) viscosity and (b) stiffness of collagen sample during the simulation of the evaporation-induced deposition process (figures taken from Kwoun, 2006) 124

Figure 6-22 Time evolution of (a) stiffness , (b) viscosity , (c) density and (d) thickness of collagen layer at 5 MHz, 15 MHz, 25 MHz and 35 MHz. 125

Figure 6-23 The MTSM/GA technique has been run 100 times for determination of the mechanical properties of 20 % glycerin/DI water. 127

Figure 6-24 Change in the resonance frequency (blue) and the frequency at the zero phase (pink) during the evaporation of collagen type-I on the MTSM sensor .. 130

Figure 7-1 Modified Butterworth-van dyke equivalent circuit of perturbed MTSM sensor loaded with two-layer viscoelastic system. 133

Figure 7-2 The physical model for two-layer viscoelastic system loaded on MTSM sensor surface. a) viscoelastic layer in air b) viscoelastic layer in deionized water (DI water) 136

Figure 7-3 The results obtained by the MTSM/GA technique for two-layer viscoelastic systems after 100 runs for a) stiffness of first layer b) viscosity of first layer c) stiffness of second layer, and d) viscosity of second layer 137

Figure 7-4 Error in the MTSM/GA technique two-layer viscoelastic systems with the number of runs 139

Figure 7-5 Zooming technique applied to a) stiffness of first layer b) viscosity of first layer c) stiffness of second layer, and d) viscosity of second layer (case: two-layer viscoelastic systems) 139

Figure 7-6 Absolute error in the MTSM/GA technique two-layer viscoelastic systems when an error is introduced to (a) first layer's thickness (b) first layer's density (c) second layer's thickness and (d) second layer's density. Analysis is done at 5 MHz. 141

Figure 7-7 Absolute error in MTSM/GA technique two-layer viscoelastic systems when an error is introduced to (a) first layer's thickness (b) first layer's density (c) second layer's thickness and (d) second layer's density. Analysis is done at 15 MHz. 142

Figure 7-8 Absolute error in (a) first layer's stiffness (b) first layer's viscosity (c) second layer's stiffness and (d) second layer's viscosity at different stiffness values of first layer (case: two-layer viscoelastic systems) 143

Figure 7-9 Absolute error in (a) first layer's stiffness (b) first layer's viscosity (c) second layer's stiffness and (d) second layer's viscosity at different stiffness values of first layer (case: two-layer viscoelastic systems) 144

Figure 7-10 Error in the MTSM/GA technique for two-layer viscoelastic systems when error in (a) resonance frequency and (b) maximum magnitude at 5 MHz 146

Figure 7-11 Error in the MTSM/GA technique for two-layer viscoelastic systems when error in (a) resonance frequency and (b) maximum magnitude at 15 MHz 146

Figure 7-12 Error in the MTSM/GA technique for two-layer viscoelastic systems when error in (a) resonance frequency and (b) maximum magnitude at 25 MHz 147

Figure 7-13 Error in the MTSM/GA technique for two-layer viscoelastic systems when error in (a) resonance frequency and (b) maximum magnitude at 35 MHz 148

Figure 7-14 Hypothetical three-layer system to investigate the effect of quality factor on the MTSM/GA technique for two-layer viscoelastic systems 149

Figure 7-15 Influence of the quality factor on the MTSM sensor's for two-aye viscoelastic systems (a) magnitude and (b) phase responses at 5 MHz (case: two-layer viscoelastic systems).....150

Figure 7-16 The effect of quality factor on the MTSM/GA technique for two-layer viscoelastic systems at 5 MHz.....150

Figure 7-17 Influence of the quality factor on the MTSM sensor's for two-layer viscoelastic systems (a) magnitude and (b) phase responses at 15 MHz.....151

Figure 7-18 The effect of the quality factor on the MTSM/GA technique for two-layer viscoelastic systems at 15 MHz.....152

Figure 7-19 Influence of quality factor on the MTSM sensor's for two-layer viscoelastic systems (a) magnitude and (b) phase responses at 25 MHz 153

Figure 7-20 The effect of the quality factor on the MTSM/GA technique for two-layer viscoelastic systems at 25 MHz.....153

Figure 7-21 Influence of the quality factor on the MTSM sensor's fro two-layer viscoelastic systems (a) magnitude and (b) phase responses at 35 MHz.....154

Figure 7-22 The effect of the quality factor on the MTSM/GA technique for two-layer viscoelastic systems at 35 MHz.....155

Figure 7-23 Change in (a) the magnitude and (b) phase responses of the MTSM sensor during evaporation process. (c) Change in maximum magnitude and resonance frequency in time at 5 MHz. (case: two-layer viscoelastic systems).....157

Figure 7-24 Effect of the changes in the two-layer viscoelastic systems viscosity and stiffness to the MTSM sensor's (a) magnitude and (b) resonance frequency responses (relative changes in resonance frequency and absolute values of magnitude in dB) at 5 MHz in Stage I. 158

Figure 7-25 The results obtained by the MTSM/GA technique for two-layer viscoelastic systems after 100 runs for a) layer-2 viscosity b) layer-2 stiffness c) layer-1 viscosity, and d) layer-1 stiffness 158

Figure 7-26Effect of the changes in the two-layer viscoelastic systems viscosity and stiffness to the MTSM sensor's (a) magnitude and (b) resonance frequency responses (relative changes in resonance frequency and absolute values of magnitude in dB) at 5 MHz in Stage II.....160

Figure 7-27 The results obtained by the MTSM/GA technique for two-layer viscoelastic systems after 100 runs for a) layer-2 viscosity b) layer-2 stiffness c) layer-1 viscosity, and d) layer-1 stiffness in stage II at 5 MHz 161

Figure 7-28Effect of the changes in the two-layer viscoelastic systems viscosity and stiffness to the MTSM sensor's (a) magnitude and (b) resonance frequency response (relative changes in resonance frequency and absolute values of magnitude in dB) at 5 MHz in Stage III 162

Figure 7-29 The results obtained by the MTSM/GA technique for two-layer viscoelastic systems after 100 runs for a) layer-1 viscosity b) layer-1 stiffness c) layer-2 viscosity, and d) layer-2 stiffness 162

Figure 7-30Effect of the changes in the two-layer viscoelastic systems viscosity and stiffness to the MTSM (a) magnitude and (b) resonance frequency responses (relative changes in resonance frequency and absolute values of magnitude in dB) at 5 MHz in Stage IV 163

Figure 7-31 The results obtained by the MTSM/GA technique for two-layer viscoelastic systems after 100 runs for a) layer 1 viscosity b) layer 1 stiffness c) layer 2 viscosity, and d) layer 2 stiffness.....164

Figure 7-32 Change in (a) magnitude and (b) phase responses of the MTSM sensor during evaporation process. (c) Change in maximum magnitude and resonance frequency by time at 15 MHz. 166

Figure 7-33Effect of the changes in the two-layer viscoelastic systems viscosity and stiffness to MTSM (a) magnitude and (b) resonance frequency response (relative changes in resonance frequency and absolute values of magnitude in dB) at 15 MHz in Stage I.....166

Figure 7-34Effect of the changes in the two-layer viscoelastic systems viscosity and stiffness to the MTSM sensor's (a) magnitude and (b) resonance frequency responses (relative changes in resonance frequency and absolute values of magnitude in dB) at 15 MHz in Stage II.....168

Figure 7-35Effect of the changes in the two-layer viscoelastic systems viscosity and stiffness to the MTSM sensor's (a) magnitude and (b) resonance frequency response (relative changes in resonance frequency and absolute values of magnitude in dB) at 15 MHz in Stage III 169

Figure 7-36Effect of the changes in the two-layer viscoelastic systems viscosity and stiffness to the MTSM sensor's (a) magnitude and (b) resonance frequency response (relative changes in resonance frequency and absolute values of magnitude in dB) at 15 MHz in Stage IV 170

Figure 7-37 Change in (a) magnitude and (b) phase responses of the MTSM sensor during evaporation process. (c) Change in maximum magnitude and resonance frequency by time at 25 MHz. (case: two-layer viscoelastic systems).....171

Figure 7-38Effect of the changes in the two-layer viscoelastic system viscosity and stiffness to the MTSM sensor's (a) magnitude and (b) resonance frequency response (relative changes in resonance frequency and absolute values of magnitude in dB) at 25 MHz in Stage I.....172

Figure 7-39Effect of the changes in the two-layer viscoelastic system viscosity and stiffness to the MTSM sensor's (a) magnitude and (b) resonance frequency response (relative changes in resonance frequency and absolute values of magnitude in dB) at 25 MHz in Stage II.....173

Figure 7-40Effect of the changes in the two-layer viscoelastic system viscosity and stiffness to the MTSM sensor's (a) magnitude and (b) resonance frequency response (relative changes in resonance frequency and absolute values of magnitude in dB) at 25 MHz in Stage III 175

Figure 7-41Effect of the changes in the two-layer viscoelastic system viscosity and stiffness to the MTSM sensor's (a) magnitude and (b) resonance frequency response (relative changes in resonance frequency and absolute values of magnitude in dB) at 25 MHz in Stage IV 176

Figure 7-42 Change in magnitude (a) and phase (b) responses of the MTSM sensor during evaporation process. (c) Change in maximum magnitude and resonance frequency by time at 35 MHz. (case: two-layer viscoelastic system) 177

Figure 7-43Effect of the changes in the two-layer viscoelastic system viscosity and stiffness to the MTSM sensor's (a) magnitude and (b) resonance frequency response (relative changes in resonance frequency and absolute values of magnitude in dB) at 35 MHz in Stage I.....178

Figure 7-44Effect of the changes in the two-layer viscoelastic system viscosity and stiffness to the MTSM sensor's (a) magnitude and (b) resonance frequency response (relative changes in resonance frequency and absolute values of magnitude in dB) at 35 MHz in Stage II.....179

Figure 7-45Effect of the changes in the two-layer viscoelastic system viscosity and stiffness to the MTSM sensors's (a) magnitude and (b) resonance frequency response (relative changes in resonance frequency and absolute values of magnitude in dB) at 35 MHz in Stage III 180

Figure 7-46Effect of the changes in the two-layer viscoelastic system viscosity and stiffness to the MTSM sensor's (a) magnitude and (b) resonance frequency response (relative changes in resonance frequency and absolute values of magnitude in dB) at 35 MHz in Stage IV 181

Figure 8-1 Single layer of 1950 nm thick of SU8-2002 layer has been modeled as two-layer viscoelastic system.....185

Figure 8-2 Single layer 1.95 μm thick SU8-2002 layer is modeled as two-layer viscoelastic layer (a) loss modulus (b) storage modulus at 5 MHz, 15 MHz, 25 MHz and 35 MHz 185

Figure 8-3 Physical model for a viscoelastic layer loaded with semi-infinite Newtonian medium 186

Figure 8-4 Comparison of the storage and loss modulus values obtained for SU8-2002 layer from single-layer (see chapter 6) and two-layer calculations. 187

Figure 8-5 Comparison of (a) the loss modulus and (b) storage modulus values obtained for DI water layer theoretically and experimentally. 187

Figure 8-6 The evaporation process of 200 µl of collagen type-I on 1.95 micron thick SU8-2002 layer at a) 5 MHz b) 15 MHz c)25 MHz and d) 35 MHz.....189

Figure 8-7 The evaporation process of 100 µl of collagen on 1.95 micron thick SU8 layer at a) 5 MHz b) 15 MHz c)25 MHz and d) 35 MHz.....191

Figure 8-8 Intensity map of a collagen type-I deposited on a ~2 µm thick SU8-2002 polymer spin coated on the MTSM sensor (image size: 0.7 µm x 0.7 µm 191

Figure 8-9Thickness of the collagen layer on at different locations; (a) thickness obtained at the end of the evaporation process of (a) 200 µl collagen and (a) 100 µl collagen on 2 µm thick SU8-2002 layer. Each point is an average of 10 measurements 192

Figure 8-10 The results obtained from the MTSM/GA technique for SU8-2002 layer before and after the formation of two-layer system; (a) storage modulus (b) loss modulus.....193

Figure 8-11 The results obtained from the MTSM/GA technique for collagen layer before and after two layer system formation.(a) loss modulus (b) storage modulus.....193

Figure 8-12 The evaporation process of 200 µl of collagen on 0.770 micron thick SU8-2002 layer at a) 5 MHz, b) 15 MHz, c)25 MHz, and d) 35 MHz.....195

Figure 8-13 The evaporation process of 100 µl of collagen on 0.770 micron thick SU8-2002 layer at a) 5 MHz b) 15 MHz c)25 MHz and d) 35 MHz.....196

Figure 8-14Thickness of the collagen layer on at different locations; (a) thickness obtained at the end of the evaporation process of (a) 200 µl collagen and (a) 100 µl collagen on 0.770 µm thick SU8-2002 layer. Each point is an average of 10 measurements 197

Figure 8-15 The results obtained from the MTSM/GA technique for SU8-2002 layer before and after two layer system formation. (a) storage modulus (b) loss modulus.....197

Figure 8-16 The results obtained from the MTSM/GA technique for collagen layer before and after two layer system formation.(a) loss modulus (b) storage modulus.....198

Figure 8-17Comparison of theoretical and experimental changes (a) resonance frequency and (b) maximum magnitude when 1.95 µm thick SU8-2002 layer spin coated on the MTSM sensor was loaded with semi-infinite DI water. Theoretical calculations were done by using TLM.....201

Figure 9-1 Time response of relative changes in (a) the resonance frequency and the (b) maximum magnitude responses of MTSM sensor to antibody binding at 15 MHz, 25 MHz and 35 MHz.....207

Figure 9-2 Physical model for MTSM sensor system at A) t=10 and B) t=70 208

Figure 9-3 MTSM sensor surfaces were rinsed with PBS at each time point and stained: (A)1 h, (B) 15 h 214

Figure 9-4 Time course of relative changes in (a) the maximum magnitude and (b) resonance frequency responses of the MTSM sensor due to the adhesion process of endothelial cells. Cell suspension was introduced to the sensor's surface at time 0. 215

Figure 9-5 MTSM sensor's response to DMEM loading (a) relative change in the resonance frequency and (b) absolute change in maximum magnitude 215

Figure 9-6 The MTSM sensor's response to gelatin coating (a) relative change in the resonance frequency and (b) relative change in maximum magnitude at 15 MHz, 25 MHz and 35 MHz 217

Figure 9-7 One-layer model of the cell attachment on the MTSM sensor.....218

Figure 9-8 Loss and storage modulus of interfacial layer at 5 MHz, 15 MHz, 25 MHz, and 35 MHz 218

Figure 9-9 Two-layer model of the cell attachment on the MTSM sensor 219

Figure 9-10 Loss and storage modulus of first and second layer at 5 MHz, 15 MHz, 25 MHz, and 35 MHz 220

Figure A2.1 Quality factor calculation by using 3dB bandwidth in S21 response of MTSM sensor…….....……..246

Figure A2.2. Quality factor calculation by using phase data of the MTSM sensor……...247

Figure A3.1 Side cross-sectional view of MTSM sensor, showing shear displacement profiles for the fundamental frequency……...248

Figure A3.2. A MTSM sensor modeled as three-port model…….253

Figure A3.3 Three port Mason model of piezoelectric quartz.…….……...259

Figure A3.4 Two port Mason model of piezoelectric quartz with one stress-free interface……...260

Figure A3.5 Mason model of composite resonator having a stress free interface on one side and two arbitrary films on the other side…….263

Figure A3.6 A lumped element model of an unloaded MTSM sensor……265

List of Tables

Table 5-1 phases of a typical viscoelastic system 42

Table 5-2 Minimum and maximum values for stiffness, viscosity, density and thickness parameters 43

Table 5-3 The convergence performance (in percentage) of the MTSM/GA technique in each the sub-space in air 49

Table 5-4 The convergence performance (in percentage) of the MTSM/GA technique in each the sub-space in DI water 49

Table 5-5 Error in percentage in the MTSM/GA technique when different combination of gene per chromosomes and number of individuals were applied..... 53

Table 5-6 Second solution for single layer viscoelastic loading in air at 5 MHz..... 55

Table 5-7Second solution for viscoelastic loading in DI water at 5 MHz 55

Table 5-8 Hypothetical mechanica and geometrical properties of single-layer viscoelastic system in each stage..... 66

Table 5-9 Properties of single viscoelastic layer determined by the MTSM/GA technique and % errors in stage I at 5 MHz 69

Table 5-10 Properties of single viscoelastic layer determined by the MTSM/GA technique and % errors in stage II at 5 MHz 71

Table 5-11 Properties of single viscoelastic layer determined by the MTSM/GA technique and % errors in stage III at 5 MHz 72

Table 5-12 Properties of single viscoelastic layer determined by the MTSM/GA technique and % errors in stage IV at 5 MHz..... 74

Table 5-13 Properties of single viscoelastic layer determined by the MTSM/GA technique and % errors in stage I at 15 MHz..... 76

Table 5-14 Properties of single viscoelastic layer determined by the MTSM/GA technique and % errors in stage II at 15 MHz 78

Table 5-15 Properties of single viscoelastic layer determined by the MTSM/GA technique and % errors in stage III at 15 MHz 79

Table 5-16 Properties of single viscoelastic layer determined by the MTSM/GA technique and % errors in stage IV at 15 MHz..... 81

Table 5-17 Properties of single viscoelastic layer determined by the MTSM/GA technique and % errors in stage I at 25 MHz..... 83

Table 5-18 Properties of single viscoelastic layer determined by the MTSM/GA technique and % errors in stage II at 25 MHz 84

Table 5-19 Absolute errors in the MTSM/GA technique for single layer viscoelastic system at 25 MHz with the change of h_f/δ ratio 86

Table 5-20 Properties of single viscoelastic layer determined by the MTSM/GA technique and % errors in stage III at 25 MHz 87

Table 5-21 Properties of single viscoelastic layer determined by the MTSM/GA technique and % errors in stage IV at 25 MHz 88

Table 5-22 Properties of single viscoelastic layer determined by the MTSM/GA technique and % errors in stage I at 35 MHz 91

Table 5-23 Properties of single viscoelastic layer determined by the MTSM/GA technique and % errors in stage II at 35 MHz 92

Table 5-24 Properties of single viscoelastic layer determined by the MTSM/GA technique and % errors in stage III at 35 MHz 93

Table 5-25 Properties of single viscoelastic layer determined by the MTSM/GA technique and % errors in stage IV at 35 MHz 94

Table 6-1 Theoretical validation of the MTSM/GA technique for determination of DI water properties at 5 MHz, 15 MHz, 25 MHz, and 35 MHz. 99

Table 6-2Experimental validation of the MTSM/GA technique for determination of DI water properties at 15 MHz, 25 MHz, and 35 MHz. 100

Table 6-3 Theoretical validation of the MTSM/GA technique for determination of 10 %glycerin/DI water properties at 5 MHz, 15 MHz, 25 MHz, and 35 MHz. 102

Table 6-4Experimental validation of the MTSM/GA technique for determination of 10% glycerin/DI water properties at 15 MHz, 25 MHz, and 35 MHz. 102

Table 6-5 Theoretical validation of the MTSM/GA technique for determination of 20 % glycerin/DI water properties at 5 MHz, 15 MHz, 25 MHz, and 35 MHz. 104

Table 6-6 Experimental validation of the MTSM/GA technique for determination of 20 % glycerin/DI water properties at 15 MHz, 25 MHz, and 35 MHz. 104

Table 6-7 Comparison density and thickness values of SU 8-2002 layer determined using MTSM/GA sensor at 5, 15, 25 and 35 MHz with profilometer and Jiang et al. (2003). 109

Table 6-8 Comparison of determined G' and G'' values of SU8 layer using MTSM/GA at 5, 15, 25 and 35 MHz and Jiang et al (2003). 109

Table 6-9 Determined density and thickness values by the MTSM/GA for 770 nm thick SU8-2002 layer at 5, 15, 25 and 35 MHz 111

Table 6-10 Comparison density and thickness values of 400 nm thick collagen layer determined using the MTSM/GA technique at 5, 15, 25 and 35 MHz with the values obtained from AFM and references. 119

Table 6-11 Comparison density and thickness values of 140 nm thick collagen layer determined using MTSM/GA technique at 5, 15, 25 and 35 MHz with the values obtained from AFM and references. 121

Table 7-1Viscosity, stiffness, density and thickness values of the viscoelastic layers forming two-layer viscoelastic systems 137

Table 7-2 Second viscoelastic layer's properties for the validation of the MTSM/GA technique for two-layer viscoelastic systems.....156

Table 7-3 Mechanical properties determined by the MTSM/GA technique for two-layer viscoelastic systems and % errors in stage I at 5 MHz.....159

Table 7-4Mechanical properties determined by the MTSM/GA technique for two-layer viscoelastic systems and % errors in stage II at 5 MHz.....161

Table 7-5Values determined by the MTSM/GA technique for two-layer viscoelastic systems and % errors in stage III at 5 MHz.....163

Table 7-6Values determined by the MTSM/GA technique for two-layer viscoelastic systems and % errors in stage IV at 5 MHz.....164

Table 7-7Values determined by the MTSM/GA technique for two-layer viscoelastic systems and % errors in stage I at 15 MHz 167

Table 7-8Values determined by the MTSM/GA technique for two-layer viscoelastic systems and % errors in stage II at 15 MHz 168

Table 7-9 Values determined by the MTSM/GA technique for two-layer viscoelastic systems and % errors in stage III at 15 MHz.....169

Table 7-10 Values determined by the MTSM/GA technique for two-layer viscoelastic systems and % errors in stage IV at 15 MHz.....170

Table 7-11Values determined by the MTSM/GA technique for two-layer viscoelastic systems and % errors in stage I at 25 MHz 173

Table 7-12Values determined by the MTSM/GA technique for two-layer viscoelastic systems and % errors in stage II at 25 MHz 174

Table 7-13Values determined by the MTSM/GA technique for two-layer viscoelastic systems and % errors in stage III at 25 MHz.....175

Table 7-14Values determined by the MTSM/GA technique for two-layer viscoelastic systems and % errors in stage III at 25 MHz.....176

Table 7-15Values determined by the MTSM/GA technique for two-layer viscoelastic systems and % errors in stage I at 35 MHz 178

Table 7-16Values determined by the MTSM/GA technique for two-layer viscoelastic systems and % errors in stage III at 35 MHz.....179

Table 7-17Values determined by the MTSM/GA technique for two-layer viscoelastic systems and % errors in stage IV at 35 MHz.....180

Table 7-18Values determined by the MTSM/GA technique for two-layer viscoelastic systems and % errors in stage IV at 35 MHz.....181

Table 8-1Single layer SU8 is modeled as two viscoelastic layers with different thicknesses (errors are average of three experiments) 186

Table 9-1Determined properties for semi-infinite Newtonian medium layer at 15 MHz, 25 MHz and 35 MHz 208

Table 9-2Determined properties for antibody layer at 15, 25 and 35 MHz 209

Table 9-3Determination of DMEM properties at 15 MHz, 25 MHz, and 35 MHz by using the MTSM/GA technique.....216

Abstract

Biological interfaces constitute one of the most dynamic and expanding fields in science and technology and affect such disciplines as tissue engineering, biomaterials, and biosensors. A typical biological interface consists of several distinct layers representing such processes as protein binding, cell adhesion and many others. It is important to know quantitative characteristics of those layers, specifically their mechanical and geometrical properties. One of very powerful technique for characterization of mechanical and geometrical properties of layered systems has been the technique based on multi-resonant thickness-shear monitor (MTSM) measurement technology. However, until this moment, the thickness shear mode (TSM) measurement technique has provided only incomplete set of quantitative data. In this project, a combination of multi-resonant thickness shear mode (MTSM) measurement technique and genetic algorithm (GA)-based data analysis method is proposed for quantitative characterization of multi-layer biological processes, and for determination of mechanical and geometrical properties of the layered structures. Specifically, MTSM measurement technique provides a unique tool capable of simultaneous interrogation of the interface at different depths ranging from tens of nanometers to several microns in real time with high accuracy. Next, a genetic algorithm (GA)-based data analysis technique capable of accurate extraction of material properties was developed and integrated with the MTSM technique. The strengths and limitations of the MTSM/GA technique were studied both theoretically and experimentally. For example, it was shown that MTSM/GA can provide the mechanical and structural properties of single and two-layer viscoelastic systems theoretically with less than %1 error. The proposed MTSM/GA was experimentally verified with several chemical systems (polymers) and biological systems (collagen, cells, and antibody). Finally, mechanical and structural properties of the antibody and bovine aortic

endothelial cells (BAECs) monolayers attached on the MTSM sensor surface were determined. The obtained results demonstrated that this novel approach can be a very useful tool in quantification and interpretation of biological, chemical, and physical interfacial structures and processes.

1 INTRODUCTION

1.1 Motivation of the Thesis

1.1.1 Biological interfacial processes

Biological interfaces constitute one of the most dynamic and expanding fields in science and technology such as tissue engineering, biomaterials, and biosensors. For instance, the interactions between scaffolds and cells have crucial importance in the development of a functional tissue ex vivo and then implantation into the human body. Furthermore controlling the interactions between biomaterials and evolving tissue by developing new smart biomaterials and biological interfaces is a promising area in the tissue engineering field (Hubbell, 1995). On the other hand cell adhesion, and the interfacial processes that depend on or are modulated by adhesion have been studied extensively due to their vital roles in many biological research areas.

Cellular adhesion plays important roles in regulation of cell behavior, such as the control of growth and differentiation during development and the modulation of cell migration in wound healing, metastasis, and angiogenesis. Biological interfacial processes have also a critical importance in determining clinical efficacy of blood-contacting materials (Greisler, 1990). Detailed understanding of these complex interactions and biological processes occurring at the interface will enable researches to develop novel blood-compatible biomaterials. Sensitivity of the biosensors is very much dependent on the specific interactions between the immobilized surface and the analyte at the sensor interface. Therefore the novel and robust immobilization of detector molecules is one the most important aspect of the biosensor field. In this aspect, interfacial science inevitably comes into play in

characterization and developing new interfaces to enhance the sensitivity and specificity of biosensors.

1.1.2 Current techniques to study biological interfacial processes; their strengths and limitations

There are four main techniques to characterize biological interfacial processes; (1) scanning force microscopy (SPM), (2) total internal reflection fluorescence microscopy (TIRFM), (3) ellipsometry and (4) surface plasmon resonance (SPR).

Scanning probe microscopy (SPM) has capability to function in the liquid environment and has nm scale resolution. In addition it can monitor cellular processes and dynamics in real time (Myhra, 2004, Davies et al., 1997). Atomic force microscopy (AFM), scanning tunneling microscopy (STM) and Near-Field Scanning Optical Microscopy (NSOM) are the well-known members of this technique.

Total internal reflection fluorescence microscopy (TIRFM) has novel applications such as monitoring the kinetics of biological processes (Klinth et. al, 2006), imaging of exocytosis or endocytosis (Yang et. al., 2003), and measurements of force transmission of cells (Mathur et. al, 2000).

Spectral ellipsometry is less convenient to monitor dynamic processes but allows the determination of thickness and refractive index of the adsorbed layer (Grant et. al, 2001, Schulz et al., 2004).

Surface Plasmon Resonance (SPR) is the most well-known optical sensing technique and has been used to study biological interfacial processes such as characterization of cell adhesion (Merve et al, 1996), polymer adsorption (Green et al. 1997), lipid bilayers (Striebel

et al., 1994) and avidin-to-biotin interactions (Cannizzaro et al., 2000). SPR has been interfaced with AFM to form a combined SPR/AFM instrument that is able to record both the kinetics of polymer surface erosion and the structural changes occurring at the interface. This allows the inter-relationship between these two variables to be directly analyzed (Chen et al., 1996).

Current technologies are limited to be mostly qualitative method. Quantification of interfacial processes is very important in many biomedical fields. For example, quantification of adsorption of macromolecules and parameterization of microstructure of thin organic layers are of high interest in research areas like biomaterials and biosensors (Arwin, 2000). Furthermore quantitative characterization of the physical interaction between cell and substrate is essential for the optimization of implants for which tissue integration is a primary determinant of performance. In tissue engineering, quantitative analysis of cell-scaffold interactions would be of great value for controlling cell behavior and the processes involved in incorporating the cells into the scaffolds for directing cellular responses and tissue formation (Nair et al, 2005).

Current technologies have limited interrogating depth into the multi-layer biological processes. It is considered essential to monitor quantitatively in real time the dynamic interactions between biomolecules and their cognate receptors in cell (Ziblat et el., 2006). The ability to visualize, track, and quantify molecules and events in living cells with high spatial and temporal resolution is essential for understanding biological systems (Schwartz et al., 2003). Biological tissue is usually composed of different constructive units of varying size and properties (Raum et al., 2003). Furthermore, it was suggested that the cell adhesion process should be modeled as a multi-layer model in which each layer shows different rheological properties (Wegener et al., 2000, Ergezen et al., 2006). Therefore it is important

to have a capability to monitor biological processes at different depths from the sensor surface with a high temporal and spatial resolution.

Current technologies give information mostly on surface chemistry and topography in great detail, but have been primarily limited to the understanding of substrate mechanics (Nair et al., 2005). Furthermore although methods to measure bulk mechanical properties are already established, accurate measurement methods are required to asses the local micro-scale mechanical properties of substrata (Wong et al., 2005). For example, Min-lo et al. (2000) showed the cell rigidity and strain could play an important controlling role in a normal and pathological processes involving cell locomotion.

In conclusion, there is a need to develop a non-destructive and quantitative tool which is capable to monitor kinetics and mechanics of multi-layer biological interfacial processes with high temporal and spatial resolution. We propose to utilize a multi-resonance thickness shear mode (MTSM) technique in this project to fill these gaps in the study of biological interfacial processes.

1.1.3 Theme of the thesis

Thickness shear mode (TSM) sensors have been used to study a variety of interfacial biological processes by other researchers and by us, Bionanosensor Research Laboratory, Drexel University.

Su et al. (1996) studied the rheological and interfacial properties of nucleic acid films. Phenomena such as diffusion (Galipeau et al., 1991), absorption and desorption (Wu et al., 1999), and adhesion (Frediksson et al., 1998, Gryte et al., 1993) in organic and biological films have been investigated using TSM sensors. Yang et al (1993) showed the importance of the liquid-solid interface in determining the response of the TSM sensor by controlling

surface free energy of the metal electrodes. The cell motility can be monitored by analyzing the noise of TSM sensor response due to its high interfacial sensitivity (Sapper et al., 2006).

Extensive research work in BioNanosensor Research Laboratory, Drexel University has been focused on quantitative characterization of variety of multilayer biological interfacial processes. After several years of experimental and theoretical effort, significant progress has been made on the development of multi-resonance thickness shear mode (MTSM) device and analysis of a variety of interfacial processes with sensor readings. These studies included cell adhesion on extracellular matrix (gelatin), blood platelet aggregation and adhesion on collagen, and bioparticle-surface interactions. These projects are shortly described below.

Project 1: Cell adhesion is a complex process involving physical interactions, chemical binding events, and biological signaling processes. MTSM technique has been used to characterize this important process. The theoretical and experimental work resulted in two journal papers and one conference paper (Hong et al., 2006, Ergezen et al., 2007, Hong et al., 2005).

Project 2: Hemostasis is required to maintain vascular system integrity, but thrombosis, formation of a clot in a blood vessel, is one of the largest causes of morbidity and mortality in the industrialized world. MTSM technique coated with collagen-I fibers to promote platelet activation and adhesion was developed and tested for sensitivity to detect these primary events. The experimental work resulted in a journal paper (Ergezen et al., 2007).

Project 3: The sensitivity of the MTSM technique in the detection of pathogens, viruses or other type of target analytes is very much dependent on the interface (immobilized interface). The MTSM technique has been used to characterize the binding of viruses and

biomarkers on antibody coated MTSM sensor. Extensive experimental and theoretical work resulted in two conference papers (Anishetty et al., 2008, Ergezen et al., 2008).

Although MTSM technique has been successfully utilized for real-time monitoring and correlation of sensor responses to specific components of these processes, they have been limited to be qualitative or semi-quantitative efforts. For viscoelastic layers, their mechanical impedance depends upon density, thickness, and complex shear modulus of the loading. Identification of all of the system parameters from the impedance measurements has been very challenging and uncertain without a priori knowledge of the thicknesses and/or some of the material properties (Lucklum and Hauptman, 1997). In particular, biological processes that exhibit strong viscoelastic behavior require more advanced modeling of both mechanical and electrical representation of the TSM sensors. A new approach merging the multi-harmonic thickness shear mode (MTSM) measurement technique and a data extraction technique based on stochastic global optimization procedure, genetic algorithm (GA), has been proposed. The MTSM/GA technique was developed and tested with polymer layers with known properties. Then it was applied to estimate the properties of protein layers with unknown properties such as antibodies and bovine aortic endothelial cells (BAEC) adsorbed on the MTSM sensor surface. MTSM/GA technique may lead to the development of quantitative tool for the characterization of a broad range of multi-layer biological interfacial processes.

1.2 Organization of the Thesis

This thesis includes 10 chapters. It starts with the introduction to the thesis work and background study in Chapter 1 and Chapter 2 respectively.

In chapter 1, motivation of the thesis, critical analysis of the current techniques and the theme of the thesis are included.

In chapter 2, the background knowledge required to understand the thesis work is introduced. A brief summary of thickness shear mode sensors, previous works for quantification of the biological interfacial processes and overview of genetic algorithm/MTSM technique are discussed. In chapter 3, the objectives of the thesis are presented.

In chapter 4, theoretical modeling of the MTSM sensor is introduced. The MTSM sensor parameters characterizing the sensor response was defined. Finally, validation of theoretical approach is pursued.

In chapter 5, a stochastic method based on the genetic algorithms is introduced and integration of the method to the MTSM technique is discussed. The theoretical validation of the MTSM/GA technique is then completed. The overall goal of this chapter is to theoretically determine the limitations and strengths of the MTSM/GA technique for determination of mechanical and structural properties of the single-layer viscoelastic systems.

Experimental validation of the MTSM/GA technique for single-layer viscoelastic systems is done in chapter 6. Two polymer systems with known paramaters, SU8-2002 and collagen, are utilized.

In chapter 7, the MTSM/GA technique is theoretically validated for two-layer viscoelastic systems. Structure of the technique and several aspects such as quality factor are discussed. Limitations and strengths of the MTSM/GA technique for determination of mechanical properties of the two-layer viscoelastic systems are analyzed.

In chapter 8, the MTSM/GA technique is experimentally validated by using two layer polymer system made of SU8-2002 (first layer) and collagen (second layer). Several

thickness combinations of two-layer system are designed and the mechanical properties are determined.

In chapter 9, the MTSM/GA technique is applied to the biological system with unknown properties. For case studies, the adsorption of antibody and the attachment of bovine aortic endothelial cells (BAEC) on the gelatin coated MTSM sensor are investigated.

The thesis work is concluded with summary, conclusions, and future work in chapter 10.

2 BACKGROUND

2.1 General features of multi-resonance thickness shear mode (MTSM) sensor operating under viscoelastic loading

Piezoelectric multi-resonance thickness shear mode (MTSM) transmits acoustic shear waves into a medium under test, and the waves interact with the medium. Shear waves monitor local properties of a medium in the vicinity of the sensor and of the medium/sensor interface (on the order of nm - μm); thus, they provide a very attractive technique to study interfacial processes. Measured parameters of acoustic waves are correlated with medium properties such as interfacial mass/density, viscosity, or elasticity that change during chemical or biological processes. Shear waves penetrate the medium over a very short distance. Fig. 2-1a shows the acoustic wave penetrating the adjacent medium and fig. 2.1b shows that the depth of penetration decreases at higher harmonic frequencies. Therefore, by changing the frequency, one can control the distance at which the wave probes the medium.

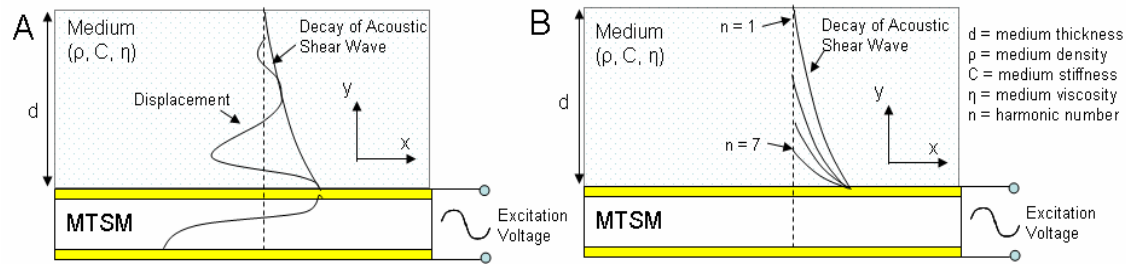

Figure 2-1 Figure2.1 Physical model of the MTSM sensor: depth of penetration for (a) fundamental and (b) harmonic resonance frequencies

Multi-resonance operation of MTSM sensor enables controlling the interrogating depth into the biological processes. Therefore it can provide more complete characterization

of the biological interfacial processes. For example, it was suggested that cell adhesion on extra cellular matrix could be modeled as a multi-layered structure (fig.2-2a) (Li et al., 2007). Therefore it was hypothesized that MTSM sensor will enable us to get information about mechanical and structural properties of the biological processes from different depths (slicing the medium) (fig. 2-2b and 2-2c).

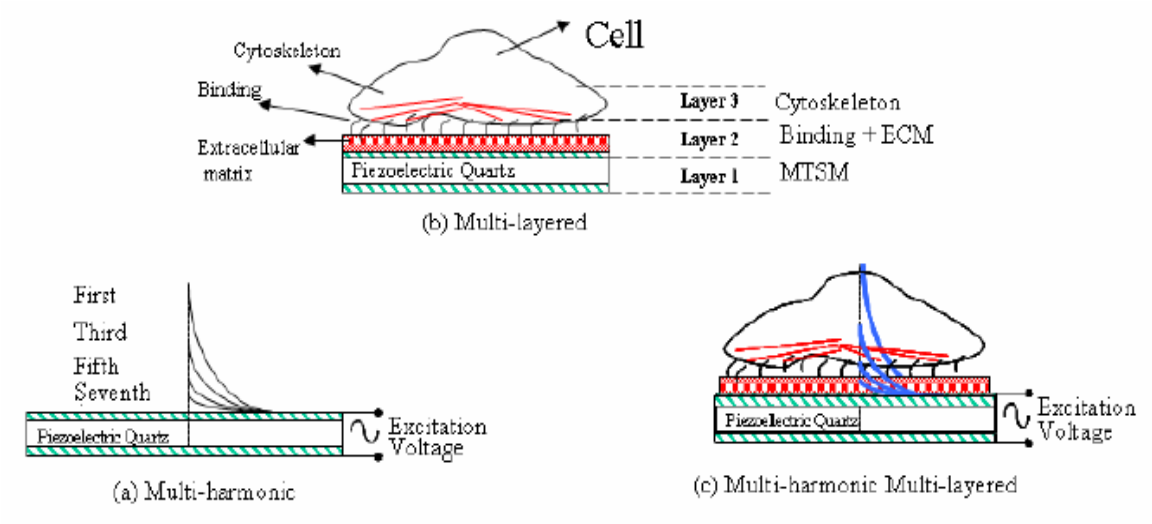

Figure 2-2 (a) Multi-layered biological process (b) Multi-harmonic operation of MTSM (c) Application of multi-harmonic operation of MTSM

2.2 Previous works with MTSM sensor for quantification of multi-layer biological interfaces

Thickness shear mode (TSM) sensors have been used in a variety of studies including interfacial biological processes, cells, tissue and properties of various proteins and their reaction (Cote et al., 2003). Phenomena such as superhydrophobicity (Kwoun et al, 2006, Roach et al., 2007), and adhesion in organic and biological films have been investigated using TSM sensors (Fredriksson et al., 1998). The rheological and interfacial properties of nucleic acid films were studied by using TSM sensors (Su and Thompson, 1996). The

number of motile sperm in a semen sample was assessed in real-time by using a flow-chamber integrated with a quartz crystal microbalance (Newton et al, 2007).

The TSM sensor response is affected by the complex nature of the interface. TSM sensor response is influenced by the geometrical and material properties of the interacting surfaces such as surface roughness (Cho et al., 2007), hydrophobicity (Ayad and Torad, 2009), interfacial slippage (Zhuang et al., 2008), coverage area (Johanssmann et al., 2008) , sensitivity profile of TSM sensor (Edvardsson et al., 2005) and penetration depth of acoustic wave (Kunze et al., 2006).

Various theoretical models have been developed for quantitative characterization of TSM sensor response to interfacial interactions. Nunalee et al (2006) developed a model to predict of the TSM sensor response to a generalized viscoelastic material spreading at the TSM sensor surface in a liquid medium. Cho et al (2007) created a model system to study the viscoelastic properties of two distinct layers, a layer of soft vesicles and a rigid bilayer. Urbakh and Daikhin (2007) developed a model to characterize the effect of surface morphology of non-uniform surface films on TSM sensor response in contact with liquid. Hovgaard et al (2007) have modeled TSM sensor data using an extension to Kevin-Voigt viscoelastic model for studying glucagon fibrillation at the solid-liquid interface. Kanazawa and Cho (2009) discussed the measurement methodologies and analytical models for characterizing macromolecular assembly dynamics.

The physical description based on a wave propagation concept in a one-dimensional approximation has been proven as the best model of thickness shear mode (TSM) sensors. The fundamentals have been published in several books (Rosenbaum, 1998). Martin et al. have (1994) applied this background to sensors by using Mason's equivalent circuit to describe the quartz crystal resonator itself and transmission lines as well as lumped elements for viscoelastic coatings, semi-infinite liquids etc. Follow-up papers have introduced a more

straightforward definition of the elements of the BvD-model (Behling et al, 1998) as well as several additional approximations, e.g. based on perturbation theory, to derive less complex equations, have suggested a simplified notation to separate the mass from so-called nongravimetric effects, or have applied the transmission line model to several subsystems (Voinova et al, 2002) for demonstration of specific situations. More recent papers deal with deviations from the one-dimensional approximations, e.g. by introducing generalized parameters by deriving specific solutions e.g. for surface roughness or with discontinuity at boundaries.

TSM sensors combined with the theoretical models mentioned above were used to determine the properties of liquids (Lin et al., 1993), high protein concentration solutions (Saluja et al., 2005), and thin polymer films (Katz et al., 1996).

For viscoelastic layers, their mechanical impedance depends upon the density, thickness, and complex shear modulus of the loading. Identification of all system parameters from the impedance measurements has been very challenging and uncertain without a priori knowledge of the thicknesses and/or some of the material properties (Lucklum et al. 1997).

Furthermore, extensive study on characterizing the biological interfacial process has been done by us in Biosensor Research Laboratory in Drexel University. Kwoun (2006) showed the beneficial features of multi-resonance operation of MTSM sensor to study the formation of biological samples, specifically collagen and albumin, on the sensor surface. In this work, it was demonstrated that each harmonic frequency clearly showed different characteristics of mechanical properties, especially shear modulus, of the biological sample. Although this work was one of the first studies to demonstrate the strengths of the MTSM measurement technique, it was limited to be semi-quantitative method. Exact values of mechanical properties of anisotropic collagen and albumin samples were not able to be defined due to complexity of the non-linear simultaneous equations of the model. An

improved MTSM technique combined with an advanced data analysis technique was proposed as a future work in Kwoun's study.

As a continuity of Kwoun's work, a new approach merging the multi-harmonic thickness shear mode (MTSM) measurement technique and genetic algorithm-based data analysis technique has been used. This novel method was utilized to solve two unmet needs:

1. Identification of all four parameters by using the MTSM sensor's single harmonic response results in an under-determined problem. The MTSM sensor response contributes to identify two parameters by providing imaginary and real components of the mechanical impedance. In other words, there are fewer equations than material/geometrical parameters of the interface, so the stochastic method is the only approach that can address this problem mathematically. In this project, a combination of the MTSM measurement technique and the genetic algorithm-based data analysis technique (called as MTSM/GA technique) was used to solve this under-determined problem. *We report, to our best knowledge, for the first time, a novel approach that enables determining all four parameters, which define the response of the MTSM technique.*

2. Most biological interfaces constitute multi-layer structures. Multi-layer modeling of biological interfacial processes was proposed by several researchers and by us (Wegener et al., 1999, Ergezen et al., 2007, Kwoun et al., 2006). In contrast, there has been very limited (Lucklum et al., 2001) theoretical study and no experimental studies based on the MTSM sensor for quantitative characterization of multi-layer biological processes. *We report, to our best knowledge, for the first time, the most comprehensive theoretical and experimental study for quantitative characterization of multi-layer biological interfacial processes.*

2.3 Structure of the MTSM/genetic algorithm (GA) technique

The general structure of the MTSM/GA technique is given in 2-3. As seen in fig. 2-3, the MTSM/GA technique utilizes two complimentary techniques, which are the MTSM measurement technique and the genetic algorithm-based data analysis method.

The MTSM measurement technique can be divided in three main components. The first component is the MTSM sensor. The MTSM sensor is an interfacial sensor, which is sensitive to the biological, chemical and structural changes at the biological interfacial processes (Kwoun, 2006, Ergezen et al., 2007, Lin et al., 1993). Therefore the MTSM sensor response can be related to the changes occurring at the interface.

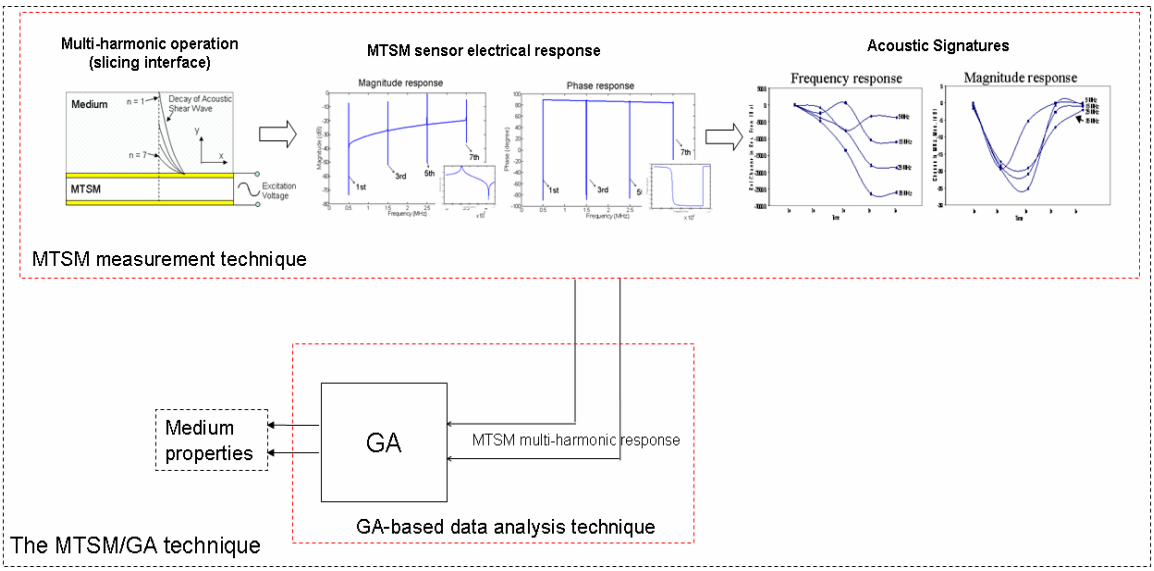

Figure 2-3 The general structure of the MTSM/GA technique combining the MTSM measurement technique and the GA-based data analysis technique

Second important component of the MTSM measurement technique is the multi-harmonic operation of the MTSM sensor. The MTSM sensor operates at different harmonic frequencies from a single sensor, thereby interrogating at different depths into the biological interface. This phenomenon can be called virtually “slicing” the interface, thus providing

information from the different layers of the biological interface. Based on this hypothesis, “acoustic signatures” concept has been introduced and it was shown theoretically and experimentally that that the acoustic signature of each harmonic response can be different, thus providing a strong tool for comprehensive understanding of the biological interfacial process (Sorial, 2000, Kwoun, 2006, Ergezen et al., 2006).

Third component of the MTSM measurement technique is that it is able to monitor the biological interfacial processes in real time. This component is especially important, since the time evolution of the mechanical and structural changes at the interface can be identified. This increases the confidence in the MTSM/GA technique results (detailed discussion can be found in chapter 6).

The acoustic signature of the MTSM measurement technique is used as the input to the genetic algorithm (GA) data analysis technique. In this project, the GA was utilized to solve the under-determine problems (discussed in detail in chapter 5 and 7).

General structure of the GA component of the MTSM/GA technique is discussed in the following section.

2.4 Structure of the MTSM/GA measurement system

General structure of the MTSM/GA measurement technique is presented in fig. 2-4. The electrical excitation of the MTSM sensor generates an acoustic shear wave which propagates in the medium over a short distance (nm – μm). The mechanical and structural changes occurring at the biological interface cause the MTSM sensor response to change by time. The changes in the MTSM sensor’s acoustic response, specifically S21 and phase responses, are monitored by using network analyzer based measurement system. The MTSM sensor responses at 5 MHz, 15 MHz, 25 MHz and 35 MHz are monitored in real-time and the

data is saved in a personal computer. A genetic algorithm-based data analysis technique programmed in MatLab is then utilized to determine four parameters which define the MTSM sensor response.

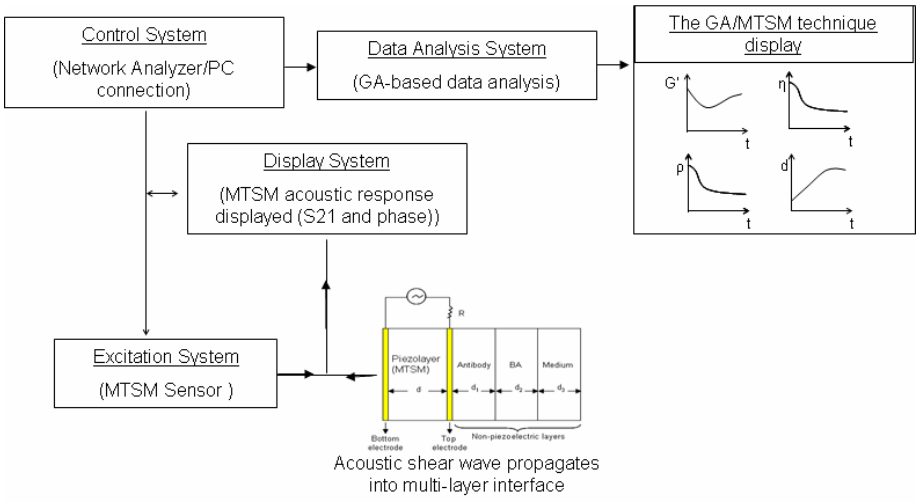

Figure 2-4 General structure of the MTSM/GA measurement system

In the next two sub-sections, the genetic algorithms, which is the last component of the MTSM/GA technique, will be introduced and the general structure of a genetic algorithm will be discussed.

2.5 Overview of genetic algorithm technique

Complex models are ubiquitous in many applications in the fields of engineering and science. Their solution often requires a global search approach. Therefore the objective of optimization techniques is to find the globally best solution of models, in the possible presence of multiple local optima. Conventional optimization and search techniques include; (1) gradient-based local optimization method, (2) random search, (3) stochastic hill climbing, (4) simulated annealing, (5) symbolic artificial intelligence and (6) genetic algorithms. The

detailed information on each technique and comparisons to genetic algorithms (GA) are already explained by Depa and Sivanandam (2008).

As discussed by Depa and Sivanandam, some of the advantages of GA over other techniques are: (1) good for multi-mode problems, (2) they are resistant to becoming trapped in local optima, (3) they perform very well for large-scale optimization problems, (4) they handle large, poorly understood search spaces easily. These advantages match very well with the requirements for an optimization technique to be applied in this project. Therefore GA was chosen as an optimization technique and successfully combined with the MTSM technique.

Genetic algorithms (GA) are a type of evolutionary computation that takes full advantage of the power of evolution. They were first analyzed and proposed by Holland in 1975. Genetic algorithms have been applied in a vast number of areas such as design, simulation and classification.

Genetic algorithms have been used to design digital filters with a determined frequency and phase response (Lee et al., 1998). Also it has been applied in artificial neural networks for designing network topologies, the study of the arrangement of the network's elements (Kim and Gen, 1999). The application of evolutionary computation in simulation helps to predict how the modeled system is going to behave. Classification using evolutionary computation has been used in many different areas such as gaming modeling the prisoner's dilemma (Back et al., 1997). In economics, an evolutionary algorithm has found rules that reflect the way in which a consumer choose one brand over another (Balakrishan and Jacob, 1996). And in biology, evolutionary algorithms helped determining the protein secondary structure (Unger and Moult, 1993), molecular modeling (Krebs, 1995) and kinetic analysis of binding (Liu et al., 2003).

2.5.1 General structure of a genetic algorithm

Genetic algorithm (GA) is based on the genetic processes of biological organisms (fig. 2.5). GA works with a population of individuals, each representing a possible solution to a given problem. Each individual is assigned a fitness score according to how good a solution to the problem it is. The highly-fit individuals are given opportunities to reproduce, by cross breeding with other individuals in the population. This produces new individuals as offspring, which share some features taken from each parent.

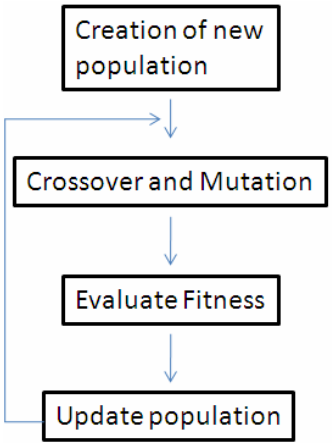

Figure 2-5 Flow chart of genetic algorithm

A genetic algorithm can be presented by its pseudo code. The pseudo code of a GA is always the same what changes is the selection method and the fitness. The pseudo code of a genetic algorithm is as follows:

```
Begin
    Generation = 0;
    Initialize Population;
    Evaluate Population Fitness;
    while termination condition not satisfied do;
        Generation = Generation +1;
        Select Individuals for reproduction;
        Generate the new population (Mutations and Crossovers);
```

```
            Evaluate New Population Fitness;
        end;
    end;
```

Genetic algorithm initializes a population within the search space defined by the user. Each individual in the population is then evaluated by using fitness function. If there is no individual that satisfies the termination criteria then GA applies mutations and crossovers to the current population to obtain a better fit population. This loop continues until the termination criteria are satisfied. This criteria can be the maximum number of the generations (such as 500, 1000 etc) and/or the minimum error to be achieved (such as 0.001% error).

Genetic algorithms have several important functions. These functions are utilized to improve the performance of GAs. Mutation, crossover and elitisms are some of the main functions integrated into GAs. Mutation is used to create variations in the population. In crossover function, given two high fitness individuals what is intended is to create a new individual that combines the best features from each of them. An elitist strategy assures that the best individual of a generation survives to the next generation. The more detailed information regarding the genetic algorithms and its functions are given in Appendix 1.

3 OBJECTIVES

Overall goal of this work is to develop a shear wave-based acoustic method for the quantitative characterization of multi-layer biological interfacial processes (BIPs). This technique will utilize multi-resonance thickness shear mode (MTSM) sensor technology, which is extremely sensitive to BIPs. Multi-layered and multi-resonance theoretical model of the biological process - sensor interactions was utilized to measure the critical aspects of BIPs in order to correlate sensor measurements with the experimental studies. In addition a genetic algorithm-based data analysis method was developed to extract mechanical and structural properties of biological interfacial processes. These goals have been achieved through 4 specific aims.

Specific Aim 1: To apply a multi-resonance and multi-layered transmission line model capable to analyze the sensor response.

In this specific aim, a multi-layer and multi-harmonic transmission line model for analyzing and predicting the MTSM sensor to variety of biological processes has been implemented. It was validated experimentally and theoretically for Newtonian liquid media.

Milestones:

- Development of multi-layer and multi-harmonic transmission line model of MTSM sensor.
- Experimental and theoretical validation of developed model with Newtonian media.

Specific Aim 2: To develop and validate the genetic algorithm (GA)/MTSM technique for quantitative characterization of single layer viscoelastic systems.

A genetic algorithm based data extraction technique has been developed to estimate mechanical (viscosity, density and elasticity) and geometrical (thickness) properties of

biological processes. The developed algorithm has been tested theoretically and experimentally for single layer viscoelastic systems

Milestones:

- Development of a technique based on genetic algorithm to estimate the mechanical and geometrical properties of single-layer viscoelastic systems.
- Experimental and theoretical testing of developed technique by using single viscoelastic layers with known properties.

Specific Aim 3: To develop and validate the MTSM/GA technique for quantitative characterization of two-layer viscoelastic systems.

A data extraction technique has been developed to estimate mechanical (viscosity and elasticity) of biological processes. The developed algorithm has been tested theoretically and experimentally for two-layer viscoelastic systems

Milestones:

- Development of a technique based on genetic algorithm to estimate the mechanical properties of two-layer viscoelastic systems.
- Experimental and theoretical testing of developed technique by using two-layer viscoelastic systems with known properties.

Specific Aim 4: To apply the developed model and the MTSM/GA technique to the experimental case studies

Genetic algorithm combined with multi-layer and multi-harmonic transmission line model of MTSM has been applied to biological interfacial processes with unknown properties

- Determination mechanical and geometrical properties of antibody layer adsorbed on the MTSM sensor

- Determination mechanical and geometrical properties of cell monolayer adsorbed on the MTSM sensor

4 THEORETICAL ANALYSIS OF THE MTSM TECHNIQUE

Acoustic sensing mechanisms formally are caused by a perturbation of mechanical boundary conditions at the surface. The theory and modeling of acoustic waves is well established and involves the simultaneous solution of the Maxwell equations and Newton equations with the appropriate boundary conditions. The measurand and the acoustic wave motion are coupled through the constitutive equations and the boundary conditions, and the measurand is expressed with the parameters of the acoustic wave motion such as the velocity, absorption or acoustic mode profile which implicitly include the acoustic/mechanical parameters of biological media such as density, viscosity and elasticity. In addition most of the biological interfaces have multiple layers and each layer shows different properties. Therefore the interactions between a biological interface and the MTSM sensor will be modeled as a layered structure.

The approach used in this project to model multiple biolayers on a MTSM sensor is based on Mason's transmission line model (Rosenbaum, 1998). This model is a one-dimensional model that describes an acoustic structure in terms of equivalent electrical parameters. Force and particle velocity in acoustical domain are equivalent to voltage and current in electrical domain. Therefore the relationship between force and particle velocity will be determined for a non-piezoelectric layer (biological layers) and a piezoelectric layer (MTSM sensor) by solving constitutive equations with proper boundary conditions. The detailed analysis of the transmission line model is presented in Appendix 3. In the following sections, a summary of theoretical development of transmission line model (TLM) will be presented and it will be correlated with relevant biological interfacial processes.

4.1 Modeling of a MTSM sensor with a viscoelastic load

Most of the biological systems consist of multiple layers and typically each layer exhibits different properties. Therefore the interactions between biological layers and the MTSM sensor could be modeled as a layered structure shown in fig.4-1.

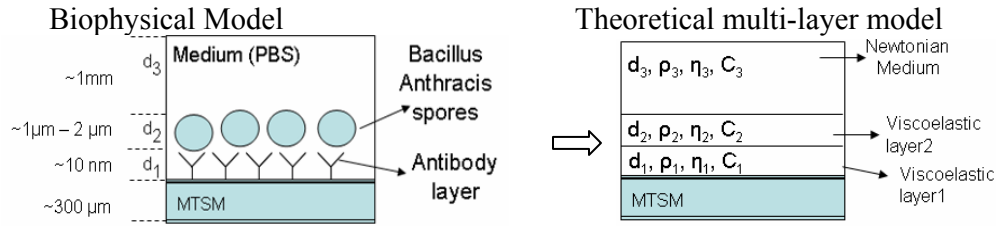

Figure 4-1 Multi-layer biological process. (Example: Bacillus anthracis (BA) spores-antibody interactions). Figure is not to scale.

As seen in fig. 4-1, the biological process consists of a piezoelectric layer (MTSM sensor) and multiple non-piezoelectric biological layers (antibody, binding, BA spores and medium). This multi-layer structure can be represented as shown in fig. 4-2.

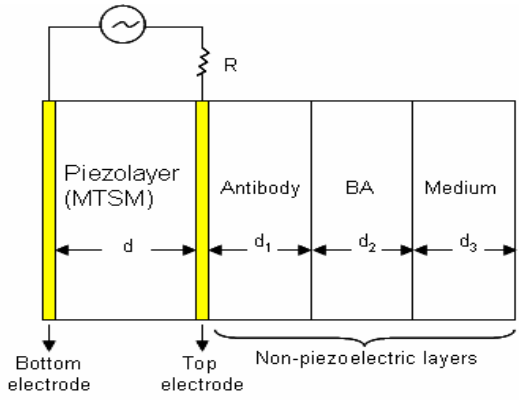

Figure 4-2 Multi-layer biological acoustic structure consisting of piezoelectric and non-piezoelectric layers

In the next two sections, modeling of non-piezoelectric and piezoelectric layers will be explained. In the last section, these two models will be combined together.

4.1.1 Modeling of a non-piezoelectric layer

Acoustic force – displacement relationship for a non-piezoelectric layer is given by (Rosenbaum, 1998):

$$F = AcS = Ac\frac{\partial u}{\partial z} \tag{4.1}$$

where F is force, c is stiffness constant, A is active sensor area of MTSM, and u is displacement. Next, we consider a finite non-piezoelectric layer bounded by the planes $z = z_1$ and $z = z_2$ as shown in fig. 4-3. There will be an acoustic reflection at the boundaries. Therefore, there are two waves in the layer (one traveling to the left, the other to the right). The particle displacement is then:

$$u = ae^{-jkz} + be^{jkz} \tag{4.2}$$

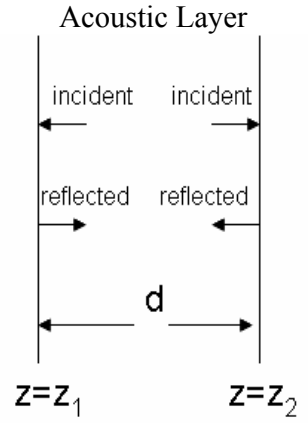

Figure 4-3 Finite thickness non-piezoelectric acoustic medium

The coefficients *a* and *b* depend on the acoustic impedance mismatch at the boundaries. At the left and right boundaries, the particle velocities are given by Eq.4.3 and Eq.4.4;

$$\dot{u}_1 = v_1 = j\omega(ae^{-jkz_1} + be^{jkz_1}) \qquad z = z_1 \tag{4.3}$$

$$\dot{u}_2 = v_2 = j\omega(ae^{-jkz_2} + be^{jkz_2}) \qquad z = z_2 \tag{4.4}$$

if coefficients, *a* and *b*, are found in terms of v_1 and v_2 (the particle velocities) and plugged into the constitutive equation (Eq.4.1), the relationship between force (*F*) and particle velocity on the left and right boundaries can be obtained, which are shown below,

$$F_1 = \frac{Z}{jSin(kd)}(v_1 - v_2) + jZ\tan(\frac{kd}{2})v_1 \tag{4.5}$$

$$F_2 = \frac{Z}{jSin(kd)}(v_1 - v_2) - jZ\tan(\frac{kd}{2})v_1 \tag{4.6}$$

k and *d* are the complex propagation constant and the layer thickness, respectively.

$Z=(\rho G)^{1/2}$ is the characteristic impedance of the layer material, where *G* is the complex shear modulus and ρ is the mass density. The complex propagation constant, k, is defined such that

$$\gamma = jk = j\omega\sqrt{\rho / G}, \tag{4.7}$$

where ω = angular frequency. Finally, these relationships can be presented with a T model of a transmission line shown in fig. 4-4.

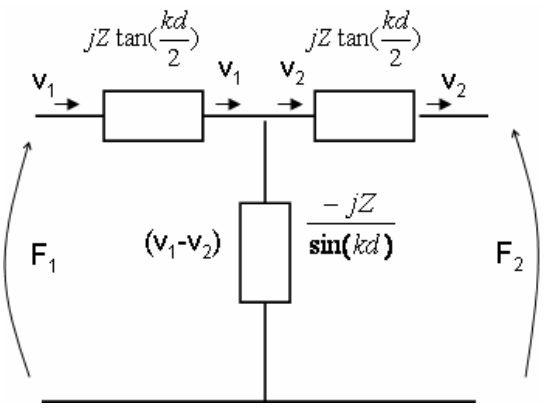

Figure 4-4 Equivalent circuit of a finite thickness acoustic line

The relationship between force and particle displacement can be expressed in matrix form.

$$\begin{bmatrix} F_1 \\ F_2 \end{bmatrix} = \begin{bmatrix} a & b \\ b & a \end{bmatrix} \begin{bmatrix} v_1 \\ v_2 \end{bmatrix} \tag{4.8}$$

where

$$a = \frac{Z}{jSin(kd)} + jZ\tan(\frac{kd}{2}) \qquad b = \frac{Z}{jSin(kd)}$$

4.1.2 Modeling of a piezoelectric layer

For a piezoelectric layer of thickness *d*, there is an extra term relating the coupling between the electrical and acoustic fields (Rosenbaum, 1998);

$$F = c^D SA - \frac{eD}{\varepsilon^S} A \tag{4.9}$$

where c^D is stiffness constant, S is strain, e is piezoelectric stress constant, D is electrical displacement, ε^S, is quartz permittivity. The first term is the mechanical term and the second term is the piezoelectric contribution. We are interested in the current-voltage characteristics, and current is given by;

$$I = j\omega DA \tag{4.10}$$

To find the voltage, we integrate the electric field.

$$E = \frac{D}{\varepsilon^S} - \frac{e}{\varepsilon^S}\frac{\partial u}{\partial z} \tag{4.11}$$

The first term is external E field and the second term is internally generated electric field by the acoustic wave. The voltage is the integration of the electrical field, then it is given by;

$$V = \frac{d}{\varepsilon^S}\frac{I}{j\omega A} + \frac{h}{j\omega}(v_1 - v_2) \tag{4.12}$$

where $h = \frac{e}{\varepsilon^S}$, transmitting constant, and $I = j\omega CoV + hCo(v_1 - v_2)$. $Co = \frac{\varepsilon^S A}{d}$ is the quartz intrinsic capacitance.

The assumption is that there is an incident wave and a reflected wave at each boundary, and the operation leads to an expression similar to the one obtained for non-piezoelectric layer with an additional term representing the electrical component.

$$F_1 = \frac{Z}{jSin(kd)}(v_1 - v_2) + jZ\tan(\frac{kd}{2})v_1 + \frac{h}{j\omega}I \tag{4.13}$$

$$F_2 = \frac{Z}{jSin(kd)}(v_1 - v_2) - jZ\tan(\frac{kd}{2})v_1 + \frac{h}{j\omega}I \tag{4.14}$$

Finally, these relationships can be presented with a T model of a transmission line shown in fig. 4-5.

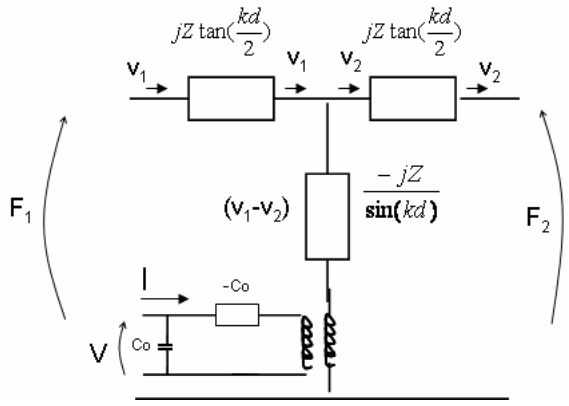

Figure 4-5 Mason model equivalent circuit of a finite thickness piezoelectric layer possesses two mechanical ports and one electrical port

The relationship between force and particle displacement can be expressed in matrix form.

$$\begin{bmatrix} F_1 \\ F_2 \end{bmatrix} = \begin{bmatrix} a_s & b_s \\ b_s & a_s \end{bmatrix} \begin{bmatrix} v_1 \\ v_2 \end{bmatrix} \tag{4.15}$$

where *s* represents sensor;

$$a_s = \frac{Z}{j\sin(kd)} + jZ\tan(\frac{kd}{2}) + \frac{hI}{j\omega} \qquad b_s = \frac{Z}{j\sin(kd)}$$

4.1.3 Combination of piezoelectric and non-piezoelectric layers

As shown in section 4.1.2 and 4.1.3, each non-piezoelectric and piezoelectric layer can be represented as a transmission line model (fig. 4-6). Also it was shown that each layer can be represented as 2x2 matrix.

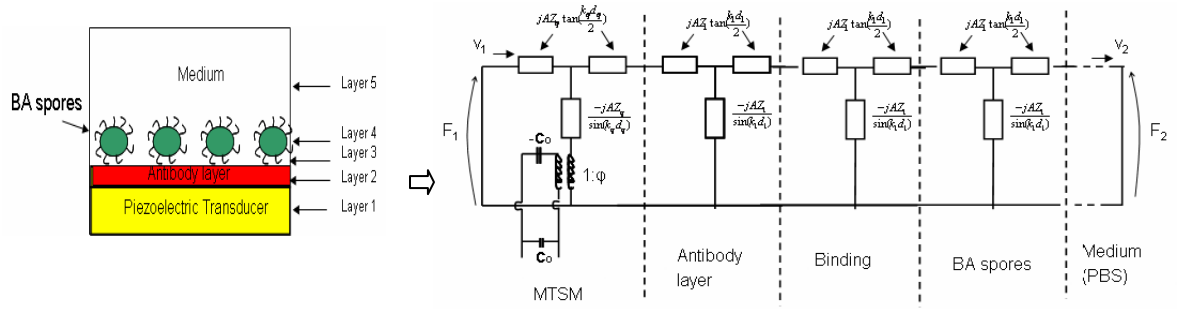

Figure 4-6 Representation of multi-layer biological process in transmission line model

Each additional layer can be added cascading another 2x2 matrix for each additional biolayer. Then the model shown in figure 4.6 can be represented in a matrix form combining a piezoelectric layer (sensor) and non-piezoelectric layers (antibody, binding, BA spores and medium).

$$\begin{bmatrix} F_1 \\ F_2 \end{bmatrix} = \underbrace{\begin{bmatrix} a_s & b_s \\ b_s & a_s \end{bmatrix}}_{\text{MTSM}} \underbrace{\begin{bmatrix} a_a & b_a \\ b_a & a_a \end{bmatrix}}_{\text{Antibody}} \underbrace{\begin{bmatrix} a_b & b_b \\ b_b & a_b \end{bmatrix}}_{\text{Binding}} \underbrace{\begin{bmatrix} a_{ba} & b_{ba} \\ b_{ba} & a_{ba} \end{bmatrix}}_{\text{BA spores}} \underbrace{\begin{bmatrix} a_m & b_m \\ b_m & a_m \end{bmatrix}}_{\text{medium}} \begin{bmatrix} v_1 \\ v_2 \end{bmatrix} \quad (4.16)$$

4.2 Definition of parameters characterizing MTSM sensor response

The MTSM sensor is a piezoelectric-based sensor which has the property that an applied alternating voltage (AC) induces mechanical shear strain and vice versa. By exciting the sensor with AC voltage, standing acoustic waves are produced within the sensor, and the sensor behaves as a resonator. The electrical response of the MTSM sensor in air over a wide frequency range is shown in fig. 4.7, where S21 is the magnitude response of the MTSM sensor. As an example, the response of MTSM sensor is presented at the first (5 MHz), third (15 MHz), fifth (25 MHz) and seventh (35 MHz) harmonics in air.

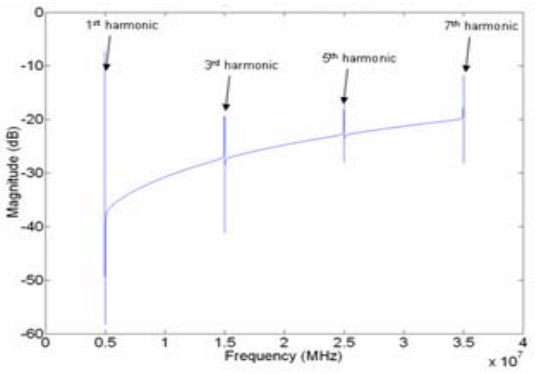

Figure 4-7 A typical magnitude vs. frequency response characteristic and the associated resonance harmonics for the MTSM sensor, spanning a wide frequency range (5 MHz to 35 MHz)

The magnitude and phase responses of the MTSM sensor in the vicinity of the fundamental resonance frequency are given below (fig. 4-8). When the MTSM sensor is loaded with a biological media, there will be a shift in S21 and phase responses of the MTSM sensor. These changes can be correlated with changes in the mechanical and geometrical properties of the medium such as thickness, viscosity, density and stiffness.

Several tracking points have been identified on S21 and phase responses of the MTSM sensor. These points are identified to be; α_R = maximum magnitude, f_R = resonance

frequency, α_{AR} = minimum magnitude, f_{AR} = anti-resonance frequency, P_R = phase at maximum magnitude, f_M = frequency at minimum phase, P_M = minimum phase.

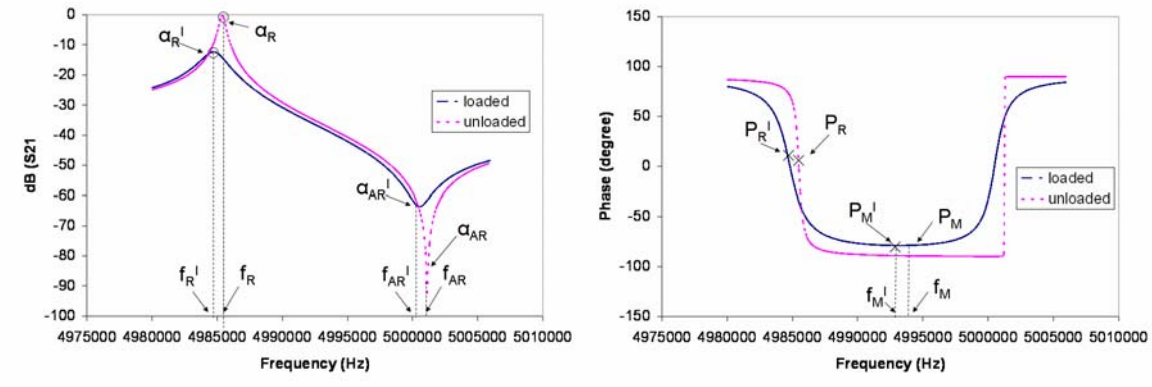

(a) (b)

Figure 4-8 Magnitude (a) and phase (b) response of MTSM sensor in the vicinity of fundamental frequency (shown at 5 MHz). α_R = maximum magnitude in air, f_R = resonance frequency in air, α_R^I = maximum magnitude when loaded, f_R^I = resonance frequency in when loaded, α_{AR} = minimum magnitude in air, f_{AR} = anti-resonance frequency in air, α_{AR}^I = minimum magnitude when loaded, f_{AR}^I = anti-resonance frequency when loaded, P_R = phase at maximum magnitude in air, P_R^I = phase at maximum magnitude when loaded, P_M^I = minimum phase when loaded, P_{AR} = phase at maximum magnitude in air, P_{AR}^I = phase at maximum magnitude when loaded

4.3 Validation of the MTSM theoretical approach: simulation and experiment of a MTSM loaded with Newtonian liquids

The response of a MTSM sensor loaded with Newtonian liquids has been analyzed. The magnitude at the resonance frequency of each harmonic and the relative changes in the resonance frequency shift at each harmonic when the MTSM sensor is loaded with a layer of Newtonian liquid on one side of the sensor were monitored. The errors between experimental and theoretical results are presented in figure 4-9. 200 µl of distilled water (DI water) and glycerin/DI water concentrations (10% and 20%) are placed on one side of the sensor and S21 and phase responses of the MTSM sensor was monitored.

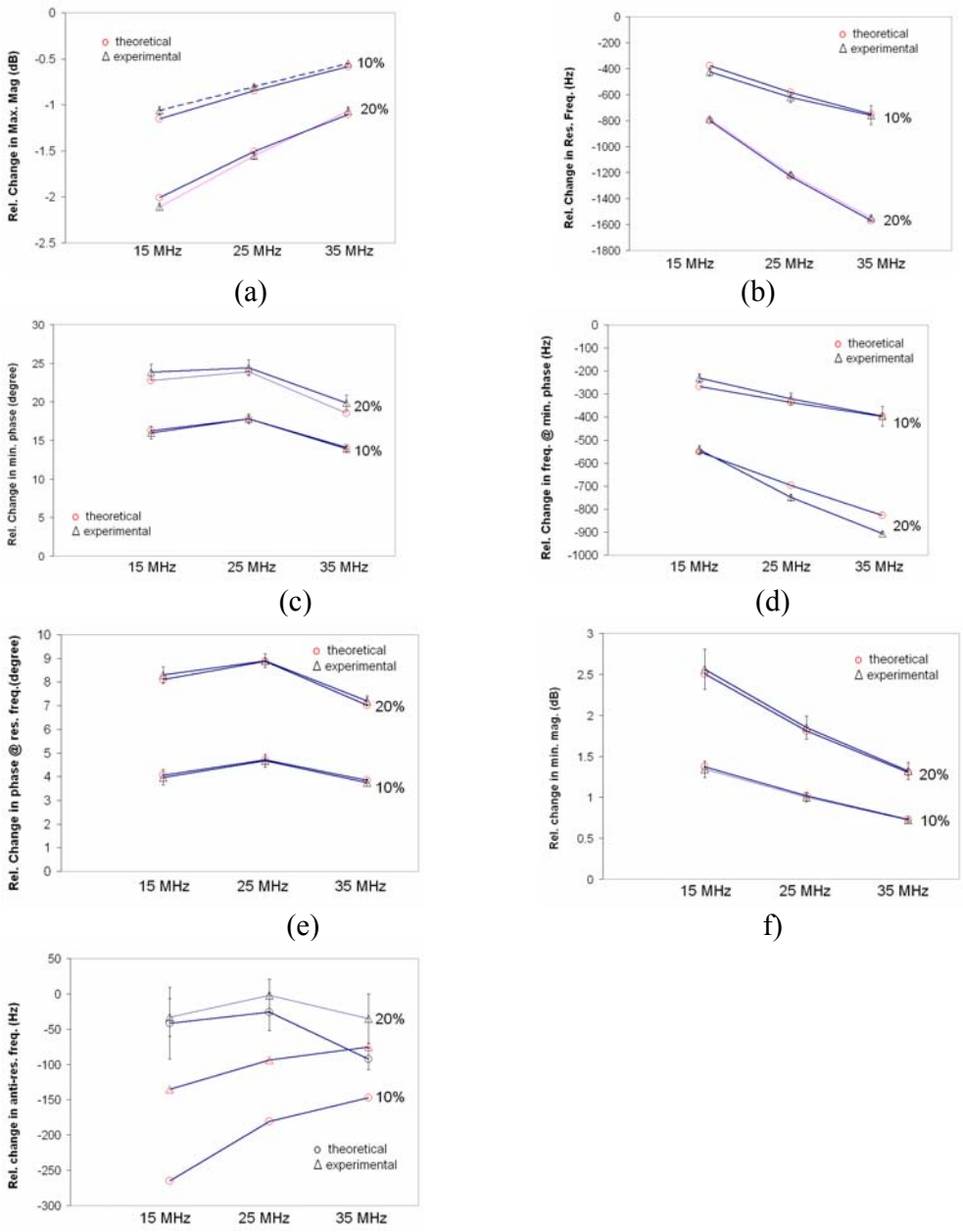

Figure 4-9 Change in (a) resonance frequency, (b) maximum magnitude, (c) minimum phase (d) frequency at minimum phase, (e) phase at resonance frequency, (f) minimum magnitude and (g) anti-resonance frequency under the loading of DI water, 10% glycerin and 20% glycerin/DI water solutions.

The experimental results at 5 MHz exhibited high fluctuations. Similar fluctuations and high error have been observed by other researchers and in our previous works (Hong et

al., 2006, Li et al., 2004). It has been shown that this phenomenon may stem from the interference of compressional wave (Martin and Hager, 1989) and the insufficient energy trappings in liquid loadings. This disagreement may also be caused by the non-plane wave feature of the acoustic wave at 5 MHz. The MTSM sensor response at 5 MHz has been used in this work when a stable response was obtained.

It was observed that experimental errors changing between 1% to 11% in tracking points at 15, 25 and 35 MHz. It has been shown that these errors between the theoretical and experimental results may stem from several reasons such as repeated use (Dewar et al., 2006), roughness of the surface (Cho et al., 2007, Macakova et al., 2007), the different mechanical properties of the water layer at the interface (Sendner et al., 2009), and slip conditions (Zhuang et al., 2008). The classical interpretation of the discrepancy is trapped mass in conjunction with surface roughness; the procedure of optical polishing as well as thermal evaporation of electrodes results in rough surfaces (Martin et al., 1995). Liquid material located in the cavities moves rigidly with the crystal surface. Surface roughness of the MTSM sensor has been measured by using atomic force microscopy (AFM) (data not shown). The roughness has been measured as 2 nm.

This roughness level is considered as atomically smooth surface and it has been shown that it will not contribute to the experimental error. There is a class of experiments where the slip of monolayers of simple liquids has been investigated (Du et al., 2004). It has been shown that the slippage in both Newtonian and liquid and amorphous solid limits is known to decouple the media from the substrate and thereby reduce both the frequency shift and damping (McHale et al., 2000). The discrepancies between experimental result and simulation are also caused by the well-ordered water molecules on the surface of gold electrodes of MTSM sensor. The mechanical properties, such as density and viscosity, of the well-ordered molecules of liquid are higher than those of bulk values (Goertz et al., 2007).

It was also observed that theoretical and experimental results do not match for the change in the anti-resonance frequency. This may stem from the fact that the parasitic capacitance of the MTSM sensor and the interference from the sensor holder interfere with the electrical response. The parasitic capacitance of the MTSM sensor dominates the sensor response away from the resonance frequency (Bandey et al., 1999).

4.4 Summary and Conclusions

The transmission line modeling (TLM) of a MTSM sensor has been studied. The model has been validated with Newtonian mediums such as deionized water and glycerin/deionized water solutions. It has been shown that the TLM can predict the MTSM sensor's experimental results with less than 11% error. Surface roughness, interfacial water layer and slip at the interface are discussed as some of the roots of this error.

Transmission line model (TLM) effectively enables multilayer modeling of the biological interfacial processes. It can be utilized to relate the changes in the resonance frequency and motional impedance to physical properties of layered structures, including material parameters and geometrical features. Combination of multi-layered modeling of the biological interface and multi-harmonic operation of the MTSM sensor provides acoustic signatures of interfacial processes, which carries in-depth information regarding the mechanical (density, elasticity and viscosity) and structural properties of biological layers at various depths and boundaries at the interface.

In the following chapters, theoretical and experimental foundation of the MTSM/GA technique, which utilizes the multi-layer modeling of sensor-interface interactions and multi-harmonic operation of the MTSM sensor, will be discussed.

.

5 THEORETICAL FOUNDATION OF THE MTSM/GA TECHNIQUE FOR SINGLE LAYER VISCOELASTIC SYSTEMS

5.1 Problem Definition

1. Physical model of a viscoelastic biological thin material loaded on the MTSM sensor surface is shown in fig 5-1. The MTSM measurement technique provides the information on the mechanical and geometrical properties of the biological material.

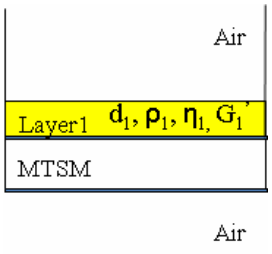

Figure 5-1 Single-layer biological viscoelastic layer loaded on the MTSM sensor

2. The mechanical impedance (Z_s) seen at the MTSM sensor interface is derived from transmission line theory and is given in eq. 5.1 (Granstaff and Martin, 1994);

$$Z_s = jZ_1 \tan(\omega\sqrt{\frac{\rho_1}{G_1}}d_1) \tag{5.1}$$

where Z_1 is the characteristic impedance of the viscoelastic coating, given by $(\rho_1 G_1)^{1/2}$ and G_1 is complex shear modulus of the viscoelastic layer and given by $G_1 = G_1' + jG_1''$; G_1' and G_1'' are storage and loss modulus respectively. As seen from eq. 5.1, surface mechanical impedance is related to density (ρ_1) and thickness (d_1) of the viscoelastic layer, and complex shear modulus (G_1). Thus the surface acoustic impedance can be defined by four independent variables.

3. The MTSM sensor response contributes two parameters by providing real and imaginary part of mechanical impedance. To understand this contribution, the modified Butterworth-Van dyke equivalent circuit of a perturbed MTSM sensor has been analyzed in fig. 5.2 (Bandey et al., 1999).

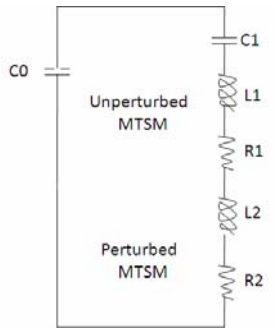

Figure 5-2 Modified Butterworth-Van Dyke equivalent circuit of loaded MTSM sensor

In fig 5.2, an electrical equivalent circuit of a perturbed MTSM sensor is shown. L1, C1 and R1 represent the unloaded MTSM sensor parameters. L2 and R2 represent perturbation caused by the loading on MTSM sensor surface. C_0 represents the intrinsic capacitance of the MTSM sensor. When the MTSM sensor is loaded with a viscoelastic medium, the motional impedance contribution of this surface load is given by the complex electrical load impedance as (Bandey et al., 1999):

$$Z_e = \frac{N\pi}{4K^2\omega C_0}\left(\frac{Z_s}{Z_q}\right) \tag{5.2}$$

where N is harmonic number, K^2 is the square of the quartz electromechanical coupling coefficient, ω is the angular frequency for the unperturbed MTSM sensors, $Z_q=(\rho_q\mu_q)^{0.5}$ is the quartz shear wave characteristics impedance where ρ_q and μ_q are mass density and shear stiffness of the quartz, Z_s is the shear mechanical impedance at the device surface. Z_s is a complex quantity. The electrical impedance element L2 and R2 can be related to the components of the surface mechanical impedance as:

$$R2 = \frac{N\pi}{4K^2\omega C_0}\left(\frac{\mathrm{Re}(Z_s)}{Z_q}\right) \tag{5.3}$$

$$L2 = \frac{N\pi}{4K^2\omega C_0}\left(\frac{\mathrm{Im}(Z_s)}{Z_q}\right) \tag{5.4}$$

Imaginary part of Z_s is related to frequency, f, taken at the in-phase impedance minimum. It is equivalent to resonance of motional arm of the equivalent circuit, not to zero phase crossing of the quartz resonator (Vives and Arnau, 2004);

$$\frac{\Delta f_s}{f_0} = -\frac{\mathrm{Im}(Z_s)}{\pi Z_q} \tag{5.5}$$

where f_0, is resonance frequency of unloaded MTSM and Δf_s is relative change in the resonance frequency when sensor is loaded, and given by $\Delta f_s = f_s - f_o$.

The real part of the acoustic load is related to acoustic energy dissipation;

$$\frac{\Delta R}{2\omega L_q} = -\frac{\mathrm{Re}(Z_s)}{\pi Z_q} \tag{5.6}$$

where f_0 is resonance frequency of MTSM sensor, ω is angular frequency.

4. As seen from eqs. 5.5 and 5.6, the change in equivalent resistance and inductance provides information about the acoustic properties of the viscoelastic medium loaded on the MTSM sensor surface. Therefore the measurement of the change in resonance frequency and losses of the MTSM sensor by time contribute the identification of two out of four variables which define the surface mechanical impedance. Thus monitoring single harmonic response of the MTSM sensor results in an under-determined problem. This problem can be overcome by using two methods:

1. Density of the viscoelastic medium can be separated out by equating its value to the bulk value indicated in the literature. The thickness of the medium can be measured with additional techniques such as profilometer and atomic force microscopy. Then

the under-determined problem can be eliminated. The disadvantage of this method is that it requires an additional technique to identify all four parameters. This technique has been utilized by several researchers (Jiang et al, 2003, Morray et al., 2002).

2. The harmonic operation of the MTSM sensor can be utilized. This mode of operation introduces additional equations to the system. Then the under-determined problem can be turned in to a determined problem. In this case, the dependency of viscoelastic properties on operating frequency of the MTSM sensor will be neglected (Yang et al., 2009).

In this project, a stochastic method based on genetic optimization has been integrated with the MTSM sensor technique to overcome the under-determined problem discussed above. It has been shown that genetic algorithm can be applied to under-determined problems to obtain approximate solutions with satisfactory accuracy. Szabad et. al. (2000) utilized genetic algorithms to locate the best solution in the force planning for co-operating manipulators. Wang and Dhawan (2008) developed an optical image reconstruction method by using genetic algorithm based optimization technique. Reasonable constraints are incorporated into the genetic algorithm to stabilize the solution. Nearchau (1998) applied genetic algorithms, hill-climbing and simulated annealing to overcome the under-determined characteristics of non-linear kinematics equations. Genetic algorithms showed particular ability to search complex, or discontinuous function spaces and showed the best performance among other techniques.

In the following sections, the integration of GA and MTSM sensor technique will be discussed and its implementation to the under-determined problem will be explained. The proposed technique will be called as “MTSM/GA technique”.

5.2 Outline of Chapter 5

This chapter will be structured in the following manner;

1. The general structure of the MTSM/GA technique will be explained. The MTSM/GA technique consists of three main parts (fig. 5-3): a) inputs, b) internal parameters/functions, and c) outputs.

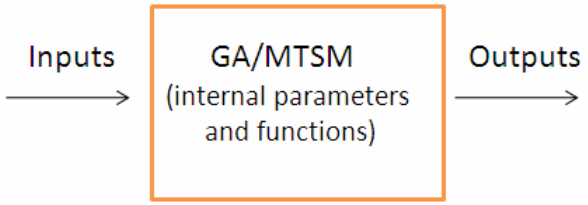

Figure 5-3 The MTSM/GA technique has three main parts: inputs, internal parameters and functions of GA and outputs

2. Next, the MTSM/GA technique will be validated theoretically. The MTSM/GA technique will be applied to determine the properties of hypothetical viscoelastic single-layer systems loaded on the MTSM sensor. The theoretical analysis of the technique will be critically discussed and the limitations and strengths of the method will be identified.
3. Finally, the MTSM/GA technique will be validated experimentally. Experimental validation of the technique will be realized by using single layer polymer systems with known parameters. Two polymer systems; namely, SU8-2002 and collagen type I, will be used for the validation of the MTSM/GA technique.

5.3 Structure of the MTSM/GA technique

Overall structure of the MTSM/GA technique is presented in fig. 5-4. There are two inputs to the MTSM/GA, namely; “range for the variables” and “MTSM sensor response”. GA outputs the “estimated” values of the variables by using GA’s sub-functions such as crossover, mutation and fitness evaluation.

Genetic algorithm is a stochastic optimization technique which searches for the solution in a “search space” (Wood, 2006). The search space is determined by the user and it is strongly dependent on the problem which is under consideration. Thus the method to identify the boundaries (maximum and minimum points) of the search space should be discussed. MTSM sensor’s response will be utilized as “fitness function” in the genetic algorithm. Fitness function will be used to evaluate the “goodness” of each solution. Depending on the fitness score, the GA functions such as mutation and crossover (see section 5.3.2) will be applied to generate better offsprings.

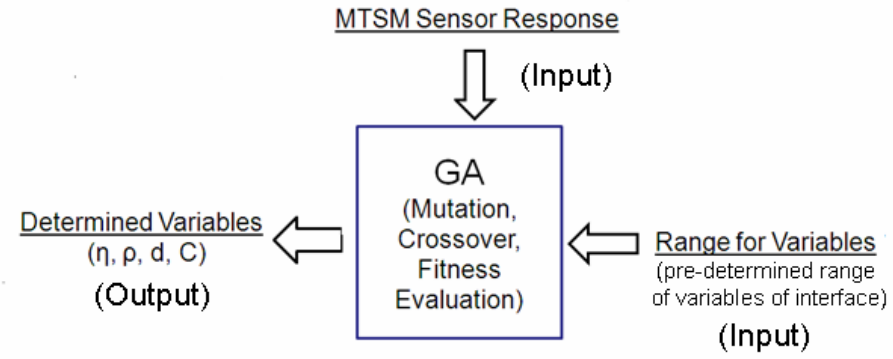

Figure 5-4 Inputs and outputs of the MTSM/GA technique

5.3.1 Inputs to the MTSM/GA technique

There are two inputs to the MTSM/GA technique. These are "range of variables" and the "MTSM sensor response". These two inputs will enable addressing two key questions;

1. Genetic algorithm seeks for a solution in a finite "search space", which is also called a state space. The space of all feasible solutions (the set of the solutions among which the desired solution resides) is called the search space (Sivanandam, 2000). The limits (maximums and minimums) of a search space are determined by the user. Therefore the question of "how to set these limits for search space" should be addressed. In other words, how we will set the "search space" to make sure that it will lead us to a right solution.
2. Genetic algorithm itself generates a theoretical MTSM sensor response by using the transmission line model. Then it compares the theoretical response with the one obtained experimentally by using a "fitness function" (Lee and Han, 2002). The fitness function guides the direction of the GA optimization process (Lee and Han, 2002). So the next question is "how does GA make this comparison?" or in other words, how will we set up the "fitness function" to compare the theoretical and experimental MTSM sensor response for calculating the error (fitness score)?

5.3.1.1 Determination of the ranges for input parameters

The space of all feasible solutions is called the search space. Search space is an important component of the GAs in determining the accurate values for the variables under consideration. For example, the ranges for stiffness value can not be set to be between 10^5 N/m^2 and 10^7 N/m^2 for a Newtonian liquid while it is well known that stiffness value should be zero. In this case the algorithm will not converge to a solution because of inappropriate

choice of maximum and minimum values of the search space for the stiffness parameter. If the range for stiffness value is set between 0 – 10^{10} N/m^2 while the value is expected to be much less than 10^{10} N/m^2 (for example, it could be 10^5 N/m^2), in this case, algorithm will converge to a value that may not be scientifically acceptable as well as computation time will increase dramatically (Wendth et al., 2002). The ranges for these variables depend on the application itself and should be determined by the user.

In this project, it is assumed that there is no prior information regarding the properties of the viscoelastic layers. Therefore the search space will be chosen to cover typical viscoelastic layer properties. As shown by Kwoun (2006) and others (Han and Lindsay, 1999, Martin and Frye, 1991, Lucklum and Hauptman, 2000) viscoelastic materials can be divided into four regimes, namely; liquid like, soft rubber, hard rubber and solid like. As seen from table 5-1, the viscosity values mostly change between 0.001 kg/m.s and 0.1 kg/m.s and stiffness values vary between 0 N/m^2 – 10^9 N/m^2. It was indicared that the density values of a typical polymer changes between 1000 – 1400 kg/m^3.

Table 5-1 phases of a typical viscoelastic system

Phases	**η (kg/m.s)**	**C (N/m^2)**
Liquid like	0.001 – 0.01	0-10^5
Soft Rubber	0.001 – 0.01	10^5 – 10^6
Hard Rubber	0.01 – 0.1	10^6 – 10^7
Solid Like	0.01 - 0.1	10^7 – 10^9

In the following sub-sections and chapters, for all GA simulations, the ranges for four variables are set to cover all these fours phases. The maximum and minimum values for the parameters are shown in table 5-2.

Table 5-2 Minimum and maximum values for stiffness, viscosity, density and thickness parameters

Variable	Minimum	Maximum
Stiffness (N/m^2)	0	10^9
Viscosity (kg/m.s)	10^{-3}	10^{-1}
Density (kg/m^3)	1000	1400
Thickness (nm)	1	10000

5.3.1.2 MTSM sensor response and fitness function

The fitness function must reflect the relevant measures to be optimized. The fitness function plays important role on the performance of the genetic algorithms (Fan and Fox, 2004). This function evaluates the function being searched for the set of parameters of each member of the population. The output of the fitness function is a vector that contains the fitness for each member of the population. This vector helps in the selection of individual for generating new offspring or individuals that will be included in the new generated population.

It has been shown in chapter 4 that transmission line modeling of the MTSM sensor can successfully predict the sensor's experimental response with less than 11% error. The importance of this observation is that the theoretical response obtained by the TLM can be utilized in forming the fitness function. The difference between these two responses will be used in the formation of "fitness function" of the MTSM/GA technique.

There are six different points which can be predicted accurately (with errors changing between 1% to 11%) by using TLM model in chapter 4. In the fitness function, all these points can be used to compare theoretical and experimental responses of the MTSM sensor. In other words, whole S21 curve can be utilized. In that case there will be two main drawbacks. 1. Each point will introduce an error to the system. Therefore total error will increase so thus accuracy of the MTSM/GA may be decreased. 2. The evaluation cost of

fitness function will increase, thus the computation time is highly elevated (Povinelli and Feng, 1999).

In this project, only maximum magnitude and resonance frequency values will be plugged into the fitness function of the MTSM/GA. The other tracking points will be utilized to check the accuracy of the results at the end of the experiments. Once the initial population is created the algorithm randomly generates a population (includes 50 individuals) chosen from the ranges of the variables. Typical population number for the genetic algorithms varies between 20 and 100 (Stathakis and Kanellopoulos, 2008). For the demonstration of the MTSM/GA technique, number of population was initially chosen to be 50. In section 5.4, the MTSM/GA technique was optimized and optimum number of population number was obtained to be used in further simulations. Each individual was then input to fitness function (transmission line model). The error between the model (TLM) and the experimental results were compared by using the following equation:

$$fit\_func = \frac{100}{1 + \sqrt{(\alpha_{\mathrm{Re}} - \alpha_{Rt})^2} + \sqrt{(f_{\mathrm{Re}} - f_{Rt})^2}} \tag{5.7}$$

The denominator of this function represents the difference between the model and the experimental data (we use the plus one in order to avoid the eventual division by zero). In this project, maximum magnitude (α_R) and resonance frequency (f_R) have been compared between the model and the experimental results. Subscript “e” indicates experimental results and subscript “t” stands for theoretical model. This function is monotonically increasing with the fitness of the solution provided by the genetic algorithm. The fitness function is used to minimize the errors in the maximum magnitude and the resonance frequency values. It is a

two-dimensional function, in which two error minimization processes are not inter-related, but they are pursued simultaneously.

5.3.2 Internal functions and outputs of the MTSM/GA technique

In the previous sections, the inputs to the MTSM/GA technique have been discussed. The ranges of the variables and the fitness function have been identified. In this section, the structure of genetic algorithm and its internal functions will be examined.

Tournament selection was implemented (please see Appendix 1 for more detailed information). In order to carry out the crossovers the entire population is divided into groups of 5 individuals each, these groups are randomly selected. From each group the individual with the highest fitness together with another individual of this group are selected for crossover. The two selected individuals are the parents and yield two sons. Both the parents and the sons pass to the next generation. This idea was implemented in order to reduce the selection pressure. The crossover between the parents is a simple one meaning that a random crossover point is selected and two kids' genome are formed with the left and right genes of the crossover point of each parent. A relatively high mutation probability is present in order to avoid local minimum, otherwise all the individuals might end up having the same genome and this genome corresponding to a not optimal solution. Also elitism was implemented to the MTSM/GA technique to transmit the best fit individual to the next generation.

The MTSM/GA will be theoretically optimized to achieve the minimum error. For a better explanation of the MTSM/GA technique, a hypothetical single-layer viscoelastic system loaded on the MTSM sensor has been simulated by using the TLM. Hypothetical values for thickness (d), stiffness (ε), viscosity (η) and density (ρ) of each layer were entered to transmission line model. The magnitude and resonance frequency values of each harmonic

(up to 7th harmonic) were obtained from the model. These values were then entered into the MTSM/GA. Next, output values of the MTSM/GA were compared with the input values of transmission line model (fig. 5.5).

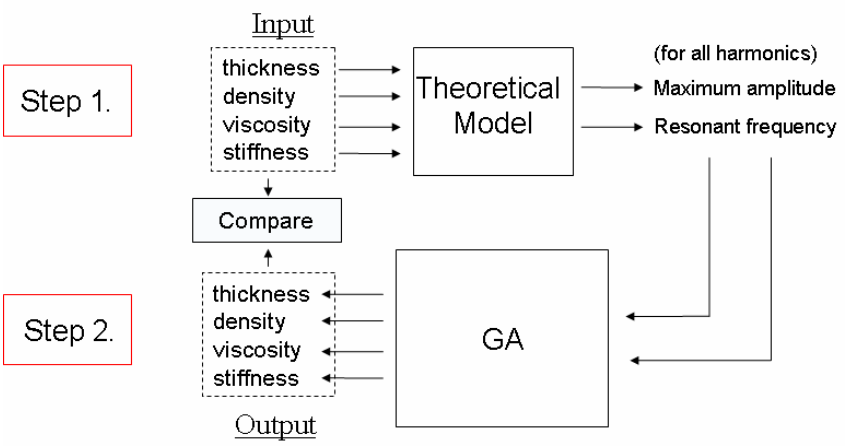

Figure 5-5 Experimental set-up for theoretical testing of the MTSM/GA technique

The typical physical models of the hypothetical viscoelastic layer have been shown in fig. 5-6. Two cases of the model have been investigated; (a) the viscoelastic layer in air, (b) the viscoelastic layer in DI water. The typical biological systems are mostly diluted in buffer solutions to maintain the necessary pH value for biological entities. Most of the buffer solutions have properties similar to DI water. Therefore the MTSM/GA technique will be developed and optimized for these two viscoelastic layer systems. The theoretical and experimental results for the case (a) in fig. 5-6 will be presented in this project. Same methodology and analysis have been done for the case (b).

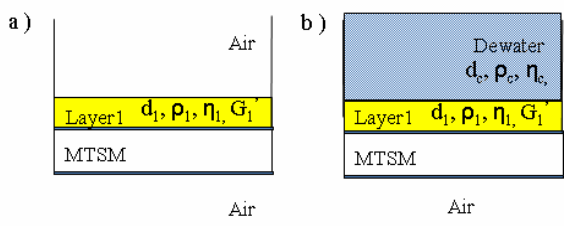

Figure 5-6 The physical model for a viscoelastic layer loaded on MTSM sensor surface. a) viscoelastic layer in air b) viscoelastic layer in deionized water (DI water)

The parameters for the hypothetical layer have been chosen similar to typical polymer layer properties (Kwoun, 2006). The properties of the layer are chosen to be; d_c= 10000 nm, and ρ_c= 1000 kg/m^3 and η_c = 1x10^{-3} kg/m.s, G_1' = 4x10^7 N/m^2, d_1= 1000 nm, and ρ_1= 1200 kg/m^3.

5.3.3 Integration of sub-spacing method to the MTSM/GA technique

As discussed in the section 5.3.1.1, a large search space has been chosen since it was assumed that there was no prior information regarding the properties of the viscoelastic layer which is under consideration. For example, the range for the viscosity is between 0.001 kg/m.s and 0.1 kg/m.s. It is 100 fold increase in the viscosity value. In addition stiffness value was set between 0 N/m^2 to 10^9 N/m^2. This is a relatively large solution space, and there have been many efforts to apply GA technique for the problems with large solution spaces (Liou et al., 2007, Paulinas and Usinskas, 2007, Godefroid and Khurshid, 2002). One frequent search strategy to deal with complex optimization problems has been the exploration of scattered points in the solution space. As there is no information about a global optimum location before solving an optimization problem, algorithms based on such strategy can evenly scan a feasible region of the search space to determine good solutions (points) for better exploration in subsequent iterations (Garai and Chaudhuri, 2007).

In this project, "Sub-spacing" method has been applied. Sub-spacing method basically gives a quick idea of where the solution can be and also decreases algorithm running time dramatically. It divides the whole search space into sub-spaces depending on the convergence status of the population and the solutions obtained so far (Boschetti et al., 2002). This method intended to deal with multi-modal problems which are difficult to be solved by the conventional genetic algorithms (Tsutsui et al., 2000).

In this project, the solution space was divided in 10 sub-spaces. The performance of the MTSM/GA after 500 generations in each sub-space is compared and the best subspace is chosen to be a candidate solution space. 1000 and 2000 generations were also utilized and it was observed that there has been no difference in the MTSM/GA technique's performance. Genetic algorithm was run 5 times in each subspace. Each subspace's convergence performance was evaluated. The sub-spaces with the best fitness scores were considered to be the "candidate" solution spaces. It was observed that the candidate sub-space had a distinct convergence performance compared to the others. This method dramatically increased the efficiency of the MTSM/GA by eliminating the irrelevant solution spaces.

As seen from table 5-3 and 5-4, the whole subspace was divided into 10 sub-spaces which are the combination of viscosity and stiffness values. There were two main reasons of choosing viscosity-stiffness values to form the subspaces. These are;

1. In a typical viscoelastic system, the density (ρ) has the small range of the variation in density between water like liquid and a crystallized polymer sample (Munson et al. 1998).
2. From our previous experiences in the Biosensors Research Laboratory, it was observed that the bandwidth of the solution space for thickness value was smaller than the solution spaces for viscosity and stiffness. This hypothesis has been visualized and proven in the following sections.

Table 5-3 The convergence performance (in percentage) of the MTSM/GA technique in each the sub-space in air

Viscosity (kg/m.s)	**Stiffness (N/m^2)**				
	$0 – 10^5$	**$10^5 – 10^6$**	**$10^6 – 10^7$**	**$10^7 – 10^8$**	**$10^8 – 10^9$**
$10^{-3} – 10^{-2}$	0.04±0.01	0.40±0.03	20.77±8.31	90.55±8.25	47.27±2.32
$10^{-2} – 10^{-1}$	0.07±0.02	0.08±0.01	2.93±0.20	97.60±3.65	71.13±19

Table 5-4 The convergence performance (in percentage) of the MTSM/GA technique in each the sub-space in DI water

Viscosity (kg/m.s)	**Stiffness (N/m^2)**				
	$0 – 10^5$	**$10^5 – 10^6$**	**$10^6 – 10^7$**	**$10^7 – 10^8$**	**$10^8 – 10^9$**
$10^{-3} – 10^{-2}$	0.08±0.001	0.18±0.001	1.70±0.04	61.00±21.00	16.65±0.01
$10^{-2} – 10^{-1}$	0.18±0.003	0.18±0.001	1.48±0.04	56.28±41.87	16.68±0.006

As seen from table 5.3 and 5.4, there are two sub-spaces in which the MTSM/GA technique shows distinctly better performances compared to others. This is an expected occurrence because the initially chosen solution space is very large. It covers all possible four viscoelastic regimes. In this example, the first search space reflects more like a “soft rubber” system. The second one represents more “hard rubber” like system. In the following sections, this phenomenon will be discussed in detail and limitations of the MTSM/GA technique will be explained.

After identifying the possible solution spaces, the GA was run 100 times in these candidate sub-spaces. Sample size of 100 provides 95 % of confidence level and 10% of confidence interval. The results of GA runs have been shown in fig. 5-7.

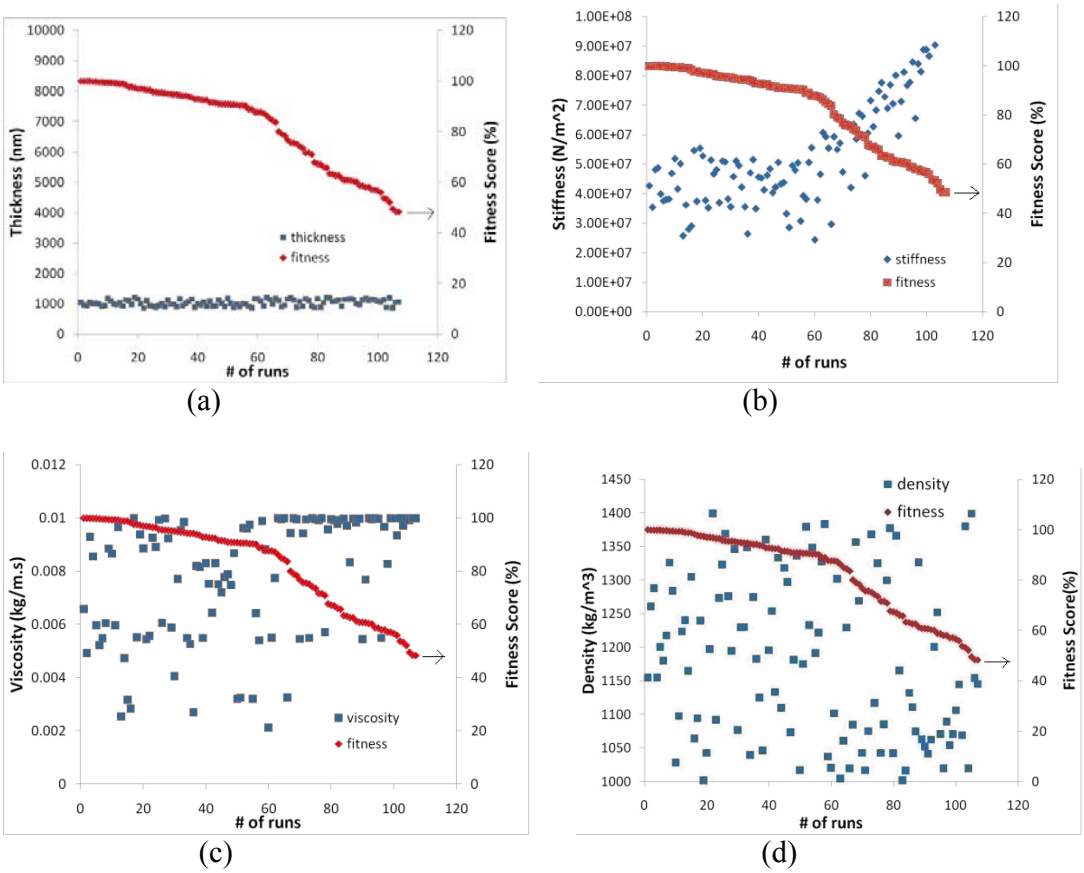

Figure 5-7 The results obtained by the MTSM/GA technique after 100 runs for a) thickness b) stiffness c) viscosity, and d) density values.

As seen from the figure 5-7, the thickness and stiffness values fall around a small range. In other words they have smaller solution bandwidths. Solutions for thickness value are between 800 nm - 1200 nm and the solutions for stiffness fall between $2x10^7$ and $6x10^7$ N/m^2. As remembered, the theoretical value for thickness and stiffness are 1000 nm and $4x10e^7$ N/m^2 respectively. Even though the search space for thickness and stiffness are between 1 nm to 10000 nm and 10^7 N/m^2 - 10^8 N/m^2, the candidate solutions only fall between ±200 nm. For stiffness, small bandwidth of $\pm 2x10^7$ N/m^2 was observed. Based on this observation, it was hypothesized that even though the system is an under-determined problem, some variables will be more dominant than the others. In other words, in this

example, if these two variables can be estimated with relatively good accuracy, the other two variables can also be estimated. In the following section, zooming method will be explained to obtain an optimum solution by forcing the MTSM/GA to a solution.

5.3.4 Integration of a zooming method with the MTSM/GA technique

Zooming method was applied to reduce the search space around a candidate optimum solution. In this way, the elitist strategy preserves the best individual of the previous iteration in the present iteration, whereas zooming technique restricts search domain, so improving in any case convergence rate. Several zooming methods have been developed for different applications (Kwon et al., 2003, Milani and Milani et al., 2007). If variable x of the best performing individuals in a number of successive previous generations has consistently been located in a small portion of the search space, then the search space for x is reduced and centralized about the current parameter value. This leads to a smaller discretization that results in fine tuning (Ndiritu and Daniell., 2001).

In this project, the MTSM/GA technique was run 30 times, and then a new search space was set between maximum and minimum of the 30 points, which is considered a “large sample size” statistically. The solution with highest fitness in each run was also maintained. The median of the points have been calculated and this number is compared with the theoretical values. This zooming continued until the error was less than 1% for all variables. This error was achieved after 6 zooming steps. Zooming is effected mainly by the confinement of the search to those regions that are promising for the particular decision variable.

As seen from fig. 5-8 both thickness and stiffness values approach to theoretical solutions which are 1000 nm and $4x10^7$ N/m^2 respectively. Similar effects are seen in density

and viscosity values. After 6 zooming steps around the candidate points, the error between the median of the solutions, for all variables, is less than 1%.

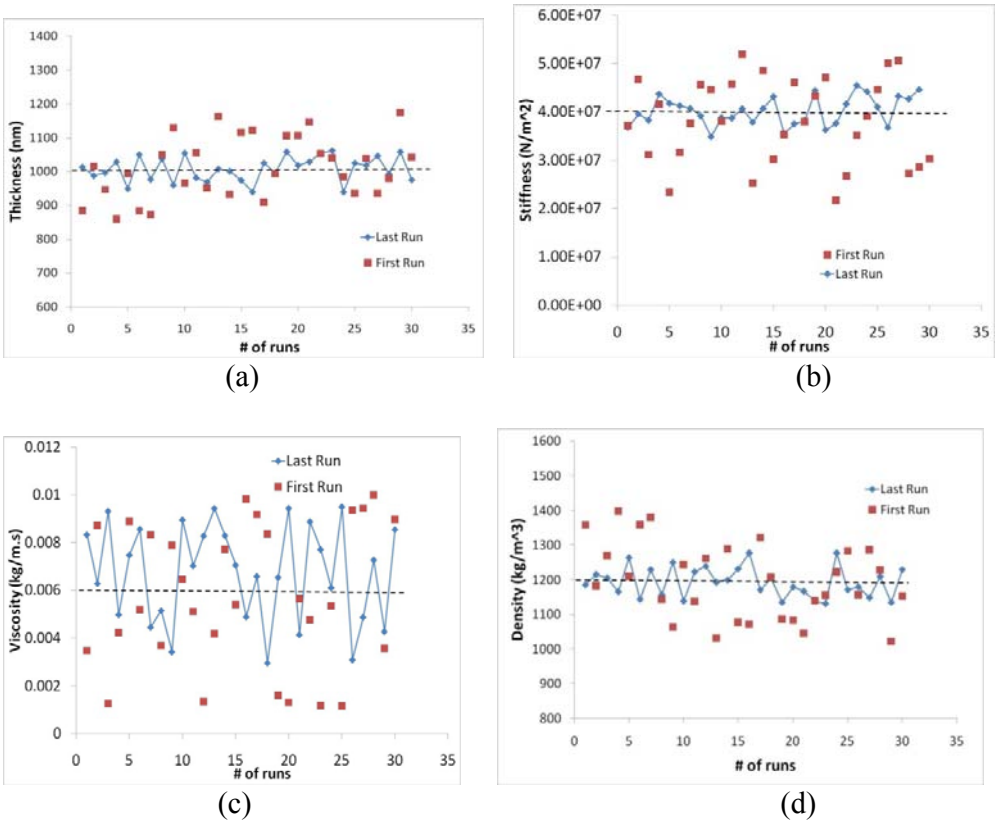

Figure 5-8 Zooming technique applied to each variable a) thickness, b) stiffness, c) viscosity, d)density

5.4 Optimization of the MTSM/GA's parameters

After explaining the general structure of the technique used in this project, the next step is to optimize the MTSM/GA parameters to obtain the best results. There are three main parameters; genes per chromosome, number of individuals and mutation rate.

A mutation operator is applied in the MTSM/GA to increase the diversity in the population. A low fixed mutation rate usually traps the search in a local optimum for a long period of time and a high fixed mutation rate may cause search to be unstable in a solution

space. To address this problem, a dynamic approach is used for setting the mutation rate to increase the effectiveness and efficiency in the search of optima (Choi and Ki-Chan, 2001). In this project, the mutation rate is chosen to be 20*rand. Rand is a Matlab function which generates a number between 0 -1.

Different combinations of genes per chromosome and number of individuals have been evaluated and the absolute errors obtained by the MTSM/GA technique for each variable are presented in table 5-5. These results are presented for the MTSM sensor operating at 5 MHz. Optimization is related to the MTSM/GA's intrinsic characteristics. Therefore it will be enough if the MTSM/GA is optimized for one harmonic.

Table 5-5 Error in percentage in the MTSM/GA technique when different combination of gene per chromosomes and number of individuals were applied.

	# of Individuals		
Genes per chromosome	25	50	100
8	5.6	1.7	4.4
16	0.3	**0.3**	0.6
32	0.2	0.7	2.9

(a) Density

	# of Individuals		
Genes per chromosome	25	50	100
8	2.1	19	5.4
16	16	**0.6**	2.8
32	7.2	10.5	22.8

(b) Viscosity

	# of Individuals		
Genes per chromosome	25	50	100
8	6.2	2.6	5
16	0.6	**0.2**	0.1
32	0.2	1.4	3.3

(c) Thickness

	# of Individuals		
Genes per chromosome	25	50	100
8	7.4	4	5.1
16	0.8	**0.2**	0.1
32	0.6	1.7	3.2

(d) Stiffness

As seen from the table 5-5, less than 1% error has been accomplished with the combination of 16 and 50 for number of genes and individuals respectively. Therefore these combinations will be used in the following sections.

5.5 Stability of the MTSM/GA Technique

The MTSM/GA technique has been run independently ten times to investigate if less than 1% error for each variable is obtained at every run. Less than 1% error was achieved for each variable in ten independent runs for viscoelastic layer in air (fig. 5.9). The same study has been done for a viscoelastic layer in DI water and similar performance has been obtained (data not shown).

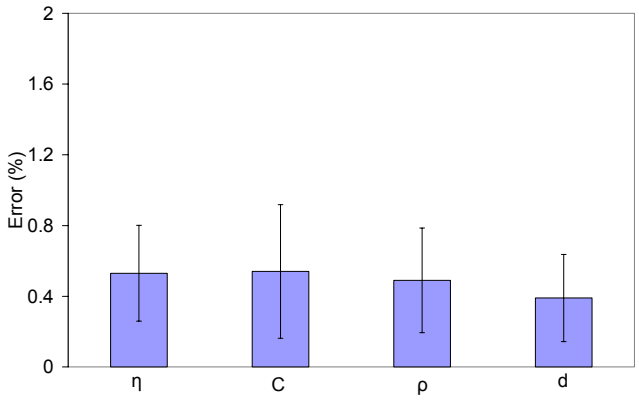

Figure 5-9 Stability of the MTSM/GA technique after 10 runs

5.6 Multiple solutions obtained by the MTSM/GA technique

It was shown in table 5.3 that there are two sub-spaces where a possible solution can be obtained. The MTSM/GA technique has been applied to find the second solution. After the second solution was obtained, the determined values for four parameters have been plugged into the TLM. As shown in table 5.6, two different solutions give exactly the same results for each tracking point. Therefore it can be concluded that there might be multiple solutions in the search space. It should be noted that the MTSM/GA technique has capability to obtain each solution. The main question then will be which solution is the right one.

This question can be answered in two ways.

1. As seen from the table 5-6 and 5-7, the second solution shows “hard rubber” like properties while the first one presents “soft rubber”. One of the solutions can be chosen if some information about the viscoelastic system is known from the literature. The appropriate solution can be correlated with the properties indicated in the literature.
2. If time evolution of the biological process is obtained by the MTSM sensor, the information regarding the properties in the prior time points can help the user to identify the right solution.

Table 5-6 Second solution for single layer viscoelastic loading in air at 5 MHz

	Res. Freq. (Hz)	Max. amp (dB)	Phase at max (degree)	Min amp (dB)	Anti-res. (Hz)	Phase at Anti-res. (Hz)	Min phase (degree)	Freq at min. phase (Hz)
First Solution	4978640	-0.047	-0.062	-108.3	4994380	75.596	-89.86	4993290
Second solution	4978640	-0.047	-0.062	-108.3	4994380	75.60	-89.86	4993290

*Values for second solution are ρ=1100 kg/m^3, η=25x10^{-3} kg/m.s, C=8.1x10^7 N/m2, d=1.1 μm

Table 5-7Second solution for viscoelastic loading in DI water at 5 MHz

	Res. Freq. (Hz)	Max. amp (dB)	Phase at max (degree)	Min amp (dB)	Anti-res. (Hz)	Phase at Anti-res. (Hz)	Min phase (degree)	Freq at min. phase (Hz)
First solution	4977850	-12.57	5.333	-63.37	4993680	5.604	-78.49	4986300
Second solution	4977850	-12.57	5.332	-63.37	4993680	5.604	-78.49	4986300

*Values for second solution are ρ=1300 kg/m^3, η=35x10^{-3} kg/m.s, C=4.3x10^7 N/m2, d=0.9 μm

5.7 Analysis of the effect of the experimental error on the MTSM/GA technique

As seen in section 4.4, it is expected to have an error between theoretical and experimental results. Possible reasons have been discussed in the chapter 4. Therefore it

needs to be discussed that how these discrepancy between theoretical and experimental results affects the MTSM/GA results.

Theoretically, an error was introduced to maximum magnitude and resonance frequency data. It was previously shown that the TLM can predict the experimental response of the MTSM sensor with less than 11 % error. Therefore hypothetically 0.5 %, 1%, 2% and 10 % errors were introduced to the resonance frequency response and 5 %, 10 %, and 20 % errors were introduced to the maximum magnitude response. The errors in the MTSM/GA technique have been presented at 5 MHz, 15 MHz, 25 MHz and 35 MHz in the following sections.

Effect of the experimental error on the MTSM/GA technique at 5 MHz has been presented in fig. 5-10. As seen from fig. 5-10, the error increases to 20 % when the error in the resonance frequency was 10 % (absolute error = 690 Hz). On the other hand, the error in the MTSM/GA technique reaches to 12 % when the error in the magnitude response is 20 % (absolute error = 0.0024 dB).

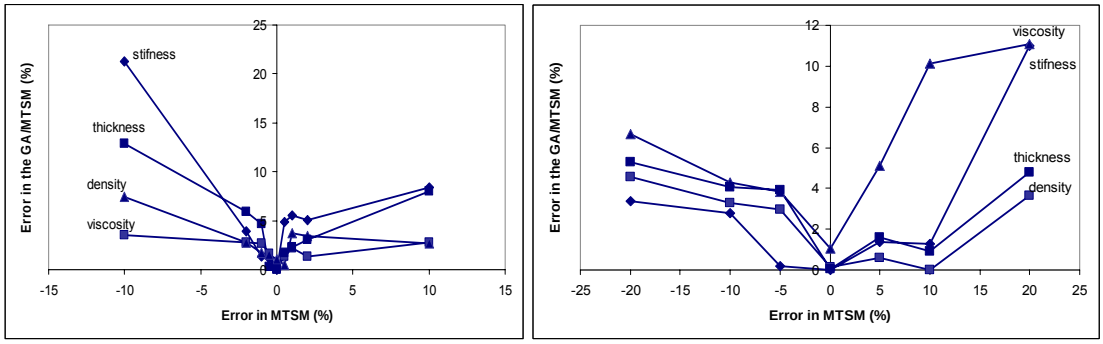

(a) (b)

Figure 5-10 Influence of experimental error in (a) resonance frequency and (b) maximum magnitude on the MTSM/GA technique for single-layer viscoelastic systems at 5 MHz

Effect of the experimental error on the MTSM/GA technique at 15 MHz has been presented in fig. 5-11. As seen from the fig. 5-11, the error increases to 20 % when the error

in the resonance frequency was 10 % (absolute error = 2230 Hz). On the other hand, the error in the MTSM/GA technique reaches to 16 % when the error in the magnitude response is 20 % (absolute error = 0.22 dB).

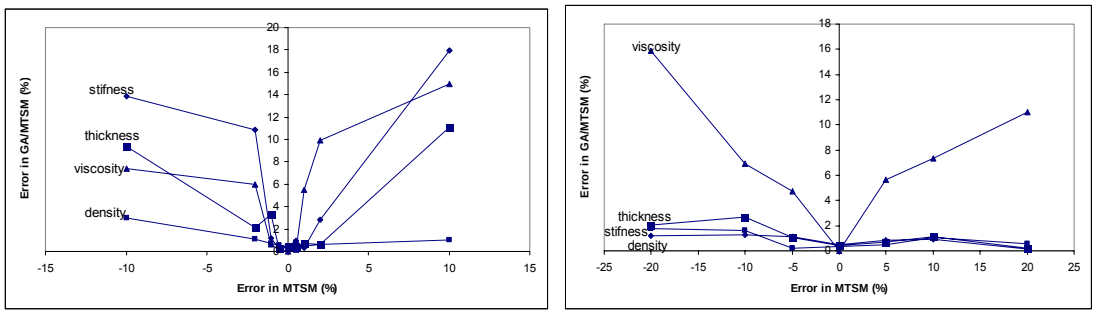

(a) (b)

Figure 5-11 Influence of experimental error in (a) resonance frequency and (b) maximum magnitude on the MTSM/GA technique for single-layer viscoelastic systems at 15 MHz

It can be concluded that the error between the theoretical and experimental data may cause ~ 20 % error in the MTSM/GA technique.

5.8 Effect of quality factor on the MTSM/GA technique

The quality of a MTSM sensor is the quality factor (Q factor), which is defined as the ratio between the stored and dissipated energy. The maximum value for Q factor is given by material constants. For the relation to the frequency the following equation can be derived (Pardo et al., 2005):

$$Q_{\max} = 1.6x10^{13} \frac{1}{f} s^{-1} \tag{5.8}$$

The Q factor is influenced by factors like impurities, mobility of impurities, dislocations, and hydrogen content of the quartz crystal, the diameter/thickness ratio and

parallelity of the quartz surfaces (Zimmermann et al., 2001). Due to additional loses, the value calculated from eq. 5.8. is therefore not reached in practice.

The Q factor can be calculated on the base of a modified Butterworth-van-Dyke circuit and the equivalent circuit values R and L and C_1

$$Q = \frac{\omega L}{R} = \frac{1}{\omega R C_1} \tag{5.9}$$

where L, R and C_1 are electrically equivalent inductance, resistance and capacitance. ω is angular frequency which is equal to 2πf (f: resonance frequency). Furthermore L and R can be related to density and viscosity of the medium loaded on MTSM sensor surface. It has been shown that the resolution of MTSM sensor measurements worsens when the density and viscosity of the liquid is increased (Pardo et al., 2005). The biological processes should occur in a biochemically favorable environment. Therefore they take place in buffer or other relevant biological mediums such as serum, whole blood and saliva. These media are more viscous and denser than deionized water. For example, blood plasma viscosity is 1.4 times higher than DI water's viscosity (Rosenson et al.,1996). Furthermore it was observed that, in our own studies, high losses (>-25 dB) may be observed. Thus it is important to study the influence of the quality factor on the MTSM/GA technique.

The quality factor has been calculated by using the two methods. In the first method, the Q factor was determined by using S21 response of the MTSM sensor. The 3dB bandwidth of the S21 response was calculated (Vives and Arnau, 2004). In the second method, the group delay time was determined by using the phase data (Kaba et al., 2006). More detailed information regarding the calculation of Q factor was given in Appendix 2.

To investigate the effect of quality factor on the MTSM/GA technique, a hypothetical two layer system is designed and simulated by using TLM (fig. 5.12). In this model, the first layer is a viscoelastic layer having stiffness (G'_1) of $4x10^7$ N/m^2, viscosity (η_1) of $6x10^{-3}$

kg/m.s, density (ρ_1) of 1200 kg/m^3 and thickness (d_1) of 1 μm. The second layer is chosen to be a semi-infinite Newtonian medium which has stiffness of 0 N/m^2 and density (ρ_c) of 1000 kg/m^3. To obtain different quality factor values, the viscosity of the Newtonian medium (η_c) is increased from 10^{-3} kg/ms to 10^{-1} kg/m.s. Performance of the MTSM/GA technique has been investigated at six different quality factors. The analysis has been done at 5 MHz, 15 MHz, 25 MHz and 35 MHz.

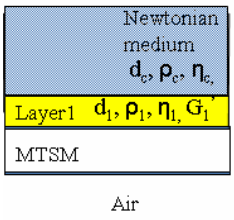

Figure 5-12 Hypothetical two layer system to investigate the effect of quality factor on the MTSM/GA technique for single layer viscoelastic systems

Increasing the viscosity of the Newtonian medium decreases the maximum magnitude and the resonance frequency of the MTSM sensor (fig. 5-13a). Dynamic range of the MTSM sensor response decreased with the decrease of the quality factor. The similar phenomenon can be seen in the phase response (fig. 5-13b).

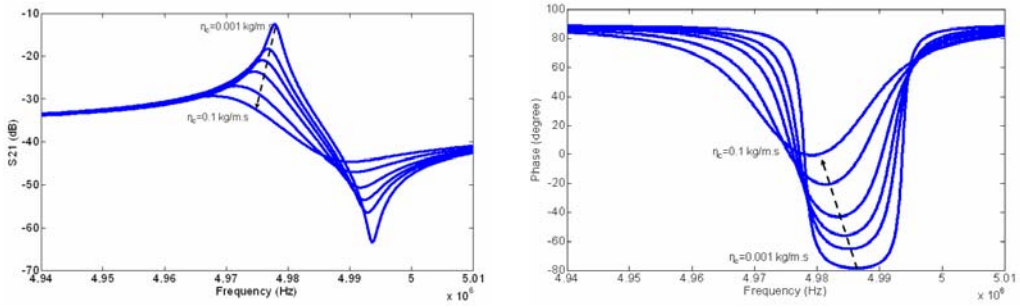

(a) (b)

Figure 5-13 Influence of quality factor on the MTSM sensor's (a) magnitude and (b) phase responses at 5 MHz (single-viscoelastic layers)

The quality factor has been changed from 2500 (2000) to 300 (200) by increasing the viscosity value of the second layer (values in parenthesis are for second method). At each viscosity value, the properties of the medium are determined by the MTSM/GA technique and the absolute error between the estimated values and the values input to the TLM model has been presented in fig. 5-14.

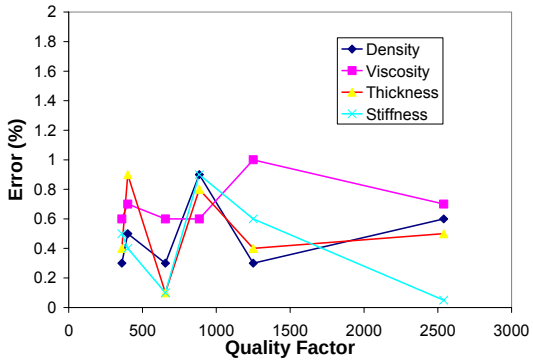

Figure 5-14 Effect of the quality factor on the MTSM/GA technique single-viscoelastic layers at 5 MHz

As seen from fig. 5-14, the absolute errors for all parameters are smaller than 1%. In other words, no affect of quality factor on the MTSM/GA technique has been observed at 5 MHz.

Change in S21 and phase responses of the MTSM sensor surface with the decrease of quality factor at 15 MHz has been presented in fig. 5-15. As seen from the graphs, the maximum magnitude decreases dramatically from -17 dB to -27 dB while the phase response no longer reaches to zero phase except at the first viscosity value ($\eta=10^{-3}$ kg/m.s).

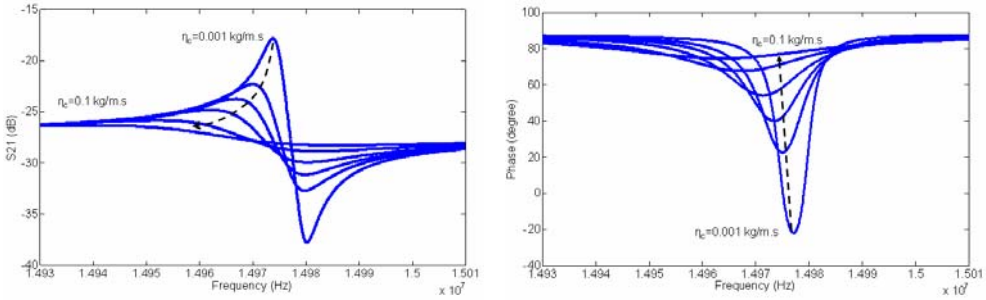

(a) (b)

Figure 5-15 Influence of quality factor on the MTSM sensor's (a) magnitude and (b) phase responses at 15 MHz (single-viscoelastic layers)

As seen in fig. 5-15, the dynamic range for the MTSM sensor at 15 MHz (between -17 dB to -38 dB) is much smaller than the one seen at 5 MHz (between -13 dB to -64 dB). The zero phase is no longer available when viscosity of the second layer is increased to $5x10^{-3}$ kg/m.s. Similar phenomenon can be also seen in the Q factor vs. error response. As seen in fig 5-16a, the quality factor changes from ~3000 initially to 0 for the last two conditions (when viscosity of the second layer is equal to 0.05 kg/m.s. and 0.1 kg/m.s.). Therefore S21 response vs. absolute error graph has been shown in fig 5-16b for a better visualization of this phenomenon. As seen in fig. 5-16b, when the maximum magnitude reaches -25 dB, the error increase above 4 % for all parameters.

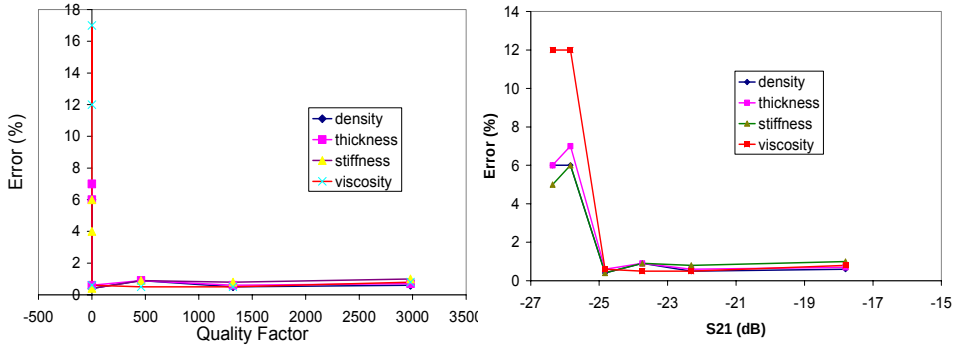

(a) (b)

Figure 5-16 (a) Effect of quality factor on the MTSM/GA technique's error at 15 MHz (b) Change in maximum magnitude vs. the MTSM/GA technique's error at 15 MHz (single-viscoelastic layers)

The change in S21 and phase responses of the MTSM sensor at 25 MHz has been shown in fig. 5-17a and b. It should be noted that there is no zero phase crossing for any case at 25 MHz. The dynamic range of the MTSM sensor also decreased compared to the ones at 5 MHz and 15 MHz. (dynamic range = -20.5 to -25.9)

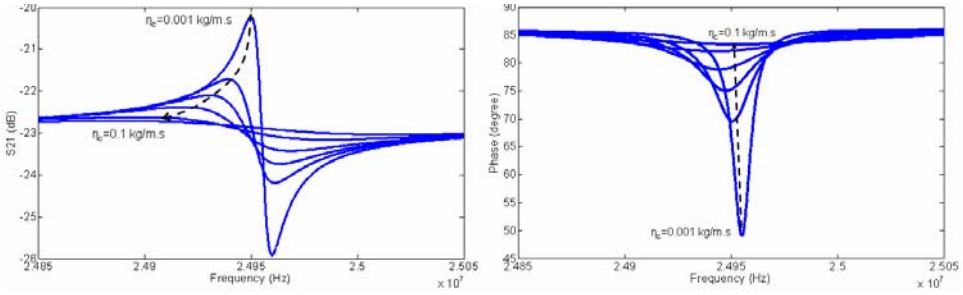

(a) (b)

Figure 5-17 Influence of quality factor on the MTSM sensor's (a) magnitude and (b) phase responses at 25 MHz (single-viscoelastic layers)

The quality factor at six viscosity values were 0 at 25 MHz. Therefore the absolute error has been presented as the maximum magnitude of the MTSM sensor response vs. error in the MTSM/GA technique and is shown in fig. 5-18. The error increases to 10 % when the maximum magnitude reaches -22.5 dB.

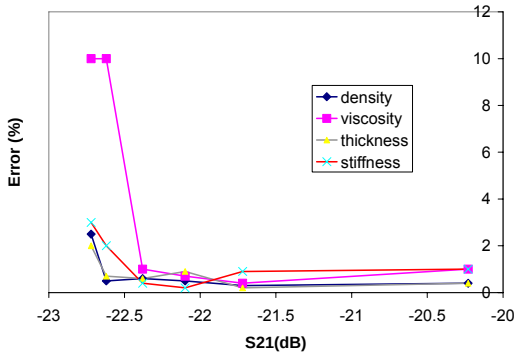

Figure 5-18 Maximum magnitude vs. the error in MTSM/GA technique for single layer viscoelastic systems at 25 MHz

The change in S21 and phase responses of the MTSM sensor at 35 MHz is shown in fig. 5-19a and b. It should be noted that there is no zero phase crossing for any case at 35 MHz. The dynamic range of the MTSM sensor also decreased compared to the ones observed

at 5 MHz and 15 MHz and 25 MHz (dynamic range = -19.6 to -20.45). Furthermore the resonance frequency is increasing after the viscosity of the second layer reaches the 0.01 kg/m.s.

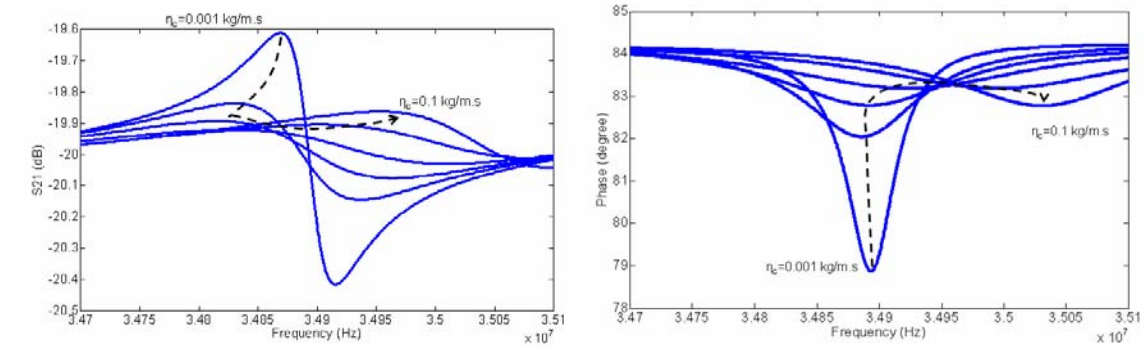

(a) (b)

Figure 5-19 Influence of quality factor on the MTSM sensor's (a) magnitude and (b) phase responses at 35 MHz (case: single-viscoelastic layers)

The quality factors for all six cases were 0 at 35 MHz. Therefore the absolute error has been presented as the maximum magnitude of the MTSM sensor response vs. error in the MTSM/GA technique and shown in fig. 5-20. As seen fig. 5-20, the error increases to 14 % when the maximum magnitude reaches -19.9 dB.

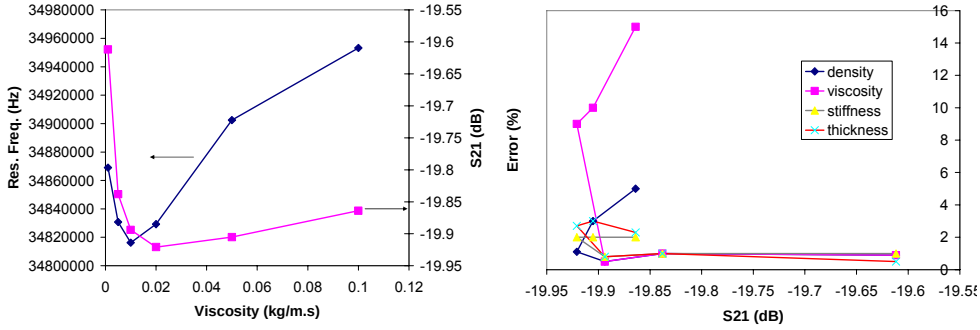

(a) (b)

Figure 5-20 (a) Change in the maximum magnitude and resonance frequency (b) Effect of the quality factor on the MTSM/GA technique's error at 35 MHz (case: single-viscoelastic layers)

It should be noted it was assumed that the MTSM sensor is optimized for the operation at the fundamental harmonic, which is 5 MHz, in this project. Here, the

optimization is considered to be the design optimization of the MTSM sensor. Literature shows that the ratio of the thickness of the quartz membrane to the diameter of gold electrode should be ~1/18 (Lin et al., 1993). This ratio has been maintained at 5 MHz but was not realized for the other harmonics. For example, MTSM sensor's acoustic response to the same loading discussed above is presented in fig. 5-21 when the sensor is optimized for the operation at 15 MHz.

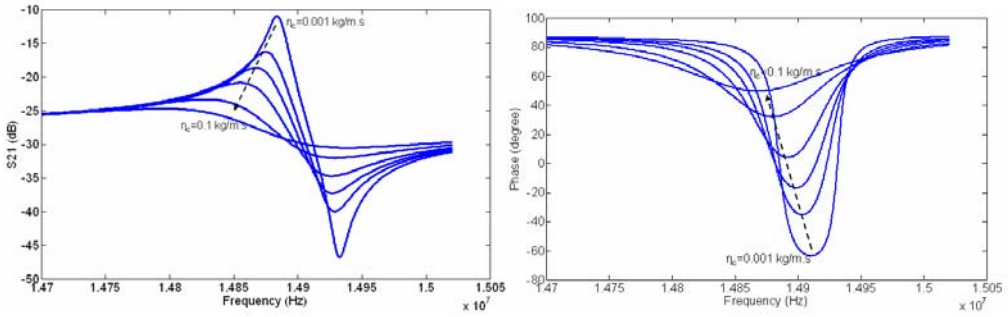

(a) (b)

Figure 5-21 Influence of quality factor on the MTSM sensor's (a) magnitude and (b) phase responses at 15 MHz, when the MTSM sensor is optimized for operation at 15 MHz (case: single-viscoelastic layers)

Theoretical studies showed that the dynamic range of the MTSM sensor operating at 15 MHz increased. In addition the zero phase crossing is maintained for the first three viscosity values of the second layer. It can be clearly seen that there is distinct difference between the performance of the MTSM sensor operated at 3rd harmonic of 5 MHz and the MTSM sensor operated at fundamental frequency of 15 MHz. Therefore, for future applications, the MTSM sensors with different fundamental frequencies can be placed on single quartz substrate. Each sensor can be optimized for fundamental operation. Therefore it will provide higher dynamic range and accuracy. This hypothesis was studied in detail by Francois et al. (2008). Biochip technology with multi-resonance operation was successfully utilized to characterize of several biological interfacial processes such as bacillus anthracis detection.

5.9 Theoretical validation of the GA/MTM technique for single-layer viscoelastic systems

To identify the limitations and strengths of the MTSM/GA technique, a hypothetical evaporation process has been analyzed and the properties of each stage were determined by the MTSM/GA technique. The evaporation starts with liquid like stage, then with continues soft rubber, hard rubber and finally solid thin layer which can be defined with solid like state (Kwoun, 2006). Figure 5-22 shows a typical four stage evaporation induced deposition processes of biological thin film on the sensor surface. The detailed analysis of these stages was discussed in Kwoun's study. In this project, this biological process was utilized as a mean to validate the MTSM/GA technique.

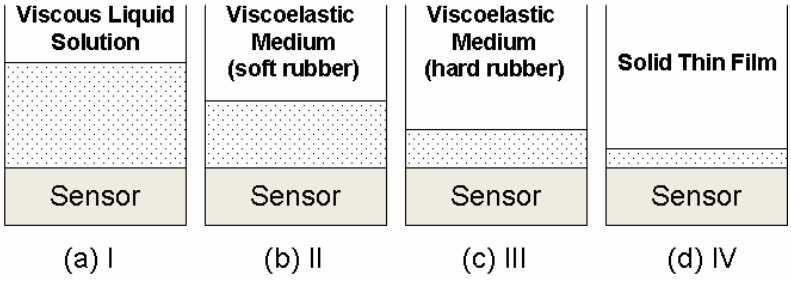

Figure 5-22 Four stages of a typical evaporation-induced deposition process of a biological film

Stage I: The stage I is characterized as a viscous liquid with a relatively low stiffness value (10^5 N/m^3). The density is also assumed to be same as water (1000 kg/m^3) for the simulation. The viscosity of the sample is set to be between 0.001 kg/ms to 0.01 kg/ms, which is 0.002 kg/m.s. The thickness of the film is assumed to be 3 μm.

Stage II: The stage II is characterized as a soft robber viscoelastic condition. In this stage, both the viscosity and stiffness are increased from the previous stage I. The range of viscosity is increased more than 3 fold, to 0.007 kg/m.s. The stiffness also has been increased to $2x10^6$ N/m^2 to present a soft rubbery stage of the sample. Density of the film is assumed to be 1100 kg/m^3 due to mass deposition on the sensor surface. The thickness of the film was decreased to 1 μm from 3 μm in the first stage due of the evaporation of the solvent.

Stage III: This stage of the sample is characterized as a hard rubber condition in this study. The viscosity of the sample is increased up to 0.02 kg/ms and the range of the stiffness has been increased from $2x10^6$ to $5x10^7$ N/m^2 to represent the hard rubber condition of the sample. Density and thickness of the film were changed to 1200 kg/m^3 and 500 nm respectively.

Stage IV: This stage is characterized as a solid like thin film. The stiffness has been increased to $5x10^8$ to indicate the rigidity of the sample condition. The viscosity value has been set to be 0.1 kg/m.s while the thickness was assumed to be constant, which is 500 nm. Density value was increased to 1300 kg/m^3. The summary of the values used to represent each stage is presented in table 5-8.

Table 5-8 Hypothetical mechanica and geometrical properties of single-layer viscoelastic system in each stage

	Four phases of biological process			
Properties	**Stage I**	**Stage II**	**Stage III**	**Stage IV**
Thickness (nm)	3000	1000	500	500
Stiffness (N/m^2)	10^5	$2x10^6$	$5x10^7$	$5x10^8$
Viscosity (kg/m.s)	$2x10^{-3}$	$7x10^{-3}$	$2x10^{-2}$	10^{-1}
Density (kg/m^3)	1000	1100	1200	1300
	Liquid like	Soft rubber	Hard Rubber	Solid like

In the following section, each stage of the deposition process discussed by analyzing the acoustic signatures of the MTSM sensor at 5 MHz, 15 MHz, 25 MHz and 35 MHz. Then

the MTSM/GA technique is applied and critically evaluated to understand its limitations and strengths in determining the viscoelastic properties of a typical biological process.

5.9.1 Analysis of the MTSM/GA technique for single layer viscoelastic systems to at 5 MHZ

The changes in the magnitude and phase responses of the MTSM sensor to the evaporation-induced deposition process in stage I, II, III and IV has been simulated using transmission line model and presented in fig. 5-23.

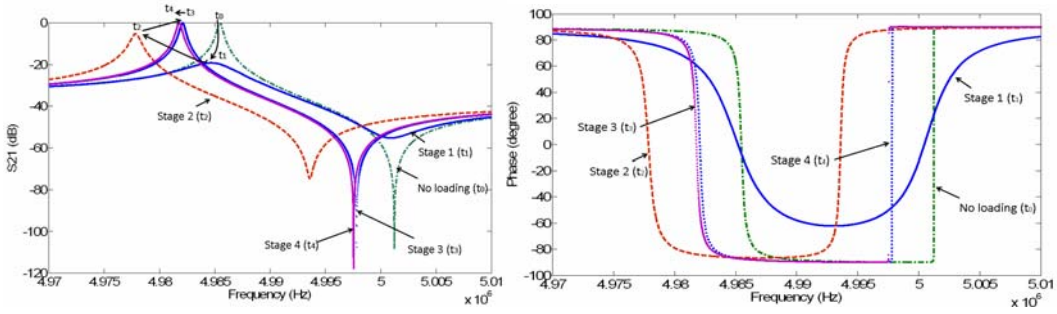

(a) (b)

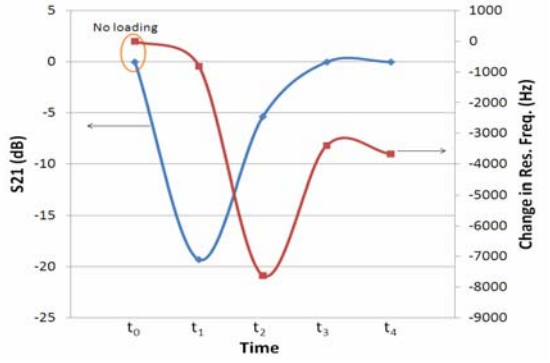

(c)

Figure 5-23 Change in the magnitude (a) and (b) phase responses of the MTSM sensor during evaporation process. (c) Change in the maximum magnitude and resonance frequency by time at 5 MHz. (case: single-viscoelastic layers)

In stage I, the viscoelastic layer shows a "transition state" properties where G" and G' are close to each other, (G' = 10^5 N/m^2 and G" = 0.63x10^5 N/m^2). The magnitude and the resonance frequency responses of the MTSM sensor decreased from the air reference (no loading). In this phase, the system can be modeled as a semi-infinite viscoelastic loading because the penetration depth (~1.3 μm) is smaller than the column thickness (3 μm). In other words, there is no reflection of acoustic wave from the column surface.

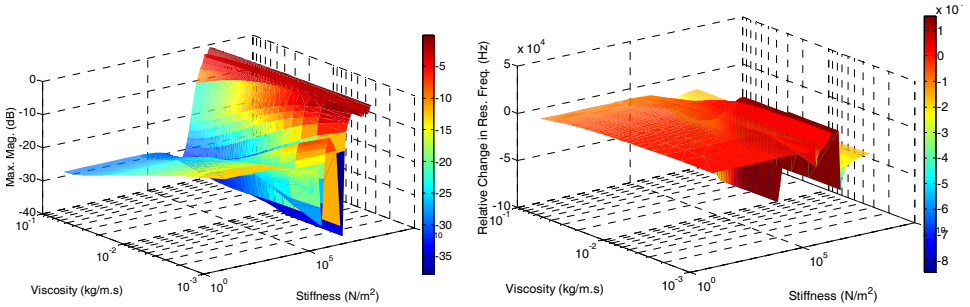

(a) (b)

Figure 5-24. Effect of the changes in the single viscoelastic layer viscosity and stiffness on the MTSM magnitude (a) and resonance frequency (b) response (relative changes in resonance frequency and absolute values of attenuation in dB) at 5 MHz in Stage I.

This phenomenon can be seen in both magnitude and frequency responses of the MTSM sensor (fig. 5-24). The penetration depth of the acoustic wave is lower than the column height when the stiffness value is a relatively lower value (C < 10^5 N/m^2). With the increase in the viscosity and stiffness values of the viscoelastic layer, the oscillations are observed in both responses. This phenomenon is called "film resonance" (Martin et al., 1994) and it is closely related to acoustic phase shift (φ) which is defined as:

$\phi = \omega h_f \, \mathrm{Re}(\rho_f G)^{1/2}$,where ω (=2πf) is the angular frequency, G=G' + jG" is the complex shear modulus of the viscoelastic layer, and ρ_f and h_f are the mass density and thickness of the film, respectively. When the film thickness and/or the shear modulus of the film increases, then the displacement applied by the quartz at the lower film surface can undergo a

significant phase shift (Martin et al., 2000). If the film is acoustically thin, i.e. $\varphi << \pi/2$, the film moves synchronously with the resonator surface. If acoustic phase shift is between 0 and $\pi/2$, then the displacement at the upper surface of the film exceeds that at the resonator surface. Finally if φ reaches $\pi/2$, then interaction between the resonator and film exhibits characteristics of coupled resonance systems: displacement in the film/resonator exhibits in-phase and out-of phase modes. In addition, the system is highly damped in the vicinity of resonance. In this compliant film regime, the resonator no longer functions as a simple microbalance; resonance frequency and damping depend upon film thickness, density, and the shear elastic properties (Martin and Frye, 1991).

The MTSM/GA technique has been applied to determine the properties of the viscoelastic layer in stage I. The results obtained from the technique and the absolute errors are presented in table 5-9.

Table 5-9 Properties of single viscoelastic layer determined by the MTSM/GA technique and % errors in stage I at 5 MHz

Properties	Values Input to TLM	Values Determined by MTSM/GA Technique	Error (%)
d_1 (nm)	3000	3300	12
G' (N/m^2)	10^5	1.006×10^5	0.7
η_1 (kg/m.s)	2×10^{-3}	1.99×10^{-3}	0.2
ρ_1 (kg/m^3)	1000	1010	1

As seen from table 5-9 the parameters are estimated with less than 1% error except the thickness value by using the MTSM/GA technique. The high error in this value stem from the fact the viscoelastic loading is seen as a semi-infinite medium by the MTSM sensor because the penetration depth (~1.3 μm) is smaller than the column height (3 μm). Therefore any thickness value which is bigger than the penetration depth will satisfy the solution. Thus it can be concluded that if the medium loaded is a semi-infinite medium, the estimated value

will be equal to or a higher value than penetration depth because of the phenomenon discussed above.

In stage II, the viscoelastic layer enters in a "soft rubbery state" where G' is ten times bigger than G" (G' = $2x10^6$ N/m^2 and G" = $0.22x10^6$ N/m^2). An increase in the magnitude response is observed while the resonance frequency continues to decrease. As seen in fig. 5-25a, the combination of given viscosity ($7x10^{-3}$ kg/m.s) and stiffness ($2x10^6$ N/m^2) values at a constant density (1100 kg/m^3) and thickness (1 μm) yields -5.39 dB which is larger than the magnitude value in stage I. At the same time the penetration depth increases to ~24 μm, which is 24 times higher than the column thickness. In this stage, the reflection of acoustic wave at the sensor surface is observed.

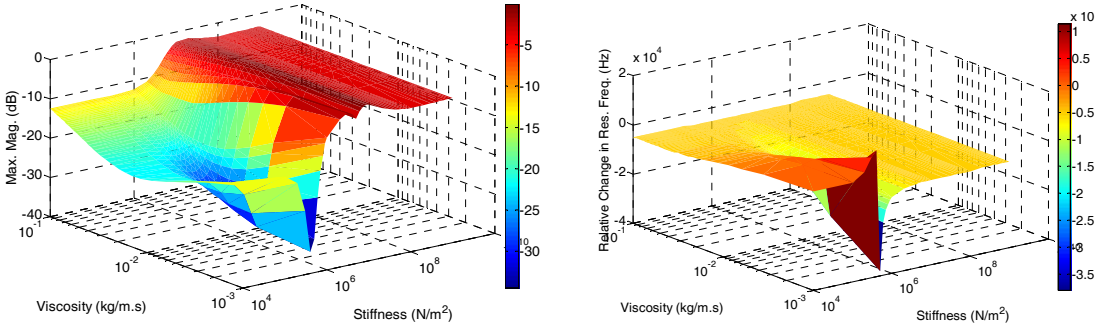

(a) (b)

Figure 5-25 Effect of the changes in the single viscoelastic layer viscosity and stiffness on the MTSM magnitude (a) and resonance frequency (b) response (relative changes in resonance frequency and absolute values of attenuation in dB) at 5 MHz in Stage II.

The MTSM/GA technique has been applied to determine the properties of the viscoelastic layer in stage II at 5 MHz. The results obtained from the technique are presented in table 5-10. As seen from the table, all four parameters are determined with less than 1% error by the MTSM/GA technique. It should be noted that a second solution has been also obtained. These values were $6x10^6$ N/m^2, 1200 kg/m^3, $6.6x10^{-2}$ kg/m.s and 1000 nm for

stiffness, density, viscosity and thickness respectively. As discussed in section 5.6, there might be multiple solutions obtained by the technique because of a large search space. The advantage of this method is that it can obtain all solutions.

Table 5-10 Properties of single viscoelastic layer determined by the MTSM/GA technique and % errors in stage II at 5 MHz

Properties	Values Input to TLM	Values Determined by MTSM/GA Technique	Error (%)
d_1 (nm)	1000	1005	0.5
G' (N/m^2)	$2x10^6$	$1.99x10^6$	0.5
η_1 (kg/m.s)	$7x10^{-3}$	$7.01x10^{-3}$	0.2
ρ_1 (kg/m^3)	1100	1090	1

In stage III, the viscoelastic layer enters in a "hard rubber" state where G' is eighty times bigger than G" (G' = $5x10^7$ N/m^2 and G" = $0.063x10^7$ N/m^2). Although the ratio of storage to loss modulus increases to around 80, small losses in magnitude response were still present, which was -0.038 dB (in air loses is -0.036 dB). Therefore small viscoelastic contribution was observed. It should be noted that no noise was introduced to the MTSM sensor response in the theoretical studies. In the experimental studies, the noise in the MTSM sensor signal may introduce higher errors in the MTSM/GA technique since the viscoelastic system is very close to "solid like" stage.

Both stiffness and viscosity values increase compared to the values in stage II. This causes the penetration depth of the acoustic wave to increase to ~0.1 cm while the thickness of the layer decreases to 500 nm. As seen in fig. 5-26 the oscillatory response initiates at earlier stiffness and viscosity values because of the smaller thickness value and higher penetration depth.

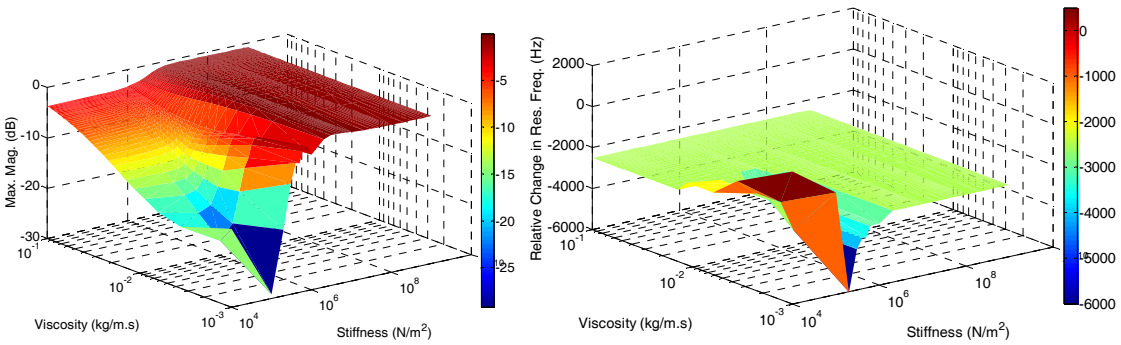

(a) (b)

Figure 5-26 Effect of the changes in the single viscoelastic layer viscosity and stiffness on the MTSM magnitude (a) and resonance frequency (b) response (relative changes in resonance frequency and absolute values of attenuation in dB) at 5 MHz in Stage III.

The MTSM/GA technique has been applied to determine the properties of the viscoelastic layer in stage III at 5 MHz. The results obtained from the technique are presented in table 5-11. As seen from the table, all four parameters are determined with less than 1% error by the MTSM/GA technique.

Table 5-11 Properties of single viscoelastic layer determined by the MTSM/GA technique and % errors in stage III at 5 MHz

Properties	Values Input to TLM	Values Determined by the MTSM/GA Technique	Error (%)
d_1 (nm)	500	497	0.6
G' (N/m^2)	$5x10^7$	5.0210^7	0.5
η_1 (kg/m.s)	$2x10^{-2}$	$2.02x10^{-2}$	1
ρ_1 (kg/m^3)	1200	1210	1

In stage IV, the viscoelastic layer enters in a "solid like" state where G' is much larger than G" (G' = $5x10^8$ N/m^2 and G" = $0.031x10^8$ N/m^2). The magnitude also increased to -0.036 dB, which is equal to the magnitude value in air. Thus no visible viscous contribution is present on the MTSM sensor response. The acoustic phase shift is calculated to be $8x10^{-5}\pi$ which is much smaller than $\pi/2$. In this case, the layer behaves as an ideal mass layer, with response following the Seuerbrey model. In this regime the device responds only to the surface mass density ρ_f, and the thickness (h_f) of the viscoelastic film. No significant power

dissipation occurs in the film, due to a lack of deformation, and the resonance remains relatively undamped. This might be referred to as the microbalance regime of operation (Martin and Frye, 1991).

This phenomenon can be clearly seen in fig. 5-27a and b. In stage IV, the stiffness and viscosity increase compared to the values in stage III. This causes the penetration depth of the acoustic wave to increase to ~6 cm while the thickness of the layer is 500 nm. Therefore the oscillation is seen in the lower values of viscosity and stiffness values; specifically 10^{-3} kg/m.s and 10^{4} N/m^2 for viscosity and stiffness respectively.

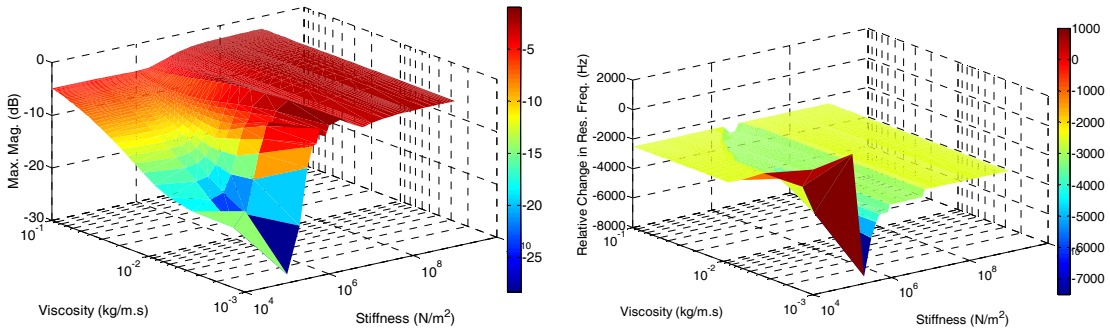

(a) (b)

Figure 5-27 Effect of the changes in the single viscoelastic layer viscosity and stiffness on the MTSM magnitude (a) and resonance frequency (b) response (relative changes in resonance frequency and absolute values of attenuation in dB) at 5 MHz in Stage IV.

The MTSM/GA technique has been applied to determine the properties of the viscoelastic layer in stage IV at 5 MHz. The results obtained from the technique are presented in table 5-12. As seen from the table, while stiffness and viscosity were not able to be determined by the MTSM/GA technique, the density and thickness variables were determined with less than 3 % errors. This stems from the fact that the viscoelastic layer shows a solid like system. Therefore MTSM sensor response is governed by the product of film density and thickness. The viscous contribution is no more visible by the MTSM sensor.

It can be concluded that if the viscoelastic layer is a solid like medium, then MTSM/GA technique will not able to determine the shear modulus efficiently and the error in the thickness and density values may increase to more than 3 %.

Table 5-12 Properties of single viscoelastic layer determined by the MTSM/GA technique and % errors in stage IV at 5 MHz

Properties	Values Input to TLM	Values Determined by MTSM/GA Technique	Error (%)
d_1 (nm)	500	510	2.5
G' (N/m^2)	$5x10^8$	NA	NA
η_1 (kg/m.s)	10^{-1}	NA	NA
ρ_1 (kg/m^3)	1300	1330	2.5

5.9.2 Analysis of the MTSM/GA technique for single layer viscoelastic systems to at 15 MHZ

The changes in the magnitude and phase responses of the MTSM sensor to the evaporation-induced deposition process has been simulated at 15 MHz using transmission line model and presented in fig. 5-28a and b. Change in maximum magnitude and resonance frequency by time is given in fig. 5-28c. As seen from the fig. 5-28c, the acoustic signature of the MTSM sensor at 15 MHz differs from the acoustic response at 5 MHz (fig 5-23c). The maximum magnitude value at 15 MHZ in stage II decreases while it increases at 5 MHz for the same stage. Also, at time t_3, the resonance frequency continues to decrease from time t_2, while the apposite is seen in the resonance frequency response at 5 MHz.

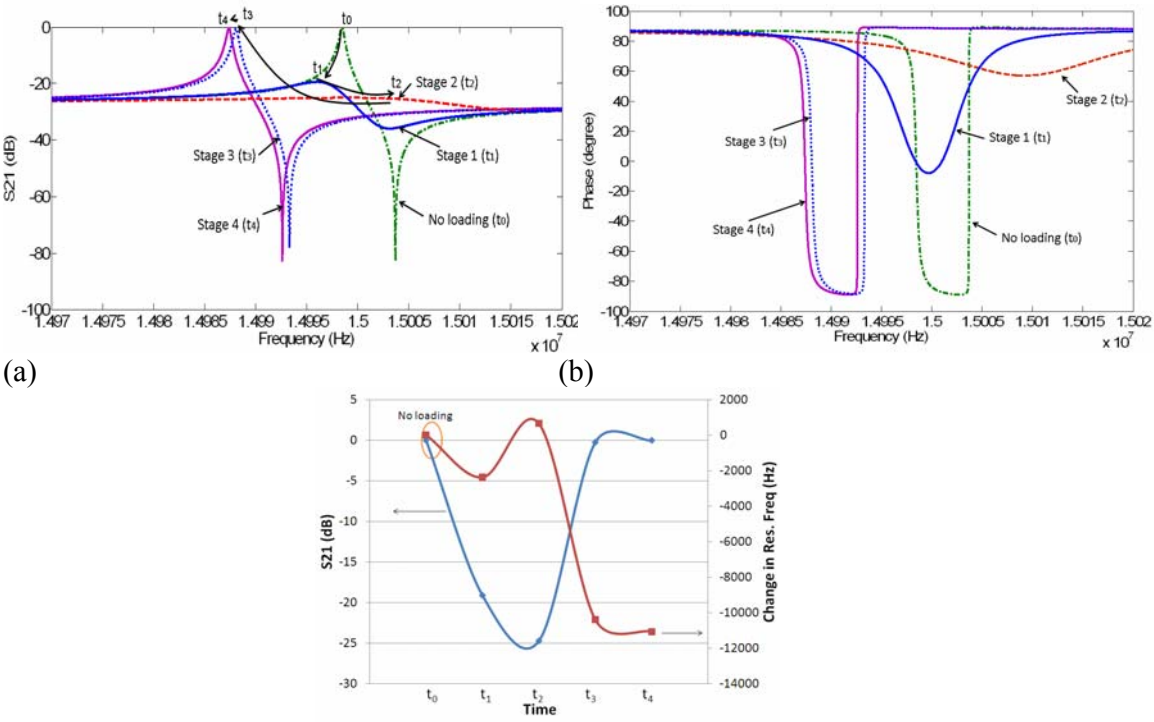

Figure 5-28 Change in magnitude (a) and phase (b) responses of the MTSM sensor during evaporation process. (c) Change in maximum magnitude and resonance frequency by time at 15 MHz. (case: single viscoelastic layer)

In stage I, the viscoelastic layer shows a "transition state" properties where G" and G' is close to each other, (G' = 10^5 N/m^2 and G" = 1.9x10^5 N/m^2). The magnitude and the resonance frequency responses of the MTSM sensor decrease compared to the values in air reference. In stage I, the similar phenomenon has been observed at the 5 MHz. The penetration depth (~300 nm) is much smaller than the column thickness (3 μm). In other words, there is no reflection of acoustic wave from the column surface. This can be seen in both in magnitude and frequency responses shown in fig. 5-29a and b. As seen from graphs in fig. 5-29a and b, no oscillation is observed when the stiffness less than 10^6 N/m^2.

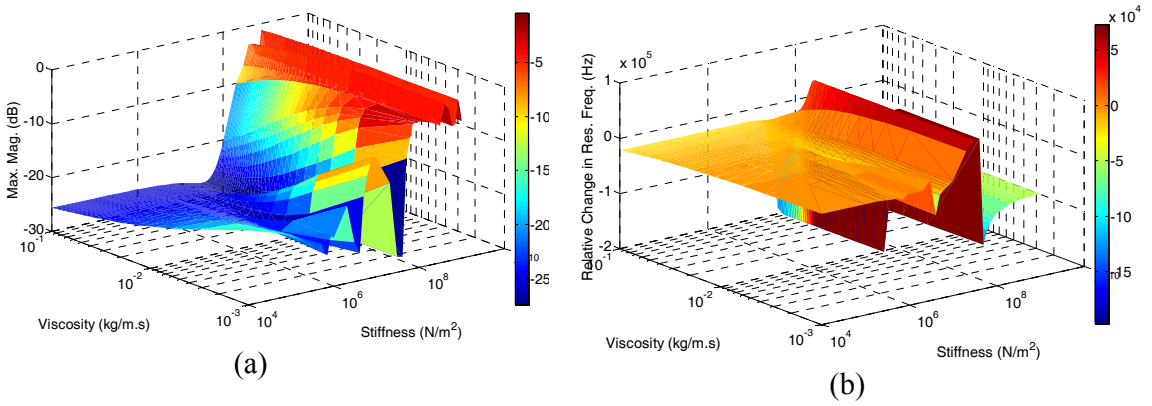

Figure 5-29 Effect of the changes in the single viscoelastic layer viscosity and stiffness on the MTSM magnitude (a) and resonance frequency (b) response (relative changes in resonance frequency and absolute values of attenuation in dB) at 15 MHz in Stage I.

The MTSM/GA technique has been applied to determine the properties of the viscoelastic layer in stage I. Single solution was obtained. The results obtained from the technique are presented in table 5-13.

Table 5-13 Properties of single viscoelastic layer determined by the MTSM/GA technique and % errors in stage I at 15 MHz

Properties	Values Input to TLM	Values Determined by MTSM/GA Technique	Error (%)
d_1 (nm)	3000	2800	7
G' (N/m^2)	10^5	0.99×10^5	1
η_1 (kg/m.s)	2×10^{-3}	1.99×10^{-3}	0.2
ρ_1 (kg/m^3)	1000	1010	1

As seen from table 5-13 the parameters are estimated with less than 1% error except thickness value by using the MTSM/GA technique (same phenomenon has been observed in stage at 5 MHz as well). This result is consistent with our hypothesis made in section 5.9.1 that if the loading is seen as a "semi-infinite medium" by the MTSM sensor, then the thickness value of the viscoelastic layer will be equal to penetration depth or higher than the penetration depth. Therefore a higher error in thickness value can be present.

In the stage II, the viscoelastic layer shows a "soft rubbery" state properties where G" is around three times bigger than G' (G' = $2x10^6$ N/m^2 and G" = $0.66x10^6$ N/m^2). In this stage, both the maximum magnitude and the resonance frequency decrease from the values in stage I. An interesting phenomenon is observed in which the resonance frequency goes higher than the resonance frequency value obtained in air. This event stems from the fact that the acoustic phase shift (φ=0.7 π) is bigger than the π/2. In this case, the frequency is higher than the uncoated the MTSM sensor. In addition the sensor is highly damped (α_R=~26 dB) in the vicinity of the resonance. The oscillations in magnitude and resonance frequency responses of MTSM sensor can be clearly seen in fig. 5-30a and b. When stiffness value is $2x10^6$ N/m^2 and viscosity is equal to $7x10^{-3}$ kg/m.s, the MTSM sensor shows an oscillatory response.

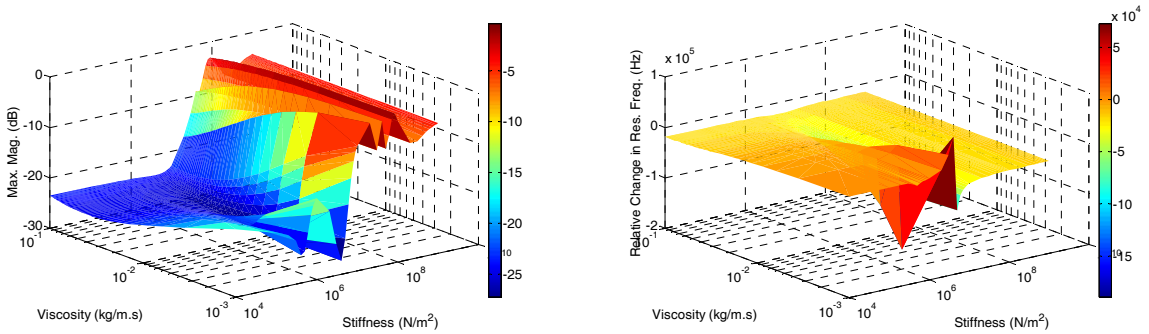

(a) (b)

Figure 5-30 Effect of the changes in the single viscoelastic layer viscosity and stiffness on the MTSM magnitude (a) and resonance frequency (b) response (relative changes in resonance frequency and absolute values of attenuation in dB) at 15 MHz in Stage II.

The MTSM/GA technique has been applied to determine the properties of the viscoelastic layer in stage II. The results obtained from the technique are presented in table 5-14.

Table 5-14 Properties of single viscoelastic layer determined by the MTSM/GA technique and % errors in stage II at 15 MHz

Properties	Values Input to TLM	Values Determined by MTSM/GA Technique	Error (%)
d_1 (nm)	1000	1020	2
G_1' (N/m^2)	2x10^6	2.01x10^6	0.5
η_1 (kg/m.s)	7x10^{-3}	7.02x10^{-3}	0.9
ρ_1 (kg/m^3)	1100	1150	5

As seen from table 5-14, stiffness and viscosity values are determined with less than 1% accuracy while the error increases for thickness and density values. It is hypothesized that the reason of higher error in stage II at 15 MHz due to the low quality factor. Experimentally observed quality factor for a MTSM sensor is ~40K and the initial loses is ~ 0.036 dB in air. In stage II, the quality factor drops to 0 and the magnitude decreases to -26 dB. The MTSM sensor becomes more damped and the sensitivity decreases. The more detailed analysis of the effect of quality factor on MTSM/GA sensor technique is discussed in section 5.8. When the MTSM sensor is highly damped (when α_R < -25dB) the accuracy of the genetic algorithm decreases. Furthermore a second solution is also observed in stage II at 15 MHz (similar phenomenon occurred at 5 MHz in stage II).

In stage III, G' becomes 27 times bigger than G", where G' = 5x10^7 N/m^2 and G" = 0.19x10^7 N/m^2. The viscoelastic system becomes more like a "hard rubbery" state. In this stage, maximum magnitude increases to -0.6 dB. The resonance frequency decreases dramatically from the value obtained in time t_2. The thickness of the layer was also decreased to 500 nm in stage III.

The magnitude and resonance frequency responses in stage III are given in fig. 5-31a and b. As seen from fig 5-31, when the viscosity is equal to 2x10^{-2} and stiffness value is 5x10^7 N/m^2, no oscillation is observed in the MTSM sensor response. The acoustic phase

shift throughout the viscoelastic layer is calculated to be 0.04π which is smaller than 0.5 π. Therefore the upper film displacement is large and in phase with the driving resonator surface. In contrast to the phenomenon seen in stage II, the frequency is lower than for the uncoated resonator.

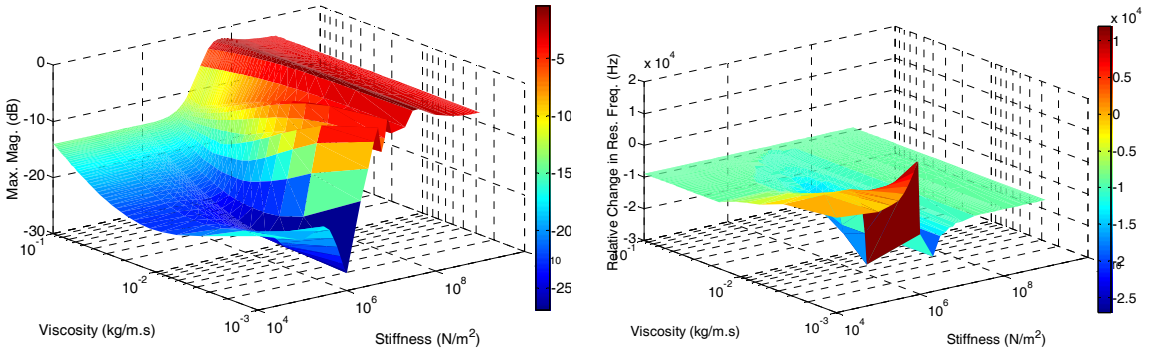

(a) (b)

Figure 5-31 Effect of the changes in the single viscoelastic layer viscosity and stiffness on the MTSM magnitude (a) and resonance frequency (b) response (relative changes in resonance frequency and absolute values of attenuation in dB) at 15 MHz in Stage III.

The MTSM/GA technique has been applied to determine the properties of the viscoelastic layer in stage III. The results obtained from the technique are presented in table 5-15. As seen from the table, all four parameters are determined with less than 1 % error by the MTSM/GA technique. Single solution was obtained.

Table 5-15 Properties of single viscoelastic layer determined by the MTSM/GA technique and % errors in stage III at 15 MHz

Properties	Values Input to TLM	Values Determined by MTSM/GA Technique	Error (%)
d_1 (nm)	500	502	0.5
G' (N/m^2)	$5x10^7$	$5.04x10^7$	0.8
η_1 (kg/m.s)	$2x10^{-2}$	$2.02x10^{-2}$	1
ρ_1 (kg/m^3)	1200	1190	1

In the stage IV, the viscoelastic layer still shows a “hard rubbery” properties where G” is around 53 times bigger than G’ (G’ = $5x10^8$ N/m^2 and G” = $0.094x10^8$ N/m^2). The losses at the resonance frequency increased to -0.33 dB, which is slightly higher than the losses in air (-0.31 dB). In this stage the viscoelastic layer is almost solid like system with a very small viscous contribution. As seen from fig. 5-32a and b, no oscillations were observed in maximum magnitude and resonance frequency response of the MTSM sensor when the stiffness and viscosity values are $5x10^8$ N/m^2 and 10^{-1} kg/m.s. The acoustic shift was calculated to be 0.012π which is ~43 times smaller than $0.5\ \pi$. Therefore the frequency value is smaller than the resonance frequency value in air and very small losses (-0.33) observed.

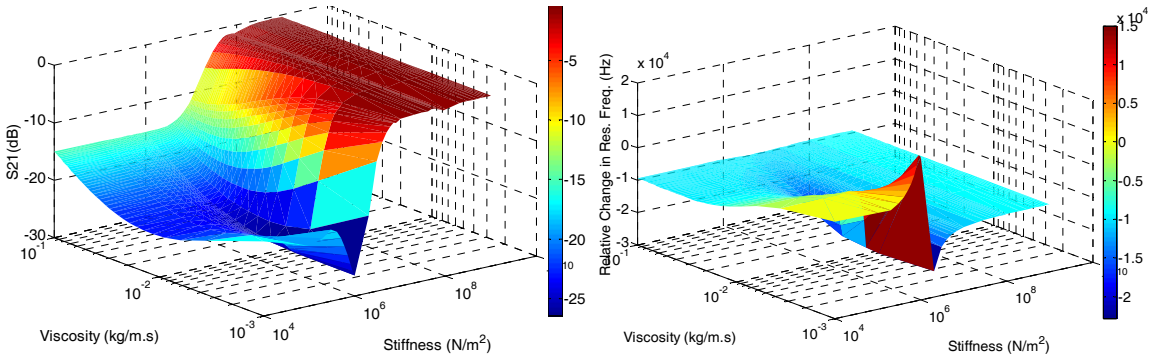

Figure 5-32 Effect of the changes in the single viscoelastic layer viscosity and stiffness to MTSM magnitude (a) and resonance frequency (b) response (relative changes in resonance frequency and absolute values of attenuation in dB) at 15 MHz in Stage IV.

The MTSM/GA technique has been applied to determine the properties of the viscoelastic layer in stage III at 15 MHz. The results obtained from the technique are presented in table 5-16. As seen from the table, all four parameters are determined with less than 1 % error by MTSM/GA technique. Single solution was obtained.

Table 5-16 Properties of single viscoelastic layer determined by the MTSM/GA technique and % errors in stage IV at 15 MHz

Properties	Values Input to TLM	Values Determined by MTSM/GA Technique	Error (%)
d_1 (nm)	500	499	0.2
G_1' (N/m^2)	$5x10^8$	$5.05x10^8$	1
η_1 (kg/m.s)	10^{-1}	$1.01x10^{-2}$	1
ρ_1 (kg/m^3)	1300	1290	1

5.9.3 Analysis of the MTSM/GA technique for single layer viscoelastic systems at 25 MHz

The changes in the magnitude and phase responses of the MTSM sensor to the evaporation-induced deposition process has been simulated at 25 MHz using transmission line model and presented in fig. 5-33a and b. Time responses of maximum magnitude and resonance frequency are given in fig. 5-33c. As seen from fig. 5-33c, the maximum magnitude decreases until time t_2, and reaches to the value of -20 dB. The resonance frequency continuously decreases until the end of evaporation process. The acoustic signature of MTSM sensor differs than the ones obtained at 5 MHz and 15 MHz.

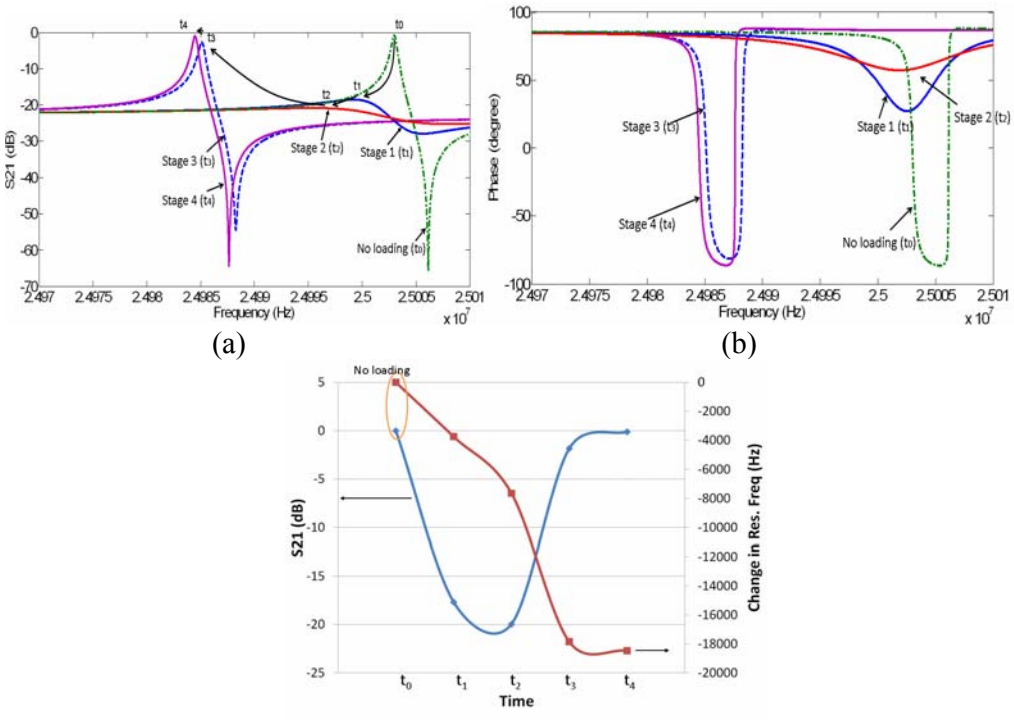

Figure 5-33 Change in magnitude (a) and phase (b) responses of the MTSM sensor during evaporation process. (c) Change in maximum magnitude and resonance frequency by time at 25 MHz. (case: single-layer viscoelastic system)

In stage I, the viscoelastic layer shows a "lossy like" properties where G" is 3 times higher than G', (G' = 10^5 N/m^2 and G" = 3.1×10^5 N/m^2). The magnitude and the resonance frequency responses of MTSM sensor decrease compared to the values in air reference. The penetration depth (~200 nm) is much smaller than the column thickness (3 μm). In other words, the loading is considered as semi-infinite medium and there is no reflection of acoustic wave from the column surface. This can be seen in both in magnitude and frequency responses shown in fig. 5-34.

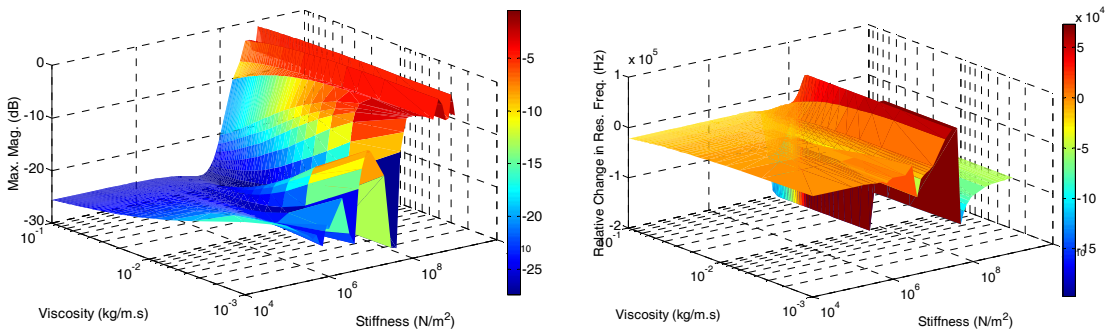

(a) (b)

Figure 5-34 Effect of the changes in the single viscoelastic layer viscosity and stiffness on the MTSM magnitude (a) and resonance frequency (b) response (relative changes in resonance frequency and absolute values of attenuation in dB) at 25 MHz in Stage I.

The MTSM/GA technique has been applied to determine the properties of the viscoelastic layer in stage I. The results obtained from the technique are presented in table 5-17. As seen from the table, stiffness, viscosity and density values are determined with less than 1 % error by MTSM/GA technique. As expected, the thickness value had a larger error (80 %) due to fact that the penetration depth is much smaller than the thickness of the column.

Table 5-17 Properties of single viscoelastic layer determined by the MTSM/GA technique and % errors in stage I at 25 MHz

Properties	Values Input to TLM	Values Determined by MTSM/GA Technique	Error (%)
d_1 (nm)	3000	5500	80
G_1' (N/m^2)	10^5	$0.99x10^5$	1
η_1 (kg/m.s)	$2x10^{-3}$	$1.98x10^{-3}$	0.2
ρ_1 (kg/m^3)	1000	1010	1

In stage II, the viscoelastic layer shows a "transition" state properties where G' is ~2 times bigger than G' (G' = $2x10^6$ N/m^2 and G" = $1.1x10^6$ N/m^2). In this stage, both the maximum magnitude and the resonance frequency decrease from the values in stage I. As seen in fig. 5-35, when stiffness value is $2x10^6$ N/m^2 and viscosity is equal to $7x10^{-3}$ kg/m.s, the MTSM sensor shows oscillatory response.

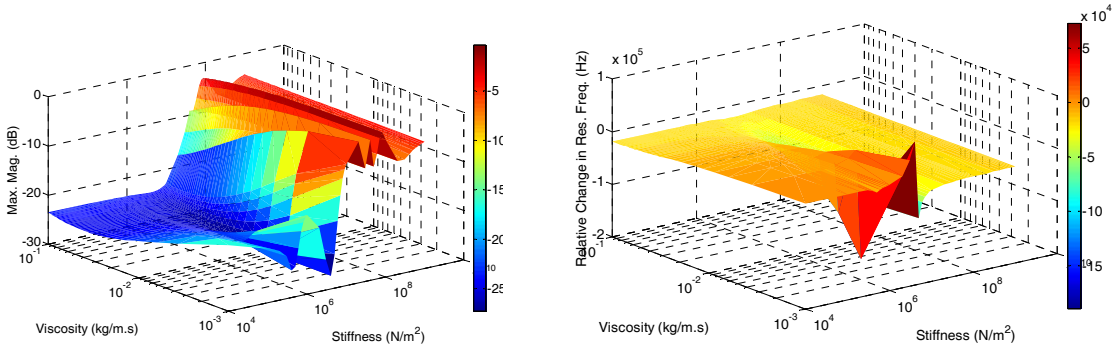

(a) (b)

Figure 5-35 Effect of the changes in the single viscoelastic layer viscosity and stiffness on the MTSM magnitude (a) and resonance frequency (b) response (relative changes in resonance frequency and absolute values of attenuation in dB) at 25 MHz in Stage II.

As seen from table 5.18, the properties were not able to be determined with less than 1 % error. While the error for viscosity and density were 30 % and 10 % respectively, the error for stiffness were even higher than 100 %. Furthermore the MTSM/GA technique was not able to converge to a single thickness value.

Table 5-18 Properties of single viscoelastic layer determined by the MTSM/GA technique and % errors in stage II at 25 MHz

Properties	Values Input to TLM	Values Determined by MTSM/GA Technique	Error (%)
d_1 (nm)	1000	NA	NA
G_1' (N/m^2)	2x10^6	10^5	NA
η_1 (kg/m.s)	7x10^{-3}	5x10^{-3}	30
ρ_1 (kg/m^3)	1100	1000	10

The penetration depth of the acoustic wave in stage 2 at 25 MHz is calculated to be 1.17 μm. The column height is 1 μm, which is very close to the penetration depth (δ) value. Therefore it can be hypothesized that if the penetration depth of the acoustic wave is close to the column height the MTSM/GA technique may not work efficiently. To test this hypothesis, several hypothetical viscoelastic layers have been loaded on the MTSM sensor

and the acoustic responses of these systems were simulated by using TLM (fig 5-36). The properties of the layer were $\eta = 7x10^{-3}$ kg/m.s, $\rho = 1100$ kg/m^3, $C = 2x10^6$ N/m^2.

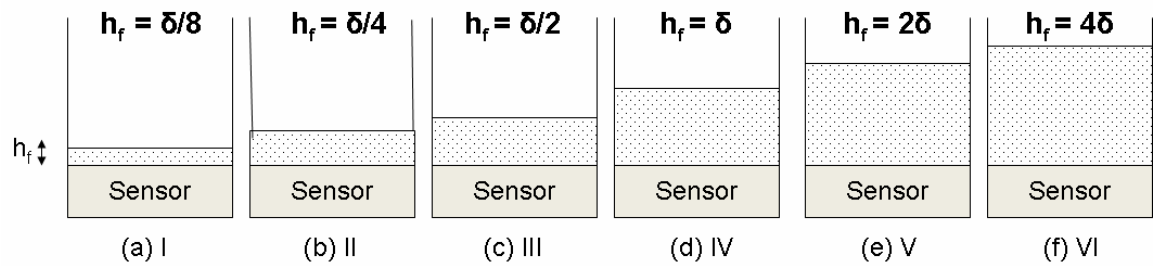

Figure 5-36 Hypothetical one-layer viscoelastic layers with difference column heights (h_f) a) $h_f = \delta/4$, b) $h_f = \delta/2$, c) $h_f = 3\delta/4$, and d) $h_f = \delta$ e) $h_f = 4\delta/3$ f) $h_f = 2\delta$

The acoustic signature of the hypothetical biological process shown above is presented in fig. 5-37. As seen from fig. 5-37, the oscillations can be seen in both responses with the increase of the thickness of the viscoelastic layer. The cause of the oscillations was discussed in the previous sections.

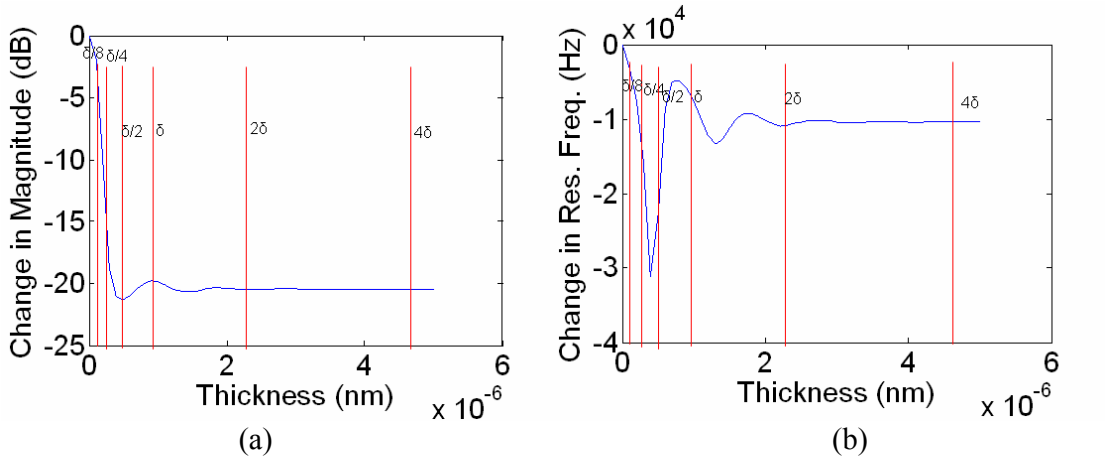

Figure 5-37 MTSM sensor's acoustic response and penetration depth relationship at 25 MHz

The decay length of the acoustic wave was ~1170 nm. The layer thickness (h_f) has been selected to be equal to δ/8, δ/4, δ/2, δ, 2δ, 4δ (δ= penetration depth). The calculated maximum magnitude and resonance frequency values were plugged into the MTSM/GA technique. The errors in the determined parameters are presented in table 5-19.

Table 5-19 Absolute errors in the MTSM/GA technique for single layer viscoelastic system at 25 MHz with the change of h_f /δ ratio

Properties	Error (%)					
	h_f =δ/8	h_f =δ/4	h_f =δ/2	h_f =δ	h_f =2δ	h_f =4δ
d (nm)	0.5	0.8	NA	50	30	25
C (N/m^2)	0.5	0.9	10	7	2.5	0.3
η (kg/m.s)	0.6	1	20	8	5	0.5
ρ (kg/m^3)	0.9	0.8	4	5	2	0.8

As seen from table 5-19, when the layer thickness approaches to the value where the oscillation occurs in the acoustic responses, the accuracy of the MTSM/GA technique dramatically decreases. When $h_f > 2\delta$, the layer is considered as semi-infinite medium, and the thickness value is no longer determined accurately but the other values are estimated with less than 1 % error value. Therefore it can be concluded that if $h_f \sim \delta$, the MTSM/GA technique will not able to provide accurate values of the layer properties.

In stage III, G' becomes 16 times higher than G", where G' = $5x10^7$ N/m^2 and G" = $0.34x10^7$ N/m^2. The viscoelastic system becomes more like a "hard rubbery" state. In this stage, maximum magnitude increases to -2.7 dB. The resonance frequency continued to decrease from the value obtained in time t_2. The thickness of the layer was also decreased to 500 nm in stage III.

The magnitude and resonance frequency responses, when the thickness and density values are set to 500 nm and 1200 kg/m^3 respectively, are given in fig. 5-38a and b. As seen

from fig 5-38, when the viscosity is equal to $2x10^{-2}$ and stiffness value is $5x10^{7}$ N/m^2, no oscillation is observed in the MTSM sensor response.

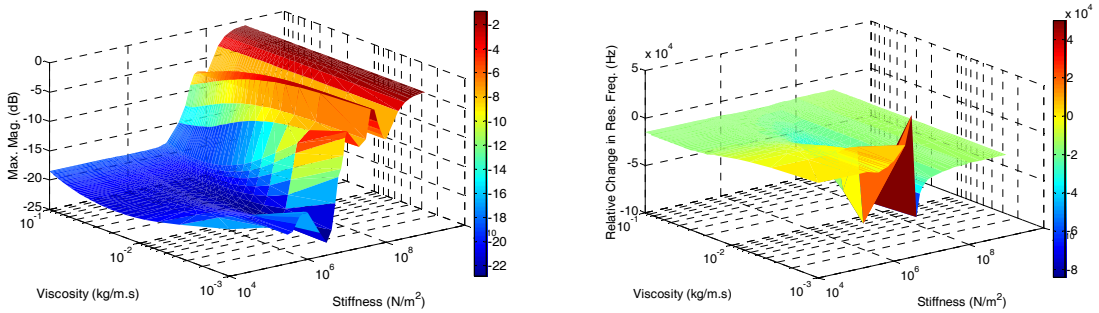

(a) (b)

Figure 5-38 Effect of the changes in the single viscoelastic layer viscosity and stiffness to MTSM magnitude (a) and resonance frequency (b) response (relative changes in resonance frequency and absolute values of attenuation in dB) at 25 MHz in Stage III.

The MTSM/GA technique has been applied to determine the properties of the viscoelastic layer in stage III at 25 MHz. The results obtained from the technique are presented in table 5-20. As seen from the table, all four parameters are determined with less than 1 % error by MTSM/GA technique.

Table 5-20 Properties of single viscoelastic layer determined by the MTSM/GA technique and % errors in stage III at 25 MHz

Properties	Values Input to TLM	Values Determined by MTSM/GA Technique	Error (%)
d_1 (nm)	500	499	0.2
G_1' (N/m^2)	$5x10^7$	$5.04x10^7$	0.8
η_1 (kg/m.s)	$2x10^{-2}$	$2.01x10^{-2}$	0.5
ρ_1 (kg/m^3)	1200	1201	0.1

In the stage IV, the viscoelastic layer still shows a “hard rubbery” properties where G” is around 32 times higher than G’ (G’ = $5x10^8$ N/m^2 and G” = $0.094x10^8$ N/m^2). The losses at the resonance frequency decreased to -0.855 dB, which is slightly higher than the losses in air (-0.85 dB). As seen from fig. 5-39a and b, no oscillations were observed in

maximum magnitude and resonance frequency response of the MTSM sensor when the stiffness and viscosity values are $5x10^8$ N/m^2 and 10^{-1} kg/m.s.

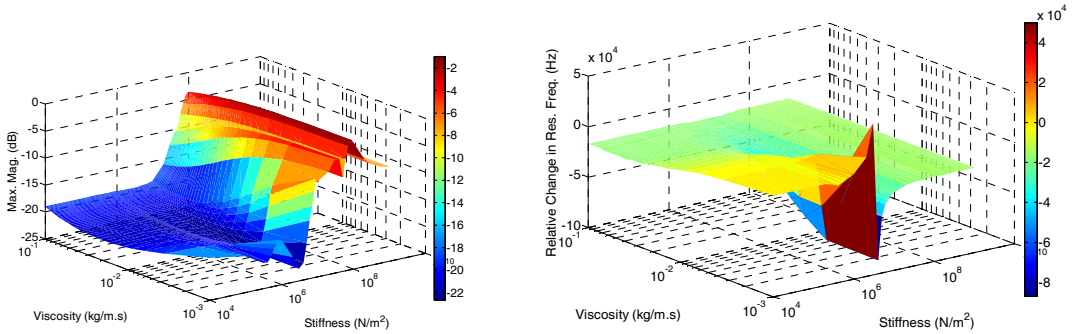

(a) (b)

Figure 5-39 Effect of the changes in the single viscoelastic layer viscosity and stiffness on the MTSM magnitude (a) and resonance frequency (b) response (relative changes in resonance frequency and absolute values of attenuation in dB) at 25 MHz in Stage IV.

The MTSM/GA technique has been applied to determine the properties of the viscoelastic layer in stage IV at 25 MHz. The results obtained from the technique are presented in table 5-21. As seen from the table, all four parameters are determined with less than 1 % error by the MTSM/GA technique.

Table 5-21 Properties of single viscoelastic layer determined by the MTSM/GA technique and % errors in stage IV at 25 MHz

Properties	Values Input to TLM	Values Determined by MTSM/GA Technique	Error (%)
d_1 (nm)	500	505	1
G_1' (N/m^2)	$5x10^8$	$4.99x10^8$	0.2
η_1 (kg/m.s)	10^{-1}	$1.01x10^{-1}$	1
ρ_1 (kg/m^3)	1300	1290	0.7

5.9.4 Analysis of the MTSM/GA technique for single layer viscoelastic systems at 35 MHz

The changes in the magnitude and phase responses of the MTSM sensor to the evaporation-induced deposition process has been simulated at 35 MHz using transmission line model and presented in fig. 5-40a and b. Time responses of maximum magnitude and resonance frequency are given in fig. 5-40c. As seen from fig. 5-40c, the maximum magnitude decreases until time t_2, and reaches to the value of -17 dB. The resonance frequency continuously decreases until t_3 and slightly increases at the end of evaporation process. The acoustic signature of he MTSM sensor again differs than the ones obtained at 5 MHz, 15 MHz and 25 MHz.

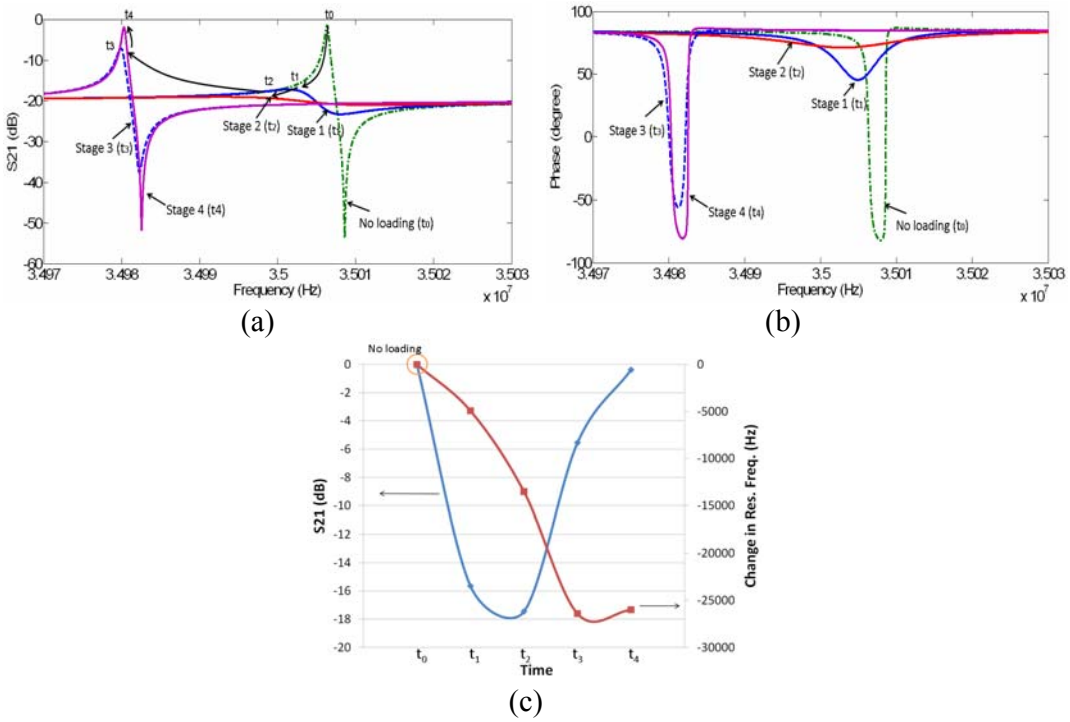

Figure 5-40 Change in magnitude (a) and phase (b) responses of MTSM sensor during evaporation process. (c) Change in maximum magnitude and resonance frequency by time at 35 MHz.

In stage I, the viscoelastic layer shows a “transition state” properties where G” is only 3 times higher than G’, (G’ = 10^5 N/m^2 and G” = 4.4x10^5 N/m^2). The magnitude and the resonance frequency responses of the MTSM sensor decrease compared to the values in air reference. The penetration depth (~200 nm) is much smaller than the column thickness (3 μm). In other words, the loading is considered as semi-infinite medium and there is no reflection of acoustic wave from the column surface. This can be seen in both in magnitude and frequency responses shown in fig. 5-41.

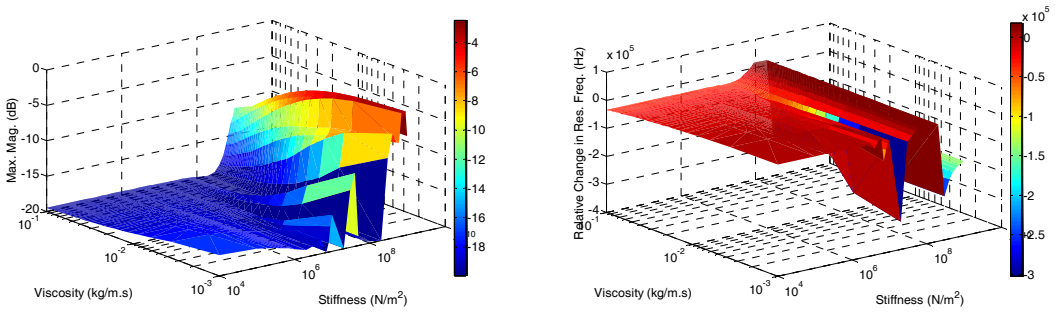

(a) (b)

Figure 5-41 Effect of the changes in the single viscoelastic layer viscosity and stiffness to MTSM magnitude (a) and resonance frequency (b) response (relative changes in resonance frequency and absolute values of attenuation in dB) at 35 MHz in Stage I.

The MTSM/GA technique has been applied to determine the properties of the viscoelastic layer in stage I. The results obtained from the technique are presented in table 5-22. As seen from the table, stiffness, viscosity and density values are determined with less than 1 % error by the MTSM/GA technique. As expected, the thickness value had a larger error (80 %) due to fact that the penetration depth is much smaller than the thickness of the column.

Table 5-22 Properties of single viscoelastic layer determined by the MTSM/GA technique and % errors in stage I at 35 MHz

Properties	Values Input to TLM	Values Determined by MTSM/GA Technique	Error (%)
d_1 (nm)	3000	5000	80
G_1' (N/m^2)	10^5	$0.99x10^5$	1
η_1 (kg/m.s)	$2x10^{-3}$	$1.98x10e^{-3}$	0.9
ρ_1 (kg/m^3)	1000	1009	1

In stage II, the viscoelastic layer shows a "soft rubbery" state properties where G' is ~1.3 times bigger than G' (G' = $2x10^6$ N/m^2 and G" = $1.54x10^6$ N/m^2). In this stage, both the maximum magnitude and the resonance frequency decrease from the values in stage I. As seen in fig. 5-42, when stiffness value is $2x10^6$ N/m^2 and viscosity is equal to $7x10^{-3}$ kg/m.s, the MTSM sensor shows oscillatory response. Therefore it is expected that the MTSM/GA technique may not provide accurate values for the viscoelastic layer and this can be seen in table 5-23.

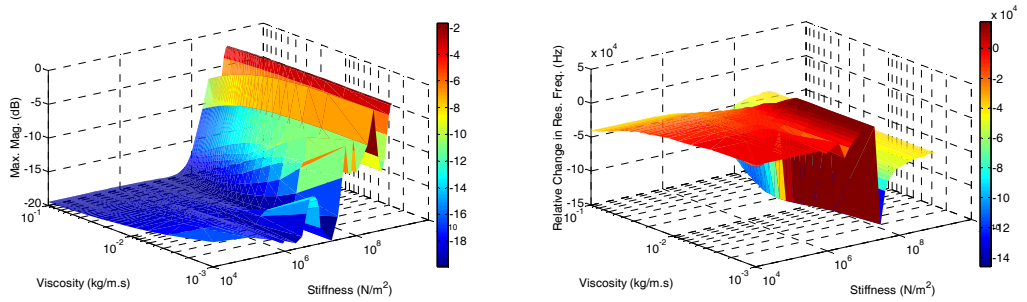

(a) (b)

Figure 5-42 Effect of the changes in the single viscoelastic layer viscosity and stiffness on the MTSM magnitude (a) and resonance frequency (b) response (relative changes in resonance frequency and absolute values of attenuation in dB) at 35 MHz in Stage II.

The penetration depth of the acoustic wave in stage II at 35 MHz is calculated to be 0.63 μm. The column height is 1 μm, which is very close to the penetration depth value. Therefore the layer properties can not determine accurately (see section 5.9.3).

Table 5-23 Properties of single viscoelastic layer determined by the MTSM/GA technique and % errors in stage II at 35 MHz

Properties	Values Input to TLM	Values Determined by MTSM/GA Technique	Error (%)
d_1 (nm)	1000	NA	NA
G_1' (N/m^2)	$2x10^6$	10^5	NA
η_1 (kg/m.s)	$7x10^{-3}$	$5x10^{-3}$	20
ρ_1 (kg/m^3)	1100	1000	15

In stage III, G' becomes 16 times higher than G", where G' = $5x10^7$ N/m^2 and G" = $0.44x10^7$ N/m^2. The viscoelastic system becomes more like a "hard rubbery" state. In this stage, maximum magnitude increases to -5.6 dB. The resonance frequency continued to decrease from the value obtained in time t_2. The thickness of the layer was also decreased to 500 nm in stage III.

The magnitude and resonance frequency responses, when the thickness and density values are set to 500 nm and 1200 kg/m^3 respectively, are given in fig. 5-43a and b. As seen from fig 5-43, when the viscosity is equal to $2x10^{-2}$ kg/m.s and stiffness value is $5x10^7$ N/m^2, no oscillation is observed in MTSM sensor response.

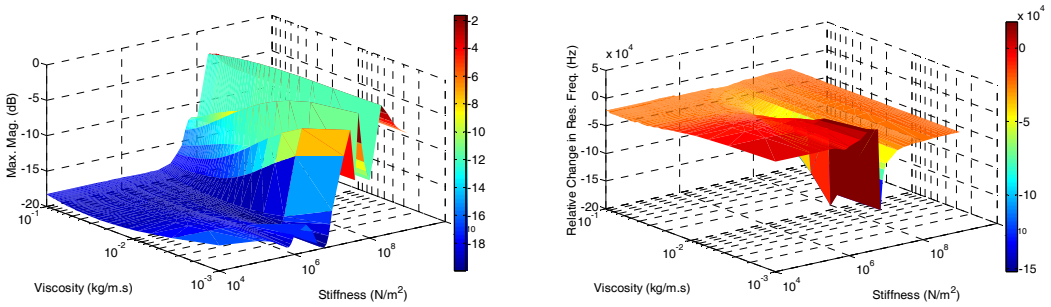

Figure 5-43 Effect of the changes in the single viscoelastic layer viscosity and stiffness to MTSM magnitude (a) and resonance frequency (b) response (relative changes in resonance frequency and absolute values of attenuation in dB) at 35 MHz in Stage III.

The MTSM/GA technique has been applied to determine the properties of the viscoelastic layer in stage III. The results obtained from the technique are presented in table 5-24. As seen from the table, all four parameters are determined with less than 1 % error by the MTSM/GA technique.

Table 5-24 Properties of single viscoelastic layer determined by the MTSM/GA technique and % errors in stage III at 35 MHz

Properties	Values Input to TLM	Values Determined by MTSM/GA Technique	Error (%)
d_1 (nm)	500	499	0.9
G' (N/m^2)	5x10^7	5.04x10^7	1
η_1 (kg/m.s)	2x10^{-2}	2.01x10^{-2}	0.5
ρ_1 (kg/m^3)	1200	1201	0.2

In stage IV, the viscoelastic layer still shows a "hard rubbery" properties where G" is around 23 times higher than G' (G' = 5x10^8 N/m^2 and G" = 0.22x10^8 N/m^2). The losses at the resonance frequency decreased to -3 dB, which is still higher than the losses in air (-1.59 dB). As seen from fig. 5-44a and b, no oscillations were observed in maximum magnitude and resonance frequency response of MTSM sensor when the stiffness and viscosity values are 5x10^8 N/m^2 and 10^{-1} kg/m.s.

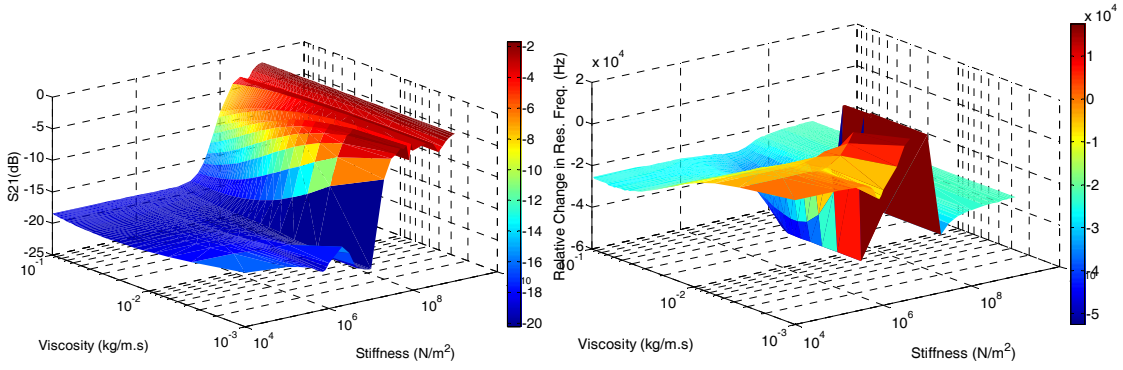

(a) (b)

Figure 5-44 Effect of the changes in the single viscoelastic layer viscosity and stiffness to MTSM magnitude (a) and resonance frequency (b) response (relative changes in resonance frequency and absolute values of attenuation in dB) at 35 MHz in Stage IV.

The MTSM/GA technique has been applied to determine the properties of the viscoelastic layer in stage IV. The results obtained from the technique are presented in table 5-25. As seen from the table, all four parameters are determined with less than 1 % error by the MTSM/GA technique.

Table 5-25 Properties of single viscoelastic layer determined by the MTSM/GA technique and % errors in stage IV at 35 MHz

Properties	Values Input to TLM	Values Determined by MTSM/GA Technique	Error (%)
d_1 (nm)	500	505	0.6
G_1' (N/m^2)	$5x10^8$	$4.99x10^8$	0.2
η_1 (kg/m.s)	10^{-1}	$1.01x10^{-2}$	0.9
ρ_1 (kg/m^3)	1300	1290	1

5.10 Summary and Conclusions

A genetic algorithm (GA)-based data analysis method combined with the MTSM measurement technique was developed and theoretically validated.

Initially, the theoretical foundation of the MTSM/GA technique for single-layer viscoelastic systems was developed. The influence of several important quantities, such as quality factor and experimental error, on the MTSM/GA technique has been critically evaluated. Finally, the MTSM/GA technique has been applied to determine the mechanical and structural processes of a hypothetical biological adsorption process (representation of collagen adsorption process).

It was demonstrated that the MTSM/GA technique for single-layer viscoelastic systems is capable of:

1. Determining the mechanical (density, elasticity, viscosity) and structural properties (thickness) of the single-layer viscoelastic system with less then 1 % error theoretically.
2. Full quantification of biological interfacial processes by providing the “acoustic signatures” of the interfacial process at each harmonic operation (resultant of multi-harmonic operation of the MTSM) and applying GA-based algorithm to determine the properties of the interfacial layer.

Also it was shown, that for some certain conditions, the accuracy of the MTSM/GA technique could decrease for one or more variables. For example, semi-infinite viscoelastic layers, acoustically thin layers and the viscoelastic layers with thicknesses value close to the shear wave penetration depth represent such special cases. Next, it was shown that in some cases more than one solution can be obtained for the same acoustic response. In this case, monitoring the kinetics of the biological interfacial processes and multi-harmonic operation can provide unique tools to identify the right solution.

In conclusion, it was shown, for the first time, that the MTSM/GA technique provides very powerful tools such as multi-layered modeling, multi-harmonic operation, monitoring real-time kinetics and GA-based data analysis algorithm, and can be used to determine quantitative mechanical and structural properties of the single-layer viscoelastic layers.

6 EXPERIMENTAL VALIDATION OF THE MTSM/GA TECHNIQUE FOR SINGLE LAYER VISCOELASTIC SYSTEMS

Development of a MTSM sensor measurement system is initially described. Then, for the calibration purposes, the MTSM sensors was loaded with different glycerin/DI water concentrations and the properties of the Newtonian mediums were determined by using the MTSM/GA technique. The results were compared to literature values. Finally, after the calibration of the MTSM system is completed, the MTSM sensor was spin-coated with SU8-2002 polymer layers, and their mechanical properties were determined by the MTSM/GA technique. Following that, the signature of an evaporation process of biological samples (type I collagen) has been characterized by using the MTSM measurement system.

The mechanical and structural properties of the SU8-2002 and collagen layers were determined theoretically. For this purpose, the thicknesses of the layers were measured by using atomic force microscopy (AFM) and profilometer devices. The density values were obtained from the literature. After two unknowns were determined, the problem was no longer under-determined, thus the other two unknown parameters (viscosity and density) were determined. The results obtained by the MTSM/GA technique was compared with the ones obtained theoretically.

6.1 Development of a MTSM sensor measurement system

A 14 mm diameter, 0.33 mm thick, 5 MHz quartz crystal with bonded 7 mm gold electrodes was placed in a custom fabricated brass sensor holder. During the experiments, only one side of the MTSM sensor was loaded with the target samples. The sensor holder was connected to a Network Analyzer (NA) (HP4395A) through a microwave switch, which

enables multiple sensor measurement simultaneously. The sensor was connected to the NA to generate a shear oscillation at each harmonic and to measure the S21 response of the MTSM sensor. A personal computer controlled the network analyzer and collected the data at 5 MHz, 15 MHz, 25 MHz and 35 MHz. The experiments were done in room temperature ($24^{o}C \pm 3^{o}C$). Tracking points which were discussed in chapter 4 were monitored during the experiments (fig. 6-1). The sampling rate was 60 seconds. Each experiment was repeated three times unless otherwise is indicated.

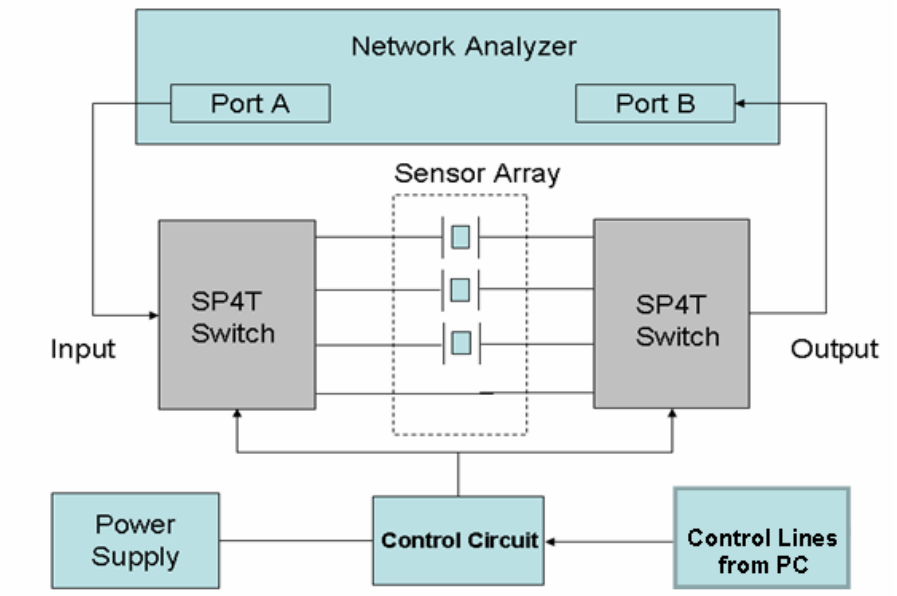

(a)

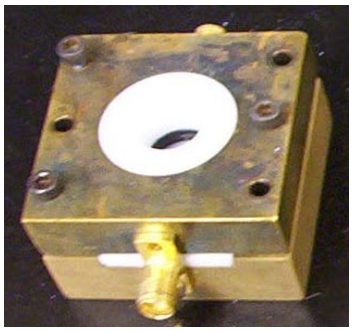

(b)

Figure 6-1 (a) MTSM sensor network analyzer based electronics measurement system (b) MTSM sensor static holder

6.2 Validation of the MTSM/GA technique using Newtonian liquids

Three concentrations of deionized/glycerin concentrations (0%, 10% and 20%) have been prepared. The MTSM sensor response to Newtonian mediums can be determined with Kanazawa equation which is shown below;

$$\Delta f = -f^{3/2}\left(\frac{\rho_l \eta_l}{\pi \rho_q \mu_q}\right)^{1/2} \tag{6.1}$$

where ρ_l and η_l are density and viscosity of liquid while ρ_q and μ_q are density and elastic modulus of the MTSM sensor and f represents the resonance frequency of the MTSM sensor. As seen in eq. 5.4, the change in the response frequency is proportional to the square root of the product of density and viscosity of the liquid. The Kanazawa equation represents the frequency change of the series resonance circuit, which excludes Co. Therefore the experimental results were compared to the theoretical results obtained from the TLM, not from Kanazawa equation.

6.2.1 Determination of deionized water properties

Initially, the MTSM/GA technique was validated theoretically for determination of DI water properties. Typical DI water properties in room temperature (η=~10^{-3} kg/m.s., C = 0 N/m^2, ρ=~1000 kg/m^3) (Greczylo and Debowska et al., 2005) were simulated by using TLM. The MTSM sensor was loaded with 200 µl of DI water in room temperature. The column height was 2 mm. The comparison of theoretical and experimental results at 15 MHz, 25 MHz and 35 MHz were compared and presented in fig. 6-2. Large error (>50 %) between theoretical and experimental results at 5 MHz have been observed. The possible reasons have

been discussed in chapter 4. Therefore only the acoustic response at higher harmonics is presented.

Initially, the MTSM/GA technique has been validated theoretically. Therefore a hypothetical DI water layer has been loaded on the MTSM sensor and acoustic response was simulated by using the TLM. The column height of the medium was kept to be much higher than the penetration depth (h (column thickness) = 10 μm, δ (penetration depth) = 250 nm). The maximum magnitude and resonance frequency values were plugged into the MTSM/GA technique. The results obtained by the MTSM/GA technique were presented in table 6-1. As seen from table 6-1, the MTSM/GA technique determines the DI water properties, except thickness value, with less than 1 % error. As discussed before, in case of semi-infinite medium loading on the MTSM sensor surface, the thickness value will be equal to penetration depth or above the penetration depth.

Table 6-1 Theoretical validation of the MTSM/GA technique for determination of DI water properties at 5 MHz, 15 MHz, 25 MHz, and 35 MHz.

MTSM Frequency (MHz)	η kg/m.s	C N/m2	ρ kg/m3	d (nm)
5	$1.01x10^{-3}$	0	1002	800
15	10^{-3}	0	1003	450
25	$1.01x10^{-3}$	0	1001	370
35	10^{-3}	0	1001	290

Next, the MTSM/GA technique has been validated experimentally. The MTSM sensors were loaded with 200 μl of DI water solution in room temperature. The relative changes in the resonance frequency and absolute changes in the magnitude responses have been monitored and presented in fig. 6-2. The experimentally obtained resonance frequency and magnitude values were plugged into the MTSM/GA technique and results were presented in table 6-2.

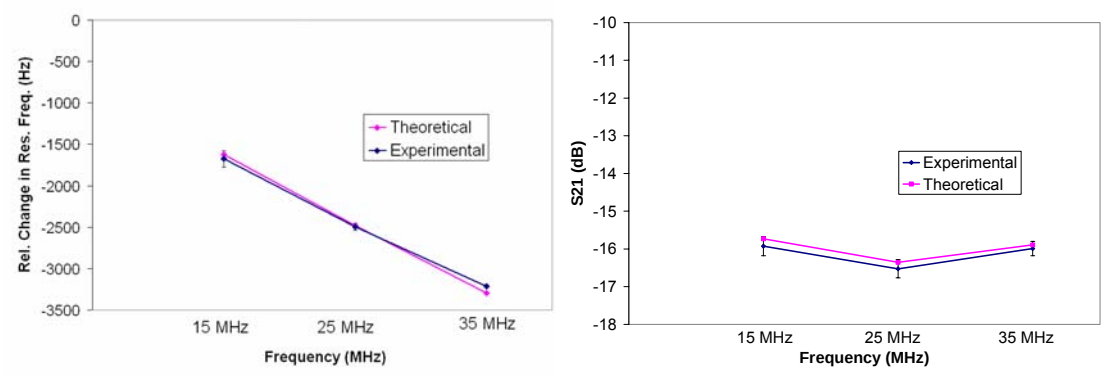

(a) (b)

Figure 6-2 Theoretical and experimental resonance frequency (a) and maximum magnitude change (b) of the MTSM sensor loaded with DI water at 15 MHz, 25 MHz and 35 MHz.

The experimentally obtained resonance frequency and magnitude values were plugged into the MTSM/GA technique and results were presented in table 6-2. As seen from the table, by only using maximum magnitude and resonance frequency values, the properties of deionized water is determined with less than 10 % error.

Table 6-2Experimental validation of the MTSM/GA technique for determination of DI water properties at 15 MHz, 25 MHz, and 35 MHz.

MTSM Frequency (MHz)	η (kg/m.s)	C (N/m^2)	ρ (kg/m^3)	d (nm)
15	$(1\pm0.012)x10^{-3}$	$(13\pm3)x10^{3}$	1001±0.2	147±3
25	$(1\pm0.08)x10^{-3}$	$(27\pm4)x10^{3}$	1001±0.4	110±1
35	$(1\pm0.02)x10^{-3}$	$(60\pm0.6)\ x10^{3}$	1001±0.5	100±3

It should be noted that the determined thickness values are close to the penetration depth of the acoustic wave which were calculated as 145 nm, 112 nm and 95 nm at 15 MHz, 25 MHz, and 35 MHz respectively.

6.2.2 Determination of 10 % glycerin/DI water solution properties

The MTSM sensors were loaded with 200 µl of 10 % glycerin/DI water solution in room temperature. The relative changes in the resonance frequency and absolute changes in the magnitude responses have been monitored and presented in fig. 6-3.

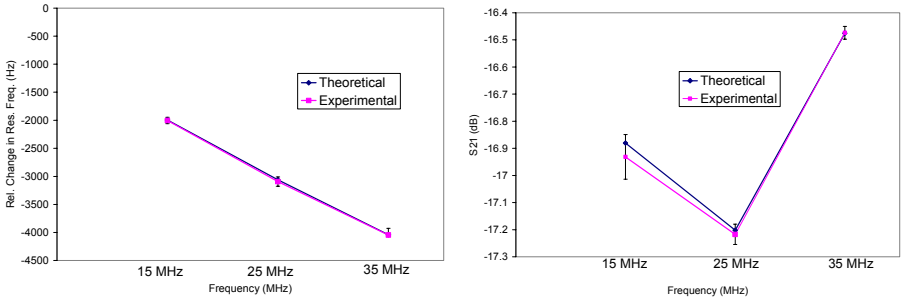

(a) (b)

Figure 6-3 Theoretical and experimental resonance frequency (a) and maximum magnitude change (b) of MTSM sensor loaded with 10% glycerin/DI water at 15 MHz, 25 MHz and 35 MHz.

Initially, the MTSM/GA technique was validated theoretically for determination of 10 % glycerin/DI water properties. Typical properties (η=1.4x10^{-3} kg/m.s., C = 0 N/m^2, ρ=1025 kg/m^3) (Greczylo and Debowska et al., 2005) were simulated by using TLM and then the maximum magnitude and frequency values were plugged into the MTSM/GA technique. The thickness of the water column (10 µm) was kept to be much larger than the penetration depth (~300 nm) at 5 MHz. The final resonance frequency and maximum magnitude values of the MTSM sensor were plugged into the MTSM/GA technique and the results are presented in table 6-3. As seen from table 6-3, the MTSM/GA technique determines 10% glycerin/DI water properties, except thickness value, with less than 1 % error. As explained before, in case of semi-infinite medium loading on MTSM sensor surface, the thickness value will be equal to penetration depth or above the penetration depth.

Table 6-3 Theoretical validation of the MTSM/GA technique for determination of 10 %glycerin/DI water properties at 5 MHz, 15 MHz, 25 MHz, and 35 MHz.

MTSM Frequency (MHz)	η (kg/m.s)	C (N/m^2)	ρ (kg/m^3)	d (nm)
5	$1.4x10^{-3}$	0	1025	950
15	$1.396x10^{-3}$	0	1028	700
25	$1.396x10^{-3}$	0	1027	540
35	$1.399x10^{-3}$	0	1025	470

Next, the MTSM/GA technique has been validated experimentally. The experimentally obtained resonance frequency and maximum magnitude values were plugged into the MTSM/GA technique and results were presented in table 6.4. As seen from the table, the properties of 10 % glycerin/DI water is determined with less than 20 % error.

Table 6-4Experimental validation of the MTSM/GA technique for determination of 10% glycerin/DI water properties at 15 MHz, 25 MHz, and 35 MHz.

MTSM Frequency (MHz)	η (kg/m.s)	C (N/m^2)	ρ (kg/m^3)	d (nm)
15	$(1.43\pm0.03)x10^{-3}$	0	1033±10	170±9
25	$(1.42\pm0.02)x10^{-3}$	0	1026±7	130±4
35	$(1.41\pm0.04)x10^{-3}$	0	1023±5	110±3

It should be noted that the determined thickness values were close to be equal to the penetration depth of the acoustic wave which were determined to be 170 nm, 130 nm and 111 nm at 15 MHz, 25 MHz, and 35 MHz respectively.

6.2.3 Determination of 20% glycerin/DI water solution's properties

The MTSM sensor was loaded with 200 μl of 20 % glycerin/DI water solution in room temperature. The relative change in resonance frequency and absolute change in the maximum magnitude have been monitored and presented in fig. 6-4.

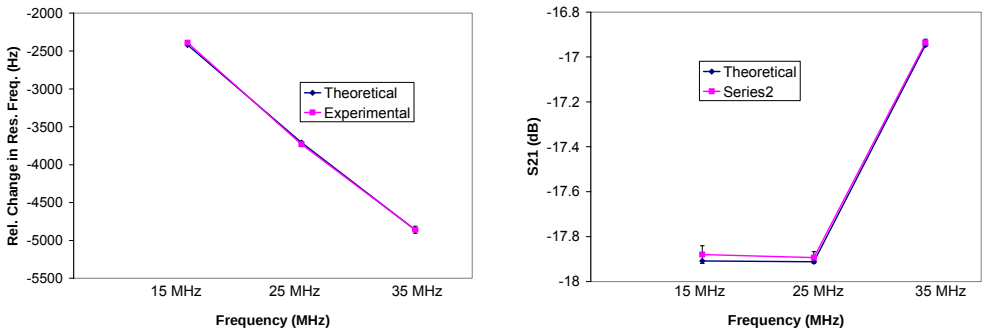

(a) (b)

Figure 6-4 Theoretical and experimental resonance frequency (a) and maximum magnitude change (b) of the MTSM sensor loaded with 20 % glycerin/DI water at 15 MHz, 25 MHz and 35 MHz.

Initially, the MTSM/GA technique was validated theoretically for determination of 20 % glycerin/DI water properties. Typical 20 % glycerin/DI water properties (η=1.9x10^{-3} kg/m.s, C = 0 N/m^2, ρ=1050 kg/m^3) (Greczylo and Debowska et al., 2005) were simulated by using the TLM and then the maximum magnitude and resonance frequency values were plugged into the MTSM/GA technique. The thickness of the water column (10 μm) was kept to be much larger than the penetration depth (~340 nm) at 5 MHz. The final resonance frequency and maximum magnitude values of the MTSM sensor were plugged into the MTSM/GA technique and the results were presented in table 6-5. As seen from table 6-5, the MTSM/GA technique determines the 20 % glycerin/DI water properties, except thickness value, with less than 1 % error. As explained before, in case of semi-infinite medium loading on MTSM sensor surface, the thickness value will be equal to penetration depth or above the penetration depth.

Table 6-5 Theoretical validation of the MTSM/GA technique for determination of 20 % glycerin/DI water properties at 5 MHz, 15 MHz, 25 MHz, and 35 MHz.

MTSM Frequency (MHz)	η kg/m.s	C N/m2	ρ kg/m3	d (nm)
5	1.901e-3	0	1049	1000
15	1.896e-3	0	1052	800
25	1.896e-3	0	1049	600
35	1.897e-3	0	1049	500

Next, the MTSM/GA technique has been validated experimentally. The experimentally obtained resonance frequency and maximum magnitude values were plugged into the MTSM/GA technique and results were presented in table 6.6. As seen from the table, the properties of 20% glycerin/deionized water is determined with less than 10% error.

Table 6-6 Experimental validation of the MTSM/GA technique for determination of 20 % glycerin/DI water properties at 15 MHz, 25 MHz, and 35 MHz.

MTSM Frequency (MHz)	η (kg/m.s)	C(N/m^2)	ρ (kg/m^3)	d (nm)
15	(2.05±0.01)e-3	0	1056±7	190±2
25	(2.02±0.04)e-3	0	1052±8	150±4
35	(2.01±0.02)e-3	0	1060±4	130±1

It should be noted that the determined thickness values were close to be equal to the penetration depth of the acoustic wave which were determined to be 200 nm, 150 nm and 130 nm at 15 MHz, 25 MHz, and 35 MHz respectively.

6.3 Validation of the MTSM/GA technique using SU8-2002 polymer layer

The MTSM/GA technique first experimentally tested with the polymer SU8-2002 layer spun coated on the sensor surface. The determined properties of the layer were compared with the values obtained from literature and independent measurements such as

atomic force microscopy and profilometer. The methods and chemicals used in the experiments are described below.

6.3.1 Materials and Methods

6.3.1.1 Deposition of the Thin Polymer Film

The SU 8-2002 (MicroChem) polymer solution was spun coated on the MTSM sensor by using the following procedure. First, the gold electrode surface of the MTSM sensors was cleaned using Piranha solution (one part of 30% H_2O_2 in three parts H_2SO_4). After 2 min exposure time, the sensors were rinsed with distilled water. The surface was dried in a stream of nitrogen gas. The SU8 – 2002 sample was dispensed on the MTSM sensor surface and sensors were spun coated for 40 seconds. The sensors were then soft baked for 1 min at 95 ^oC. The SU 8-2002 films were exposed to UV light for 4 seconds under 25 mJ/cm^2. It was followed by 1 min hard baking on hot plate at 95 ^oC.

6.3.1.2 Characterization of geometrical properties of the thin film

The thicknesses of the SU8 – 2002 films were determined by using optical profilometer (Zygo Inc. Model #: NV6200). For the thickness measurements, a very small portion of MTSM sensor surface was not exposed to UV light. After the films were developed, the SU 8-2002 layer was removed from this portion. To obtain different thicknesses of film layer, 1:1 solution of SU8-2002 and cyclopentanone (Acros Organics) was prepared. The surface topography of the film layer was measured by using atomic force microscopy (AFM). The prepared samples were gently placed on the glass slide installed on the atomic force microscope (Bioscope; Veeco), that was mounted on the inverted

fluorescence microscope (TE2000; Nikon, Melville, N.Y.). Measurements were done in contact mode and scan rate was 2 Hz. AFM method was also utilized for thickness measurement of the polymer layers.

Two different thicknesses of SU8 2002 layers were spin coated on the sensor surface and changes in the resonance frequency and maximum magnitude responses were monitored at 5 MHz, 15 MHz, 25 MHz and 35 MHz. The thicknesses of the layers were measured by using optical profilometer (fig. 6-5a). The average thicknesses of the layers were 1950±50 nm and 770±50 nm respectively. Surface topography of the SU8 - 2002 layers was measured by using AFM (fig. 6-5b). The average roughness of the layer was 20 nm and no cracks on the surface were observed.

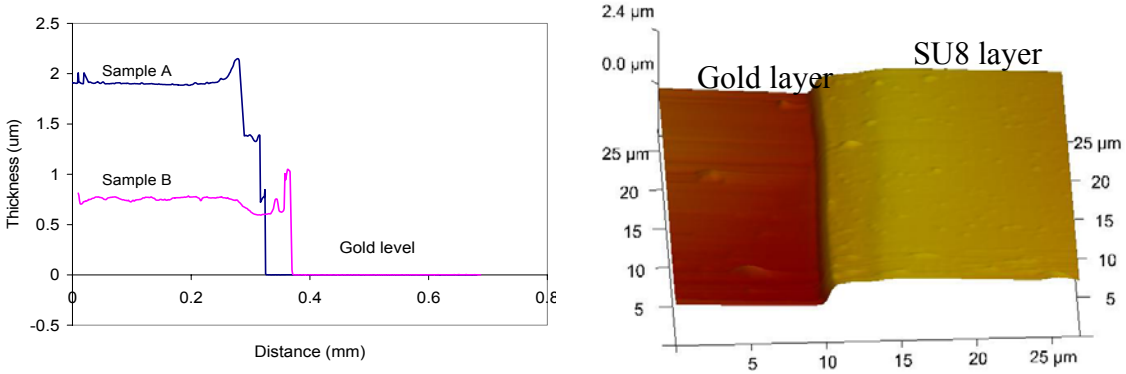

(a) (b)

Figure 6-5 a) Thickness measurements from optical profilometer sample A. SU8-2000 solution sample B. 1:1 dilution of SU8-2002 and cyclopentanone b) Surface topography of SU8 layer obtained by AFM.

The surface profile of SU8-2002 layer spun coated on the MTSM sensor has been investigated. Accurate measurement of the thickness profile of the SU8-2002 layers throughout the sensor surface is important since the thickness value contribute the viscoelastic response of the MTSM sensor. To do so, the 2 micron thick SU8-2002 polymer

has been spin coated on the MTSM sensor. Small sections (approximately at the right edge, in the middle and at the left edge) were not cured. After the polymer samples were developed, thickness measurements were pursued by using AFM at each section and depicted in the figure 6-6. Ten measurements were done at each section. As seen from the fig 6-6, the SU8-2002 layer can be considered relatively flat on the MTSM sensor. The variation among the surface is less than 10 nm. Similar results have been observed for 770 nm thick SU8 layer (results are not shown).

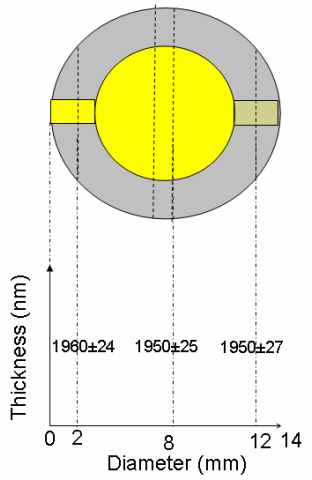

Figure 6-6 Variations in the thickness of SU8-2002 polymer layer coated on the MTSM sensor surface

6.3.2 Determination of mechanical and geometrical properties of SU8-2002 layer of 1.95 µm thickness

First set of experiments were performed by spin coating 1.95 µm thick SU8 - 2002 layer on the MTSM sensor surface. The change in the resonance frequency and the maximum magnitude are given in fig. 6.7. As seen from the fig. 6.7, the change in the resonance frequency is linear among the harmonics. It should be noted that there are losses present in

the system. The viscoelastic layer shows a “hard rubber” system with low losses. This can be seen from the magnitude response of the MTSM sensor. The relative changes in the average losses are -0.3 dB, -1.7 dB, -6.5 dB and -10.99 dB at 5 MHz, 15 MHz, 25 MHz and 35 MHz respectively. Therefore the viscoelastic properties can be calculated since the system is not in Sauerbrey region yet.

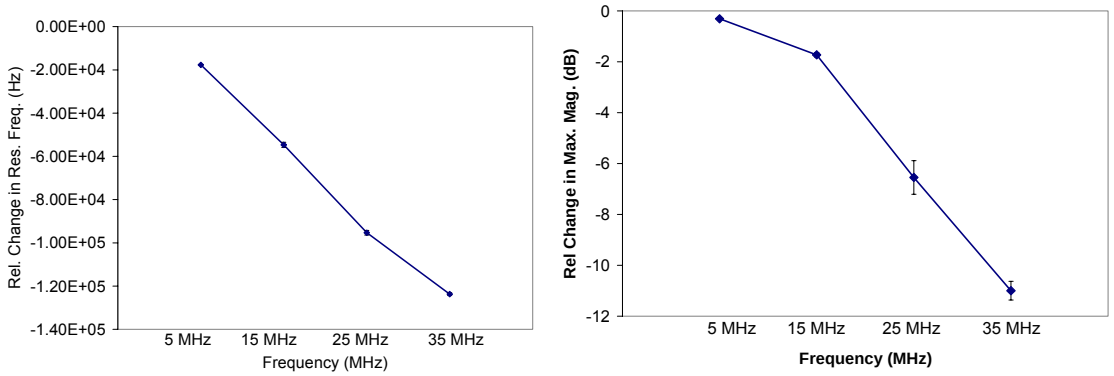

(a) (b)

Figure 6-7 Relative changes in resonance frequency and the maximum magnitude under 2 μm thick SU8-2002 layer at 5 MHz, 15 MHz, 25 MHz and 35 MHz. (error bars are smaller than symbols when not visible)

Layer properties determined by the MTSM/GA technique are presented in table 6-7. The average thickness of the polymer layer varied between 1900 nm and 1960 nm among the harmonics. Although these values are slightly higher than the value (1950±50 nm) obtained in control experiments, they are still in less than 5 % experimental errors. The variation between the frequencies for density value was also very small, which was changing from 1180 to 1220 kg/m^3. These numbers are very close to the literature value which is 1200 kg/m^3 (Jiang et al. 2003).

Table 6-7 Comparison density and thickness values of SU 8-2002 layer determined using MTSM/GA sensor at 5, 15, 25 and 35 MHz with profilometer and Jiang et al. (2003).

MTSM Frequency	MTSM/GA Results		Profilometer	Jiang et al. [2003]
(MHz)	d(nm)	ρ (kg/m^3)	d (nm)	ρ (kg/m^3)
5	1900±60	1210±10	1950±50	1200
15	1960±30	1220±10		
25	1970±10	1180±40		
35	1960±50	1210±30		

The frequency dependent shear modulus of SU8-2002 layer is presented in table 6-8. Both loss and storage modulus varies with the operating frequency. These determined values were compared with the values obtained by independent measurements and by Jiang et al (2003) (table 6-8). Jiang et al calculated the shear modulus of SU8 layer by using the impedance-admittance characteristics of the equivalent circuit models of loaded and unperturbed TSM sensors operating at 9 MHz.

Table 6-8 Comparison of determined G' and G'' values of SU8 layer using MTSM/GA at 5, 15, 25 and 35 MHz and Jiang et al (2003).

MTSM Frequency	MTSM/GA Results		Jiang et al.(2003) (at 9 MHz)	
(MHz)	G^I (N/m^2)	G^{II} (N/m^2)	G' (N/m^2)	G'' (N/m^2)
5	(8±0.6) $x10^6$	(0.3±0.06) $x10^5$	7.80e7	2.00e5
15	(8±0.18)$x10^7$	(2.6±0.1) $x10^5$		
25	(2±0.52)$x10^8$	(1.6±0.52) $x10^6$		
35	(3.2e8±0.71) $x10^8$	(5.8±0.18) $x10^6$		

As seen in table 6-8, the values obtained by Jiang et al. fall between the values obtained here at 5 and 15 MHz. The small deviations in the G' and G'' may be due to difference in the film preparations protocol. Alig et al. (1996) has shown that variations in film preparation methods can affect the mechanical properties of the polymer layers. The comparison between the theoretical and experimental results is presented in fig. 6-8. As seen

from fig. 6-8, there is a good correlation between the experimental and theoretical results with less than 10 % error.

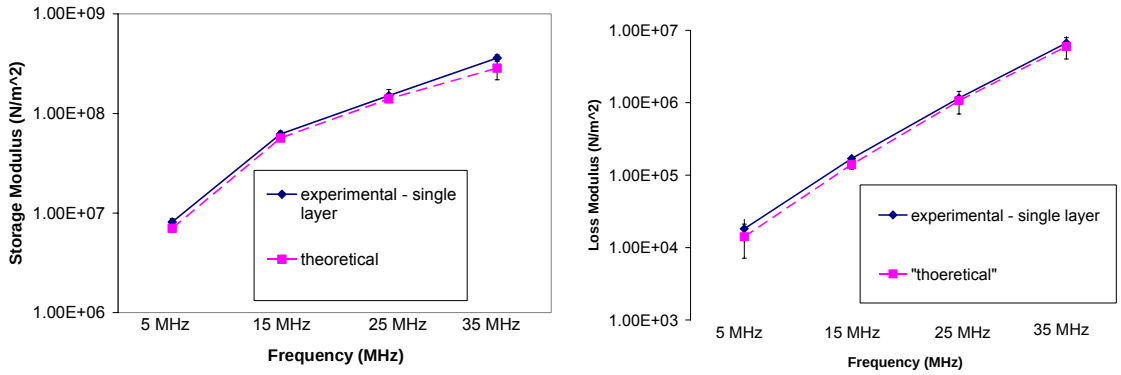

(a) (b)

Figure 6-8 Determined G' and G'' values of SU8-2002 layer using the MTSM/GA technique at 5, 15, 25 and 35 MHz and comparison with theoretical results

6.3.3 Determination of mechanical and geometrical properties of SU8-2002 layer of 0.770 µm thickness

Second set of experiments were performed by spin coating 0.77 µm thick SU 8 - 2002 layer on the sensor surface. The change in the resonance frequency and the maximum magnitude are given in fig. 6-9. As seen from the fig. 6-9, the change in the resonance frequency is linear among the harmonics. It should be noted that there are still losses present in the system. The viscoelastic layer shows a "hard rubber" system with low loses. This can be seen from the magnitude response of the MTSM sensor. The relative changed in the average losses are -0.3 dB, -0.5 dB, -1.4 dB and -2.05 dB at 5, 15, 25 and 35 MHz respectively. Therefore the viscoelastic properties can be calculated since the system is not in the Seuerbrey region yet. As seen in fig. 6-9b, the error in the magnitude responses are relatively higher compared to the ones obtained for 2 µm. This higher error may stem from

the film preparation method. It can be expected that the error in the loss modulus obtained by the MTSM/GA results will be higher compared to the ones in 2 μm thick SU8 layer.

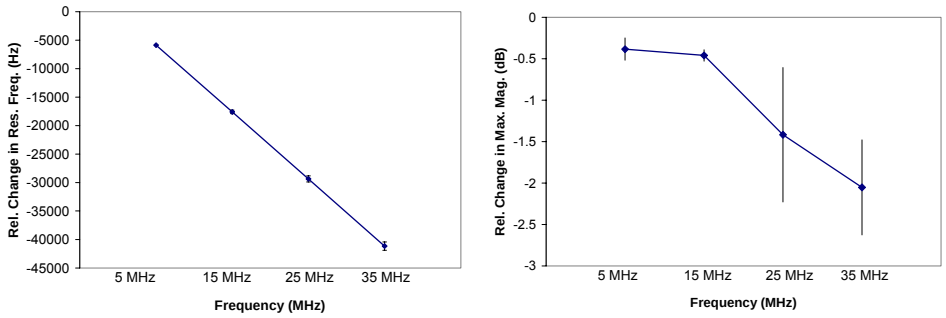

(a) (b)

Figure 6-9 Relative changes in (a) the resonance frequency and (b) the maximum magnitude under 0.77 μm thick SU8 layer at 5 MHz, 15 MHz, 25 MHz and 35 MHz.

As seen from the table 6-9, the thickness of the layer was determined with less than 10% error for each harmonic. Furthermore the results vary only 10 nm between the harmonics. Similarly, determined values for density were very consistent between the harmonics, which is around ~1200 kg/m^3.

Table 6-9 Determined density and thickness values by the MTSM/GA for 770 nm thick SU8-2002 layer at 5, 15, 25 and 35 MHz

MTSM Frequency	MTSM/GA Results		Profilometer	Jiang et al.[2003]
(MHz)	d(nm)	ρ (kg/m^3)	d (nm)	P (kg/m^3)
5	770±8	1220±10	770±50	1200
15	780±6	1190±5		
25	760±13	1190±10		
35	770±20	1200±16		

The average relative changes in maximum magnitude are -0.3 dB and -2.05 dB for 5 MHz and 35 MHz respectively. As seen from these results, the losses remain relatively low when the thickness of the layer was decreased to 770 nm in contrast to the phenomenon observed

when the film thickness was 2 µm. The determined shear modulus values were presented in figure 6-10. Both loss and storage modulus were decreased compared to the values obtained when film thickness was 2 µm. It has been shown that the scale effect on the mechanical properties of the polymers (Liu et al., 2009, Lu et al., 2003, Dylkov et al., 1966). This might be the reason for the decrease in the values. As seen in fig 6-10, the error in experimental and theoretical results in the determination of loss modulus is higher than the ones observed for 2 um thick SU8 layer. In contrast the error is relatively lower for storage modulus, which is more related to the change in resonance frequency.

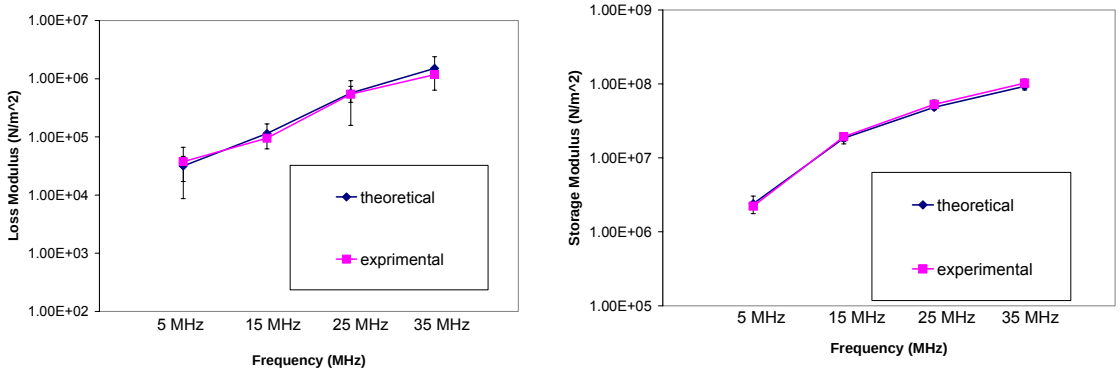

(a) (b)

Figure 6-10 Determined G' and G'' values of SU8 layer using the MTSM/GA at 5 MHz, 15 MHz, 25 MHz and 35 MHz and comparison with theoretical results

6.4 Analysis of mechanical and geometrical properties of SU8-2002 layers with different thicknesses

Four different thicknesses of SU8-2002 layer have been spun coated on the MTSM sensor surface and the mechanical properties determined by the MTSM/GA technique has been presented in fig. 6.11.

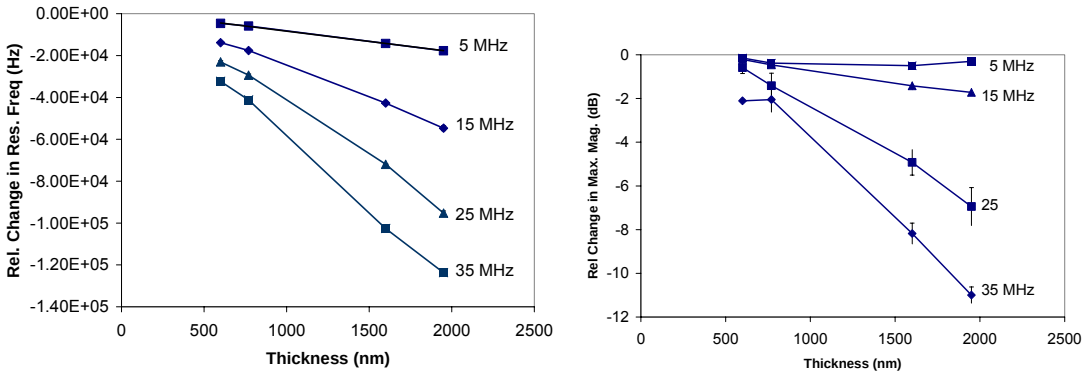

(a) (b)

Figure 6-11 Change in the resonance frequency and maximum magnitude with thickness change for SU8-2002 layers

As seen from fig. 6-11, the change in the resonance frequency can be considered linear for each harmonic. This can be expected because the SU8 layer behaves as hard rubber system with relatively small losses. On the other hand, the error between the experiments increases for the maximum magnitude response. This can be clearly seen in fig 6-11b. The storage modulus and the loss modulus calculated by the MTSM/GA technique has presented in fig. 6-12.

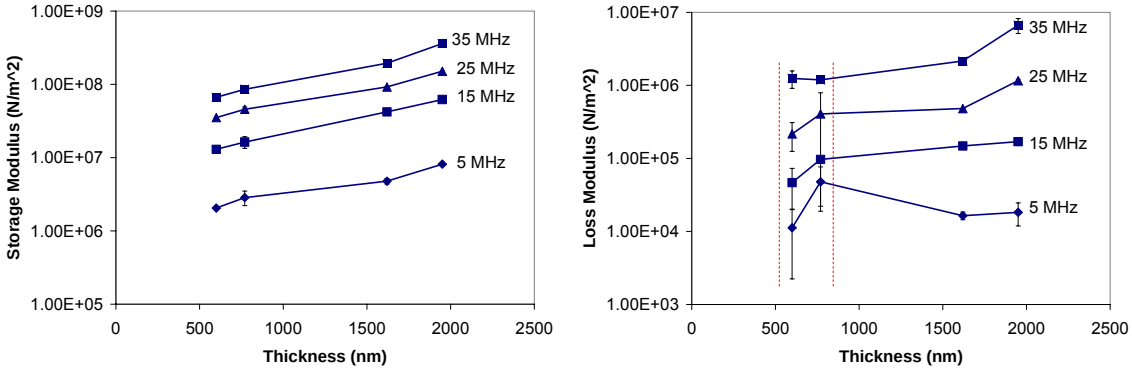

(a) (b)

Figure 6-12 Storage (a) and loss (b) modulus determined by the MTSM/GA technique for different thickness of SU8 layer

As seen from the fig. 6-12, the error in the loss modulus increases more than 50 % because of high experimental error. It should be noted that the error especially increases with the lower thickness values of the SU8-2002 layer.

6.5 Validation of the MTSM/GA technique using collagen type-I layer deposited on the MTSM sensor surface

Collagen is a fibrous protein found mostly in skin, bone, and other connective tissues of animals. As a component of the vascular extracellular matrix (ECM), type I collagen plays an essential structural role as well as a role in regulating proliferation and migration of cells such as vascular smooth muscle cells (Raines et al., 2000) and it is important in providing tensile stress and rigidity in lungs (Hermanjatinder et al., 2001). The deposition of collagen type-I is important in scar formation (Kopecki et al., 2008). The mechanical and structural properties of thin films of collagen affect the morphology of smooth muscle cell morphology (Elliot et al., 2003).

The viscoelastic mechanical properties of collagen during the evaporation process are mainly depend on the concentration of the collagen solutes and the condition of the fibrous collagen protein. The MTSM/GA technique experimentally tested with the collagen layer deposited on MTSM sensor surface. The layer properties determined by the MTSM/GA technique were compared with the values obtained from the literature and an independent measurement system, tomic force microscopy. The methods and chemicals used in the experiments are described below.

6.5.1 Materials and Methods

6.5.1.1 Deposition of the collagen type-I layer on the MTSM sensor surface

Insoluble fibrillar collagen type I (bovine Achilles tendon, Sigma) was deposited on the MTSM sensor surface by adsorption from acetic acid solution. The concentration of the collagen solution was 1 mg/ml. The experiments were done in room temperature (24C±3C). The temperature was monitored continuously during the experiment.

6.5.1.2 Characterization of geometrical properties of the thin film

The surface topography and thicknesses of the collagen films were determined using atomic force microscopy. The prepared samples were gently placed on the glass slide installed on the atomic force microscope (Bioscope; Veeco), that was mounted on the inverted fluorescence microscope (TE2000; Nikon, Melville, N.Y.). Measurements were done in contact mode and scan rate was 2 Hz. The surface profile of collagen layer deposited on the MTSM sensor has been investigated. To do so, the 200 µl and 100 µl of collagen solutions have been adsorbed on the MTSM sensors. Small sections (at the right edge, in the middle and at the left edge) were gently scratched and collagen layer was removed. Ten thickness measurements were done by using AFM at each section and depicted in the figure 6-13. The collagen layer forms a concave shape on the MTSM sensor. For first sensor, the variation among the surface is around 100 nm. For 150 nm thick collagen layer, the variations among the surface was around 50 nm. For theoretical calculations, average thicknesses of the collagen are taken as 400 nm and 140 nm.

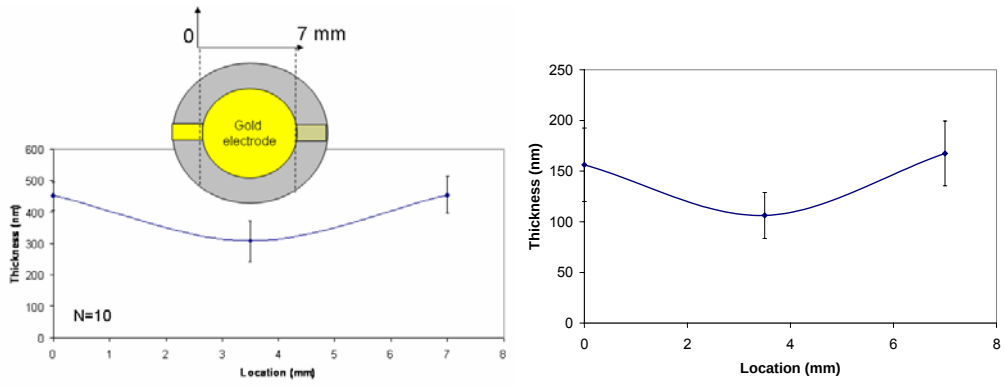

(a) (b)

Figure 6-13 The surface profiles of collagen polymer layers coated on the MTSM sensor surface (a) 400 nm and (b) 140 nm. (N=10)

6.5.2 Results and Discussions

200 µl and 100 µl of collagen samples were loaded on the MTSM sensor. The acoustic signatures of the evaporation-induced deposition process has been monitored at 5 MHz, 15 MHz, 25 MHz, and 35 MHz. Collagen solution formed a thin (polycrystalline) film under an evaporation-induced deposition process at the end. Graphs in figures 6.14 show the changes in the relative resonance frequency (Δf) and change in maximum magnitude of the MTSM sensor during the evaporation-induced deposition process of collagen solution as a function of time. All graphs clearly show that there are four consecutive stages of a viscoelastic system during the evaporation-induced deposition process. Time 0 indicates the addition of the collagen samples. The graphs are presented as relative changes to the time 0.

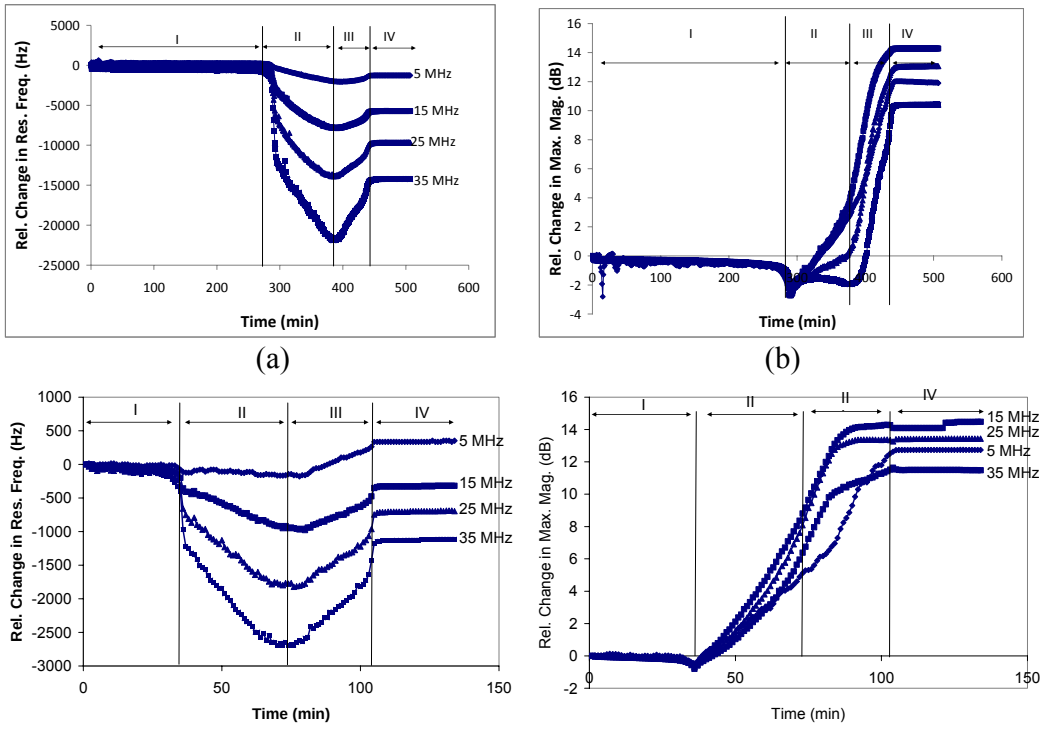

Figure 6-14 Relative changes in maximum magnitude and resonance frequency in the harmonic resonance frequencies of the MTSM with collagen sample as a function of time. (a) and (b) 400 nm, (c) and (d) 140 nm

The first stage I is indicated by either small or almost no changes in the relative Δf and α. During the first stage, solvent evaporates through the open top surface; hence, the change in the thickness of the liquid medium is the main parameter that affects the response of the MTSM sensor. The first part of the second stage is indicated by sudden slight (about ~ 2 and 1 dB for 450 nm and 150 thick collagen samples) increase in magnitude and lasts for a short period of time (less than 30 minutes). The phase of the sample starts to transform from a Newtonian viscous liquid to viscoelastic (VE) condition during this stage because of the increase in the concentration of the solute. The second part of the second stage is characterized by a sudden decrease in the relative Δf and α. It is hypothesized that the most of the liquid solvent is evaporated and only left with a gel type, soft rubber condition, viscoelastic thin film on the MTSM sensor surface. The third stage is characterized by

increase in relative Δf and decrease in the magnitude. The resonance frequency and magnitude of each harmonic in stage IV stabilize and become close to zero which means that the film behaves more rigidly.

As discussed above, two different thicknesses of collagen layer have been deposited on the MTSM sensor surface. The final thicknesses of the collagen layers were ~400 nm and ~140 nm. In the following section, initially the properties of 400 nm thick collagen layer will be examined. It will be followed by the discussion on the determination of mechanical properties of 140 nm thick collagen layer.

400 nm thick of collagen layer was formed on the MTSM sensor surface by evaporation process. The final thickness of the collagen layer was measured by using atomic force microscopy (AFM) as shown in fig 6-15. Thickness of the final collagen layer after 8 hours was measured as 400±50 nm. The MTSM's surface was fully covered by collagen. Average roughness was measured as 50 nm. Peak-to-peak roughness was measured as ~100 nm.

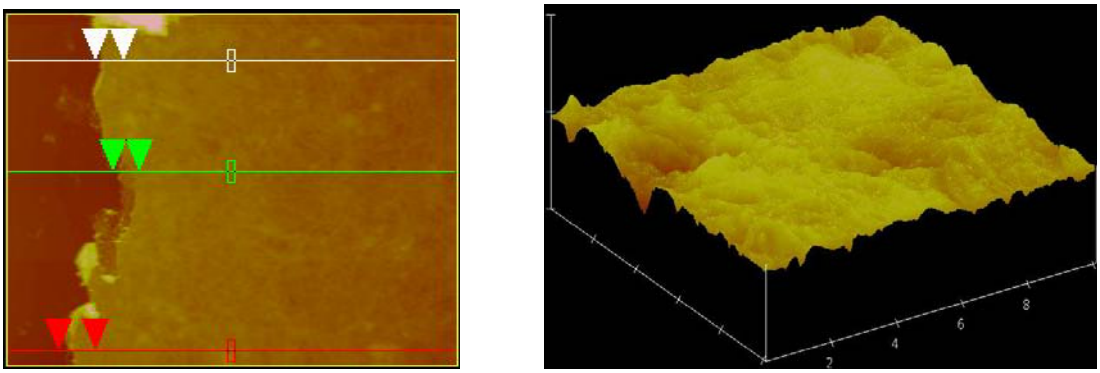

(a) (b)

Figure 6-15 The step analysis (a) of 400 nm thick collagen layer for thickness measurement and surface topography image (b) roughness measurement

The density of collagen has been given by several references. Hulmes et al (1977) indicated that the density of collagen in its native state is between 1160 – 1330 kg/m^3. Black and Mattson (1982) showed that the density of collagen is 1230 kg/m^3. Langevin et al. (2007) has given the collagen density between 1100 kg/m^3 – 1200 kg/m^3. It can be seen that the density of collagen can be between 1100 kg/m^3 to 1300 kg/m^3. For theoretical calculations, density of the collagen was taken as 1200 kg/m^3.

After the collagen layer is formed on the surface, the final resonance frequency and magnitude values of the MTSM sensor have been plugged into the MTSM/GA technique to determine the mechanical and geometrical properties of collagen layer. The comparison between the thickness and density values obtained from the MTSM/GA technique and the values obtained from AFM and references is shown in table 6-10.

Table 6-10 Comparison density and thickness values of 400 nm thick collagen layer determined using the MTSM/GA technique at 5, 15, 25 and 35 MHz with the values obtained from AFM and references.

MTSM Frequency	MTSM/GA Technique		AFM	Langevin et al., Hulmes et al. Black et al.
(MHz)	d(nm)	P (kg/m^3)	d (nm)	ρ (kg/m^3)
5	420	1130	400±50	1100 – 1300
15	390	1140		
25	380	1130		
35	380	1120		

The determined density values are consistent among the harmonics, between 1120 kg/m^3 to 1140 kg/m^3. These values are consistent with previously reported values.

The determined values for storage and loss modulus for collagen layer are presented in fig. 6-16. It can clearly seen that both storage and loss modulus increase with the frequency. The

error between the theoretical and experimental result are between 3 % to 14 % for storage modulus and between 2 % to 24 % for loss modulus.

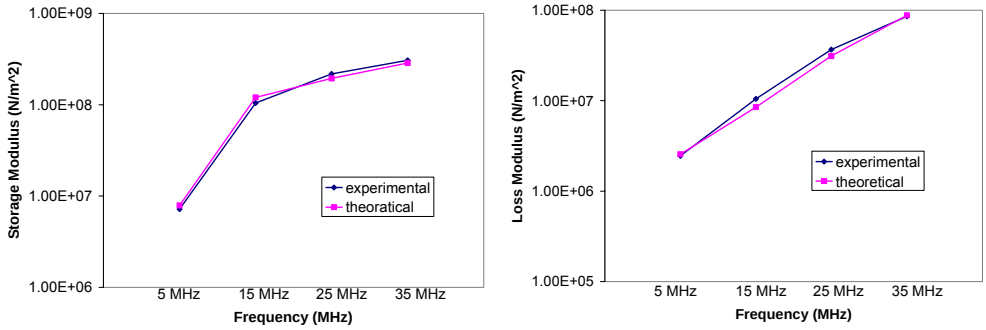

Figure 6-16 Determined G' and G" values of 400 nm of collagen layer using MTSM/GA technique at 5 MHz, 15 MHz, 25 MHz and 35 MHz and comparison with theoretical values

Next, 140 nm thick collagen layer was formed on the MTSM sensor surface by evaporation process. The final thickness of the collagen layer was measured by using atomic force microscopy (AFM) as shown in fig 6-17.

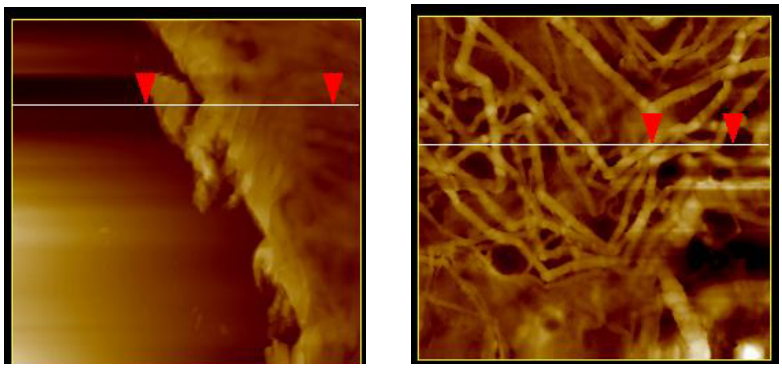

Figure 6-17 The step analysis (a) of 140 nm thick collagen layer for thickness measurement and surface topography image (b) for roughness measurement

As seen from the table 6-11, the thickness values were determined at 140 nm at 5 MHz and 120 nm, 110 nm and 110 nm at 15 MHz, 25 MHz and 35 MHz respectively. The determined density values are consistent among the harmonics, between 1115 kg/m^3 to 1130 kg/m^3.

Table 6-11 Comparison density and thickness values of 140 nm thick collagen layer determined using MTSM/GA technique at 5, 15, 25 and 35 MHz with the values obtained from AFM and references.

MTSM Frequency	MTSM/GA Results		AFM	Langevin et al., Hulmes et al. Black et al.
(MHz)	d(nm)	P (kg/m^3)	D (nm)	ρ (kg/m^3)
5	140	1120	140±50	1100 – 1300
15	120	1115		
25	110	1120		
35	110	1130		

The determined values for storage and loss modulus for collagen layer are presented in fig. 6.18. It can clearly seen that both storage and loss modulus increases with the frequency. But the storage and loss modulus at 15 MHz, 25 MHz and 35 MHz are in the same magnitude order while the storage and loss modulus at 5 MHz is one magnitude order lower than the other harmonics. The error between the theoretical and experimental result are between 2 % to 16 % for storage modulus and between 9 % to 24 % for loss modulus.

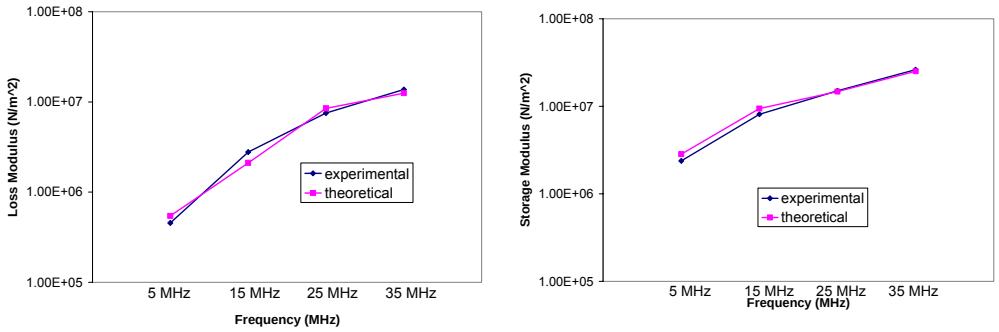

(a) (b)

Figure 6-18 Determined G$^{'}$ and G$^{''}$ values of 140 nm thick collagen layer using the MTSM/GA technique at 5, 15, 25 and 35 MHz and comparison with theoretical results

It should be noted that the collagen experiments have been repeated only once because of the large difference between the different experiments. This phenomenon can be clearly seen in fig. 6.19. 100 µl of collagen sample has been introduced to the surfaces of

fours MTSM sensors. The maximum magnitude and the resonance frequency responses of the sensors have been monitored simultaneously in room temperature. Even though the same volume of sample has been added on the sensors, the relative changes in the magnitude and frequency responses show more than 50 % errors. At the end of the experiments, the thicknesses of the collagen layers have been measured by using atomic force microscopy. The obtained results for thickness values were around 120 nm, 80 nm, 170 nm, and 140 nm. As seen from these results, the reproducibility of the collagen experiments is very poor.

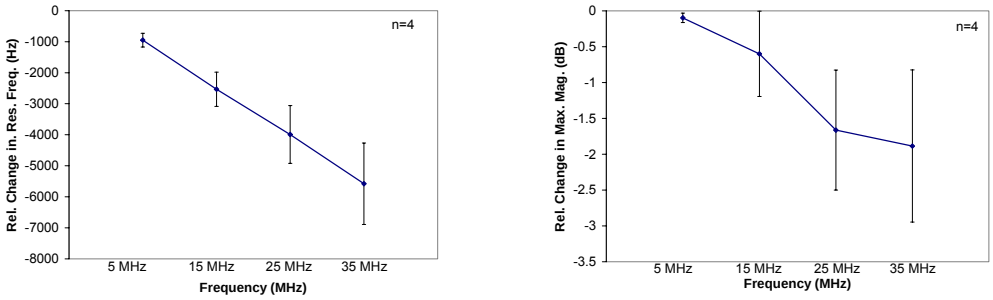

(a) (b)

Figure 6-19 Relative changes in (a) resonance frequency and (b) maximum magnitude of the MTSM sensor loaded with 100 μl of collagen samples.

To overcome this disadvantage, a calibration curve is obtained by adsorbing collagen layers with three different thicknesses on the MTSM sensor. The mechanical properties were determined by the MTSM/GA technique and compared with the theoretical values. Results are presented in fig. 6-20. Thickness measurements were done by using AFM. As seen from the fig. 6-20, both storage and loss modulus of the collagen are thickness dependent. They both decrease with the decrease of the thickness. This graph will be used as a calibration curve for the collagen experiments which will be presented in the section 8.

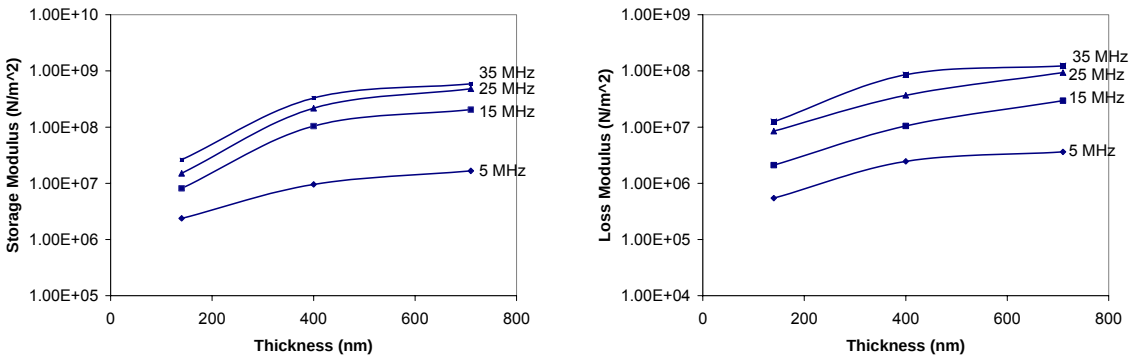

(a) (b)

Figure 6-20 Storage (a) and loss (b) modulus values for different thickness of collagen layer

6.5.3 Time evolution of the properties during collagen evaporation process

Theoretical modeling of collagen evaporation has been extensively investigated by Kwoun et al. It has been shown that the initial viscosity and stiffness are at the value of water (0.001 kg/ms and 0 N/m^2) to represent the water like condition and maintained at similar value to indicate the stage I. This stage I in figure 6-20 also corresponds to region I in fig. 6-14. At the end of the stage I (about 300 minutes), the viscosity starts to increase suddenly because of the increase in the concentration of the collagen solute. The stiffness is maintained at the liquid like value to describe the phase transition of the medium from water like to a higher viscous soft rubber condition. The stiffness of the sample starts to increase (up to 10^7 N/m^2) at the middle of the stage II while the viscosity is already high (0.1 ~ 1 kg/ms). During the stage III, the stiffness of the sample keeps increase (up to 10^9 N/m^2) and the viscosity decrease slightly (from ~ 1 to 0.7 kg/ms) to describe the hardening and fibrillation processes of the collagen sample. The viscosity and stiffness are generally fixed at the end of the stage III and stayed during the stage IV to reveal the final stabilization process of the evaporation-induced deposition process of collage sample.

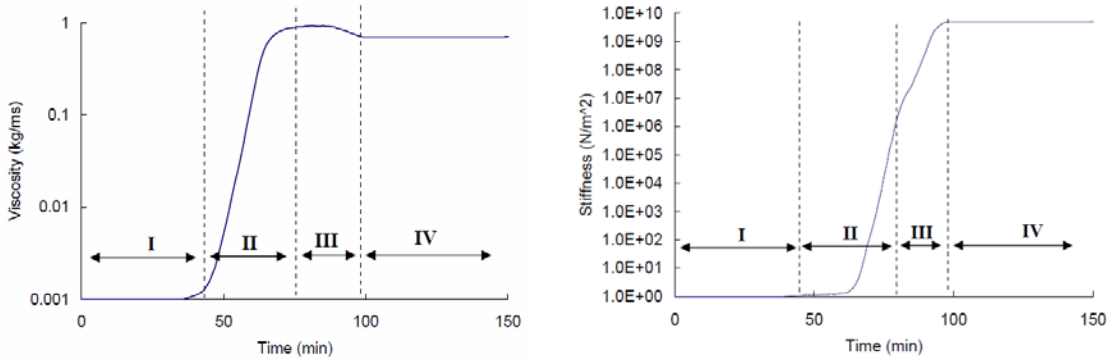

Figure 6-21 Theoretical changes in the (a) viscosity and (b) stiffness of collagen sample during the simulation of the evaporation-induced deposition process (figures taken from Kwoun, 2006)

The time evolution of the geometrical and mechanical properties of collagen evaporation process has been studied experimentally. For this purpose, the 400 nm thick collagen layer was deposited on MTSM sensor response. During the evaporation process, the properties were monitored at specific time points which fall into four stages of collagen evaporation process. The obtained results have been compared with the theoretical results shown in fig. 6-21.

The experimental results at all harmonics have been shown in fig.6-22. As seen from the fig. 6-22, the stiffness values are slightly increasing in stage II. It is followed by a sudden increase in stage III. This is in good correlation in the theoretical model. In contrast, the viscosity values are increases in stage II and slightly decrease in stage III.

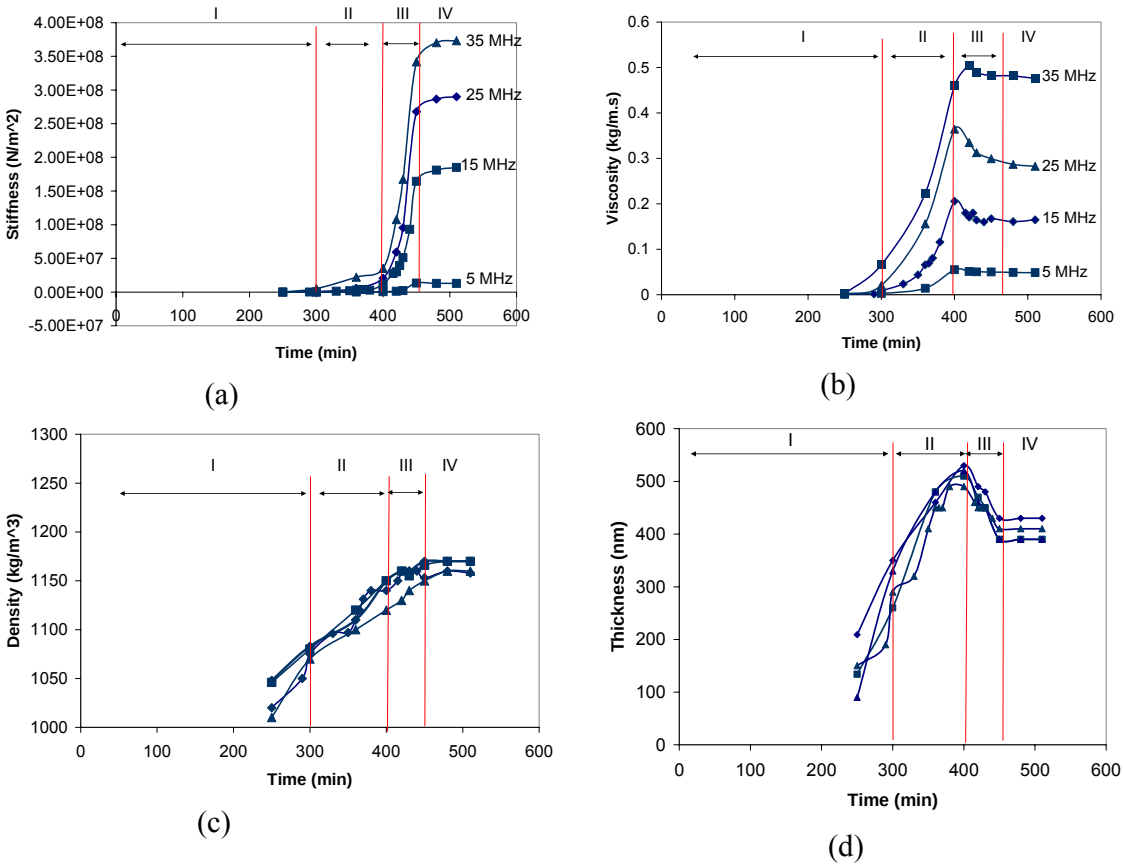

Figure 6-22 Time evolution of (a) stiffness , (b) viscosity , (c) density and (d) thickness of collagen layer at 5 MHz, 15 MHz, 25 MHz and 35 MHz.

The collagen properties show liquid like behavior during stage I. The viscosity (changing between ~0.0012 kg/m.s to ~0.0018 kg/m.s among the harmonics) and the stiffness (0 N/m^2) are close to the water values (η_{water}=0.001 kg/m.s and C_{water}=0 N/m^2). In this stage, the thickness is close to the penetration depth because the system is seen as a semi-infinite medium by the MTSM sensor. The thickness values calculated at 250 minute are equal to 210 nm, 160 nm, 130 nm and 90 nm for 5 MHz, 15 MHz, 25 MHz and 35 MHz respectively. The density value is changing between 1010 kg/m^3 - 1030 kg/m^3 among the harmonics which is very close the water value (ρ_{water} = 1000 kg/m^3).

In stage II, the viscosity value increases almost 40 - 50 times in stage II while stiffness values increase to the order of 10^6 to 10^7 values among the harmonics. Density value

continues to increase and reaches to 1100- 1150 kg/m^3 value. Thickness of the layer increases to a peak value which is around 500 nm.

In stage III, the viscosity value start decreasing while the stiffness value rapidly increases more than ~10 fold in 30 min. This stage represents the stiffening of the collagen layer. Thickness value also decreases in this stage representing the hardening and structural changes of collagen layer. Density value stays almost constant in this stage.

In stage IV, all parameters are fixed constant representing the final stabilization of the process.

As seen from fig. 6-21 and 6-22, the theoretical and experimental results reveal the same characteristics of the collagen evaporation process. The difference between theoretical (fig. 6-21) and experimental results (fig. 6-22) are the absolute values of the viscosity and stiffness values (no information is available in the literature regarding the density and thickness change). It is hypothesized that these differences stem from the fact that the viscoelastic properties are thickness dependent. For example, the viscosity and stiffness values reach to 0.8 kg/m.s and 5x10^8 N/m^2 when the thickness of the collagen is ~700 nm. It should also be noted that the viscoelastic properties are affected by the temperature, sample preparation, humidity and surface properties.

6.6 Discussions on experimental validation of the MTSM/GA technique for single-layer viscoelastic systems

Single-layer viscoelastic systems with different thickness combinations of SU8-2002 photoresist and collagen type-I polymers have been realized on the MTSM sensor. For calibration purposes, three different glycerin – DI water concentrations (0 %, 10 % and 20 %) were prepared and loaded on the MTSM sensor. The density and viscosity values of semi-

infinite mediums have been determined with less than 20 % error by the MTSM/GA technique. The thickness values were determined to be close to penetration depth value since the mediums were semi-infinite. As seen in the Kanazawa equation (eq. 6.1), which describes the sensor response to Newtonian medium, is the product of the density and viscosity values of the medium. Even though the equation describing the viscoelastic system only depends on the density and viscosity values, it was observed that the stiffness value was always zero.

To demonstrate this observation, the MTSM/GA technique's solutions for 20 % glycerin/DI water concentration was presented in fig 6-23. Stiffness values are always to be 0 or very close to 0 value ($<10^3$ N/m^2). The viscosity values also fell around 1.9×10^{-3} kg/m.s, which is equal to literature value.

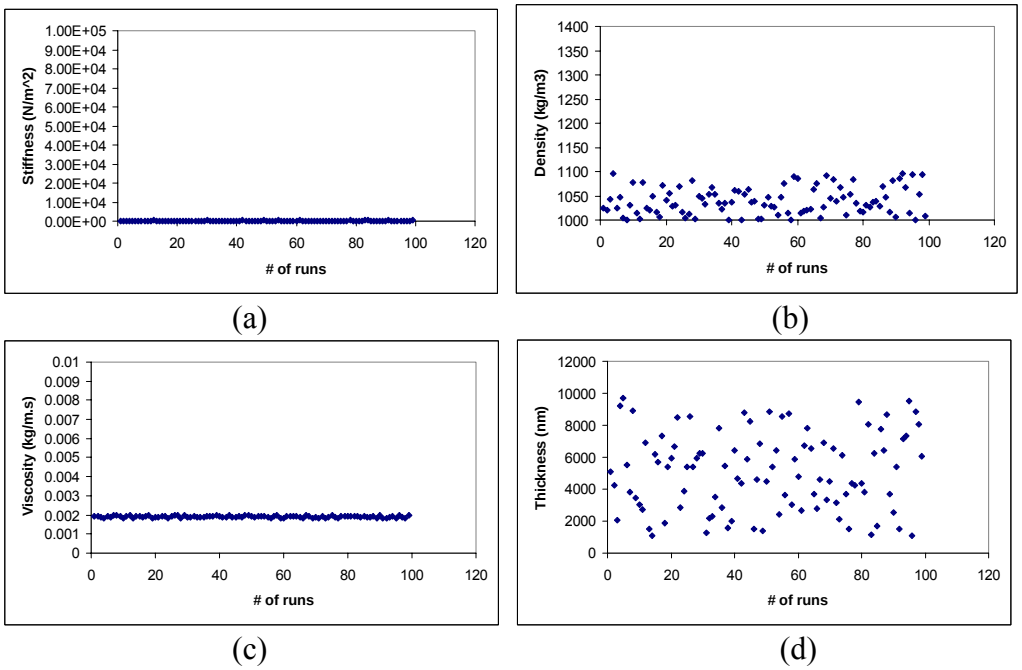

Figure 6-23 The MTSM/GA technique has been run 100 times for determination of the mechanical properties of 20 % glycerin/DI water.

Similar results were seen for other concentrations of glycerin/DI water solutions (data not shown). Therefore it can be concluded that, the MTSM/GA technique can identify the density and viscosity values of the Newtonian mediums.

Next set of experiments were done by spin coating SU-2002 layers on the MTSM sensors. The spin coating process was reproducible in repeated measurements and provided a uniform polymer layers on the sensors (fig. 6-6). No cracks were observed. The thickness of the viscoelastic layer has been measured by using atomic force microscopy and profilometer. Two different thicknesses of the SU8-2002 layer were formed, which were ~1.95 μm and ~0.77 μm. The density value for the negative photoresist was obtained from the literature which was 1200 kg/m^3. Therefore other two unknowns were thus calculated. These values were then compared with the ones obtained from the MTSM/GA technique. It was shown that the MTSM/GA technique can determine that all four properties less than 10 % error. It was observed that the experimental error for 0.77 μm thick SU8-2002 layer increased, especially for the magnitude response. Therefore these variations were reflected in the determination of the loss modulus. The scale effect on the mechanical properties of the polymer layers was also observed.

Third set of experiments were done by adsorbing collagen type – I on the MTSM sensor. Different volumes of 1 mg/ml of collagen solutions (100 μl and 200 μl) were added on the sensor's surface to obtain different thicknesses of the collagen layer. It was observed that the collagen was uniform on the MTSM sensor but the shape of the layer was concave. Therefore the thickness of the layer was measured at different locations. The average thickness of the layer was calculated. These values were well correlated with the thickness values obtained with the MTSM/GA technique.

The time response of the collagen deposition process consisted of four viscoelastic regimes; namely, Newtonian medium, soft rubber, hard rubber and solid like. Detailed

theoretical modeling of the collagen evaporation process was done by Kwoun (2006). The experimental findings were in good agreement with the theoretical study pursued by Kwoun. Specifically, it was indicated by Kwoun that the initial viscosity and stiffness are at the value of water (0.001 kg/ms and 0 N/m^2) to represent the water like condition and maintained at similar value to indicate the stage I. Experimentally, it was observed that the collagen properties showed liquid like behavior during the stage I. The viscosity (changing between ~0.0012 kg/m.s to ~0.0018 kg/m.s among the harmonics) and the stiffness (0 N/m^2) are close to the water values (η_{water}=0.001 kg/m.s and C_{water}=0 N/m^2). In this stage, the thickness is close to the penetration depth because the system is seen as a semi-infinite medium by the MTSM sensor. The thickness values calculated at 250. minute are equal to 210 nm, 160 nm, 130 nm and 90 nm for 5 MHz, 15 MHz, 25 MHz and 35 MHz respectively. The density value is changing between 1010 kg/m^3 - 1030 kg/m^3 among the harmonics which is very close the water value (ρ_{water} = 1000 kg/m^3).

In stage II, the viscosity value increases almost 40 - 50 times in stage II while stiffness values increase to the order of 10^6 to 10^7 values among the harmonics. Density value continues to increase and reaches to 1100- 1150 kg/m^3 value. Thickness of the layer increases to a peak value which is around 500 nm. In stage III, the viscosity value start decreasing while the stiffness value rapidly increases more than ~10 fold in 30 min. This stage represents the stiffening of the collagen layer. Thickness value also decreases in this stage representing the hardening and structural changes of collagen layer. Density value stays almost constant in this stage. In stage IV, all parameters are fixed constant representing the final stabilization of the process.

As seen in fig. 6.20d, the thickness value of the collagen layer increases until the end of the stage II, then surprisingly decreases in the stage III. No change was observed in the stage IV. The increase in the thickness value in the first two stages can be explained by the

adsorption of the collagen on the MTSM sensor surface. It was expected that the thickness will increase until the end of the stage III, but surprisingly it decreased in the stage III. To explain this phenomenon, the changes in the resonance frequency and the frequency value at the zero phase during the evaporation process at 5 MHz were shown in the fig. 6-24.As seen in fig. 6-24, changes in the two frequency values show the same time characteristics, but the absolute values differ each other. During the experiments, it was observed that the resonance frequency and the frequency value at the zero phase differ each other when the MTSM sensor loaded with a viscous medium such as DI water and glycerin/DI water concentrations. Detailed study of this phenomenon was discussed by Francois (2008).

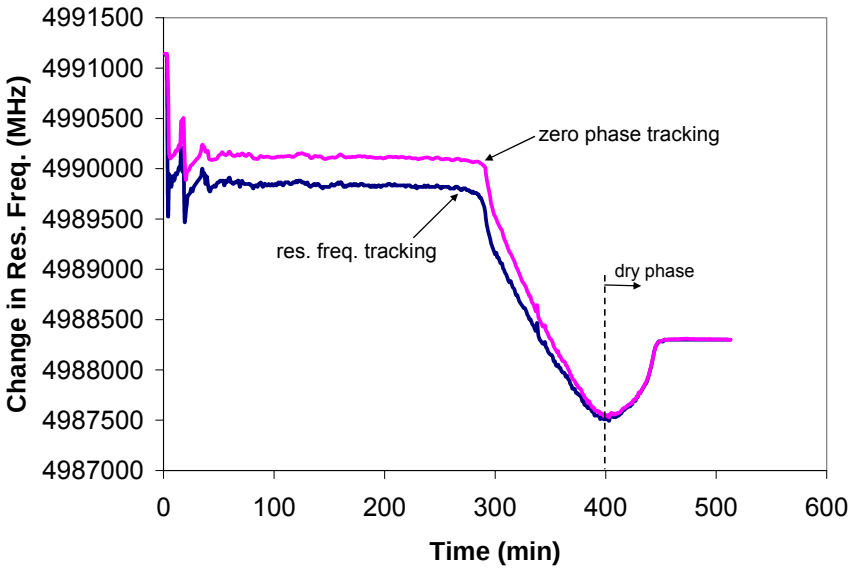

Figure 6-24 Change in the resonance frequency (blue) and the frequency at the zero phase (pink) during the evaporation of collagen type-I on the MTSM sensor

As seen in fig. 6-24, two frequency values aligned each other at the end of stage II, where the thickness value started decreasing. It can be hypothesized that the medium enters so called “dry phase” at this time point. The collagen fibers swell in solution which results in the increase in the thickness increase of collagen fibers Shrinkage of the collagen fibers may

cause the conformational change in the collagen matrix as well (Maeda et al., 1999). From these preliminary findings, it can be hypothesized that the MTSM/GA technique may be used as a novel tool to measure the degree of the swelling of collagen. Further studies are required to test this hypothesis, which will be subject of the following research.

6.7 Summary and Conclusions

The MTSM/GA technique has been tested with well-defined experimental media such as semi-infinite Newtonian fluids, polymers (SU8-2002)and collagens (type-I) that represent very broad range of mechanical properties and structural features. Polymer layers were formed on the MTSM sensor by using spin coating method and adsorption process. The thickness profiles of polymer layers were identified by using control experiments such as atomic force microscopy and profilometer. The density values of the polymer and collagen and the mechanical properties (viscosity, density and stiffness) of Newtonian media were obtained from literature.

It was shown that the MTSM/GA can determine the mechanical (density, complex shear modulus) and structural properties (thickness) of semi-infinite Newtonian media and finite thickness of SU8-2002 polymer and collagen layers with less than 20 % error.

Furthermore, it was demonstrated, for the first time, that the MTSM/GA technique is capable of providing time evolution of all four parameters during the collagen adsorption process.

7 THEORETICAL FOUNDATION OF THE MTSM/GA TECHNIQUE FOR TWO-LAYER VISCOELASTIC SYSTEMS

7.1 Problem Definition

1. There is a two-layer viscoelastic biological layer which the mechanical and structural properties are needed to be determined.

2. The mechanical impedance seen at the MTSM sensor loaded with multiple viscoelastic layer is derived from transmission line theory and is given in eq. 7.1 (Lucklum and Hauptman, 2000);

$$Z_m = Z_1 \frac{Z_2 + jZ_1 \tan(\omega\sqrt{\frac{\rho_1}{G_1}}h_1)}{Z_1 + jZ_2 \tan(\omega\sqrt{\frac{\rho_1}{Z_1}}h_1)} \tag{7.1}$$

where $Z_1 = \sqrt{\rho_1 G_1}$ is the acoustic impedance of the first layer adjacent to the MTSM sensor; ρ_1, h_1 and $G_1 = G'_1 + G''_1$ are the density, thickness and the complex shear modulus of the first layer respectively. Z_2 represents the acoustic load acting on the top of the first coating. This load may be provided by a second film, a multilayer or a semi-infinite material. The surface acoustic impedance can be defined by eight independent variables.

The modified Butterworth-Van dyke equivalent circuit of a perturbed MTSM sensor loaded with a two-layer viscoelastic system has been given in fig. 7-1.

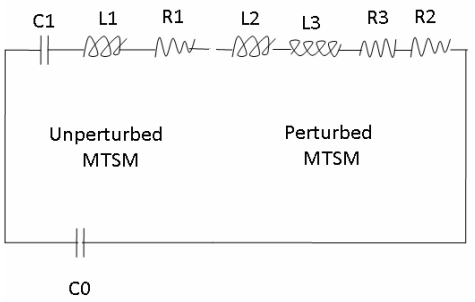

Figure 7-1 Modified Butterworth-van dyke equivalent circuit of perturbed MTSM sensor loaded with two-layer viscoelastic system.

In fig 7-1, an electrical equivalent circuit of a perturbed MTSM sensor is shown. L1, C1 and R1 represent the unloaded MTSM sensor parameters. L2 and R2 represent the properties of first viscoelastic layer. L3 and R3 represent the second layer's properties.

The measurement of the change in resonance frequency and loses of MTSM sensor by time contribute the identification of two out of four variables which define the surface mechanical impedance. Thus monitoring single harmonic response of MTSM sensor results in an under-determined problem.

3. For the determination of the properties of two layer viscoelastic layers, the four parameters out of eight unknown will be kept constant. It will not be possible to determine all these eight parameters by using only single harmonic's response. In this case, two methods can be applied to overcome this problem. First, more than single harmonic can be utilized to determine the geometrical and viscoelastic properties of the two-layer system. Each harmonic will introduce identification of two variables. Main drawback of this technique is that it assumes that the viscoelastic properties of the layers are not frequency-dependent. This issue has been also discussed in the chapter 5 and it was shown that this assumption forces the MTSM/GA technique's to be applied to very limited viscoelastic systems. Therefore this method was not favored in this project.

The second method is to keep density and thickness values of the layers constant. The problem will stay as an under-determined problem but the number of unknowns will be reduced to four. It has been discussed in chapter 5 that the change in the density of a typical viscoelastic system (<40 %) is much smaller than the change in the viscoelastic properties (100 folds or more). It will be a valid assumption to keep the density values constant. The user can find the viscoelastic properties at different density values if necessary.

Thickness values of the layers can be obtained by the literature search. For example, cell adhesion process has been studied extensively since it has crucial importance in the regulation of cell behavior, such as the control of growth and differentiation during development. Interactions between cells and the substrate have been modeled as multi-layer system. Wegener et al.(2000) proposed that the cell adhesion process should be modeled as two-layer viscoelastic system. The first layer is the attachment site between the cells and the substrate. It has been also shown that there is a considerable gap between plasma membrane and aqueous/proteinacous intermediate layer. This layer was proposed to have ~100 nm thickness (Giebel et al., 1999). The second layer consists of the cell membrane and the cell body. This can be set to be several micron depending on the cell type and the stage of the cell adhesion. As seen from the cell adhesion example, the multi-layer modeling of the biological processes can be found in the literature since they have crucial importance in science and engineering fields such biosensors and tissue engineering. Therefore, in this project, it was proposed that the density and the thickness values of the layers will be kept constant, and the complex shear modulus of the layers will be the interest of chapter 7 and 8.

7.2 Outline of Chapter 7

This chapter will be outlined in the following manner;

1. The structure of the MTSM/GA technique for determination mechanical properties of a two-layer viscoelastic system will be explained.

2. The MTSM/GA technique will be validated theoretically by simulating a typical evaporation process of a polymer viscoelastic layer. Accuracy and the limitations of the technique will be discussed by analyzing the acoustic response of the MTSM sensor and the performance of the MTSM/GA technique in each stage.

7.3 Structure of the MTSM/GA technique for determination of properties of two-layer viscoelastic system

Same methodology and structure, which have been developed in chapter 5, were used to determine the mechanical properties of two-layer viscoelastic systems. Shortly, two auxiliary techniques were integrated to the MTSM/GA technique: sub-spacing and zooming. While zooming has been applied in the same manner, the search space was divided into 64 sub-spaces rather than only ten, which was the case in the single layer systems. The combination of viscosity and stiffness values has been used. The sub-functions and the parameters of the MTSM/GA technique have been kept the same. The MTSM/GA technique has been already optimized in chapter 5, therefore no optimization study was done in this chapter.

The MTSM/GA technique was developed for both cases (fig. 7-2); 1. two-layer viscoelastic system in air 2. two-layer viscoelastic system in DI water. It has been discussed in chapter 5 that the typical biological systems are mostly diluted in buffer solutions to

maintain certain biological activities. The results for the viscoelastic system in air were presented in this chapter.

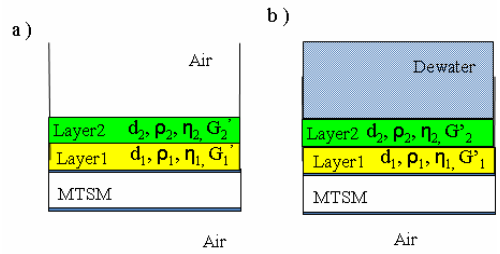

Figure 7-2 The physical model for two-layer viscoelastic system loaded on MTSM sensor surface. a) viscoelastic layer in air b) viscoelastic layer in deionized water (DI water)

The mechanical and geometrical parameters for the first viscoelastic layer have been chosen similar to the one used in chapter 5. The properties of the second viscoelastic layer were chosen to be close to the properties of collagen layer, which was used to validate the MTSM/GA technique in chapter 5. This configuration of the viscoelastic layers were chosen to depict the structure of the MTSM/GA technique since it is closely related to the experimental validation of the technique. In the chapter 8, the two-layer viscoelastic systems consisting of SU8-2002 layer as a first viscoelastic layer and collagen as a second viscoelastic layer will be utilized to validate the MTSM/GA technique. The aim of this project is to develop a quantitative tool and validate it with controlled experiments. Therefore it will be impossible to realize all the possible configurations of a two-layer viscoelastic system. For the explanation of the theoretical structure of the MTSM/GA technique, chosen properties of two-layer viscoelastic layer system were shown in table 7-1.

Table 7-1Viscosity, stiffness, density and thickness values of the viscoelastic layers forming two-layer viscoelastic systems

Viscoelastic layer	Density (kg/m^3)	Thickness (nm)	Viscosity (kg/m.s)	Stiffness (N/m^2)
1	1200	1000	$6x10^{-3}$	$4x10^{7}$
2	1100	300	$5x10^{-2}$	$8x10^{6}$

7.3.1 Integration of sub-spacing method to the MTSM/GA technique for two-layer viscoelastic systems

The search space has been divided into 64 different sub-spaces consisting of different stiffness and viscosity values. The sub-spaces, in which the MTSM/GA shows distinctly better performances, were chosen to be the candidate solutions spaces. After identifying the possible solution spaces, the MTSM/GA was run 100 times in these candidate sub-spaces. The results have been shown in fig. 7-3.

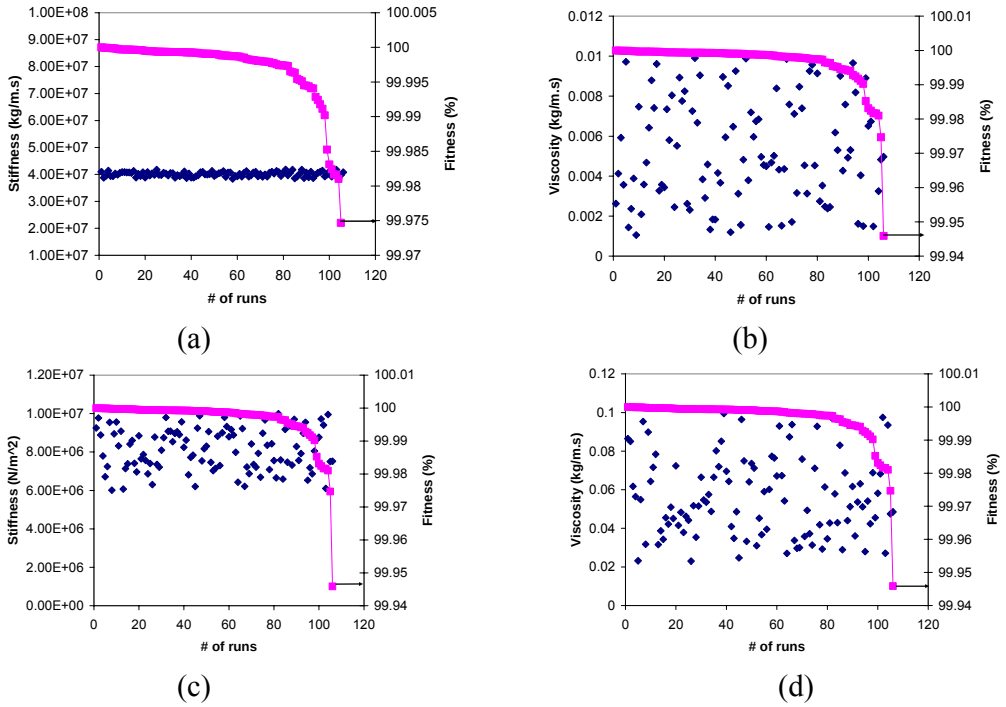

Figure 7-3 The results obtained by the MTSM/GA technique for two-layer viscoelastic systems after 100 runs for a) stiffness of first layer b) viscosity of first layer c) stiffness of second layer, and d) viscosity of second layer

As seen from the figure 7.3, the stiffness values for first layer fell around a very narrow solution space, which is between $3.8x10^7$ N/m^2 and $4.2x10^7$ N/m^2. Similarly the stiffness values for second layer are located in a restricted area between $6x10^6$ N/m^2 and 10^7 N/m^2. As remembered, the theoretical value for stiffness values for first and second layer were $4x10^7$ N/m^2 and $8x10^6$ N/m^2 respectively. It can be hypothesized that even though the system is an underdetermined problem, some variables will be more dominant than the others. In other words, in this example, if these two variables can be estimated with relatively good accuracy, the other two variables can also be estimated. Similar phenomenon has been observed in chapter 5 in the development of the MTSM/GA technique for single-layer viscoelastic system. In the following section, zooming method will be explained for fine tuning of the solutions.

7.3.2 Integration of zooming technique into the MTSM/GA technique for two-layer viscoelastic systems

The MTSM/GA was run 30 times, and then the new range was set to be between maximum and minimum numbers of the 30 points for each variable. The median of the points have been calculated and this number was then compared with the theoretical values. This zooming continued until the error was less than 1% for all variables. This error was achieved after 4 zooming (fig. 7-4). To increase the confidence, 6-time zooming has been utilized in this project.

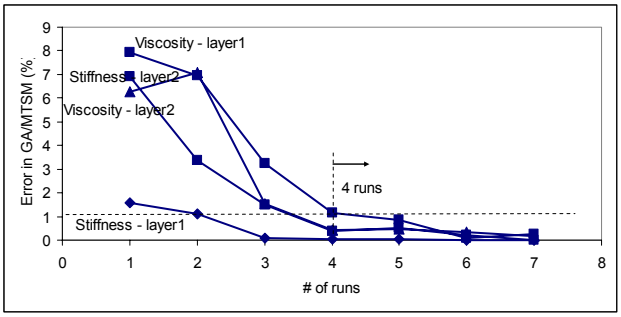

Figure 7-4 Error in the MTSM/GA technique two-layer viscoelastic systems with the number of runs

As seen from fig. 7-5, the stiffness values for first and second layers approach to the theoretical solutions which are $4x10^7$ N/m^2 and $8x10^6$ N/m^2 respectively. Similar effects are seen in density and viscosity values as well. It was shown that the after 6-zooming around the candidate points, the error between the median of the candidate points and for all variables are achieved to be less than 1%.

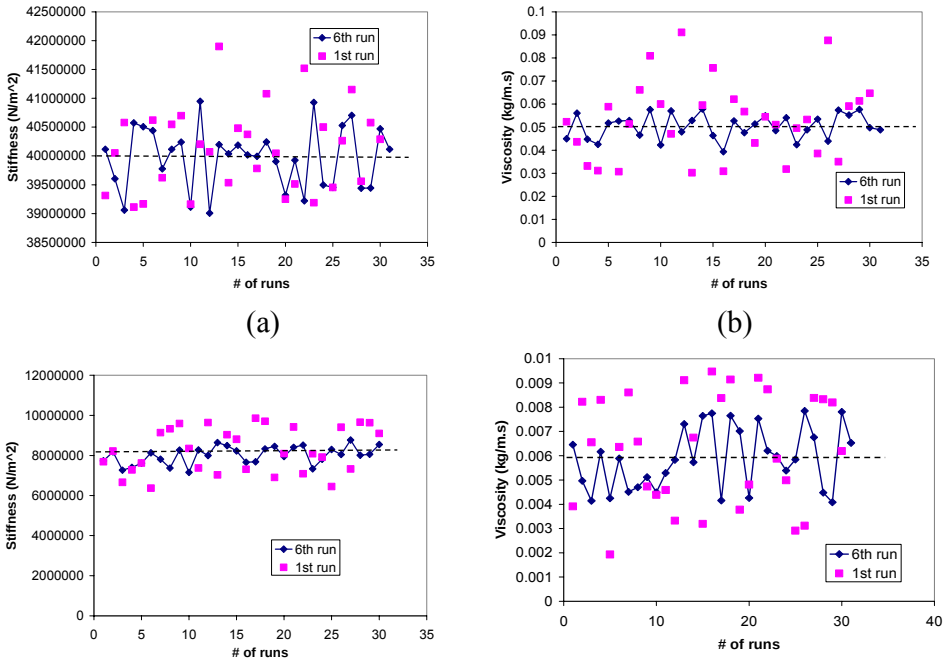

Figure 7-5 Zooming technique applied to a) stiffness of first layer b) viscosity of first layer c) stiffness of second layer, and d) viscosity of second layer (case: two-layer viscoelastic systems)

7.4 The effect of accurate estimation of the thickness and density values on the MTSM/GA technique

As discussed in section 7.1, the density and the thickness values of a two-layer viscoelastic system will be kept constant in the MTSM/GA technique. Therefore this requirement brings a question of "how the accuracy in estimation of the thickness and density values affect the MTSM/GA output". To answer this question, a hypothetical two-layer system is designed and simulated by using the TLM. Then the obtained maximum magnitude and the resonance frequency values were plugged into the MTSM/GA technique. Different combinations of errors introduced to the density and thickness values of the first and second viscoelastic layers. Figure 7-6 presents the error in the MTSM/GA technique depending on the errors introduced into the thickness and density values of the layers. As seen from the fig. 7-6, the error in determination of the stiffness value of the first layer increases to more than 2000 % if the error in the first layer's thickness is only 2 %. The errors for other parameters change between 1% to 100 % depending on the errors in the layers' properties. Error is presented as an absolute error.

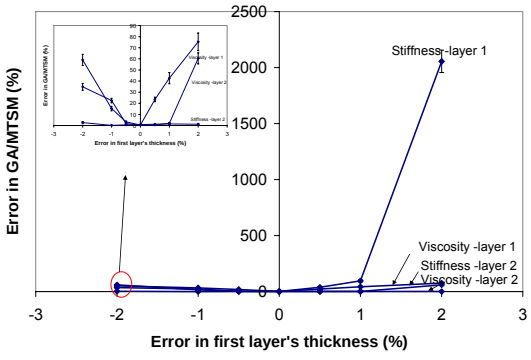

(a)

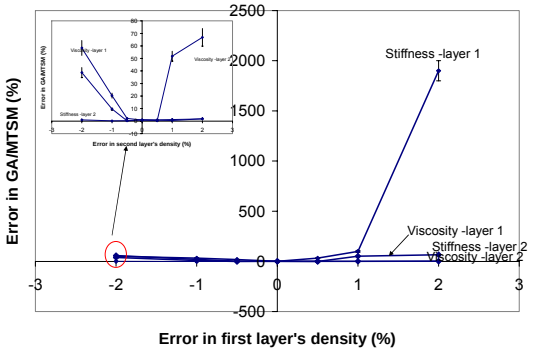

(b)

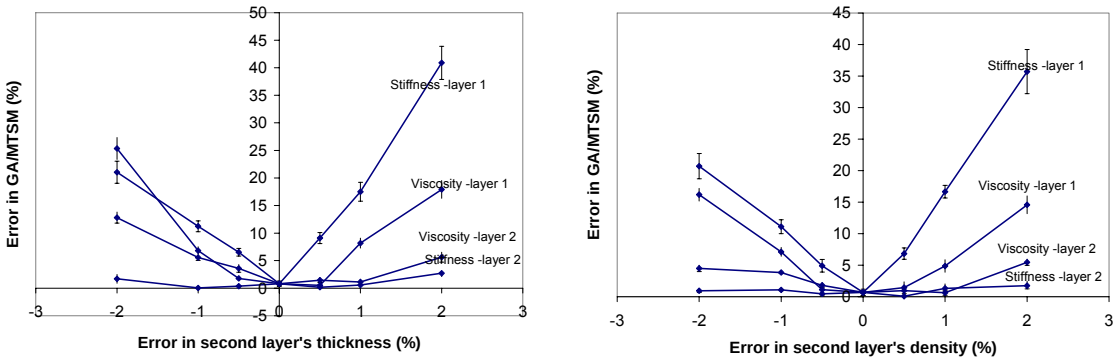

(c) (d)

Figure 7-6 Absolute error in the MTSM/GA technique two-layer viscoelastic systems when an error is introduced to (a) first layer's thickness (b) first layer's density (c) second layer's thickness and (d) second layer's density. Analysis is done at 5 MHz.

The similar analysis has been done at 15 MHz. As seen from fig. 7-7, the errors for each parameter are less than 20 %, which is much smaller than 2000 % that was seen at 5 MHz. Therefore it can be hypothesized that the error in the MTSM/GA technique will depend on the layers' properties.

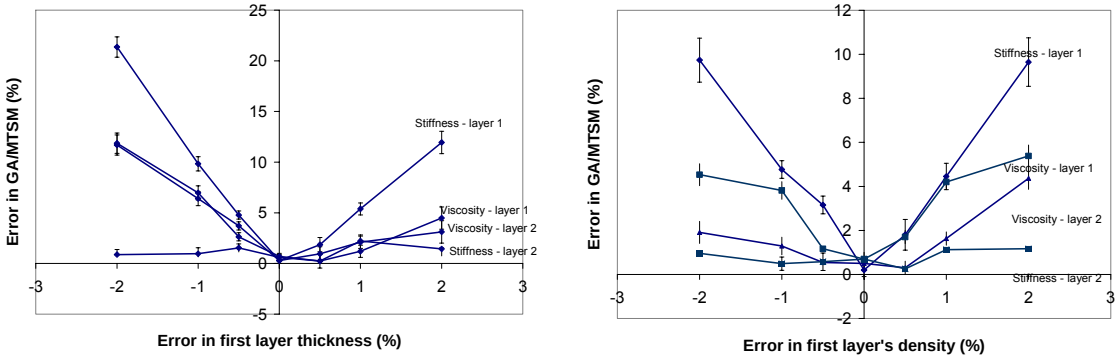

(a) (b)

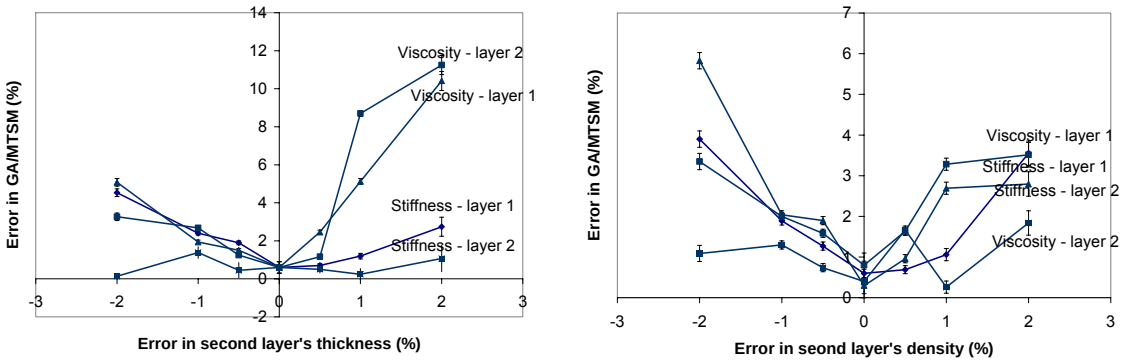

(c) (d)

Figure 7-7 Absolute error in MTSM/GA technique two-layer viscoelastic systems when an error is introduced to (a) first layer's thickness (b) first layer's density (c) second layer's thickness and (d) second layer's density. Analysis is done at 15 MHz.

To test this hypothesis, several different configurations of viscoelastic layers have been created by changing the stiffness value of the first layer. The stiffness value of the first layer was changed from $3x10^6$ N/m^2 to $4x10^7$ N/m^2. The 2 % error was introduced to the first layer's thickness. The errors in the stiffness value of the first layer determined by the MTSM/GA technique have been presented in fig. 7-8. As seen from the fig. 7-8, the error has reached to more than 2000 % when the first layer stiffness value reaches to $4x10^7$ N/m^2. In other words, the first layer acts more like hard rubber with very small loss value (-0.037) (α_{air} = 0.036 dB). Then it is hypothesized that if the first layer exhibits solid like properties, then the errors in the MTSM/GA technique may reach more than 1000 %. It should be noted that the error in the stiffness values increases with the increase in the stiffness value of the first layer. On the other hand, it is shown that the error in the viscosity values of the layers does not depend on the first layer's stiffness value.

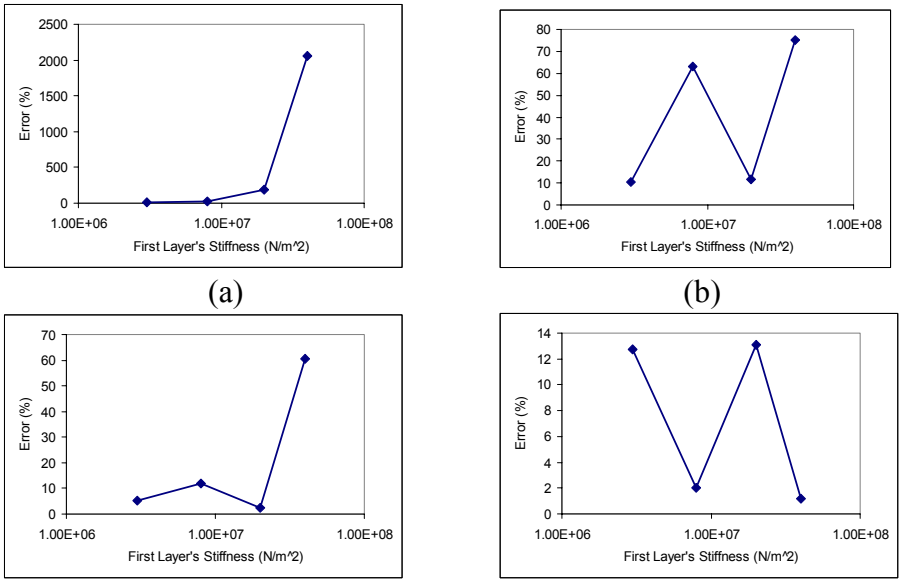

Figure 7-8 Absolute error in (a) first layer's stiffness (b) first layer's viscosity (c) second layer's stiffness and (d) second layer's viscosity at different stiffness values of first layer (case: two-layer viscoelastic systems)

Similar study was done at 15 MHz. The first layer's stiffness value has been increased from $4x10^6$ N/m^2 to $4x10^8$ N/m^2. The error in the MTSM/GA technique for each parameter is presented in fig.7-9.

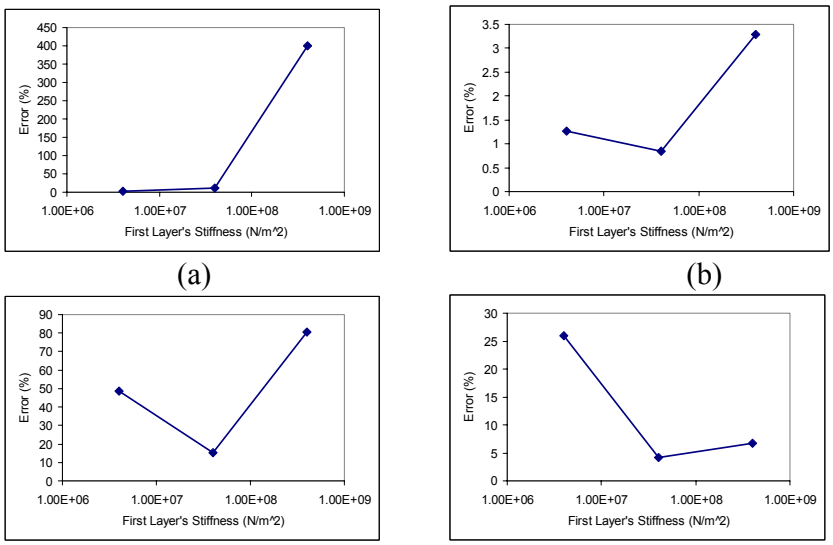

Figure 7-9 Absolute error in (a) first layer's stiffness (b) first layer's viscosity (c) second layer's stiffness and (d) second layer's viscosity at different stiffness values of first layer (case: two-layer viscoelastic systems)

As seen in the fig. 7-9, the error in the first layer's stiffness value increases with the increase in the stiffness value of first layer. The first layer approaches to hard rubber state with very low loss (-0.36) (α_{air} = 0.35 dB). Therefore it can be concluded that if the first layer's properties are hard rubber with very low loss or solid like system, then the MTSM/GA technique will be very sensitive to the error in the layers thickness and the density.

The two-layer viscoelastic system which is under consideration in this project also reflects a hard rubber system as first layer and a lossy system as a second layer. Therefore it should be expected the error in the experiments might be relatively higher (>30 %).

7.5 Effect of the error between experimental and theoretical results on the MTSM/GA technique

It has been shown in chapter 4 that there was an error observed between the experimental and theoretical values. The roots of this error have been discussed in detail in chapter 4. Therefore, here, the effect of this error on the MTSM/GA technique for two-layer viscoelastic layers has been investigated.

The hypothetical error is introduced to both magnitude and frequency responses. Initially the analysis has been done at 5 MHz. 0.5 %, 1 % and 1.5 % errors were introduced to the MTSM sensor's frequency response and 5 %, 10 %, and 20 % errors were introduced to the MTSM sensor's maximum magnitude response. As seen from the fig. 7-10, the error increases to 1800 % when the error in the resonance frequency was 1% (absolute error = 130 Hz). On the other hand, the error in the MTSM/GA technique reaches to 25 % when the error in the magnitude response is 20 % (absolute error = 0.016). As seen from the results, the stiffness value of the first layer is very sensitive to the experimental error. Even 1.5 % error in the MTSM sensor frequency response causes more than 1000 % error in the MTSM/GA sensor response for the stiffness value. The error for other variable varies 20 % to 70 %. The error in the magnitude response introduces only 25 % error in the MTSM/GA technique.

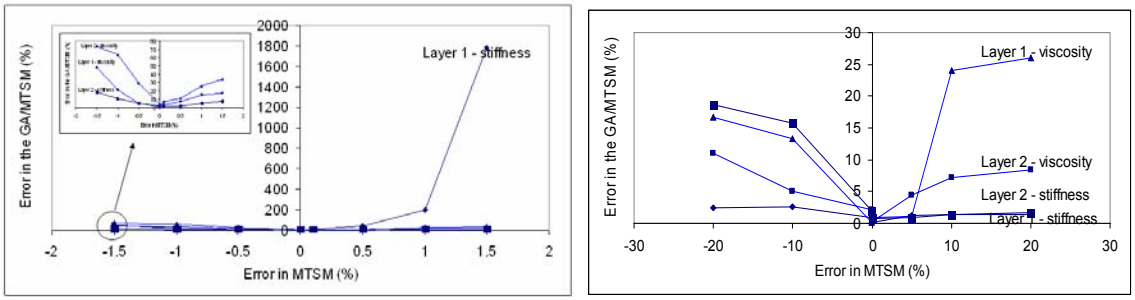

(a) (b)

Figure 7-10 Error in the MTSM/GA technique for two-layer viscoelastic systems when error in (a) resonance frequency and (b) maximum magnitude at 5 MHz

The hypothetical error is introduced to both magnitude and frequency responses at 15 MHz. The analysis has been done at 15 MHz. 0.5 %, 1 % and 10 % errors were introduced to the MTSM sensor's frequency response and 5 %, 10 %, and 20 % errors were introduced to the MTSM sensor's maximum magnitude response. The errors in the MTSM/GA technique for all parameters have been presented in fig. 7-11. As seen from the fig. 7-11, the error increases to ~150 % when the error in the resonance frequency was 10 % (absolute error = 3000 Hz). On the other hand, the error in the MTSM/GA technique reaches to 30 % when the error in the magnitude response is 20 % (absolute error = 1.17 dB).

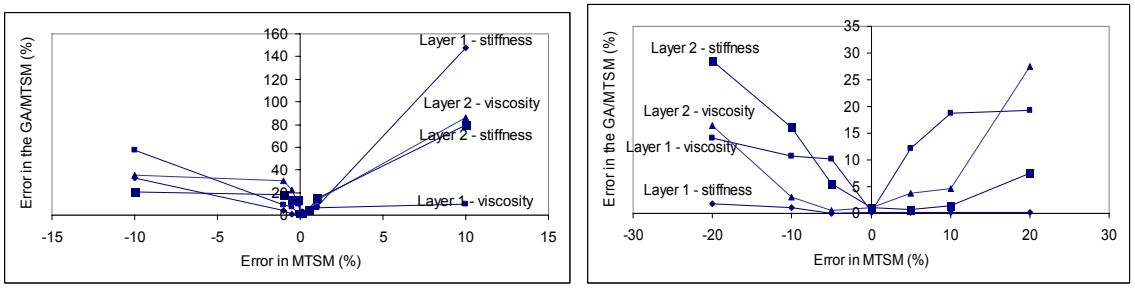

(a) (b)

Figure 7-11 Error in the MTSM/GA technique for two-layer viscoelastic systems when error in (a) resonance frequency and (b) maximum magnitude at 15 MHz

The hypothetical error is introduced to both amplitude and frequency responses at 25 MHz. The analysis has been done at 25 MHz. 0.5 %, 1% and 10 %errors were introduced to

the MTSM sensor's frequency response and 5 %, 10 %, and 20 % errors were introduced to the MTSM sensor's maximum magnitude response. The errors in the MTSM/GA technique for all parameters have been presented in fig. 7-12. As seen from the fig. 7-12, the error increases to ~50 % when the error in the resonance frequency was 10 % (absolute error = 8000 Hz). On the other hand, the error in the MTSM/GA technique reaches to 700 % when the error in the magnitude response is 20 % (absolute error = 3.8 dB).

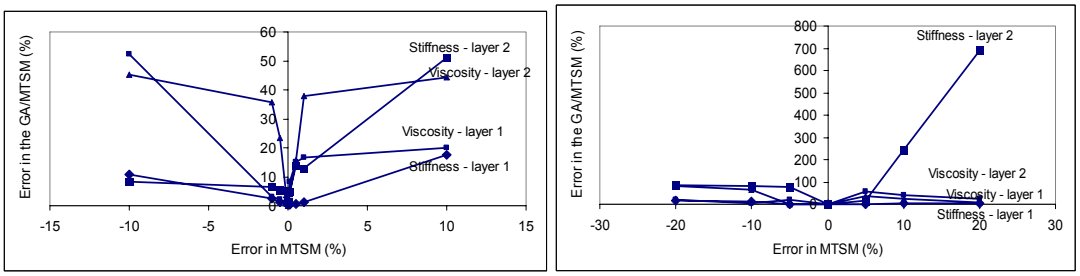

Figure 7-12 Error in the MTSM/GA technique for two-layer viscoelastic systems when error in (a) resonance frequency and (b) maximum magnitude at 25 MHz

At 35 MHz, it was seen that the MTSM sensor response was damped so that there was no visible maximum pick. Therefore the viscoelastic properties of the layer have been changed to $\eta_1 = 6x10^{-2}$ kg/m.s, $C_1 = 5x10^8$ N/m^2, and $\eta_2 = 5x10^{-2}$ kg/m.s, $C_2 = 8x10^7$ N/m^2. The hypothetical error is introduced to both maximum magnitude and frequency responses at 35 MHz. The analysis has been done at 25 MHz. 0.5 %, and 1% errors were introduced to the MTSM sensor's frequency response and 5 %, 10 %, and 20 % errors were introduced to the MTSM sensor's maximum magnitude response. The errors in the MTSM/GA technique for all parameters have been presented in fig. 7-13. As seen from the fig. 7-13, the error increases to ~45% when the error in the resonance frequency was 1% (absolute error = 650 Hz). On the other hand, the error in the MTSM/GA technique reaches to 40% when the error in the magnitude response is 20% (absolute error = 0.8 dB). When ±10% error was introduced to

the resonance frequency, it has been observed that there was no solution obtained for the two-layer system.

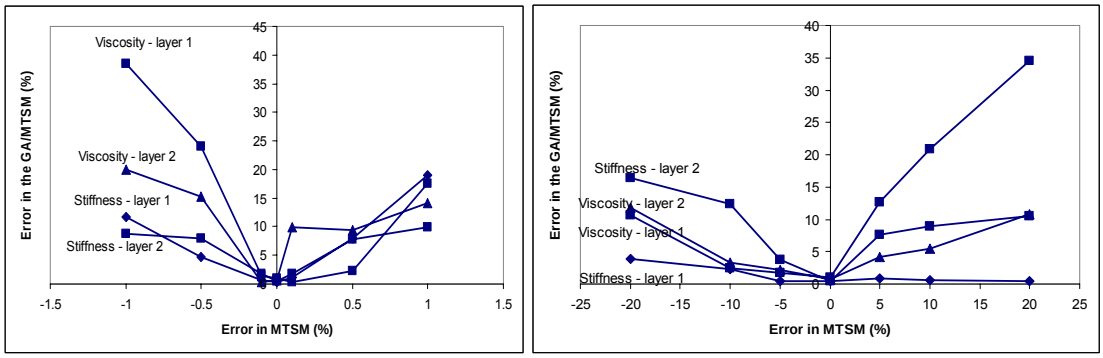

Figure 7-13 Error in the MTSM/GA technique for two-layer viscoelastic systems when error in (a) resonance frequency and (b) maximum magnitude at 35 MHz

7.6 Effect of the quality factor on the MTSM/GA technique for two-layer viscoelastic systems

To investigate the effect of quality factor on the MTSM/GA technique, a hypothetical three-layer system was designed and simulated by using the TLM (fig. 7-14). In this model, the first layer is a viscoelastic layer having stiffness (G'_1) of $4x10^7$ N/m^2, viscosity (η_1) of $6x10^{-3}$ kg/m.s, density (ρ_1) of 1200 kg/m^3 and thickness (d_1) of 1 μm. The second layer is a viscoelastic layer having stiffness (G'_2) of $8x10^6$ N/m^2, viscosity (η_2) of $5x10^{-2}$ kg/m.s, density (ρ_2) of 1100 kg/m^3 and thickness (d_2) of 0.3 μm. The third layer is chosen to be a semi-infinite Newtonian medium which has stiffness of 0 N/m^2 and density (ρ_c) of 1000 kg/m^3. To obtain different quality factor values, the viscosity of the Newtonian medium (η_c) is increased from 10^{-3} kg/ms to 10^{-1} kg/m.s. Performance of the MTSM/GA technique has been investigated at four different quality factors of the MTSM sensor. The analysis has been done at 5 MHz, 15 MHz, 25 MHz and 35 MHz. Calculation of the quality factor from the MTSM sensor's S21 response is given in Appendix 2.

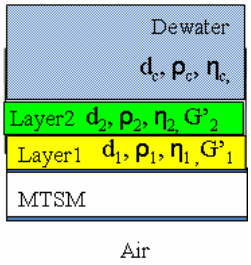

Figure 7-14 Hypothetical three-layer system to investigate the effect of quality factor on the MTSM/GA technique for two-layer viscoelastic systems

7.6.1 Effect of quality factor on the MTSM/GA technique for two-layer viscoelastic layers at 5 MHz

The viscosity of the Newtonian medium has been increased from 10^{-3} kg/ms to 10^{-1} kg/m.s to obtained different quality factors of the MTSM sensor. Five different viscosity values used in the theoretical experiments were 10^{-3} kg/m.s, $5x10^{-3}$ kg/m.s, 10^{-2} kg/m.s and 10^{-1} kg/m.s. Response of the MTSM sensor's resonance frequency and maximum magnitude to the different viscosity values of the third layer have been given in fig. 7-15. As seen from the fig. 7-15, both maximum magnitude and resonance frequency of the MTSM sensor decreased. Dynamic range of the MTSM sensor response decreased with the decrease of the quality factor. Dynamic range is defined as the difference between the maximum and minimum magnitude of the MTSM sensor's S21 response. As seen in fig. 7-14b, no zero phase is observed when the viscosity of the third layer was 10^{-1} kg/m.s.

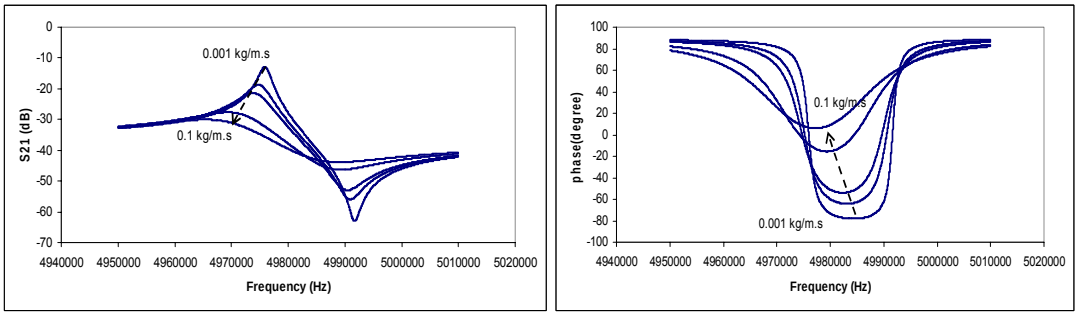

(a) (b)

Figure 7-15 Influence of the quality factor on the MTSM sensor's for two-aye viscoelastic systems (a) magnitude and (b) phase responses at 5 MHz (case: two-layer viscoelastic systems)

The quality factor has been change from 2600 to 0 by increasing the viscosity value of the third layer. At each viscosity value, the properties of the medium are determined by the MTSM/GA technique and the absolute error between the estimated values and the values input to the TLM model has been presented in fig. 7-16.

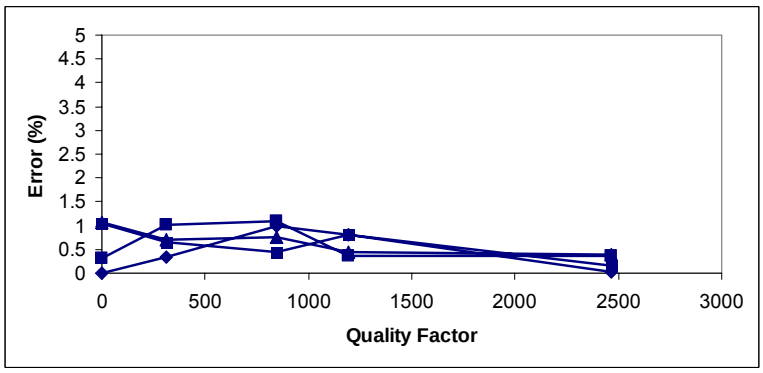

Figure 7-16 The effect of quality factor on the MTSM/GA technique for two-layer viscoelastic systems at 5 MHz

As seen from fig. 7-16, the error in the MTSM/GA technique is always equal or less than 1 % when the quality factor decreases to 0. Loses value reached to ~-30.00 dB when quality factor became 0.

7.6.2 Effect of quality factor on the MTSM/GA technique for two-layer viscoelastic layers at 15 MHz

The MTSM sensor's magnitude and phase responses to the change in the quality factor at 15 MHz are give in fig. 7-17. As seen from the fig. 7-17, both the maximum magnitude and the resonance frequency of the MTSM sensor decrease at 15 MHz. Dynamic range of the MTSM sensor response decreased with the decrease of the quality factor. It should be noted that the zero phase is achieved when the viscosity value of the third layer is 10^{-3} kg/m.s. When the viscosity value increases to 10^{-1} kg/m.s, the MTSM sensor is so damped that no maximum pick is observed in the magnitude response.

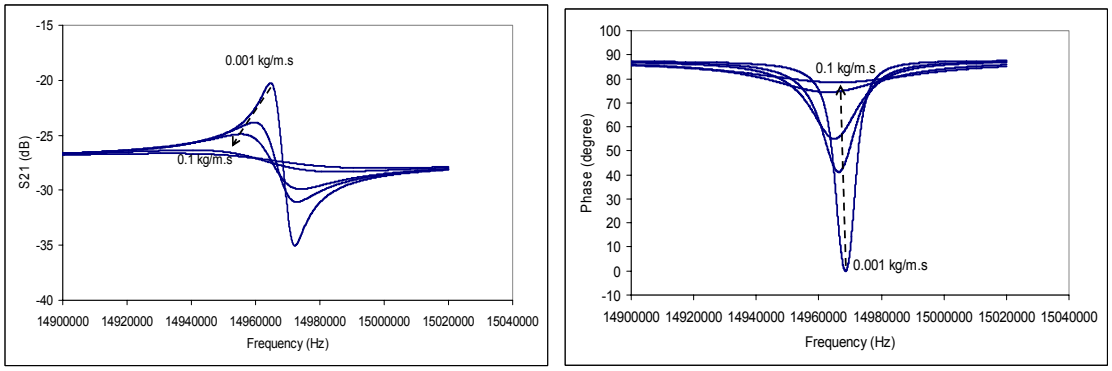

Figure 7-17 Influence of the quality factor on the MTSM sensor's for two-layer viscoelastic systems (a) magnitude and (b) phase responses at 15 MHz

The quality factor has been changed from 1600 to 0 by increasing the viscosity value of the third layer. The quality factor reaches to 0 when the viscosity value of the third layer becomes 10^{-2} kg/m.s. Therefore the absolute error vs. quality factor graph is presented as absolute error vs. maximum magnitude. At each viscosity value, the properties of the medium are determined by the MTSM/GA technique and the absolute error between the estimated values and the values input to the TLM model has been presented in fig. 7-18. As seen from

the fig. 7-18, the error in the MTSM/GA technique increases to more than 1 % when the maximum magnitude decreases to -24 dB.

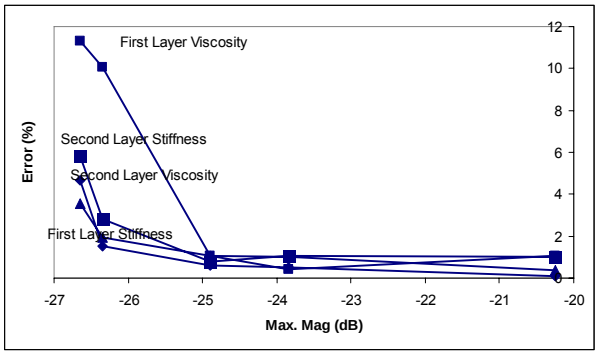

Figure 7-18 The effect of the quality factor on the MTSM/GA technique for two-layer viscoelastic systems at 15 MHz

7.6.3 Effect of quality factor on the MTSM/GA technique for two-layer viscoelastic layers at 25 MHz

At 25 MHz, it was seen that the MTSM sensor response was damped so that there was no visible maximum pick. Therefore the viscoelastic properties of the first two layers have been changed to $\eta_1 = 6x10^{-2}$ kg/m.s, $C_1 = 5x10^{8}$ N/m^2, and $\eta_2 = 5x10^{-2}$ kg/m.s, $C_2 = 8x10^{7}$ N/m^2.

The MTSM sensor's magnitude and phase responses to the change in the quality factor at 25 MHz are given in fig. 7-19. As seen from the fig. 7-19, both the maximum magnitude and the resonance frequency of the MTSM sensor decrease with the decrease in the quality factor. Dynamic range of the MTSM sensor response decreased as well. It should be noted that the zero phase is achieved at any quality factor. When the viscosity value increases to 10^{-1} kg/m.s, the MTSM sensor is so damped that no maximum pick is observed in the magnitude response.

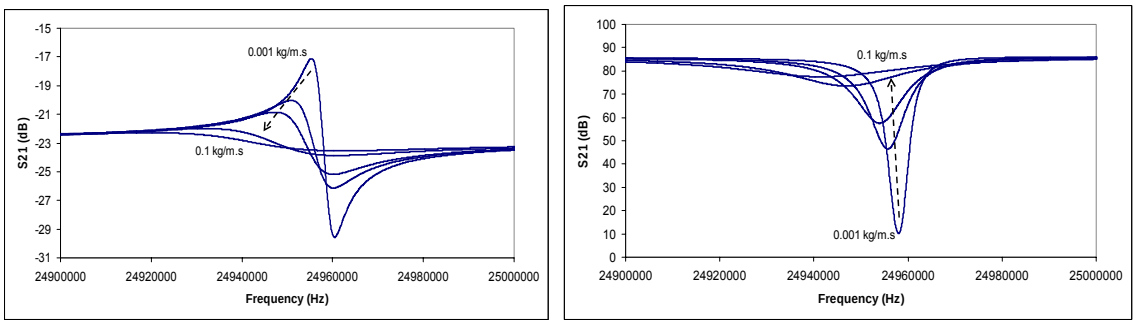

(a) (b)

Figure 7-19 Influence of quality factor on the MTSM sensor's for two-layer viscoelastic systems (a) magnitude and (b) phase responses at 25 MHz

The quality factor has been changed from 3000 to 0 by increasing the viscosity value of the third layer. The quality factor reaches to 0 when the viscosity value of the third layer becomes 0.001 kg/m.s. Therefore the absolute error vs. quality factor graph is presented as absolute error vs. maximum magnitude. At each viscosity value, the properties of the medium are determined by the MTSM/GA technique and the absolute error between the estimated values and the values input to the TLM model has been presented in fig. 7-20. As seen from the fig. 7-19, the error in the MTSM/GA technique increases to more than 1 % when the maximum magnitude decreases to -22 dB.

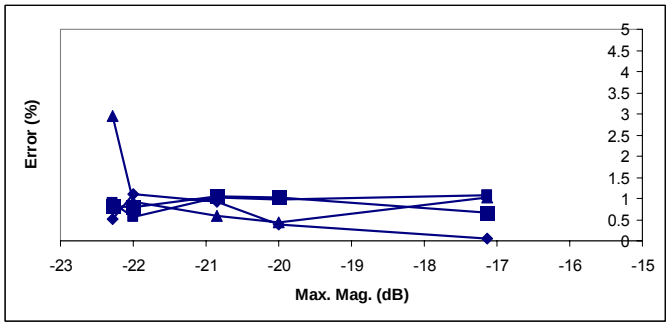

Figure 7-20 The effect of the quality factor on the MTSM/GA technique for two-layer viscoelastic systems at 25 MHz

7.6.4 Effect of Quality Factor on the MTSM/GA technique for two-layer viscoelastic systems at 35 MHz

At 35 MHz, it was seen that the MTSM sensor response was damped so that there was no visible maximum pick. Therefore the viscoelastic properties of the first two layers have been changed to $\eta_1 = 6x10^{-2}$ kg/m.s, $C_1 = 5x10^8$ N/m^2, and $\eta_2 = 5x10^{-2}$ kg/m.s, $C_2 = 8x10^7$ N/m^2.

The MTSM sensor's magnitude and phase responses to the change in the quality factor at 35 MHz are given in fig. 7-21. As seen from the fig. 7-21, both the maximum magnitude and the resonance frequency of the MTSM sensor decrease with the decrease in the quality factor.

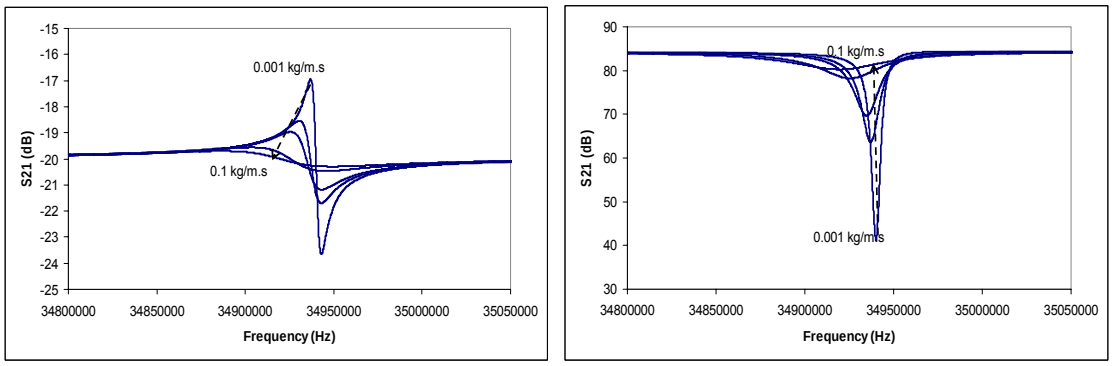

(a) (b)

Figure 7-21 Influence of the quality factor on the MTSM sensor's fro two-layer viscoelastic systems (a) magnitude and (b) phase responses at 35 MHz

The quality factor reaches to 0 when the viscosity value of the third layer is 0.001 kg/m.s. Therefore the absolute error vs. quality factor graph is presented as absolute error vs. maximum magnitude. At each viscosity value, the properties of the medium are determined by the MTSM/GA technique and the absolute error between the estimated values and the values input to the TLM model has been presented in fig. 7-22. As seen from the fig. 7-22, the error in the MTSM/GA technique increases to more than 1% when the maximum magnitude decreases to -19 dB.

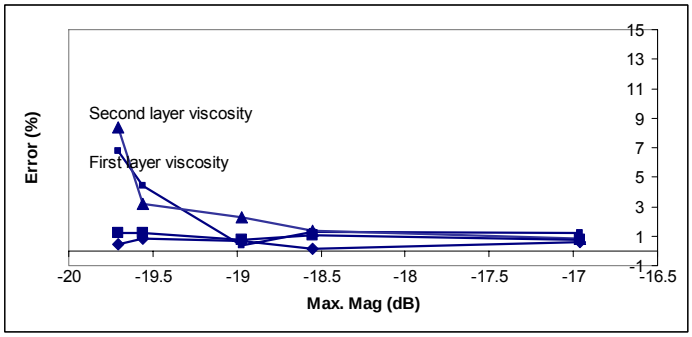

Figure 7-22 The effect of the quality factor on the MTSM/GA technique for two-layer viscoelastic systems at 35 MHz

7.7 Analysis of the MTSM sensor response to a polymer deposition process for the theoretical validation of the GA/MTM technique for two-layer viscoelastic systems

There are eight parameters which define the acoustic impedance for two-layer viscoelastic systems. Thus there might be unlimited different combination of these parameters. The aim of this project is to validate the MTSM/GA technique. It will not possible to cover all different combinations. Therefore the layers' properties are chosen to be the closest to the experimental system's which will be made of SU8-2002 and collagen polymers. The SU8-2002 represents a hard rubber like system and collagen evaporation which covers all four viscoelastic regimes which were discussed in the chapter 5. The properties of the first layer of the multilayer system will be $4x10^7$ N/m^2, $6x10^{-3}$ kg/m.s, 1000 nm and 1200 kg/m^3 for stiffness, viscosity, thickness and density values respectively. The second layer properties will be changing according to the evaporation process which was discussed in chapter 5 (table 7-2).

Table 7-2 Second viscoelastic layer's properties for the validation of the MTSM/GA technique for two-layer viscoelastic systems

	Four phases of second viscoelastic layer			
Properties	**Stage I**	**Stage II**	**Stage III**	**Stage IV**
Thickness (nm)	3000	1000	500	500
Stiffness (N/m^2)	10^5	$2x10^6$	$5x10^7$	$5x10^8$
Viscosity (kg/m.s)	$2x10^{-3}$	$7x10^{-3}$	$2x10^{-2}$	10^{-1}
Density (kg/m^3)	1000	1100	1200	1300
	Liquid like	Soft rubber	Hard Rubber	Solid like

In the following section, each stage of the deposition process discussed by analyzing the acoustic signatures of the MTSM sensor at 5 MHz, 15 MHz, 25 MHz and 35 MHz. Then the MTSM/GA technique was applied and critically evaluated to understand its limitations and strengths in determining the viscoelastic properties of two-layer biological layers.

7.7.1 Analysis of the MTSM/GA technique for two-layer viscoelastic systems to deposition process at 5 MHZ

The changes in the magnitude and phase responses of the MTSM sensor to the five different viscoelastic systems has been simulated at 5 MHz using transmission line model and presented in fig. 7.23a and b. The response at t_1 represents the response to the single layer (the MTSM is loaded with only one layer). Time responses of the maximum magnitude and the resonance frequency are given in fig. 7-23c. As seen from fig. 7-23c, the maximum magnitude decreases until time t_3, and reaches to the value of -21 dB. Then it sharply increases to -5 dB at t_4. The resonance frequency continuously decreases until time t_2 then increases. Here, time t_2 represents the MTSM sensor response to the first viscoelastic layer. In other words, the MTSM sensor was loaded with only single viscoelastic layer.

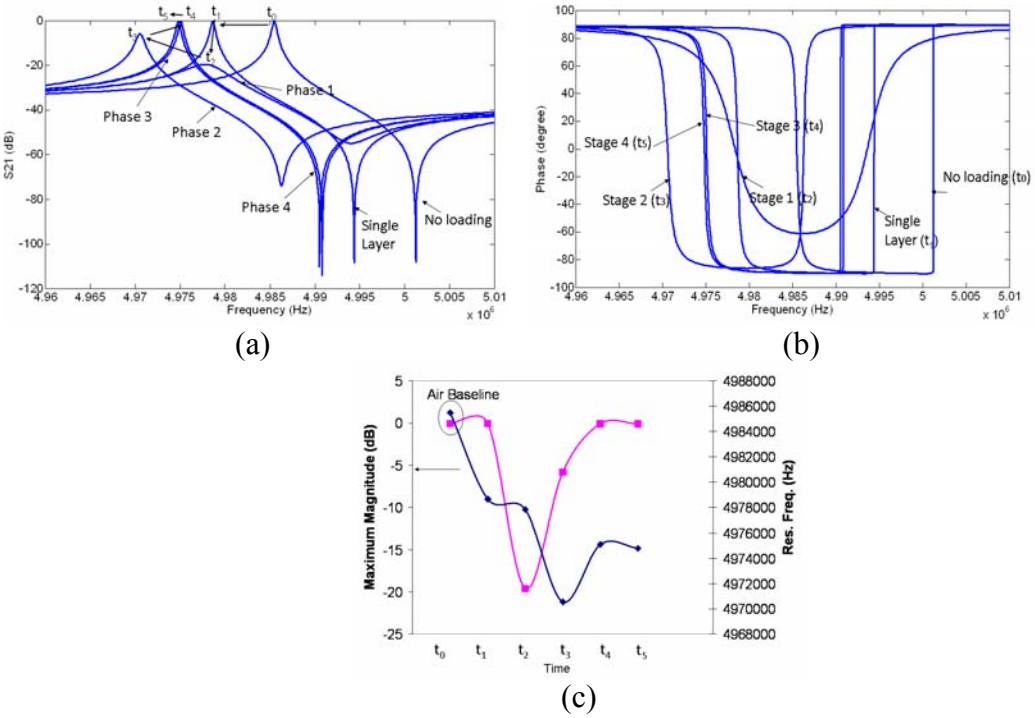

(a) (b)

(c)

Figure 7-23 Change in (a) the magnitude and (b) phase responses of the MTSM sensor during evaporation process. (c) Change in maximum magnitude and resonance frequency in time at 5 MHz. (case: two-layer viscoelastic systems)

In the stage I, the second viscoelastic layer shows a "transition state" properties where G" and G' is close to each other (G' = 10^5 N/m^2 and G" = 0.63x10^5 N/m^2). The first viscoelastic layer has G' = 4x10^7 N/m^2 and G" = 1.9x10^5 N/m2. The ratio of first layer's complex shear modulus to second layer's shear modulus is ~400. The change in the maximum magnitude and the resonance frequency responses of the MTSM sensor with the different viscosity and stiffness values of second layer at 5 MHz are given in fig.7-24a and b. As seen from the fig. 7-24a, the oscillations start when the stiffness value of the second layer reaches to 2x10^5 N/m^2. In other words, the penetration depth reached close to the column height which is 4 μm.

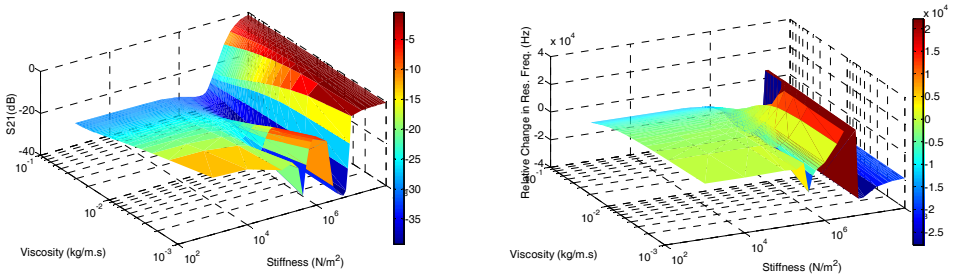

(a) (b)

Figure 7-24 Effect of the changes in the two-layer viscoelastic systems viscosity and stiffness to the MTSM sensor's (a) magnitude and (b) resonance frequency responses (relative changes in resonance frequency and absolute values of magnitude in dB) at 5 MHz in Stage I.

The MTSM/GA technique was then applied to determine the layer properties. It is clearly seen in fig 7-25, after 100 runs of the MTSM/GA technique, there are two distinct solutions for viscosity and stiffness values of the second viscoelastic layer. As seen in fig. 7-25, solution bandwidths for the second layer's properties are very small.

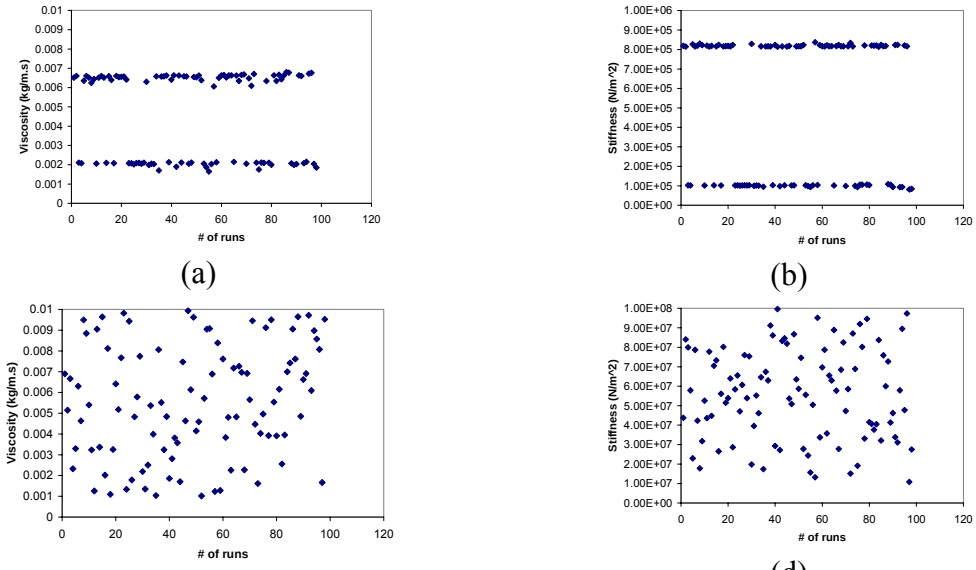

(a) (b)

(c) (d)

Figure 7-25 The results obtained by the MTSM/GA technique for two-layer viscoelastic systems after 100 runs for a) layer-2 viscosity b) layer-2 stiffness c) layer-1 viscosity, and d) layer-1 stiffness

The mechanical properties of the layers were determined with less than 1% error and presented in table 7-3. On the other hand, it should be noted that there was a second solution for the viscoelastic system.

Table 7-3 Mechanical properties determined by the MTSM/GA technique for two-layer viscoelastic systems and % errors in stage I at 5 MHz

Properties	Values Input to TLM	Values Determined by MTSM/GA Technique	Error (%)
G'_1 (N/m^2)	$4x10^7$	$4.01x10^7$	0.3
G'_2 (N/m^2)	10^5	$0.99x10^5$	0.2
η_1 (kg/m.s)	$6x10^{-3}$	$6.02x10^{-3}$	0.3
η_2 (kg/m.s)	$2x10^{-3}$	$2.01x10^{-3}$	0.5

It can be concluded that the viscoelastic system may have more than one solution. In this case, other points in the S21 response can be utilized. It has been observed that the anti-resonance frequency and the frequency at minimum phase show difference for two solutions. The difference is 40 Hz and it is much higher than the typical noise level in air (1-2 Hz). Therefore this point can be utilized for the selection of the correct solution in this example. Furthermore it was suggested that monitoring time response of the biological process may overcome the multiple solution problem, since it can provide the time evolution of the change in the layer's properties. The second method to overcome the multiple-solution problem is to utilize the real time kinetics monitoring technique. This has been discussed in chapter 5 and 6.

In the stage II, the second viscoelastic layer shows a "soft rubber" properties where G" is 9 times higher than G' (G' = $2x10^6$ N/m^2 and G" = $0.23x10^6$ N/m^2). The first viscoelastic layer has G' = $4x10^7$ N/m^2 and G" = $1.9x10^5$ N/m2. The ratio of first layer's complex shear modulus to second layer's shear modulus is ~20. The thickness of the second layer was also decreased to 1000 nm.

The change in the maximum magnitude and the resonance frequency responses of the MTSM sensor with the different configurations of viscosity and stiffness of second layer at 5 MHz in stage II are given in fig.7-26. As seen from the fig. 7-26, the oscillations start when the stiffness value of the second layer reaches to $2x10^5$ N/m^2. In other words, the penetration depth reached the column height which is ~2 μm.

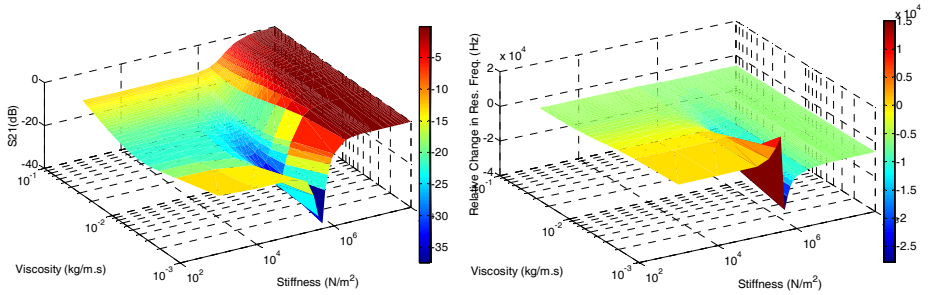

(a) (b)

Figure 7-26Effect of the changes in the two-layer viscoelastic systems viscosity and stiffness to the MTSM sensor's (a) magnitude and (b) resonance frequency responses (relative changes in resonance frequency and absolute values of magnitude in dB) at 5 MHz in Stage II.

The MTSM/GA technique has been run 100 times and the results are presented in the fig. 7-27. As seen from the fig. 7-27, the viscosity values for second viscoelastic layer are fall between $5x10^{-3}$ kg/m.s and $9x10^{-3}$ kg/m.s. Similarly, the solutions for the stiffness value for second layer fall between $1.7x10^6$ N/m^2 and $2.3x10^6$ N/m^2.

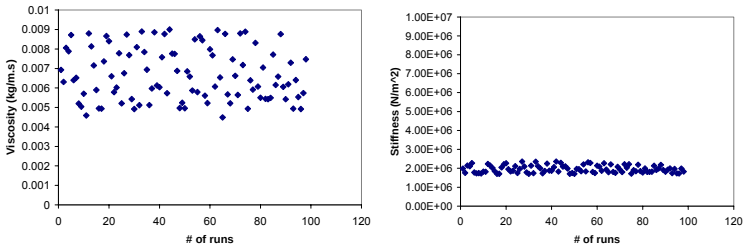

(a) (b)

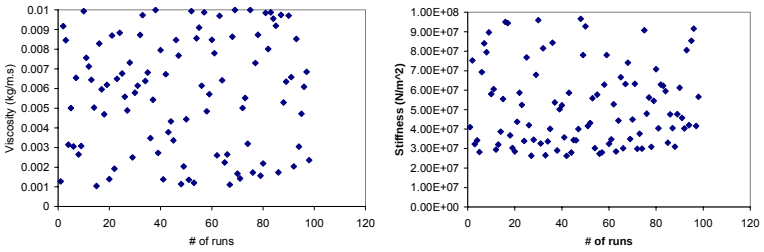

(c) (d)

Figure 7-27 The results obtained by the MTSM/GA technique for two-layer viscoelastic systems after 100 runs for a) layer-2 viscosity b) layer-2 stiffness c) layer-1 viscosity, and d) layer-1 stiffness in stage II at 5 MHz

The zooming technique has been applied for fine tuning of the solutions. Tow solutions were obtained. The first solution was determined with less than 1% error. The other tracking points have been checked and it was observed that the results were the same.

Table 7-4Mechanical properties determined by the MTSM/GA technique for two-layer viscoelastic systems and % errors in stage II at 5 MHz

Properties	Values Input to TLM	Values Determined by MTSM/GA Technique	Error (%)
G'_1 (N/m^2)	$4x10^7$	$4.01x10^7$	0.3
G'_2 (N/m^2)	$2x10^6$	$2.01x10^6$	0.2
η_1 (kg/m.s)	$6x10^{-3}$	$6.01x10^{-3}$	0.3
η_2 (kg/m.s)	$7x10^{-3}$	$7.02x10^{-3}$	0.5

In the stage III, the second viscoelastic layer shows a “hard rubber” properties where G’ is 80 times higher than G” (G’ = $5x10^7$ N/m^2 and G” = $6.3x10^5$ N/m^2). The first viscoelastic layer has G’ = $4x10^7$ N/m^2 and G” = $1.9x10^5$ N/m2. The ratio of first layer’s complex shear modulus to second layer’s shear modulus is ~0.8. The thickness of the second layer was also decreased to 500 nm. The change in the maximum magnitude and the resonance frequency responses of the MTSM sensor are given in fig.7-28. As seen from the fig. 7-28, the oscillations start when the stiffness value of the second layer reaches to 10^4 N/m^2. In other words, the penetration depth reached the column height which is 1.5 μm.

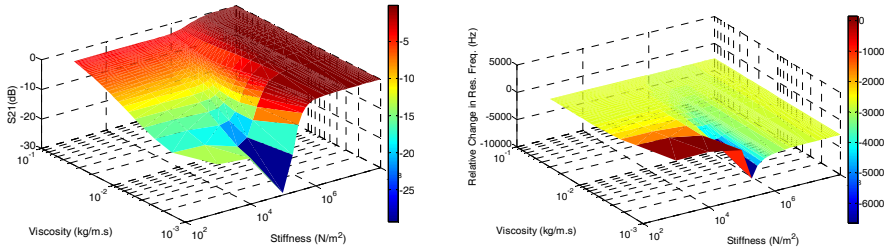

(a) (b)

Figure 7-28Effect of the changes in the two-layer viscoelastic systems viscosity and stiffness to the MTSM sensor's (a) magnitude and (b) resonance frequency response (relative changes in resonance frequency and absolute values of magnitude in dB) at 5 MHz in Stage III

The MTSM/GA technique has been run 100 times and the results are presented in the fig. 7.29. As seen from the fig. 7.29, the viscosity values for first viscoelastic layer are fall between $4x10^{-3}$ kg/m.s and $7x10^{-3}$ kg/m.s. Similarly, the solutions for the stiffness value for second layer fall between $3.8x10^{7}$ N/m^2 and $4.2x10^{7}$ N/m^2.

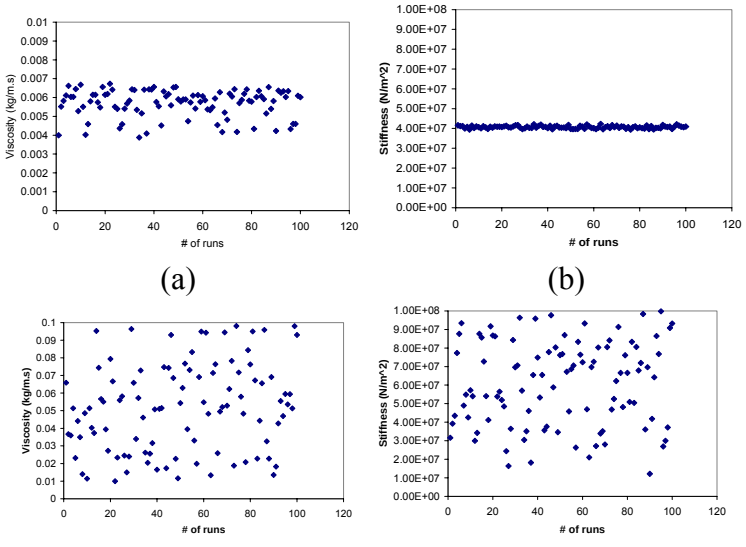

(a) (b)

(c) (d)

Figure 7-29 The results obtained by the MTSM/GA technique for two-layer viscoelastic systems after 100 runs for a) layer-1 viscosity b) layer-1 stiffness c) layer-2 viscosity, and d) layer-2 stiffness

The zooming technique has been applied for fine tuning of the solutions. The only one solution obtained from the MTSM/GA technique has been presented in table 7-5. As seen from the table 7.5, the solutions were obtained with less than 1% error.

Table 7-5Values determined by the MTSM/GA technique for two-layer viscoelastic systems and % errors in stage III at 5 MHz

Properties	Values Input to TLM	Values Determined by MTSM/GA Technique	Error (%)
G'_1 (N/m^2)	$4x10^7$	$4.03x10^7$	0.8
G'_2 (N/m^2)	$5x10^7$	$5.05x10^7$	1
η_1 (kg/m.s)	$6x10^{-3}$	$6.04x10e^{-3}$	0.6
η_2 (kg/m.s)	$2x10^{-2}$	$1.98x10^{-2}$	0.1

In the stage IV, the second viscoelastic layer shows a "solid like" properties where G' is 160 times higher than G" (G' = $5x10^8$ N/m^2 and G" = $3.14x10^6$ N/m^2). The first viscoelastic layer has G' = $4x10^7$ N/m^2 and G" = $1.9x10^5$ N/m2. The ratio of first layer's complex shear modulus to second layer's shear modulus is ~0.08. The thickness of the second layer is 500 nm. The change in the maximum magnitude and the resonance frequency responses of MTSM sensor at 5 MHz are given in fig.7-30. As seen from the fig. 7-30, the oscillations start when the stiffness value of the second layer reaches to 10^4 N/m^2. In other words, the penetration depth reached the column height which is 1.5 μm.

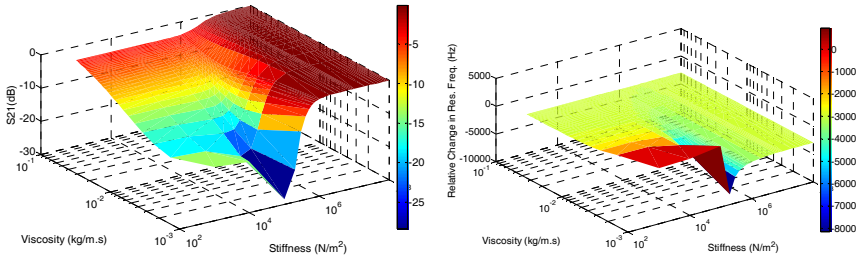

(a) (b)

Figure 7-30Effect of the changes in the two-layer viscoelastic systems viscosity and stiffness to the MTSM (a) magnitude and (b) resonance frequency responses (relative changes in resonance frequency and absolute values of magnitude in dB) at 5 MHz in Stage IV

The MTSM/GA technique has been run 100 times and the results are presented in the fig. 7.31. As seen from the fig. 7-31, the viscosity values for first viscoelastic layer are fall between $5x10^{-3}$ kg/m.s and $6.1x10^{-3}$ kg/m.s. Similarly, the solutions for the stiffness value for second layer fall between $3.9x10^{7}$ N/m^2 and $4.1x10^{7}$ N/m^2.

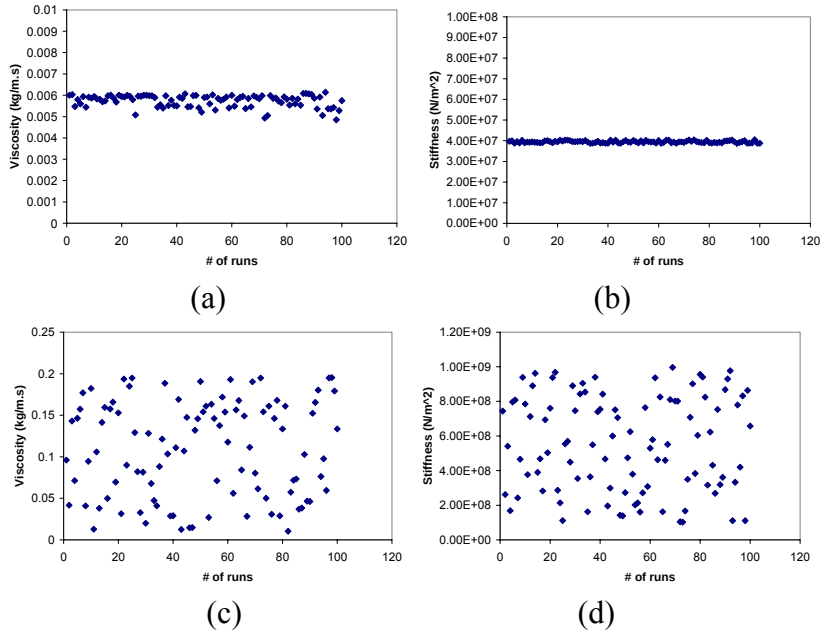

Figure 7-31 The results obtained by the MTSM/GA technique for two-layer viscoelastic systems after 100 runs for a) layer 1 viscosity b) layer 1 stiffness c) layer 2 viscosity, and d) layer 2 stiffness

The zooming technique has been applied for fine tuning of the solutions. The only one solution obtained from the MTSM/GA technique has been presented in table 7-5.

Table 7-6Values determined by the MTSM/GA technique for two-layer viscoelastic systems and % errors in stage IV at 5 MHz

Properties	Values Input to TLM	Values Determined by MTSM/GA Technique	Error (%)
G'_1 (N/m^2)	$4x10^{7}$	$4.03x10^{7}$	0.9
G'_2 (N/m^2)	$5x10^{8}$	$5.5x10^{8}$	10
η_1 (kg/m.s)	$6x10^{-3}$	$5.99x10^{-3}$	0.6
η_2 (kg/m.s)	10^{-1}	$9.9x10^{-2}$	10

It should be noted that the error in the second layer's properties increases to more than 1% (~10 %). In this stage second layer shows solid like system. It was shown in the chapter 5 that the MTSM/GA technique will not able to determine the viscoelastic properties of a solid like system because the sensor response is determine by the density and the thickness product. Thus it can be concluded that even though the first layer's viscoelastic properties are determined with less than 1 % error, the second layer's properties will not be determined with less than 1 % error if the second layer exhibits solid-like properties.

7.7.2 Analysis of the MTSM/GA technique for two-layer viscoelastic systems to deposition process at 15 MHZ

The changes in the magnitude and phase responses of the MTSM sensor to the five different viscoelastic systems has been simulated at 15 MHz using transmission line model and presented in fig. 7-32a and b. The response at t_1 represents the response to the single layer (the MTSM is loaded with only one layer). Time responses of the maximum magnitude and resonance frequency are given in fig. 7-32c. As seen from fig. 7-32c, the maximum magnitude decreases until time t_3, and reaches to the value of -25 dB. Then it sharply increases to -5 dB at t_4. The resonance frequency decreases until time t_2 then increases at t_3, then again decreases at t_4 and t_5.

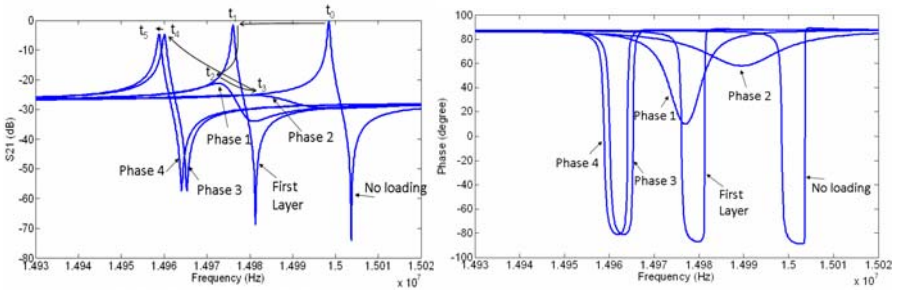

(a) (b)

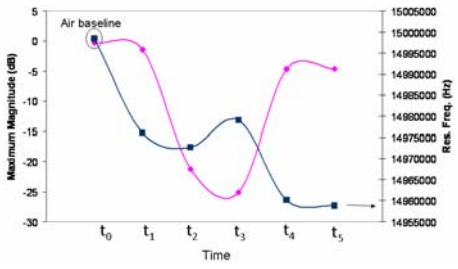

(c)

Figure 7-32 Change in (a) magnitude and (b) phase responses of the MTSM sensor during evaporation process. (c) Change in maximum magnitude and resonance frequency by time at 15 MHz.

In the stage I, the second viscoelastic layer shows a "transition like" properties where G" is ~2 times higher than G'. (G' = 10^5 N/m^2 and G" = 1.9x10^5 N/m^2). The first viscoelastic layer has G' = 4x10^7 N/m^2 and G" = 1.9x10^5 N/m2. The ratio of first layer's complex shear modulus to second layer's shear modulus is ~190. The thickness of the second layer is 3000 nm. The change in the maximum magnitude and the resonance frequency responses of the MTSM sensor as a function of viscosity and stiffness of second layer in stage I at 15 MHz are given in fig. 7-33. As seen from the fig. 7-33, the oscillations start when the stiffness value of the second layer reaches to 10^5 N/m^2. In other words, the penetration depth reached the column height which is 4 μm.

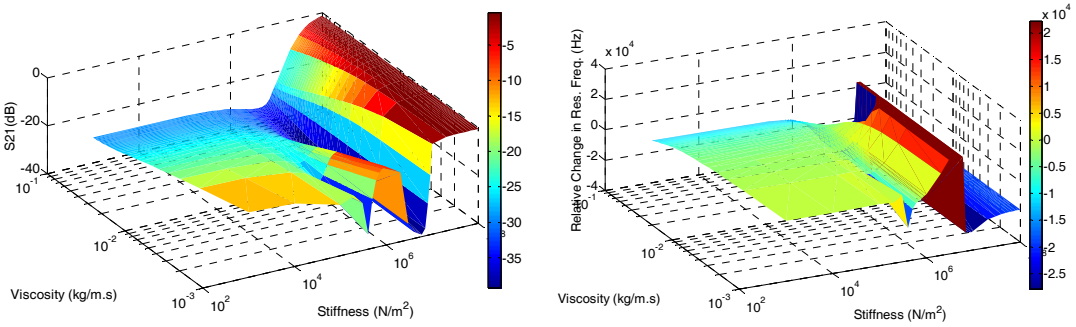

(a) (b)

Figure 7-33Effect of the changes in the two-layer viscoelastic systems viscosity and stiffness to MTSM (a) magnitude and (b) resonance frequency response (relative changes in resonance frequency and absolute values of magnitude in dB) at 15 MHz in Stage I

The zooming technique has been applied for fine tuning of the solutions. The single solution obtained from the MTSM/GA technique has been presented in table 7.6. Less than 1% error has been accomplished for each variable.

Table 7-7Values determined by the MTSM/GA technique for two-layer viscoelastic systems and % errors in stage I at 15 MHz

Properties	Values Input to TLM	Values Determined by MTSM/GA Technique	Error (%)
G'_1 (N/m^2)	$4x10^7$	$3.99x10^7$	0.2
G'_2 (N/m^2)	10^5	$1.01x10^5$	1
η_1 (kg/m.s)	$6x10^{-3}$	$6.03x10^{-3}$	0.5
η_2 (kg/m.s)	$2x10^{-3}$	$2.01x10^{-3}$	0.5

In the stage II, the second viscoelastic layer shows a "transition like" properties where G' is 3 times higher than G". (G' = $2x10^6$ N/m^2 and G" = $6.6x10^5$ N/m^2). The first viscoelastic layer has G' = $4x10^7$ N/m^2 and G" = $6.6x10^5$ N/m2. The ratio of first layer's complex shear modulus to second layer's shear modulus is ~19. The thickness of the second layer is 1000 nm. The change in the maximum magnitude and the resonance frequency responses of the MTSM sensor as a function of viscosity and stiffness of second layer in stage II at 15 MHz are given in fig.7-34. As seen from the fig. 7-34, the oscillations start when the stiffness value of the second layer reaches to 10^4 N/m^2. In other words, the penetration depth reached the column height which is 2 μm.

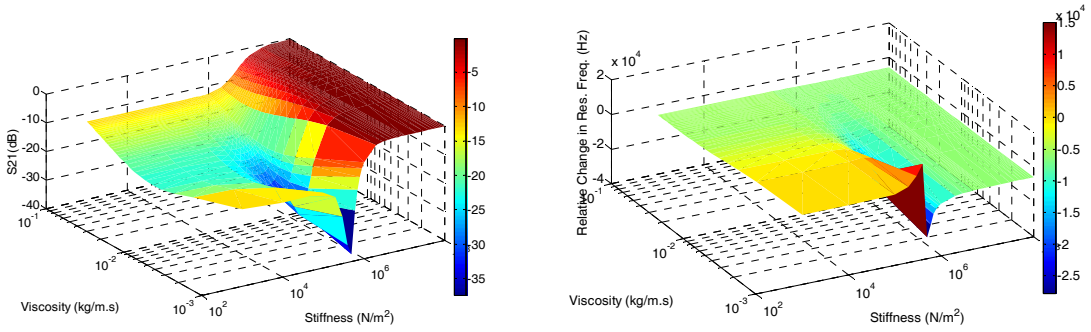

(a) (b)

Figure 7-34Effect of the changes in the two-layer viscoelastic systems viscosity and stiffness to the MTSM sensor's (a) magnitude and (b) resonance frequency responses (relative changes in resonance frequency and absolute values of magnitude in dB) at 15 MHz in Stage II

The zooming technique has been applied for fine tuning of the solutions. As seen from the table 7-8, the solution was obtained with less than 1 % error. In stage II, two solutions obtained from the MTSM/GA technique.

Table 7-8Values determined by the MTSM/GA technique for two-layer viscoelastic systems and % errors in stage II at 15 MHz

Properties	Values Input to TLM	Values Determined by MTSM/GA Technique	Error (%)
G'_1 (N/m^2)	$4x10^7$	$3.99x10^7$	0.2
G'_2 (N/m^2)	$2x10^6$	$1.99x10^6$	0.2
η_1 (kg/m.s)	$6x10^{-3}$	$5.98x10^{-3}$	0.5
η_2 (kg/m.s)	$7x10^{-3}$	$6.9x10^{-3}$	0.9

In the stage III, the second viscoelastic layer shows a "soft rubber" properties where G' is 27 times higher than G" (G' = $5x10^7$ N/m^2 and G" = $1.9x10^6$ N/m^2). The first viscoelastic layer has G' = $4x10^7$ N/m^2 and G" = $6.6x10^5$ N/m2. The ratio of first layer's complex shear modulus to second layer's shear modulus is ~0.8. The thickness of the second layer is 500 nm. The change in the maximum magnitude and the resonance frequency responses of the MTSM sensor as a function of viscosity and stiffness of second layer in stage III at 15 MHz are given in fig.7-35. As seen from the fig. 7-35, the oscillations start when the stiffness value of the second layer reaches to 10^4 N/m^2. In other words, the penetration depth reached the column height which is 1.5 μm.

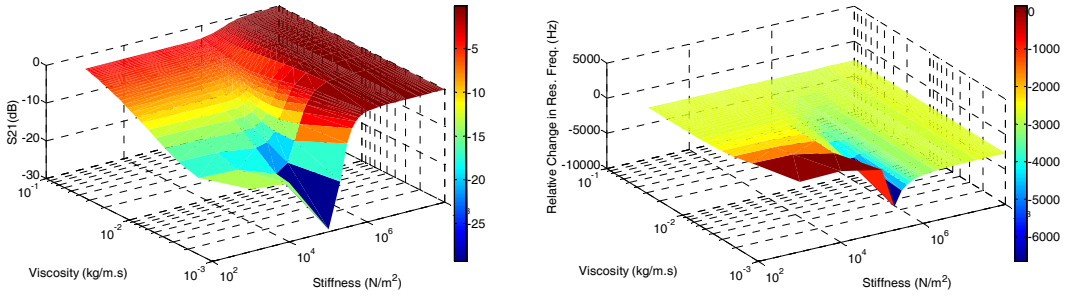

(a) (b)

Figure 7-35Effect of the changes in the two-layer viscoelastic systems viscosity and stiffness to the MTSM sensor's (a) magnitude and (b) resonance frequency response (relative changes in resonance frequency and absolute values of magnitude in dB) at 15 MHz in Stage III

The zooming technique has been applied for fine tuning of the solutions. The single solution obtained from the MTSM/GA technique has been presented in table 7-9. Layers' properties are determined with less than 1 % error.

Table 7-9 Values determined by the MTSM/GA technique for two-layer viscoelastic systems and % errors in stage III at 15 MHz

Properties	Values Input to TLM	Values Determined by MTSM/GA Technique	Error (%)
G'_1 (N/m^2)	$4x10^7$	$3.99x10^7$	0.2
G'_2 (N/m^2)	$5x10^7$	$5.05x10^7$	1
η_1 (kg/m.s)	$6x10^{-3}$	$5.99x10e^{-2}$	0.2
η_2 (kg/m.s)	$2x10^{-2}$	$2.02x10^{-2}$	1

In the stage IV, the second viscoelastic layer shows a "hard rubber" properties where G' is 53 times higher than G". (G' = $5x10^8$ N/m^2 and G" = $9.4x10^6$ N/m^2). The first viscoelastic layer has G' = $4x10^7$ N/m^2 and G" = $6.6x10^5$ N/m2. The ratio of first layer's complex shear modulus to second layer's shear modulus is ~0.08. The thickness of the second layer is 500 nm. The change in the maximum magnitude and the resonance frequency responses of the MTSM sensor as a function of viscosity and stiffness of second layer in

stage IV at 15 MHz are given in fig.7-36. As seen from the fig. 7-36, the oscillations start when the stiffness value of the second layer reaches to 10^4 N/m^2. In other words, the penetration depth reached the column height which is 1.5 μm.

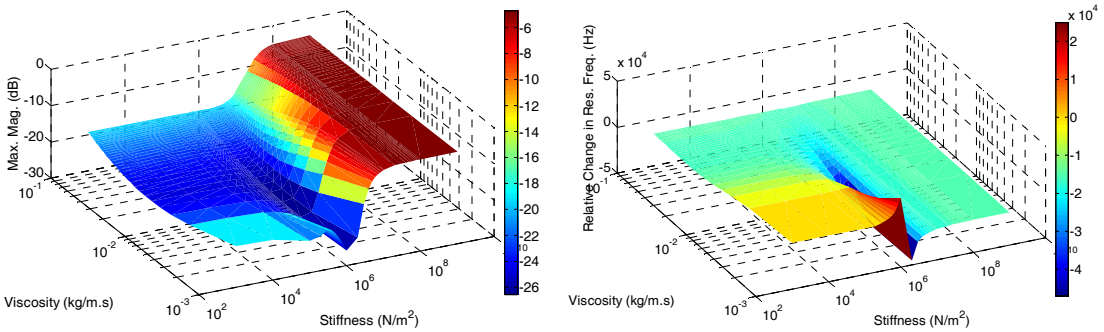

(a) (b)

Figure 7-36Effect of the changes in the two-layer viscoelastic systems viscosity and stiffness to the MTSM sensor's (a) magnitude and (b) resonance frequency response (relative changes in resonance frequency and absolute values of magnitude in dB) at 15 MHz in Stage IV

The zooming technique has been applied for fine tuning of the solutions. The single solution obtained from the MTSM/GA technique has been presented in table 7-10. Layers' properties are determined with less than 1 % error.

Table 7-10 Values determined by the MTSM/GA technique for two-layer viscoelastic systems and % errors in stage IV at 15 MHz

Properties	Values Input to TLM	Values Determined by MTSM/GA Technique	Error (%)
G'_1 (N/m^2)	$4x10^7$	$4.01x10^7$	0.3
G'_2 (N/m^2)	$5x10^8$	$5.05x10^8$	1
η_1 (kg/m.s)	$6x10^{-3}$	$6.01x10^{-3}$	0.2
η_2 (kg/m.s)	10^{-1}	$0.98x10^{-1}$	1

7.7.3 Analysis of the MTSM/GA technique for two-layer viscoelastic systems to deposition process at 25 MHZ

The changes in the magnitude and phase responses of the MTSM sensor to the five different viscoelastic systems has been simulated at 25 MHz using transmission line model and presented in fig. 7-37a and b. The response at t_1 represents the response to the single layer (the MTSM is loaded with only one layer). Time responses of maximum magnitude and resonance frequency are given in fig. 7-37c. As seen from fig. 7-37c, the maximum magnitude decreases dramatically at time t_3, to the value of -25 dB, and then slightly increases t_3, t_4 and t_5. The resonance frequency slightly decreases at time t_1, t_2 and t_3. Then it decreases sharply at t_4.

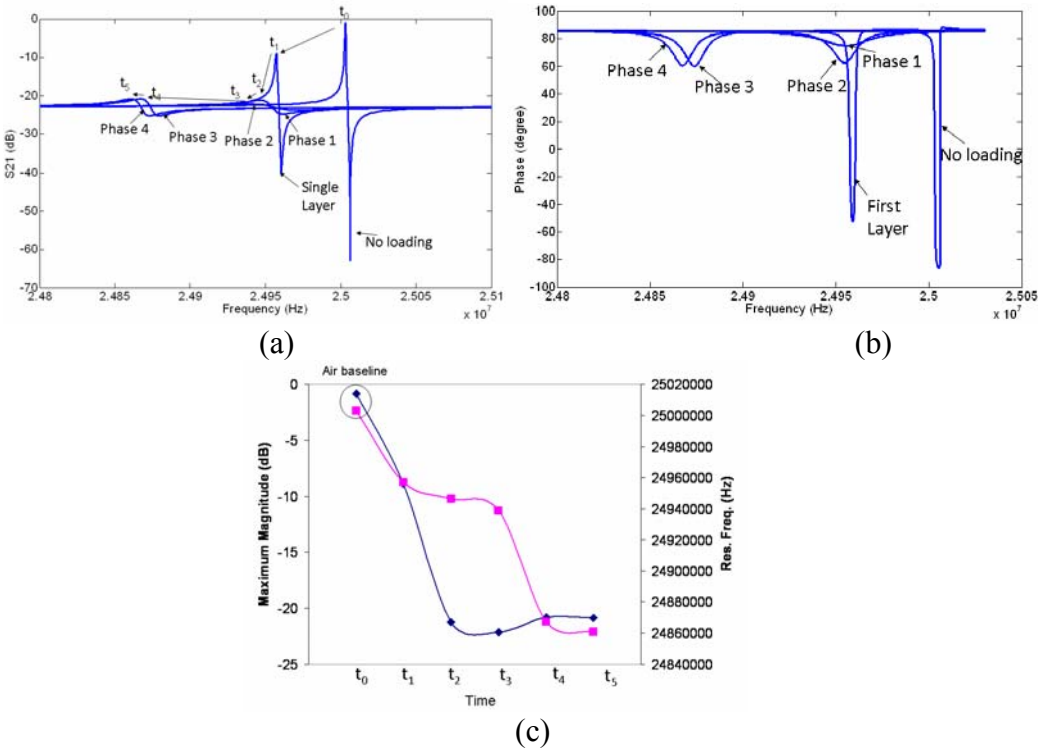

Figure 7-37 Change in (a) magnitude and (b) phase responses of the MTSM sensor during evaporation process. (c) Change in maximum magnitude and resonance frequency by time at 25 MHz. (case: two-layer viscoelastic systems)

In the stage I, the second viscoelastic layer shows a “transition like” properties where G” is ~3 times higher than G’ (G’ = 10^5 N/m^2 and G” = 3.14x10^5 N/m^2). The first viscoelastic layer has G’ = 4x10^7 N/m^2 and G” = 9.4x10^5 N/m2. The ratio of first layer’s complex shear modulus to second layer’s shear modulus is ~120. The thickness of the second layer is 3000 nm. The change in the maximum magnitude and the resonance frequency responses of the MTSM sensor as a function of viscosity and stiffness of second layer in stage I at 25 MHz are given in fig.7-38. As seen from the fig. 7-38, the oscillations start when the stiffness value of the second layer reaches to 5x10^5 N/m^2. In other words, the penetration depth reached the column height which is 4 μm.

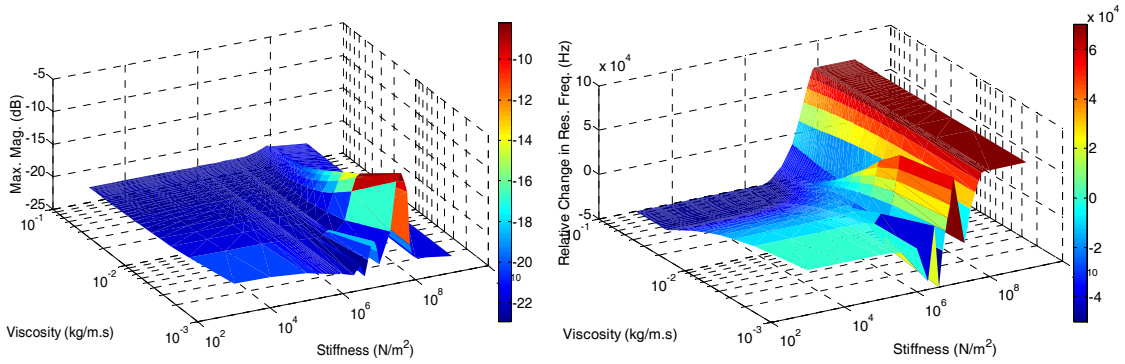

(a) (b)

Figure 7-38Effect of the changes in the two-layer viscoelastic system viscosity and stiffness to the MTSM sensor’s (a) magnitude and (b) resonance frequency response (relative changes in resonance frequency and absolute values of magnitude in dB) at 25 MHz in Stage I

The two solutions obtained from the MTSM/GA technique. Second solution for the first layer was in the same magnitude order while the second solution for the second layer two magnitude (for stiffness) and one magnitude order (for viscosity) higher than the first solution. As seen from the table 7-11, the first solution was determined with less than 1 % error.

Table 7-11Values determined by the MTSM/GA technique for two-layer viscoelastic systems and % errors in stage I at 25 MHz

Properties	Values Input to TLM	Values Determined by MTSM/GA Technique	Error (%)
G'_1 (N/m^2)	$4x10^7$	$3.99x10^7$	0.3
G'_2 (N/m^2)	10^5	$1.01x10^5$	1
η_1 (kg/m.s)	$6x10^{-3}$	$5.94x10^{-3}$	1
η_2 (kg/m.s)	$2x10^{-3}$	$2.01x10^{-3}$	0.5

In the stage II, the second viscoelastic layer shows a "transition like" properties where G' is ~2 times higher than G". (G' = $2x10^6$ N/m^2 and G" = $1.1x10^6$ N/m^2). The first viscoelastic layer has G' = $4x10^7$ N/m^2 and G" = $9.4x10^5$ N/m2. The ratio of first layer's complex shear modulus to second layer's shear modulus is ~18. The thickness of the second layer is 1000 nm. The change in the maximum magnitude and the resonance frequency responses of the MTSM sensor as a function of viscosity and stiffness of second layer in stage II at 25 MHz are given in fig.7-39. As seen from the fig. 7-39, the oscillations start when the stiffness value of the second layer reaches to 10^6 N/m^2. In other words, the penetration depth reached the column height which is 2 μm.

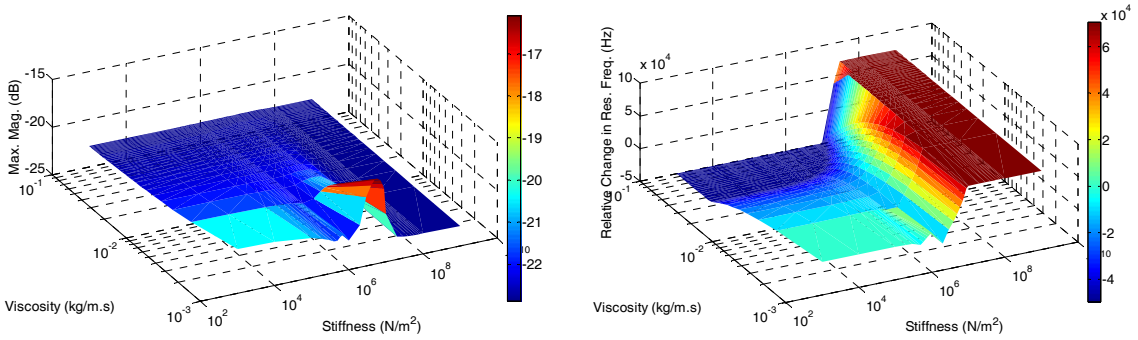

(a) (b)

Figure 7-39Effect of the changes in the two-layer viscoelastic system viscosity and stiffness to the MTSM sensor's (a) magnitude and (b) resonance frequency response (relative changes in resonance frequency and absolute values of magnitude in dB) at 25 MHz in Stage II

The two solutions obtained from the MTSM/GA technique has been presented in table 7.12. As seen from the table 7.12, there are two distinct solutions. The error in the MTSM/GA technique also increased to more than 1 % for stiffness values of the layers. This may stem from the fact that the sensor's response highly damped (losses = ~22.1 dB). It was shown that the error increases to be more than 1 % when the maximum magnitude decreases more than -22 dB for two-layer viscoelastic systems.

Table 7-12Values determined by the MTSM/GA technique for two-layer viscoelastic systems and % errors in stage II at 25 MHz

Properties	Values Input to TLM	Values Determined by MTSM/GA Technique	Error (%)
G'_1 (N/m^2)	$4x10^7$	$4.1x10^7$	2
G'_2 (N/m^2)	$2x10^6$	$1.9x10^6$	2
η_1 (kg/m.s)	$6x10^{-3}$	$6.06x10^{-3}$	1
η_2 (kg/m.s)	$7x10^{-3}$	$7.07x10^{-3}$	1

In the stage III, the second viscoelastic layer shows a "soft rubber" properties where G' is 16 times higher than G" (G' = $5x10^7$ N/m^2 and G" = $3.14x10^6$ N/m^2). The first viscoelastic layer has G' = $4x10^7$ N/m^2 and G" = $9.4x10^5$ N/m2. The ratio of first layer's complex shear modulus to second layer's shear modulus is ~0.8. The thickness of the second layer is 500 nm. The change in the maximum magnitude and the resonance frequency responses of the MTSM sensor as a function of viscosity and stiffness of second layer in stage III at 25 MHz are given in fig.7-40. As seen from the fig. 7-40, the oscillations start when the stiffness value of the second layer reaches to 10^4 N/m^2. In other words, the penetration depth reached the column height which is 1.5 μm.

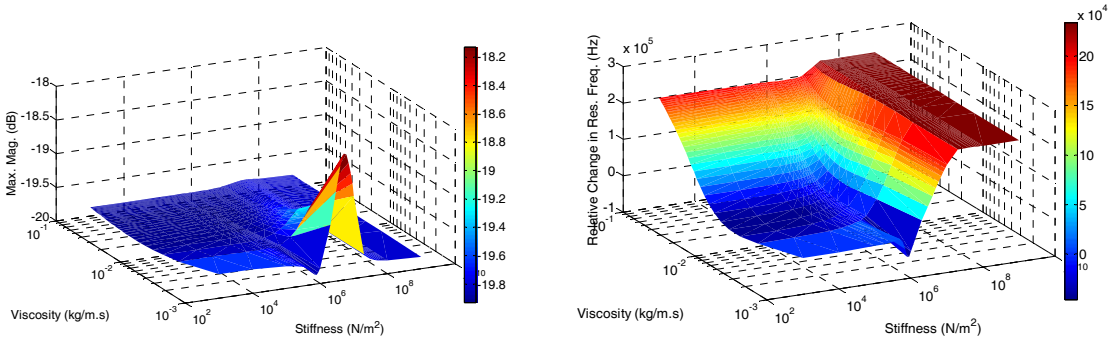

(a) (b)

Figure 7-40Effect of the changes in the two-layer viscoelastic system viscosity and stiffness to the MTSM sensor's (a) magnitude and (b) resonance frequency response (relative changes in resonance frequency and absolute values of magnitude in dB) at 25 MHz in Stage III

The single solution obtained from the MTSM/GA technique has been presented in table 7.13. Layers' properties are determined with less than 1 % error.

Table 7-13Values determined by the MTSM/GA technique for two-layer viscoelastic systems and % errors in stage III at 25 MHz

Properties	Values Input to TLM	Values Determined by MTSM/GA Technique	Error (%)
G'_1 (N/m^2)	$4x10^7$	$4.01x10^7$	0.3
G'_2 (N/m^2)	$5x10^7$	$4.97x10^7$	0.7
η_1 (kg/m.s)	$6x10^{-3}$	$6.06x10^{-3}$	1
η_2 (kg/m.s)	$2x10^{-2}$	$1.99x10^{-2}$	0.5

In the stage IV, the second viscoelastic layer shows a "hard rubber" properties where G' is 23 times higher than G". (G' = $5x10^8$ N/m^2 and G" = $2.2x10^7$ N/m^2). The first viscoelastic layer has G' = $4x10^7$ N/m^2 and G" = $9.4x10^5$ N/m2. The ratio of first layer's complex shear modulus to second layer's shear modulus is ~0.08. The thickness of the second layer is 500 nm. The change in the maximum magnitude and the resonance frequency responses of the MTSM sensor as a function of viscosity and stiffness of second layer in stage IV at 25 MHz are given in fig.7-41. As seen from the fig. 7-41, the oscillations start when the stiffness value of the second layer reaches to 10^4 N/m^2. In other words, the penetration depth reached the column height which is 1.5 μm.

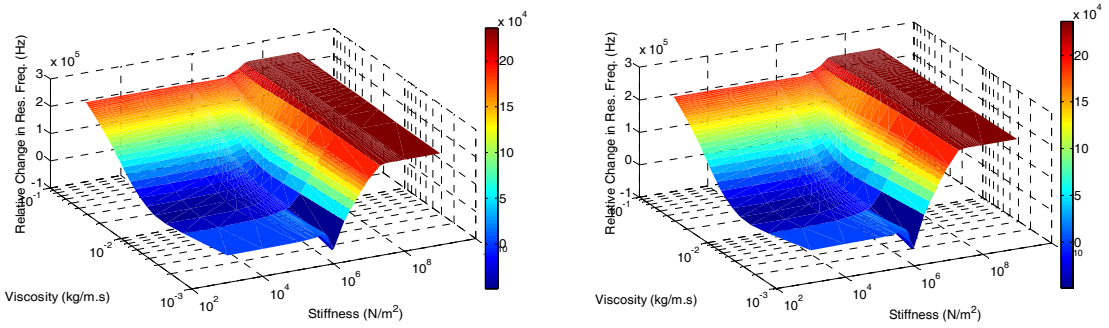

Figure 7-41Effect of the changes in the two-layer viscoelastic system viscosity and stiffness to the MTSM sensor's (a) magnitude and (b) resonance frequency response (relative changes in resonance frequency and absolute values of magnitude in dB) at 25 MHz in Stage IV

The single solution with less than 1% error obtained from the MTSM/GA technique has been presented in table 7-14.

Table 7-14Values determined by the MTSM/GA technique for two-layer viscoelastic systems and % errors in stage III at 25 MHz

Properties	Values Input to TLM	Values Determined by MTSM/GA Technique	Error (%)
G'_1 (N/m^2)	$4x10^7$	$4.01x10^7$	0.3
G'_2 (N/m^2)	$5x10^8$	$4.96x10^8$	0.7
η_1 (kg/m.s)	$6x10^{-3}$	$6.01x10^{-3}$	0.3
η_2 (kg/m.s)	10^{-1}	$9.9x10^{-1}$	0.2

7.7.4 Analysis of the MTSM/GA technique for two-layer viscoelastic systems to deposition process at 35 MHZ

The changes in the magnitude and phase responses of the MTSM sensor to the five different viscoelastic systems has been simulated at 35 MHz using transmission line model and presented in fig. 7-42a and b. The response at t_1 represents the response to the single layer (the MTSM is loaded with only one layer). Time responses of maximum magnitude and resonance frequency are given in fig. 7-42c. As seen from fig. 7-42c, the maximum magnitude decreases dramatically at time t_3, to the value of -20 dB, and then stabilizes at t_3, t_4

and t_5. The resonance frequency slightly decreases at time t_1, t_2 and t_3. Then it increases sharply at t_4.

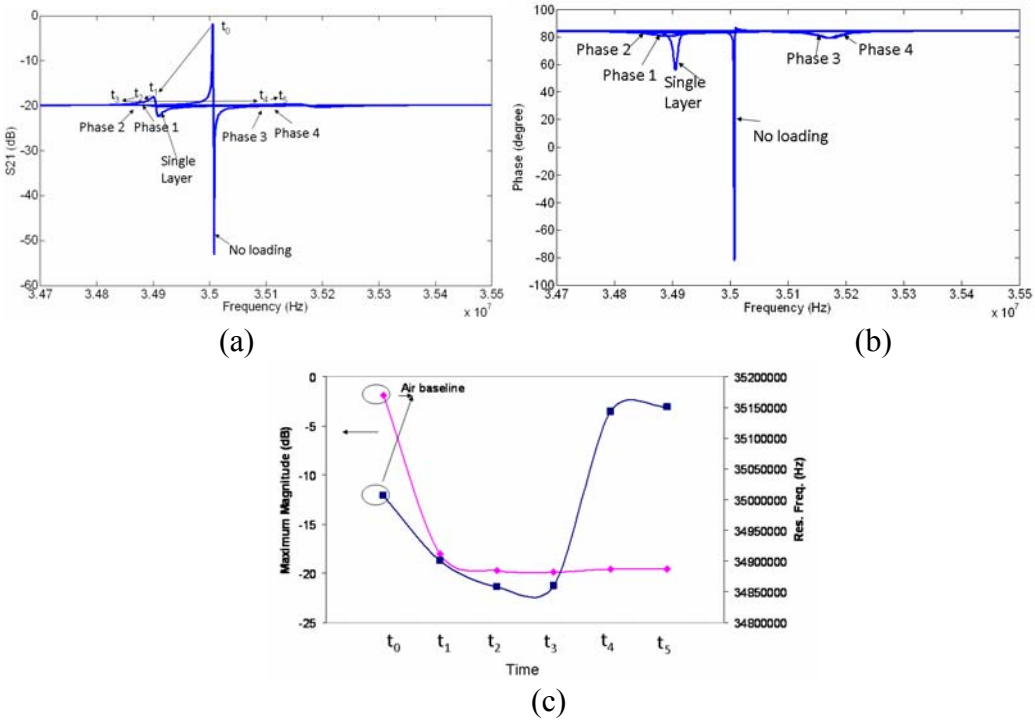

Figure 7-42 Change in magnitude (a) and phase (b) responses of the MTSM sensor during evaporation process. (c) Change in maximum magnitude and resonance frequency by time at 35 MHz. (case: two-layer viscoelastic system)

In the stage I, the second viscoelastic layer shows a "lossy" properties where G" is ~4 times higher than G' (G' = 10^5 N/m^2 and G" = 4.4x10^5 N/m^2). The first viscoelastic layer has G' = 4x10^7 N/m^2 and G" = 1.32x10^6 N/m^2. The ratio of first layer's complex shear modulus to second layer's shear modulus is ~90. The thickness of the second layer is 3000 nm. The change in the maximum magnitude and the resonance frequency responses of the MTSM sensor as a function of viscosity and stiffness of second layer in stage I at 35 MHz are given in fig. 7-43. As seen from the fig. 7-43, the oscillations start when the stiffness value of the

second layer reaches to $1x10^6$ N/m^2. In other words, the penetration depth reached the column height which is 4 μm.

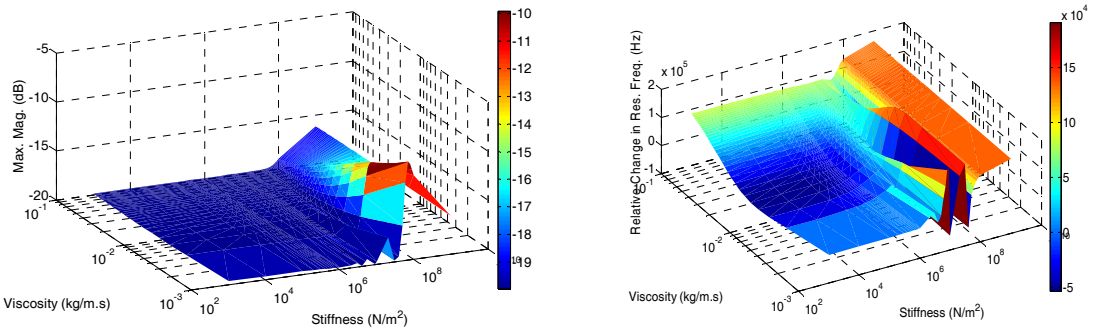

(a) (b)

Figure 7-43Effect of the changes in the two-layer viscoelastic system viscosity and stiffness to the MTSM sensor's (a) magnitude and (b) resonance frequency response (relative changes in resonance frequency and absolute values of magnitude in dB) at 35 MHz in Stage I

The single solution obtained from the MTSM/GA technique has been presented in table 7.15. It should be noted that the error is more than 1 % because of the low quality factor. It has been shown in section 7.6.4, the error in the MTSM/GA technique increases to more than 1% when the maximum magnitude decreases to -19 dB. In this stage, the maximum magnitude was -19.7 dB.

Table 7-15Values determined by the MTSM/GA technique for two-layer viscoelastic systems and % errors in stage I at 35 MHz

Properties	Values Input to TLM	Values Determined by MTSM/GA Technique	Error (%)
G'_1 (N/m^2)	$4x10^7$	$4.05x10^7$	2
G'_2 (N/m^2)	10^5	$1.04x10^5$	5
η_1 (kg/m.s)	$6x10^{-3}$	$5.95x10^{-3}$	0.5
η_2 (kg/m.s)	$2x10^{-3}$	$2.04x10^{-3}$	2

In the stage II, the second viscoelastic layer shows a "transition like" properties where G' is ~1.3 times higher than G". (G' = $2x10^6$ N/m^2 and G" = $1.54x10^6$ N/m^2). The first viscoelastic layer has G' = $4x10^7$ N/m^2 and G" = $1.32x10^6$ N/m^2. The ratio of first layer's complex shear modulus to second layer's shear modulus is ~16. The thickness of the second

layer is 1000 nm. The change in the maximum magnitude and the resonance frequency responses of the MTSM sensor as a function of viscosity and stiffness of second layer in stage II at 35 MHz are given in fig.7-44. As seen from the fig. 7-44, the oscillations start when the stiffness value of the second layer reaches to 10^6 N/m^2. In other words, the penetration depth reached the column height which is 2 μm.

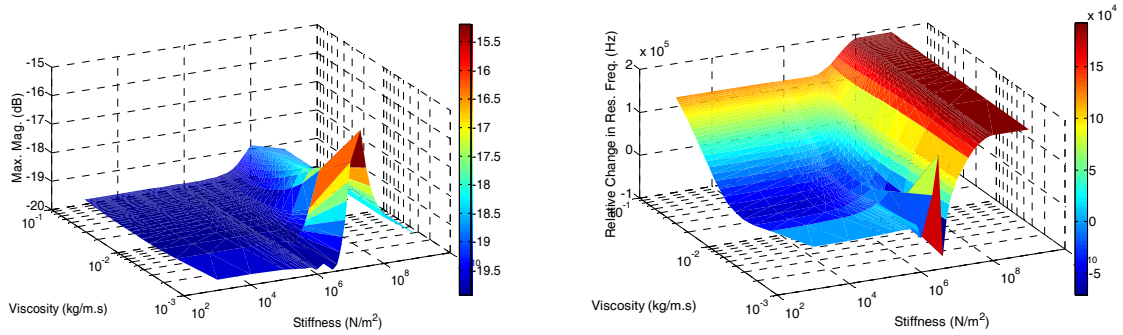

(a) (b)

Figure 7-44Effect of the changes in the two-layer viscoelastic system viscosity and stiffness to the MTSM sensor's (a) magnitude and (b) resonance frequency response (relative changes in resonance frequency and absolute values of magnitude in dB) at 35 MHz in Stage II

Two solutions obtained by the MTSM/GA technique. As seen from the table 7-16, the first solution was also calculated with more than 1%error because of the low quality factor.

Table 7-16Values determined by the MTSM/GA technique for two-layer viscoelastic systems and % errors in stage III at 35 MHz

Properties	Values Input to TLM	Values Determined by MTSM/GA Technique	Error (%)
G'_1 (N/m^2)	$4x10^7$	$4.1x10^7$	5
G'_2 (N/m^2)	$2x10^6$	$1.9x10^6$	10
η_1 (kg/m.s)	$6x10^{-3}$	$6.06x10^{-2}$	1
η_2 (kg/m.s)	$7x10^{-3}$	$7.07x10^{-3}$	1

In the stage III, the second viscoelastic layer shows a "soft rubber" properties where G' is 11 times higher than G". (G' = $5x10^7$ N/m^2 and G" = $4.4x10^6$ N/m^2). The first viscoelastic layer has G' = $4x10^7$ N/m^2 and G" = $1.32x10^6$ N/m^2. The ratio of first layer's

complex shear modulus to second layer's shear modulus is ~0.8. The thickness of the second layer is 500 nm. The change in the maximum magnitude and the resonance frequency responses of the MTSM sensor as a function of viscosity and stiffness of second layer in stage III at 35 MHz are given in fig.7-45. As seen from the fig. 7-45, the oscillations start when the stiffness value of the second layer reaches to 10^4 N/m^2. In other words, the penetration depth reached the column height which is 1.5 μm.

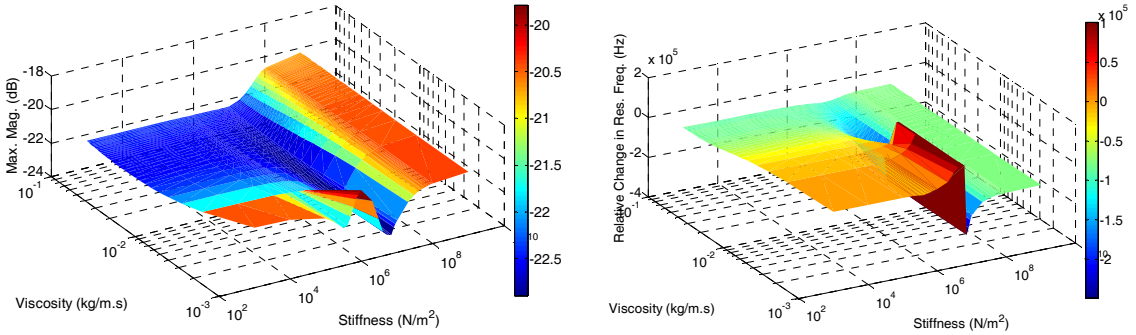

(a) (b)

Figure 7-45Effect of the changes in the two-layer viscoelastic system viscosity and stiffness to the MTSM sensors's (a) magnitude and (b) resonance frequency response (relative changes in resonance frequency and absolute values of magnitude in dB) at 35 MHz in Stage III

The single solution with less than 1 % error for each variable obtained from the MTSM/GA technique has been presented in table 7-17

Table 7-17Values determined by the MTSM/GA technique for two-layer viscoelastic systems and % errors in stage IV at 35 MHz

Properties	Values Input to TLM	Values Determined by MTSM/GA Technique	Error (%)
G'_1 (N/m^2)	$4x10^7$	$4.04x10^7$	1
G'_2 (N/m^2)	$5x10^7$	$4.95x10^7$	1
η_1 (kg/m.s)	$6x10^{-3}$	$6.05x10e^{-2}$	0.9
η_2 (kg/m.s)	$2x10^{-2}$	$2.02x10^{-2}$	1

In the stage IV, the second viscoelastic layer shows a "hard rubber" properties where G' is 31 times higher than G". (G' = $5x10^8$ N/m^2 and G" = $1.6x10^7$ N/m^2). The first viscoelastic layer has G' = $4x10^7$ N/m^2 and G" = $1.32x10^6$ N/m2. The ratio of first layer's complex shear modulus to second layer's shear modulus is ~0.08. The thickness of the second layer is 500 nm. The change in the maximum magnitude and the resonance frequency responses of the MTSM sensor as a function of viscosity and stiffness of second layer in stage IV at 35 MHz are given in fig.7-46. As seen from the fig. 7-46, the oscillations start when the stiffness value of the second layer reaches to 10^4 N/m^2. In other words, the penetration depth reached the column height which is 1.5 μm.

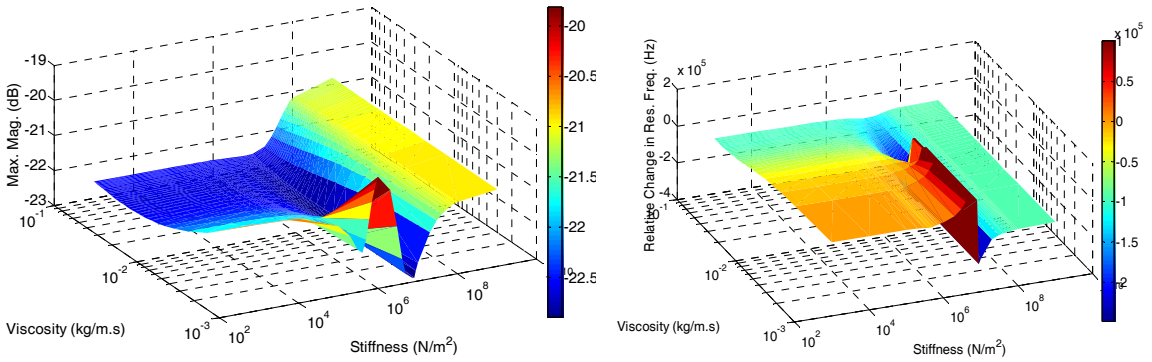

(a) (b)

Figure 7-46Effect of the changes in the two-layer viscoelastic system viscosity and stiffness to the MTSM sensor's (a) magnitude and (b) resonance frequency response (relative changes in resonance frequency and absolute values of magnitude in dB) at 35 MHz in Stage IV

Single solution with less than 1 % error for each variable was obtained from the MTSM/GA technique and shown in the table 7-18.

Table 7-18Values determined by the MTSM/GA technique for two-layer viscoelastic systems and % errors in stage IV at 35 MHz

Properties	Values Input to TLM	Values Determined by MTSM/GA Technique	Error (%)
C_1 (N/m^2)	$4x10^7$	$4.04x10^7$	1
C_2 (N/m^2)	$5x10^8$	$5.02x10^8$	0.4
η_1 (kg/m.s)	$6x10^{-3}$	$6.05x10^{-2}$	0.9
η_2 (kg/m.s)	10^{-1}	$1.01x10^{-1}$	1

7.8 Summary and conclusions

The MTSM/GA technique was extended to two-layer viscoelastic systems. First, the theoretical foundation of the MTSM/GA technique for two-layer viscoelastic systems was developed. The influence of several important quantities, such as quality factor and experimental error, on the MTSM/GA technique has been critically evaluated. Finally, the MTSM/GA technique has been applied to determine the mechanical properties of several combinations of two-layer viscoelastic systems. Its strengths and limitations were identified.

It was demonstrated that the MTSM/GA technique is capable of determining the mechanical properties of each layer forming the two-layer viscoelastic system with less than 1% error theoretically.

For the first time, it was shown that the MTSM/GA technique can be used to determine mechanical properties of the two-layer viscoelastic layers.

8 EXPERIMENTAL VALIDATION OF THE MTSM/GA TECHNIQUE FOR TWO-LAYER VISCOELASTIC SYSTEMS

Practical application of multi-layer structures loaded on the MTSM sensor requires several considerations. First, the first layer of the system should be uniform and homogenous. It has been suggested that spin coating followed by a thermal treatment of the film could be the best preparation method (Lucklum et al., 1999). In this project, as discussed in chapter 6, SU8-2002 thin polymer film has been spun coated and thermally treated on the MTSM sensor. The polymer layer's uniformity and the homogeneity have been investigated in detail. It was shown that the polymer's thickness was uniform over the sensor's surface. No micro cracks have been observed. These issues become a serious problem with the double layer arrangement because, e.g., the second film might be trapped in micro cracks. In consequence, the complex shear modulus of these "mixed" layer parts effective for the acoustic wave increase.

Second, the preparation of the second layer must not attack the first layer. SU8-2002 is very stable and difficult to dissolve in many liquids. It is also an electrically non-conducting material, and the surface of SU8-2002 is strong if hard baked (Evans et al.,2005). Typical SU8 developers are ethyl lactate and diacetone alcohol. In this project, the insoluble collagen was adsorbed in 0.1 M acetic acid. After the adsorption, it was observed that there was no degradation of the SU8 layer-2002. Under certain circumstances it can be advantageous to introduce a separation layer to overcome this and the next problem

Third, the chemical nature of the material–protein interface can have a significant effect on the structural features of the adsorbed protein layer. Chen et al suggested that fibroblast populated collagen lattices show different mechanical properties on bacteriological

grade polystyrene (BGPS) plates and tissue culture polystyrene (TCPS) plates (2007). Fereol et al showed that stiffness of both cortical and deep cytoskeleton strongly depends on the substrate rigidity (2008). Domke et al. (2000) investigated the substrate dependent differences in morphology and elasticity of living osteoblasts. Therefore it can be expected that the mechanical properties of the collagen layer, used in this project, might depend on the substrate properties (in this case, there are two substrates; gold layer and SU8-2002 layer).

For experimental validation of the MTSM/GA technique, three different experiments have been designed and analyzed. Initially, a single layer viscoelastic layer has been modeled as two-layer viscoelastic layer. For this purpose, 1950 nm thick SU8-2002 layer has been used. Secondly, the two layer models which were made of viscoelastic layer as first layer and a semi-infinite Newtonian medium (DI water) as second layer. The MTSM/GA technique has been applied to determine the properties of these two layers. Thirdly, two layer viscoelastic systems have been realized by using SU8-2002 as first layer and collagen as second layer. In addition, the structural properties of the polymer samples were analyzed using atomic force microscopy (AFM) and profilometer devices.

8.1 Validation of the MTSM/GA technique with single-layer viscoelastic system modeled as two-layer viscoelastic system

First set of experiments were done by using 1950 nm thick of SU8-2002 layer. Single layer of SU8-2002 layer has been modeled as two-layer system (fig.8-1). Experimental results obtained in chapter 6 were used for this purpose

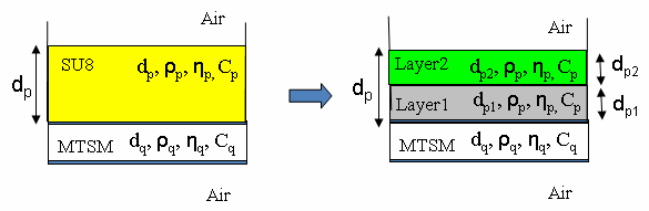

(a) (b)

Figure 8-1 Single layer of 1950 nm thick of SU8-2002 layer has been modeled as two-layer viscoelastic system

The single SU8-2002 layers have been divided into two viscoelastic layers with the same thickness and density values (d=1 μm and ρ=1200 kg/m^3). The MTSM/GA technique has been applied to determine the properties of these two layers. It was expected to be that each layer's storage and loss modulus will be equal to the properties of the single SU8-2002 layer's properties. Comparison of the determined properties is presented in fig. 8-2. As seen from the fig. 8-2, the MTSM/GA technique was able to determine the properties of two layer system with 1 %- 40 % error.

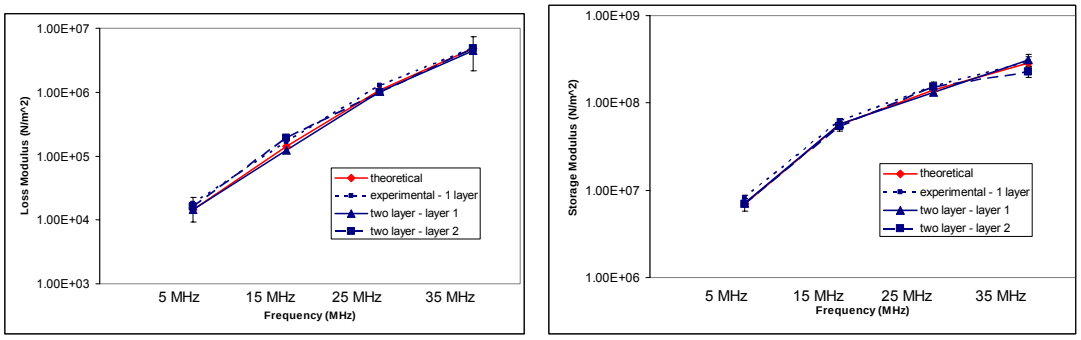

(a) (b)

Figure 8-2 Single layer 1.95 μm thick SU8-2002 layer is modeled as two-layer viscoelastic layer (a) loss modulus (b) storage modulus at 5 MHz, 15 MHz, 25 MHz and 35 MHz

Next, it was shown that the different combinations of the thickness values of the first and the second layer do not affect the MTSM/GA technique's results. Three combinations of the thickness value were used. These combinations were 550 nm -1400 nm, 975 nm – 975

nm, and 1400 nm – 550 nm (first layer's thickness – second layer's thickness). The results at 5 MHz were presented in the table 7-20.

Table 8-1Single layer SU8 is modeled as two viscoelastic layers with different thicknesses (errors are average of three experiments)

Properties	Min and max % errors in the MTSM/GA Technique		
	550-1400	975 - 975	1400 - 550
G_1" (N/m^2)	3-6	1-3	1-3
G_2" (N/m^2)	1-6	1-40	4-8
G_1' (N/m^2)	1-10	1-10	4-10
G_2' (N/m^2)	1-10	3-10	1-10

8.2 Validation of the MTSM/GA technique with two-layer system combination of SU8-2002 viscoelastic layer and semi-infinite Newtonian medium

Second set of experiments were done with two-layer viscoelastic system which consists of a finite thickness of a viscoelastic layer (SU8-2002) as first layer and a semi-infinite Newtonian medium (DI water) as second layer (fig 8-3).

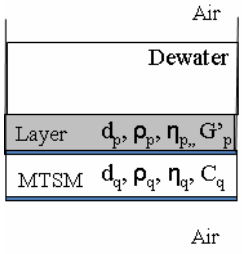

Figure 8-3 Physical model for a viscoelastic layer loaded with semi-infinite Newtonian medium

1950 nm thick SU8-2002 layer which was spun coated on the MTSM sensor was loaded with DI water in room temperature. The thickness of DI water was 2 mm which is much higher than the penetration depth of the acoustic wave (δ=2 μm). Therefore the viscoelastic system

can be modeled as two layer system in which the first layer is a finite viscoelastic layer (SU8-2002) and the second layer is a semi-infinite Newtonian medium (DI water).The obtained results are presented in fig. 8-4.

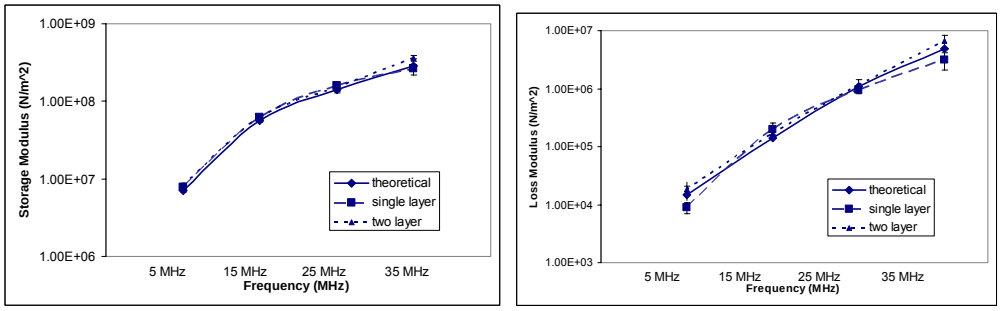

(a) **(b)**

Figure 8-4 Comparison of the storage and loss modulus values obtained for SU8-2002 layer from single-layer (see chapter 6) and two-layer calculations.

Figure 8.5 shows the comparisons between the theoretical and calculated results for DI water layer. As seen from the fig. 8-5, the experimental error changes between 30 % to 50 % among the harmonics for loss modulus. On the other hand, it was expected that there should not be any storage modulus for DI water. In other words, the stiffness should be equal to 0 N/m^2 for a typical Newtonian medium. But small stiffness ($<2x10^4$ N/m^2) was observed.

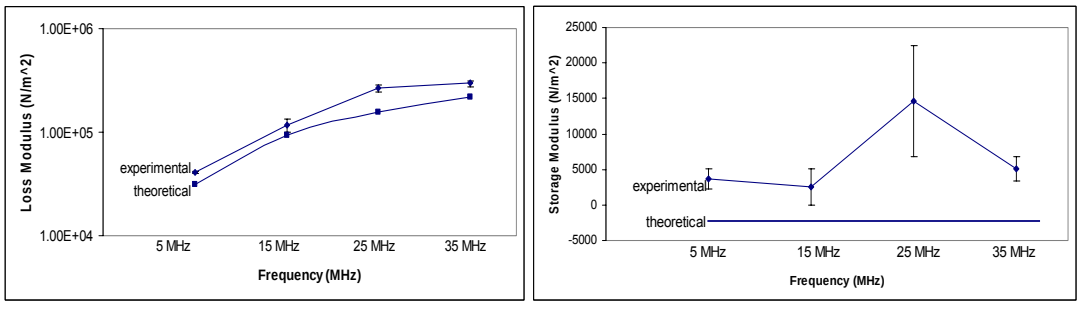

(a) (b)

Figure 8-5 Comparison of (a) the loss modulus and (b) storage modulus values obtained for DI water layer theoretically and experimentally.

8.3 Validation of the MTSM/GA technique by using two-layer viscoelastic system with known properties

The MTSM/GA technique has been validated by using two-layer viscoelastic system with known properties. The single layer viscoelastic systems made of SU8-2002 layer and collagen layer have been investigated in detail in chapter 6. Here the first layer of SU8-2002 has been created and then the collagen layer has been adsorbed on the first layer. The time response of the collagen evaporation on SU8-2002 layer was monitored. Two different thickness of the SU8-2002 layer (770 nm and 1950 nm) and two different thicknesses of collagen layers (~450 nm and ~150 nm) have been used in the experiments.

8.3.1 Two-layer viscoelastic system consists of 2 μm SU8-2002 layer as first layer and 400 nm and 200 nm thick collagen layers as second layer

200 μl of collagen solution was added on 1.95 μm thick SU8-2002 layer. The evaporation process of the collagen layer has been monitored. Changes in the maximum magnitude and the resonance frequency were presented in fig. 8-6. All graphs clearly show that there are four consecutive stages of the MTSM sensor response during the evaporation-induced deposition process of each sample (stages shown in fig.8-6a). These stages have been discussed in chapter 6 in detail but here it will be summarized again. During the first stage, solvent evaporates through the open top surface; hence, the change in the thickness of the liquid medium is the main parameter that affects the response of the MTSM sensor. The first part of the second stage is indicated by sudden slight (about 1 ~ 2 dB depending on the harmonic) decrease in magnitude and last short period of time (less than 5 minutes). The phase of the sample starts to transform from a Newtonian viscous liquid to viscoelastic (VE)

condition during this stage because of the increase in the concentration of the solute. The second part of the second stage is shown by a sudden increase in magnitude response and decrease in frequency response. In this stage, most of the liquid solvent is evaporated and only left with a gel type, soft rubber condition, viscoelastic thin film on the MTSM sensor surface. The third stage is indicated by small increase in resonance frequency. The last stage (IV) is shown by a stabilized phase in both responses.

It should be noted that the kinetics of the evaporation process at 35 MHz is qualitatively different than the ones obtained at 5 MHz, 15 MHz and 25 MHz. As seen from fig. 8.6d, the magnitude response continuously decreases during the stage II. Magnitude response increases very slightly (0.25 dB) at stages III and IV. On the other hand, frequency response contains all four stages which are presence in lower frequencies. The dynamic range of the sensor response is also very small (changing from -15.5 to -17 dB) at 35 MHz.

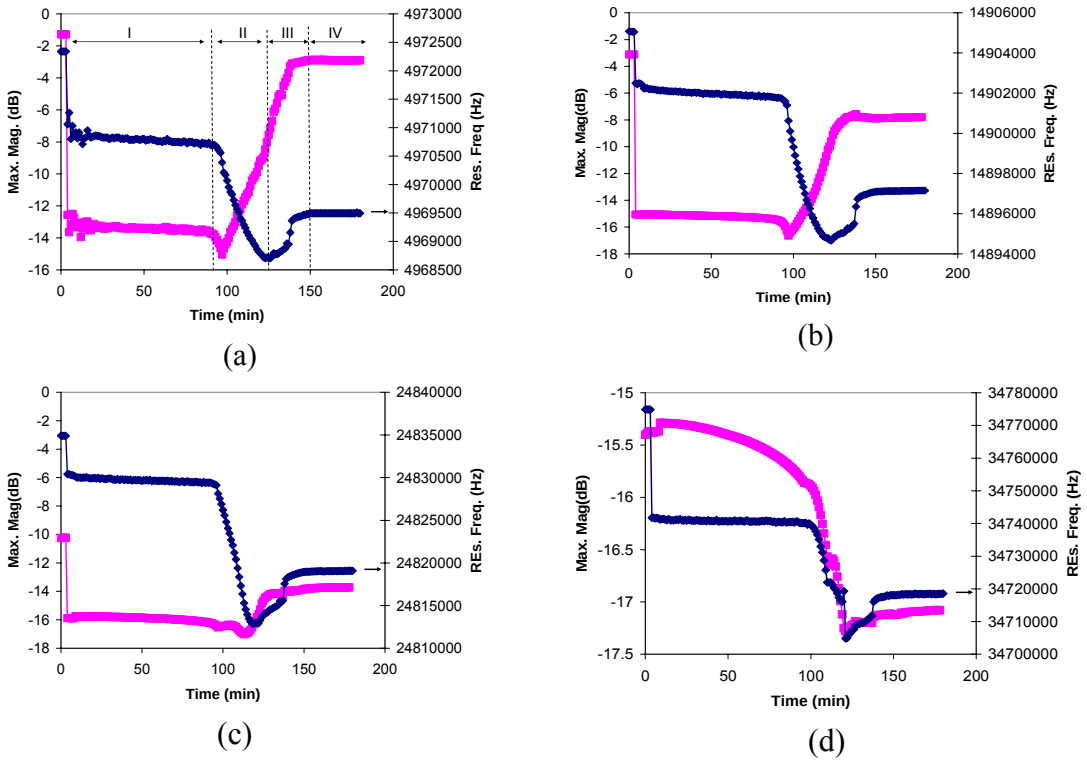

Figure 8-6 The evaporation process of 200 µl of collagen type-I on 1.95 micron thick SU8-2002 layer at a) 5 MHz b) 15 MHz c)25 MHz and d) 35 MHz

Next, 100 µl of collagen type-I suspension has been placed on the 1.95 micron thick SU8-2002 layer and maximum magnitude and resonance frequency responses of the MTSM sensor were monitored during the evaporation process (fig. 8-7). Time 0 indicates the air reference point. All graphs clearly show that there are four consecutive stages of the MTSM sensor response during the evaporation-induced deposition process of each sample (stages shown in fig.8-7a). During the first stage (first 45 min), the resonance frequency and the magnitude responses are relatively flat. The first part of the second stage is indicated by sudden slight (about 1 ~ 1.5 dB depending on the harmonic) decrease in magnitude and last short period of time (less than 5 minutes). In the second part of the second stage is magnitude response increases and resonance frequency continues decreasing. In the third stage resonance frequency increases and magnitude response continues increasing. In the last stage both responses stabilize.

It should be noted that the kinetics of the evaporation process at 35 MHz is qualitatively different than the ones obtained at 5 MHz, 15 MHz and 25 MHz. Similar phenomena has been observed for evaporation of 200 µl of collagen type-I on 1.95 µm SU8-2002 polymer layer (fig 8-6). As seen from fig. 8-7d, the magnitude response continuously decreases during the stage II. Magnitude response increases sharply (~0.4 dB) at the end of at stages III. On the other hand, frequency response contains all four stages which are presence in lower frequencies. The dynamic range of the sensor response is also very small (changing from -15.5 to -17 dB) at 35 MHz. It should also be noted that there is also visible qualitative difference in the magnitude responses. For example, the magnitude response continuously increases with the same slope at 5 MHz. In contrast rate of increase in the magnitude response at 25 MHz decreases at stage III.

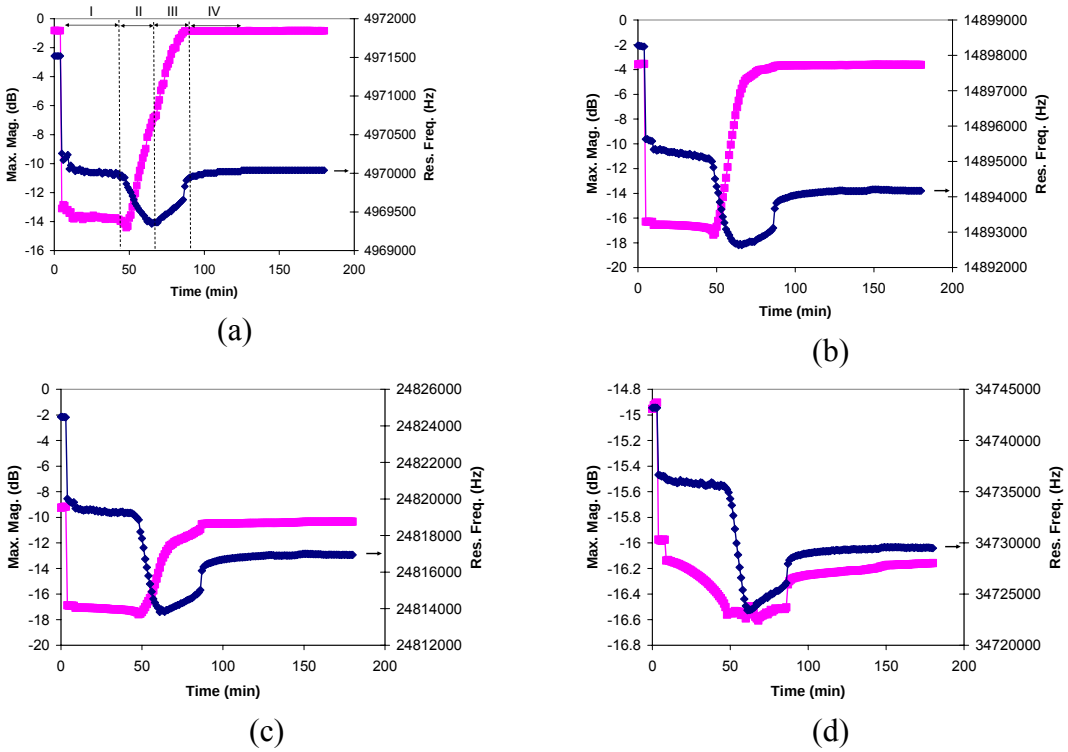

Figure 8-7 The evaporation process of 100 µl of collagen on 1.95 micron thick SU8 layer at a) 5 MHz b) 15 MHz c)25 MHz and d) 35 MHz

The collagen layer has been gently removed with a sharp object from some part of the SU8-2002 layer. Since collagen layer does form a covalent attachment on the SU8-2002 layer, it can be easily removed the top surface. The image of a collagen type-I on the SU8-2002 polymer layer obtained from a profilometer has been shown in fig. 8-8.

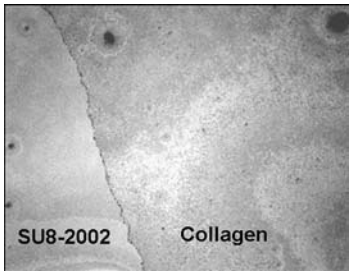

Figure 8-8 Intensity map of a collagen type-I deposited on a ~2 µm thick SU8-2002 polymer spin coated on the MTSM sensor (image size: 0.7 µm x 0.7 µm

It has been shown in chapter 5, the collagen does not form a flat layer on the MTSM sensor. Therefore the thickness of the collagen was measured at different locations at the MTSM sensor's gold electrode which has diameter of 7 mm. (fig. 8-9)

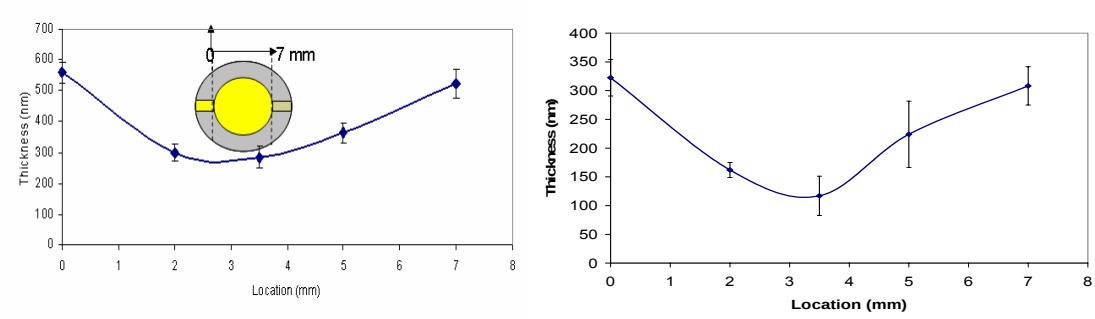

(a) (b)

Figure 8-9Thickness of the collagen layer on at different locations; (a) thickness obtained at the end of the evaporation process of (a) 200 µl collagen and (a) 100 µl collagen on 2 µm thick SU8-2002 layer. Each point is an average of 10 measurements

The thickness of the collagen layer has been calculated by using the MTSM/GA technique and it was compared to the one measured by using profilometer. As seen from the fig. 8-9, the thickness of the collagen varies at the surface. The average thickness can be estimated to be around 400±50 nm and 200±50 nm. The calculated thickness of the collagen by using the MTSM/GA technique is 370±20 nm and 150±20 nm.

Mechanical and geometrical properties of SU8-2002 layer have been already characterized in chapter 6. Here, at the end of the experiments, the maximum magnitude and resonance frequency values of the MTSM sensor were plugged into the MTSM/GA technique. The obtained viscoelastic properties of the SU8-2002 layer are presented and compared with the values obtained in single-layer experiments (fig. 8-10).

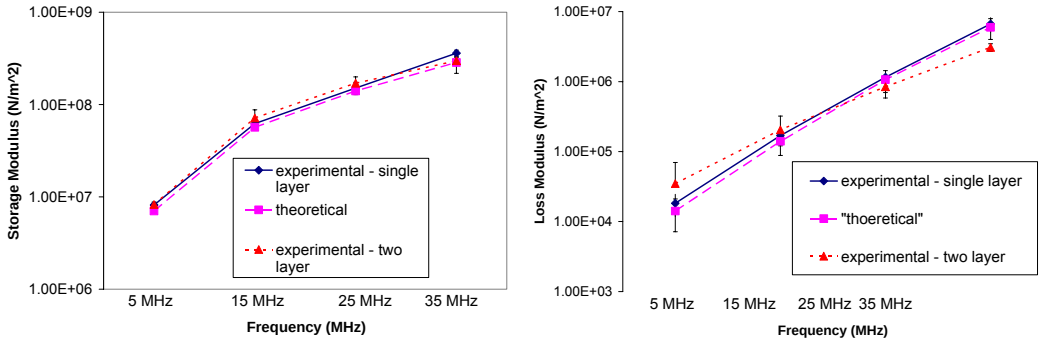

(a) (b)

Figure 8-10 The results obtained from the MTSM/GA technique for SU8-2002 layer before and after the formation of two-layer system; (a) storage modulus (b) loss modulus

As seen from fig.8.10, the storage modulus of the SU8-2002 layer has been estimated with less than 10 % error for harmonics. In contrast, the error was increased to more than 50 % at 5 MHz and 35 MHz for loss modulus estimation.

The collagen layers' viscoelastic properties are also presented in fig. 8-11. As seen from the fig. 8-11, the determined properties of the collagen fit to the calibration curve which was obtained in chapter 6.

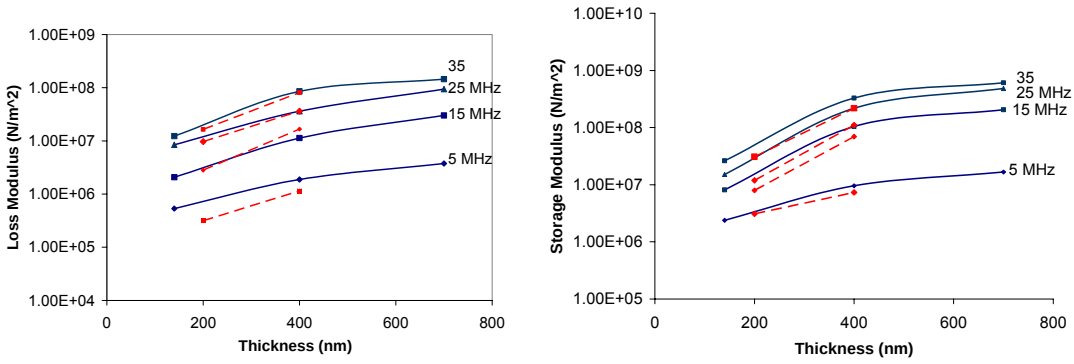

(a) (b)

Figure 8-11 The results obtained from the MTSM/GA technique for collagen layer before and after two layer system formation.(a) loss modulus (b) storage modulus

8.3.2 Two-layer viscoelastic system consists of 0.770 µm SU8 layer as first layer and 300 nm and 100 nm thick collagen layers as second layer

200 µl of collagen type-I suspension has been placed on the 0.770 micron thick SU8-2002 layer and maximum magnitude and resonance frequency responses of the MTSM sensor were monitored during the evaporation process (fig. 8-12). Time 0 indicates the air reference point. All graphs clearly show that there are four consecutive stages of the MTSM sensor response during the evaporation-induced deposition process of each sample (stages shown in fig.8-12a). During the first stage (first 95 min), the resonance frequency and the magnitude responses are relatively flat. The first part of the second stage is indicated by sudden slight (about 1 ~ 1.5 dB depending on the harmonic) decrease in magnitude and last short period of time (less than 5 minutes). In the second part of the second stage is magnitude response increases and resonance frequency continues decreasing. In the third stage resonance frequency increases and magnitude response continues increasing. In the last stage both responses stabilize.

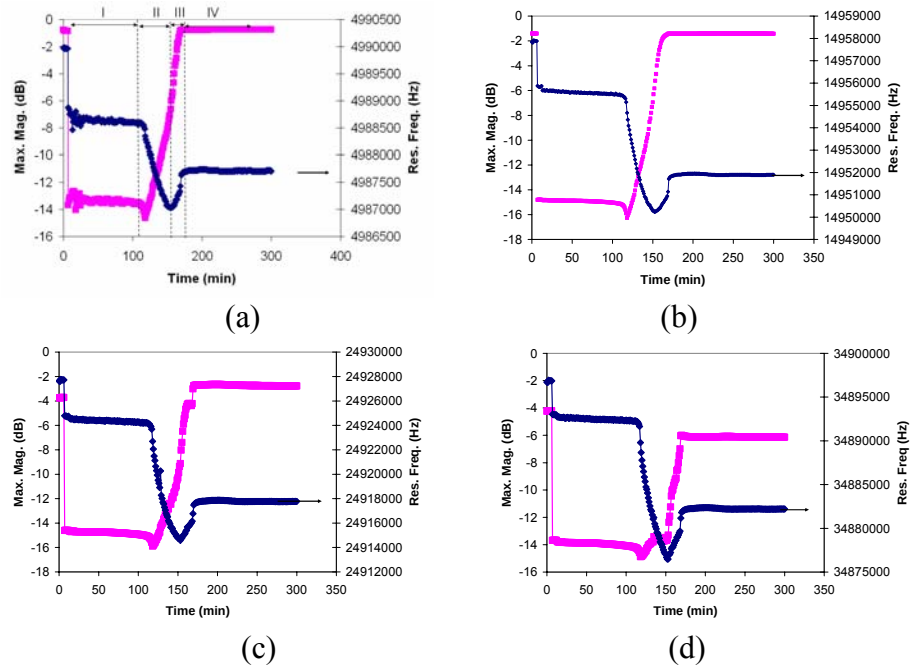

Figure 8-12 The evaporation process of 200 µl of collagen on 0.770 micron thick SU8-2002 layer at a) 5 MHz, b) 15 MHz, c)25 MHz, and d) 35 MHz

Next, 100 µl of collagen type-I suspension has been placed on the 0.770 micron thick SU8-2002 layer and maximum magnitude and resonance frequency responses of the MTSM sensor were monitored during the evaporation process (fig. 8-13). Time 0 indicates the air reference point. All graphs clearly show that there are four consecutive stages of the MTSM sensor response during the evaporation-induced deposition process of each sample (stages shown in fig.8.13a). During the first stage (first 45 min), the resonance frequency and the magnitude responses are relatively flat. The first part of the second stage is indicated by sudden slight (about 0.1 ~ 0.5 dB depending on the harmonic) decrease in magnitude and last short period of time (less than 5 minutes). This drop is relatively small compared to the ones obtained in previous experiments shown in fig. 8-6., 8-8, and 8-11. In the second part of the second stage is magnitude response increases and resonance frequency continues decreasing. In the third stage resonance frequency increases and magnitude response continues increasing. In the last stage both responses stabilize.

It should be noted that the kinetics of the evaporation process is different at each harmonic. As seen from fig. 8-13a, the frequency response stays almost flat during the stage II at 5 MHz. Magnitude response decreases sharply (~2 dB) at the end of at stages III at 25 MHz. The magnitude response continuously increases with the same slope at 5 MHz. In contrast the rate of increase in the magnitude response slows down at 15 MHz (almost flat during stage III), 25 MHz and 35 MHz decreases at initial part of stage III, then increases sharply at 15 MHz and 35 MHz.

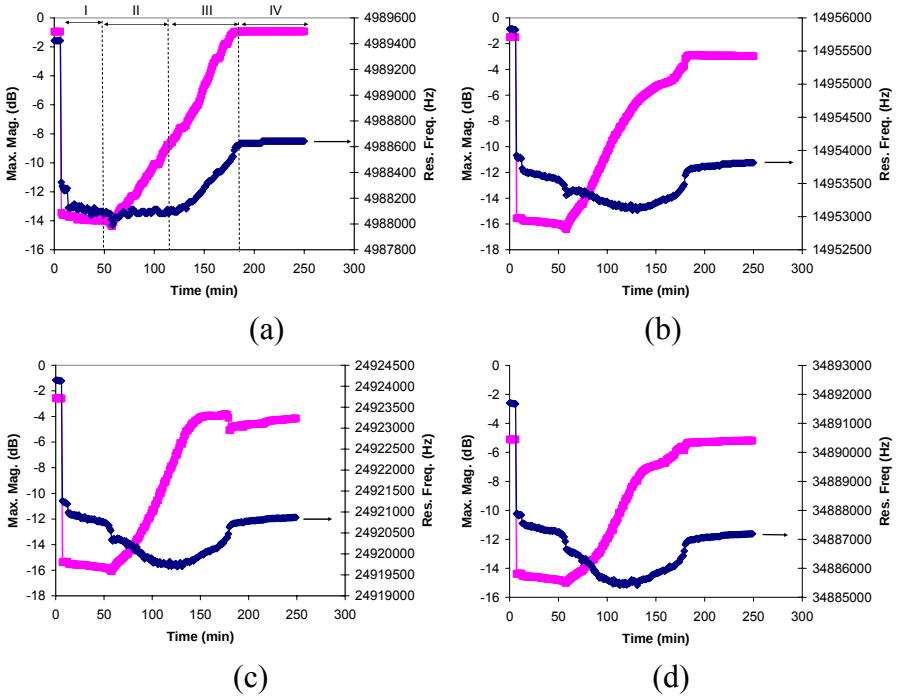

Figure 8-13 The evaporation process of 100 µl of collagen on 0.770 micron thick SU8-2002 layer at a) 5 MHz b) 15 MHz c)25 MHz and d) 35 MHz

The thickness of the collagen layer has been calculated by using the MTSM/GA technique and it was compared to the one measured by using profilometer. It has been shown in chapter 5, the collagen does not form a flat layer on the MTSM sensor. Therefore the thickness of the collagen was measured at different locations at the surface (fig. 8-14)

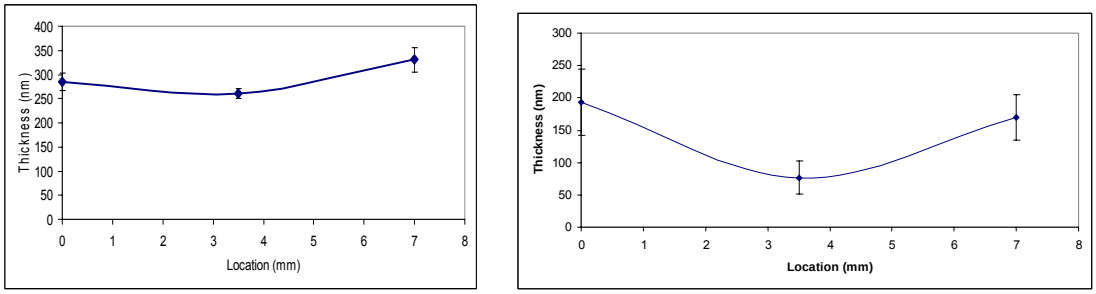

(a) (b)

Figure 8-14Thickness of the collagen layer on at different locations; (a) thickness obtained at the end of the evaporation process of (a) 200 µl collagen and (a) 100 µl collagen on 0.770 µm thick SU8-2002 layer. Each point is an average of 10 measurements

As seen from the fig. 8-14, the thickness of the collagen varies at the surface. The average thickness can be estimated to be around 300±50 (50 nm is calculated roughness) nm and 100±50 nm. The calculated thickness of the collagen by using the MTSM/GA technique is 270±30 nm and 100±20 nm. At the end of the experiments, the maximum magnitude and resonance frequency values of the MTSM sensor were plugged into the MTSM/GA technique. The obtained viscoelastic properties of the layers are presented in the fig. 8-15.

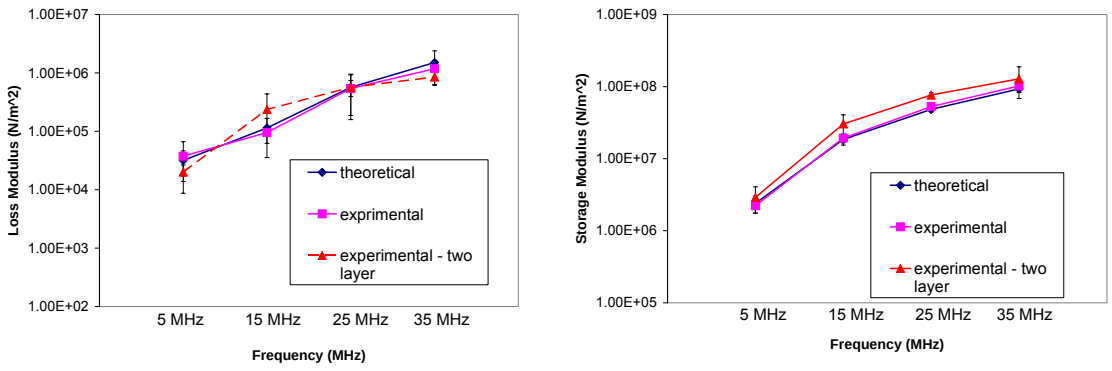

(a) (b)

Figure 8-15 The results obtained from the MTSM/GA technique for SU8-2002 layer before and after two layer system formation. (a) storage modulus (b) loss modulus

As seen from fig.8-15, the storage modulus of the SU8-2002 layer has been estimated with less than 30 % error for harmonics. In contrast, the error was increased to more than 50 % at 5 MHz and 15 MHz for loss modulus estimation.

The collagen layers' viscoelastic properties are also presented in fig. 8-16. As seen from the fig. 8-16, the determined properties of the collagen fit to the calibration curve which was obtained in chapter 5.

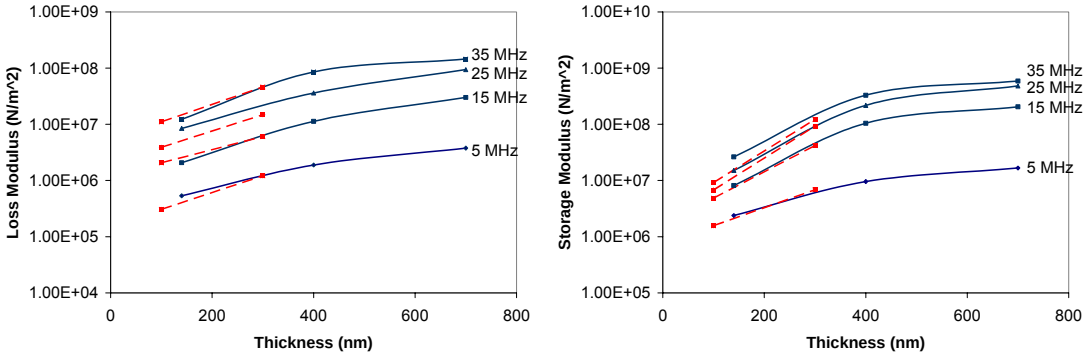

(a) (b)

Figure 8-16 The results obtained from the MTSM/GA technique for collagen layer before and after two layer system formation.(a) loss modulus (b) storage modulus

8.4 Discussions on experimental validation of the MTSM/GA technique for two-layer viscoelastic systems

Multi-layer viscoelastic systems with different thickness combinations of SU8-2002 and collagen type-I polymers have been realized. SU8-2002 has been utilized as first layer and collagen layers were deposited on the SU8-2002 layers which were spun coated on the MTSM sensor. Several important considerations have been identified before the experimental procedure has been implemented. It has been shown that SU8-2002 layers form a homogenous and uniform layer on the sensor surface. Optical studies revealed that SU8-2002 polymer layer's thickness is uniform throughout the surface. There were no micro-cracks formed during the spin coating and thermal heating of the polymer. Therefore it was assumed that there was no trapping of the second layer into the first layer.

The second important consideration was to prevent second layer's attack into the first layer during the evaporation process. It has been shown that the SU8-2002 layer's surface is very stable in many chemicals if hard baking method is applied. No developer for SU8-2002 has been used in this project. Therefore it was assumed that the SU8-2002 layer stayed stable during the collagen evaporation process. Under these valid assumptions, the SU8-2002 and collagens was considered as two distinct polymer layers without any interference to each other.

It was expected that the mechanical properties of the collagen layers absorbed on the SU8-2002 might be different than the ones absorbed on the gold layer. Surface of untreated SU8 layer is hydrophobic. The level of hydrophobicity affect the adsorption rate of the collagen on the surfaces (Yin et al., 2004). Therefore the different level of hydrophobicity of gold and SU8-2002 layers might have an affect on the mechanical and structural properties of the collagen layer.

The average surface roughness of SU8-2002 layer was measured to be around ~20 nm. This roughness level is 10 times higher than the roughness of the gold layer. Surface roughness affect the MTSM sensor response (Daikhin and Urkbah et al., 1996). Thus, the larger-than predicted responses commonly observed for resonators operated in contact with liquid are likely due to enhanced solid/liquid interactions caused by surface roughness. It can be hypothesized that a "third" layer with thickness of ~50 nm may be formed at collegen-SU8 interface. This transition layer may have an affect the MTSM sensor response, thus overall mechanical properties of the collagen layer. This brings another issue which is related to the "continuity" of the collagen-SU8 layer interface. It has been discussed that one of the basic assumptions of the TLM is that there is "continuity" of displacement at the solid-solid, solid-liquid, and liquid-liquid interfaces. In this case the interface is formed by two polymers.

After these assumptions and the considerations, three main experiments have been designed and implemented for validation of the MTSM/GA technique for two-layer viscoelastic systems. The experiments were designed to test the performance of the GA/MSM technique with the simplest to most complex viscoelastic systems.

First, a single-layer viscoelastic system has been modeled as two viscoelastic layers (depicted in fig. 8-1). For this purpose, 1.95 μm thick SU8-2002 layer has been modeled as two viscoelastic layers with different thicknesses. It was shown that the MTSM/GA technique can determine the mechanical properties of each viscoelastic layer with less than 40 % error. Less than 10 % error was achieved for the storage modulus (shown in table 8.1). In addition it was shown that the different thickness values do not affect the MTSM/GA technique's output.

Second set of experiments were designed to identify the performance of the MTSM/GA technique for determination the viscoelastic properties of a two-layer system formed by a viscoelastic polymer as first layer and Newtonian medium as second layer. For this purpose, 1.95 μm thick SU8-2002 layer spin coated on the MTSM sensor was loaded with DI water in room temperature. This physical experimental system was modeled as a two layer system made by a viscoelastic layer with finite thickness and a semi-infinite Newtonian medium. Therefore the thickness of the Newtonian medium was chosen to be at least several magnitudes higher than the penetration depth of the acoustic wave (2 μm). In the experiments the column height of DI water layer was 5 mm. After realizing these conditions, the MTSM/GA technique has been applied to determine the properties of the viscoelastic layers. It was shown that the MTSM/GA technique can predict the viscoelastic properties of the SU8-2002 layer with 6 % - 40 % error. On the other hand, the error increased to be between 30 % - 80 % for determination of DI water's viscosity value. The stiffness value of the water layer was expected to be 0 N/m^2 at all harmonics but the predicted values varied between

$2x10^3$ N/m^2 to $15x10^3$ N/m^2. It should be note that the error in determination mechanical properties of DI water loaded on gold surface was only 1 %- 2 % (table 6-2). In addition the spin coating of polymer layer on the MTSM sensor decreased the fluctuations in the sensor's response at 5 MHz. Thus reasonable results were able to be obtained at this frequency. The increase in the error may stem from the fact that the roughness of the surface increased. Therefore DI water trapped by surface microstructure or accelerated by asperities protruding into the liquid behaves as a rigidly attached mass layer, giving a kinetic energy contribution that increases frequency response (Gollas et al., 2000). To test this hypothesis, resonance frequency and maximum magnitude response of the MTSM sensor loaded with 1.95 μm thick SU8-2002 layer was simulated by using transmission line model. The mechanical properties of the layer were already calculated in chapter 6 (section 6.3.4). Then, hypothetically, the MTSM sensor coated with SU8 layer was loaded with semi-infinite DI water layer. Theoretically obtained resonance frequency and maximum magnitude values were compared with the ones obtained experimentally. The comparison was presented in fig. 8-16. Relative changes are calculated to the values when the MTSM sensor was loaded with SU8-layer.

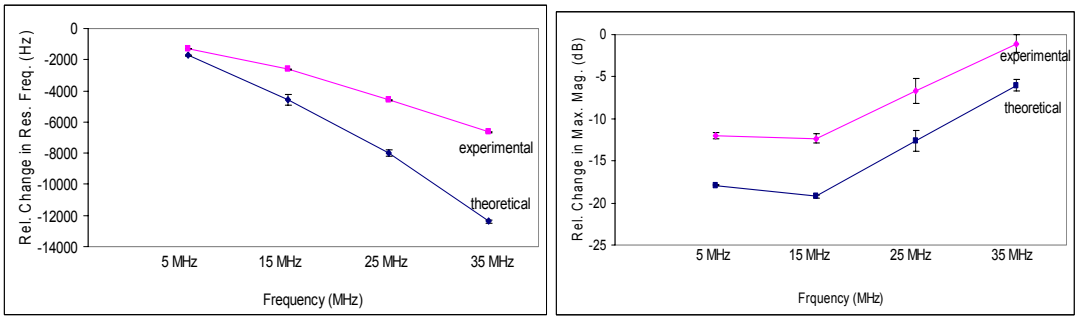

(a) (b)

Figure 8-17Comparison of theoretical and experimental changes (a) resonance frequency and (b) maximum magnitude when 1.95 μm thick SU8-2002 layer spin coated on the MTSM sensor was loaded with semi-infinite DI water. Theoretical calculations were done by using TLM

As seen from fig. 8-17, the theoretical values are ~1.7 times higher than the experimentally obtained values in both resonance frequency and maximum magnitude responses. These findings are apposite what it was predicted by the roughness theory. Therefore the error in the MTSM/GA technique may stem from the discrepancy between the TLM and the experimental results.

Final experiments were realized by forming two-layer viscoelastic systems on the MTSM sensor. The 1.95 μm and 0.77 μm thick SU8-2002 layers have been spin coated on the MTSM sensor. Then 200 μl and 100 μl of collagen type-I suspension has been added on the polymer layers. The adsorption process of the collagen suspensions has been monitored. Final thicknesses of the collagen layers have been measured by using profilometer. The detailed analysis of the stages of the evaporation process has already been discussed in section 6.8.

In first set of experiments, 1.95 μm thick SU8-2002 layer was spin coated on the MTSM sensor and collagen evaporation process on the SU8 layers has been monitored. It was shown that the acoustic signatures of the MTSM sensor show difference among the harmonic frequencies. Specifically, as seen in fig. 8-6., the magnitude response continuously decreases until the end of stage II, then increases very slightly (~0.2 dB) in the stage III and IV at 35 MHz. On the other hand, the magnitude responses stay relatively stable during stage I, decrease sharply in the beginning of the stage II, and then increase during the second part of the stage II at 5 MHz, 15 MHz, and 25 MHz. It should be noted that the penetration depth of the acoustic wave changes with the operating frequency. Thus the harmonic operation of the MTSM sensor provides the information regarding the mechanical properties of the interface at different depth from the interface. Furthermore the acoustic signatures of the collagen deposition on the SU8 layer and on the gold surface show similarities. As seen fig. 6-14b, the magnitude response of the MTSM sensor to deposition process of the collagen on

the gold surface also decrease sharply (~2dB) in the beginning of stage II and stays almost the same until the end of the stage II. Then it increases during the stage III.

At the end of the experiments, the maximum magnitude and the resonance frequency values were plugged into the MTSM/GA technique and the viscoelastic properties of the layers were determined.

As seen in fig. 8-9, while the storage modulus of the SU8-layer was determined with 4 % - 25 % error, the loss modulus was determined with 10 % - 100 % error by the MTSM/GA sensor. The error especially increased to 60% and 100% at 5 MHz and 35 MHz respectively.

The storage modulus and loss modulus of the collagen layers were presented in the fig. 8.10. The loss modulus values for 400 nm and 200 nm thick collagen layer at 15 MHz, 25 MHz, and 35 MHz show very good agreement with the values shown in the calibration curve. On the other hand the loss modulus values at 5 MHz were ~50% less than the values shown in the calibration curve, but they were still in the same magnitude order. In contrast the storage modulus values determined by the MTSM/GA technique at 5 MHz showed very good agreement with the calibration curve at 5 MHz while the same agreement was not observed at the higher harmonics. The discrepancies are around 30%, 100% and 100% at 15 MHz, 25 MHz and 35 MHz respectively (values at ~400 nm values). As seen clearly discrepancy increases with the harmonic number.

In the second set of experiments, 0.770 μm thick SU8-2002 layer was spin coated on the MTSM sensor and collagen evaporation process on the SU8 layers has been monitored. It was shown that the acoustic signatures of the MTSM sensor show difference among the harmonic frequencies. Specifically, as seen in fig. 8-12, the magnitude response sharply decreases (~2 dB) at the end of the stage III at 25 MHz. The magnitude response continuously increases until the end of stage II, then rate of the increase decreases until the

end of the stage III, and then it increases at a higher rate again until stage IV at 25 MHz and 35 MHz. On the other hand, the magnitude responses stay relatively stable during stage III at 25 MHz. It should be noted that the frequency responses at each harmonic decrease sharply in the beginning of the stage II. This phenomenon has not been observed before and shows the importance of the multi-harmonic operation of the MTSM sensors.

At the end of the experiments, the maximum magnitude and the resonance frequency values were plugged into the MTSM/GA technique and the viscoelastic properties of the layers were determined.

As seen in fig. 8.14, while the storage modulus of the SU8-layer was determined with 25% - 50% error, the loss modulus was determined with 30% - 100% error by the MTSM/GA sensor. The error especially increased to 50% and 100% at 5 MHz and 15 MHz respectively.

The storage modulus and loss modulus of the collagen layers were presented in the fig. 8-15. The both loss and storage modulus values for 300 nm and 100 nm thick collagen layer at 5 MHz, 15 MHz, 25 MHz, and 35 MHz show very good agreement with the values shown in the calibration curve.

8.5 Summary and Conclusions

The MTSM/GA technique for two-layer viscoelastic systems has been tested with judiciously prepared experimental systems. Mechanical properties of a two-layer viscoelastic system, consisting of finite thickness of a polymer as a first layer and semi-infinite Newtonian medium as a second layer, were studied. Final experiments were realized by forming two-layer viscoelastic systems made of SU8-2002 as first layer and collagen type-I

as second layer. The collagen layer was formed on the SU8-2002 polymer by adsorption process. Different thickness configurations of layered structure were studied.

Experimental studies of the MTSM/GA technique for two-layer viscoelastic systems revealed that the MTSM/GA technique is capable of determining the mechanical properties of two-layer viscoelastic systems. The error in the MTSM/GA technique was observed to increase depending on the complexity of the interface. In addition it was shown that the error can be decreased with some improvements in the multi-layer modeling of the MTSM sensor-interface interactions, which will be the focus of the further studies.

For the first time, a comprehensive experimental study on multi-layer interfaces on the MTSM sensor was realized. It was shown that the MTSM/GA technique can be a powerful tool for quantitative characterization of two-layer viscoelastic systems, which can be extended to multiple-layers with more advanced modeling and data analysis technique.

9 APPLICATION OF THE MTSM/GA TECHNIQUE FOR DETERMINATION OF MECHANICAL AND GEOMETRTICAL PROPERTIES OF BIOLOGICAL INTERFACIAL PROCESSES

The MTSM/GA technique has been applied for determination of the mechanical and geometrical properties of the biological interfacial properties. For experimental studies, antibody attachment on the MTSM sensor's gold surface by passive adsorption and attachment of the bovine aortic endothelial cells (BEAC) on the gelatin coated surface have been investigated. Antibody attachment process was used as a single-layer model on the MTSM sensor and the cell adhesion was modeled as a two-layer viscoelastic system.

9.1 Determination of properties of antibody adhesion on the MTSM sensor's gold surface

Antibodies play crucial importance in many applications. For example, due to the highly selective molecular recognition afforded by the immune system, assays involving antibody-antigen reactions are commonly used in chemical, biological, and environmental analysis (Dong and Shannon et al., 2000). It has been shown that physical stability of antibodies in the development of a high concentration stable protein formulation is dependent on the solution rheology (Shire et al., 2004). This phenomenon is crucially important in the drug delivery. Furthermore the sensitivity of the biosensors in the detection of pathogens, viruses or other type of target analytes is very much dependent on the interface (immobilized interface) (Johne, 2008).

b. Materials and methods

The reference measurements were taken for air and phosphate buffer saline (PBS). Next, the sensors were exposed to rabbit-immunoglobulin G (IgG) (0.50 μg/ml) suspended in DI water (Fisher Scientific, pH: 5.34, Cat No: 25—555-CM) for 50 minutes to allow IgG coating of the sensor surface by adsorption.

The experiments were done by adsorbing antibody layer on the MTSM sensor surface under static conditions at 5 MHz, 15 MHz, 25 MHz and 35 MHz. The sensor surface was saturated with antibody to form a uniform protein layer on the surface. Relative change in the resonance frequency and maximum magnitude responses at 15 MHz, 25 MHz and 35 MHz are presented in figure 9-1. At the fundamental frequency (5 MHz), high fluctuations observed in sensor response likely due to insufficient energy trapping as described by others (described in chapter 4). The MTSM sensor surface was saturated with the antibody by keep adding the antibody solution until no frequency and magnitude changes are observed.

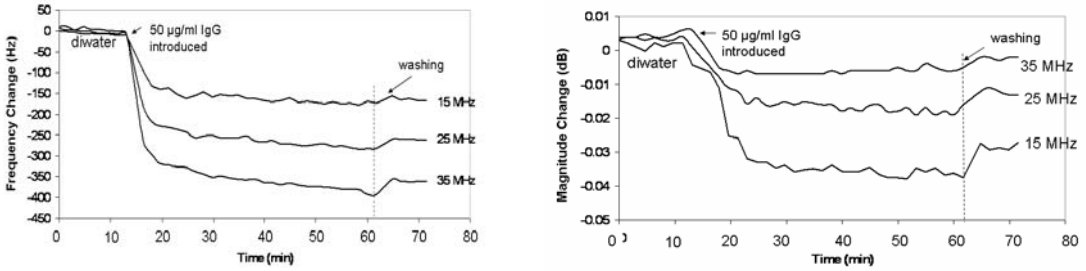

(a) (b)

Figure 9-1 Time response of relative changes in (a) the resonance frequency and the (b) maximum magnitude responses of MTSM sensor to antibody binding at 15 MHz, 25 MHz and 35 MHz

The properties of the medium were determined at t_1 = 10 and t_2 = 70 minutes. At t_1 = 10, the system is modeled as MTSM sensor loaded with semi-infinite Newtonian medium (DI water) (fig 9-2a). The height of the column (2 mm) was much higher than the penetration depth of the acoustic wave at 5 MHz (~250 nm).

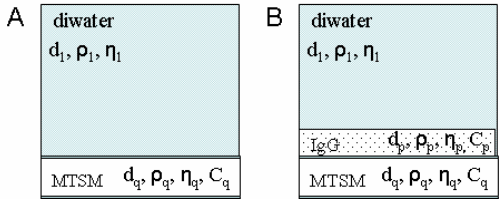

Figure 9-2 Physical model for MTSM sensor system at A) t=10 and B) t=70

At t_2 = 10 min., the determined properties of the layer at 15 MHz, 25 MHz and 35 MHz were presented in table 5. The variations in the thickness values were very high (ranging from 300 nm to 5 μm) due to the fact that column height was much larger than the penetration depth. Due to the high fluctuations in thickness values, it was not presented here. In contrast the solutions for ρ_1, η_1 and C_1 match with the literature values very well. (Literature values are ρ_1 = 1000 kg/m^3, η_1 = 0.001 kg/m.s and C_1 = 0 N/m^2 at room temperature (Greczylo and Deboswka, 2005)).

Table 9-1Determined properties for semi-infinite Newtonian medium layer at 15 MHz, 25 MHz and 35 MHz

MTSM Frequency	Density (kg/m^3)	C^I (N/m^2)	η (kg/m.s)
15	1006±5	(2.00±1.00) x10^2	(1.05±.004) x10^{-3}
25	1003±2	(5.00±3.00) x10^2	(1.08±0.03) x10^{-3}
35	1004±4	(1.00±1.00) x10^2	(1.06±0.04) x10^{-3}

At t = 70 min., the physical model is presented in fig 10b. A viscoelastic layer (protein layer) with finite thickness and semi-infinite Newtonian medium were loaded on the MTSM sensor. The properties for DI water layer were entered into the algorithm as known

variables and the unknown properties (ρ_p, η_p, C_p' and d_p) of the viscoelastic layer were determined. The results are presented in table 6. The thickness of the layer was determined between 10.3 to 11 nm for the harmonics. This number matches with the values presented by the other researches very well. Westphal et al (2002) calculated the height of antibody layer as 9.2 nm. Furthermore Liao et al (2004) measured the average height of the antibody layer as 10.1±3.3 nm.

The density of the antibody layer was also calculated as 1030±14 kg/m^3. This density value is close to the water density in which the antibodies were suspended. Hook et al. (2002) considered the density of antibody layer as 1050 kg/m^3 when the antibodies were not attached to gold surface by using covalent binding. After the cross-linking, the density value of 1300 kg/m^3, this is closer to the density value of dry protein. Voros (2004) also showed that the wet density of antibody layer is significantly different than the dry protein density value due to the solvent present in the adsorbed proteins. Therefore we believe that the determined value of the density is in a reasonable range.

Table 9-2Determined properties for antibody layer at 15, 25 and 35 MHz

MTSM Frequency	Thickness (nm)	Density (kg/m^3)	G^I (N/m^2)	G^{II} (N/m^2)
15	11±0.3	1050±10	(5.20±0.5) x10^4	(4.80±0.58) x10^5
25	10.4±0.6	1080±12	(5.00±0.13) x10^4	(9.50±1.40) x10^5
35	10.3±0.4	1040±14	(5.60±0.12) x10^4	(1.52±0.31) x10^6

As seen from the table 9.2, the adsorbed antibody layer has low storage modulus (<1e5 N/m^2), and relatively higher loss modulus (>4.8 N/m^2) While storage modulus was same for each harmonic, loss modulus was changed with frequency. It has been experimentally shown that the adsorbed protein layers on the MTSM sensor such as antibody, vesicles and cells do not behave like “rigid and thin” films (Voinova et al., 2002). Therefore

the linear relationship between resonance frequency shift and mass deposition is not observed. Saluja et al. (2005) indicated low concentrations (less than 60 mg/ml) of antibody suspension behave like Newtonian medium. But it should not be expected that the properties of adsorbed layer will not be the same as the properties of antibody suspension. The effect of the binding between protein layer and gold layer should be considered. There has been no literature value were found to be used for direct comparison. Therefore we believe that the MTSM/GA technique will lead to development of a quantitative tool for study of biological interfacial processes.

9.2 Determination of viscoelastic properties of bovine aortic endothelial cells (BAEC) attached on gelatin coated MTSM sensor surface

Cell adhesion is a complex process involving physical interactions, chemical binding events, and biological signaling processes. Cellular adhesion plays important roles in the regulation of cell behavior, such as the control of growth, differentiation during development and the modulation of cell migration in wound healing, metastasis, and angiogenesis. Cell adhesion has been one of the important criteria for evaluating the tissue integration of implanted biomaterials. In particular, quantitative characterization of cell adhesion and its kinetics provides valuable information for the development of biomaterials. Therefore, a lot of effort has been made to elucidate dynamic mechanism of cell adhesion. Current techniques for evaluating the cell spreading and cell adhesion strength are labor intensive and destructive (e.g. flow detachment assay). Especially, they are not sufficient in providing the detailed kinetics of adhesion process. Initial attachment and spreading patterns have been studied and various techniques have been introduced to quantify the cell adhesion strength (Thaler et al., 2004, Garcia et al., 1997). Morphology and topographical distribution of focal adhesions

have been investigated in real-time with confocal microscopy and immuno-staining technique (Davies et al.,1993, Neyfakh et al.,1983).

Recently, the thickness shear mode (TSM) sensor technique has been used to detect cells adhering to the sensor surface. Since TSM sensor is capable of detecting nano-scale changes in mass and mechanical properties of interfacial material, it is possible to detect ligand-receptor binding in real time. This technique has been used in monitoring the cell adhesion process using resonance frequency shifts (Redepenning et al.,1993). Wegener et al. (1998) have shown that different cell types have their own characteristic frequency changes when they formed confluent monolayers, and tried to explain frequency shifts with geometrical properties of cells. Marx et al. (2001) has shown that morphological changes of cells due to the depolymerization of cytoskeleton caused frequency and resistance shifts. Li et al. (2004) assessed the integrin-mediated cellular interactions with extracellular matrix (ECM) proteins by evaluating the bandwidth shift.

9.2.1 Material and methods

9.2.1.1 Endothelial cell culture

Bovine aortic endothelial cells (BAECs) were isolated from calf ascending aorta as previously described [ref]. The BAECs were cultured in complete media [Dulbecco's modified Eagle's medium (Mediatech, Inc., Herndon, VA), 100 units/ml penicillin, 100 mg/ml streptomycin, 250 ng/ml amphotericin B (Sigma Chemical Co., St. Louis, MO), 2mM/ml Lglutamine and 10% heat-inactivated calf serum (Invitrogen Co., Carlsbad, CA)] in a humidified, 37 ^{0}C incubator with 5% CO_2 in air. Passage numbers were between 6 and 14. Cell suspensions were made by treating the confluent monolayer of BAECs with 0.25% trypsin for 90 s, centrifuging at 200g for 5 min, and resuspending in serum-free media

[Dulbecco's modified Eagle's medium (Mediatech, Inc.), 100 units/ml penicillin, 100 mg/ml streptomycin, 250 ng/ml amphotericin B (Sigma Chemical Co.), 2mM/ml L-glutamine (Invitrogen Co.)]

9.2.1.2 MTSM sensor device and measurement system

The sensing device was built on a disk-shaped AT-cut quartz crystal operated at 5 MHz, 15 MHz, 25 MHz and 35 MHz by attaching a Teflon cylinder of which inner diameter and height were 11 and 8 mm, respectively. The 0.33 mm thick crystal was 14 mm in diameter with gold electrodes 7 mm in diameter. The sensor device was then placed in a humidified, 37 ^{0}C incubator with 5% CO_2 in air. The sensor device was connected to a network analyzer (HP 4395A), and a personal computer was used for controlling the network analyzer and collecting the data. Thus, the results reported here are for the sensor operating at 5 MHz, 15 MHz, 25 MHz and 35 MHz. The MTSM sensor response was measured using network analyzer (NA).

9.2.1.3 Surface coating of the MTSM sensor

All experiments were performed in serum-free medium to avoid variability due to uncontrolled concentration of adhesion molecules and growth factors present in serum. Except as noted, a gelatin coating of the sensor surface was used as the adhesive substrate. Gelatin coating was used to provide a uniform surface presenting Arg–Gly–Asp (RGD) peptide sequence for integrin binding. The MTSM sensor was immersed in 0.5% (v/v) gelatin solution (Sigma Chemical Co.) for 30 min at room temperature. The surplus of gelatin was removed by aspiration and the surface was rinsed with PBS two times. The thickness of the

gelatin coating was ~10 nm, as assessed by AFM, and produced a negligible change in sensor readings.

9.2.1.4 Experimental protocol

Prior to adding the cell suspension, 0.1 ml of serum-free media was placed in the MTSM sensor chamber and allowed to equilibrate to 37 ^{0}C. The equilibrium of the temperature was confirmed by checking the stability of sensor signal. Next, 0.4 ml of cell suspension (37 ^{0}C, 3.75x10^5 cells/ml) was gently pipetted into the chamber for a final concentration of 3x10^5 cells/ml. The total number of cells per sensor area was approximately the density of a confluent monolayer of ECs. The initial projected area of the unspread cells was approximately 15–20% of the sensor surface area. The density of cells was chosen to give the maximal response without overly constraining their ability to spread.

9.2.1.5 Optical measurements

` At each time point (1 hour and 20 hour), following inoculation, one of the sensors was rinsed to remove the weakly attached and unattached cells from the surface. Care was taken to make the rinsing procedure consistent between trials. After removing the cylinder from the sensor, the sensor was held at approximately 45^0 angle (from horizontal) while 2 ml of PBS was slowly pipetted onto the upper edge of the sensor and allowed to flow down the tilted surface driven by gravity alone. Cells that remained attached after two rinses were stained with Calcein Green (Invitrogen Co.) to allow visualization on the opaque sensors. Calcein Green is introduced to the cells in a non-polar ester form that can diffuse across the plasma membrane. It is then modified by nonspecific esterases into a polar fluorescent

molecule that cannot escape the cell if the membrane is intact. Thus, it also serves as a viability marker. The cells were imaged using an epifluorescence microscopy, and the total number of cells in five randomly selected microscope fields was counted (fig. 9.3).

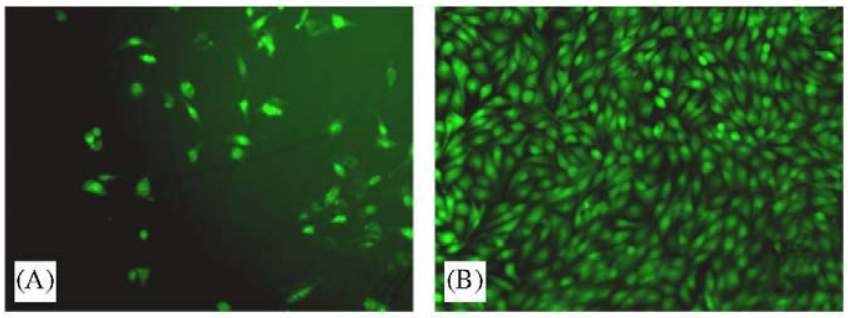

Figure 9-3 MTSM sensor surfaces were rinsed with PBS at each time point and stained: (A)1 h, (B) 15 h

9.2.2 Characterization of the MTSM sensor readings

The time course of the maximum magnitude change and the resonance frequency change following inoculation was used to characterize the cell adhesion process (fig. 9.4). In the typical response, following an initial delay time (10 min), there was a sharp increase in resistance to a new plateau (primary plateau). Subsequently, there was slower increase in resistance to a new minimum value (secondary plateau) that either persisted or gradually increased or decreased. The predicted sedimentation time was approximately 10 min. The changes in adhesion response due to the various interventions were characterized by changes in the delay time, the slope of the initial decrease in magnitude response, and the size of magnitude response at the primary plateau.

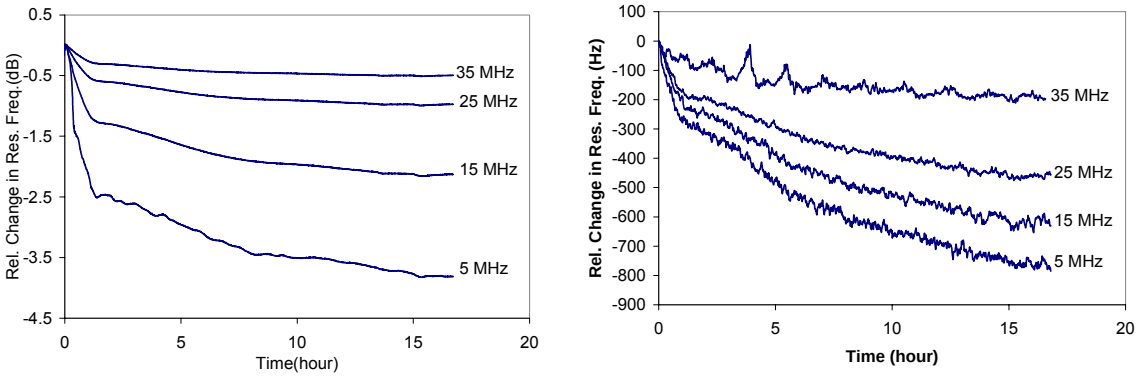

Figure 9-4 Time course of relative changes in (a) the maximum magnitude and (b) resonance frequency responses of the MTSM sensor due to the adhesion process of endothelial cells. Cell suspension was introduced to the sensor's surface at time 0.

9.2.3 Determination of the mechanical properties of DMEM loaded on the MTSM sensor

As discussed in the experimental procedure section (section 9.4), the BAEC cells were suspended in the DMEM solution. For calibration purposes, the mechanical properties of the DMEM solution should be determined first. Change in the maximum magnitude and the resonance frequency of the MTSM sensor loaded with 200 µl of DMEM solution in 37 ^{0}C have been shown in fig. 9.5.

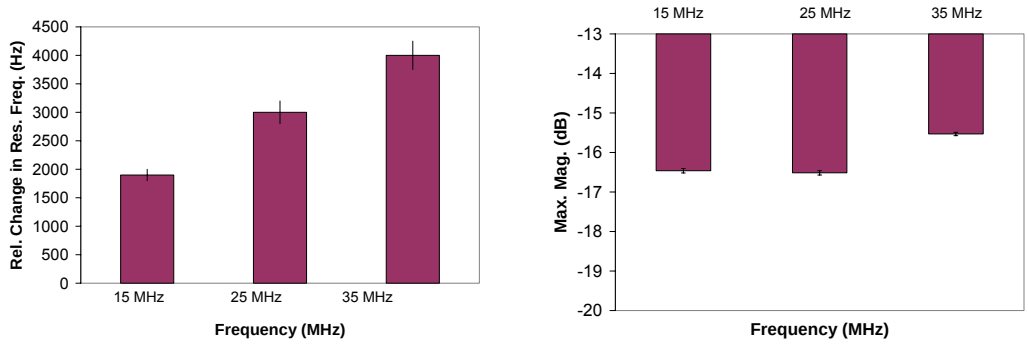

(a) (b)

Figure 9-5 MTSM sensor's response to DMEM loading (a) relative change in the resonance frequency and (b) absolute change in maximum magnitude

In table 9.3, the properties of DMEM determined by the MTSM/GA technique are presented. As seen from the table 9.3, it can be seen that DMEM solution is a Newtonian look system with zero stiffness. The viscosity is ~$1.1x10^{-3}$ kg/m.s and density is ~1020 kg/m^3. Variations in the thickness values are relatively larger (±200) since the medium is semi-infinite. As discussed in chapter 5, the thickness value will be equal and/or higher than the penetration depth of the acoustic wave (δ=250 nm at 5 MHz).

Table 9-3Determination of DMEM properties at 15 MHz, 25 MHz, and 35 MHz by using the MTSM/GA technique.

MTSM Frequency (MHz)	η (kg/m.s)	C (N/m^2)	ρ (kg/m^3)	d (nm)
15	$(1.12\pm0.01)x10^{-3}$	$(1\pm0.3)x10^3$	1020±5	700±200
25	$(1.1\pm0.08)x10^{-3}$	$(3\pm2)x10^3$	1015±5	130±10
35	$(1.1\pm0.02)x10^{-3}$	$(8\pm3)\ x10^3$	1020±0.5	100±10

9.2.4 Determination of the mechanical properties of gelatin layer coated on the MTSM sensor

Next, the properties of gelatin layer coated on the MTSM sensor surface were determined by the MTSM/GA technique. The MTSM sensor was immersed in 0.5% (v/v) gelatin solution for 60 min at room temperature. The acoustic response of the gelatin coating was presented in fig. 9.6.

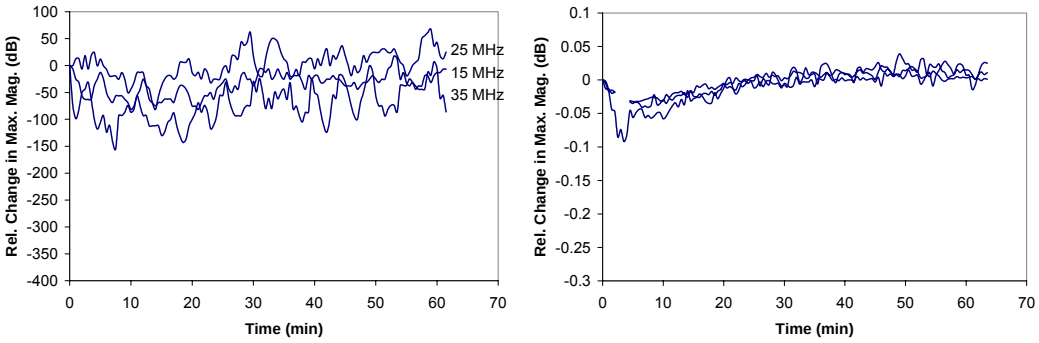

(a) (b)

Figure 9-6 The MTSM sensor's response to gelatin coating (a) relative change in the resonance frequency and (b) relative change in maximum magnitude at 15 MHz, 25 MHz and 35 MHz

As seen from the fig. 9.6, no visible change has been observed in the resonance frequency and the magnitude responses of the MTSM sensor. The noise is relatively higher (~100 Hz) in the signals since the curve fitting algorithm was not applied to these data. Therefore the MTSM/GA technique was not able to determine the properties of the gelatin layer. The thickness of the gelatin layer coated on the MTSM sensor after 60 minutes was measured by using atomic force microscopy and it was determined to be ~10 nm.

9.2.5 Determination of the mechanical properties of cells attached on the gelatin coated MTSM sensor

Time response of the MTSM sensor to the attachment of the BAEC cells on gelatin was presented in fig. 9.4. The mechanical and structural properties of the cells were determined at time 20 h since it was shown in fig. 9.3 that the cells form a monolayer on the MTSM sensor. When the MTSM/GA technique is extended to the heterogonous layers, then the mechanical properties of the cells can be determined in the other time points.

Initially cell attachment on the MTSM sensor was modeled as one layer system (fig. 9.7). Gelatin layer and cell monolayer attached on the gelatin layer were considered as one-layer viscoelastic system. Mechanical and structural properties were determined by the MTSM/GA technique.

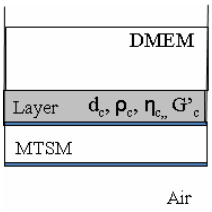

Figure 9-7 One-layer model of the cell attachment on the MTSM sensor

In fig.9.8, the properties of viscoelastic layer determined by the MTSM/GA technique are presented. The shear modulus of the cell monolayer increases with the frequency. Density and thickness values are determine to be 1040 kg/m^3 – 1080 kg/m^3, and 5000 nm – 5700 nm respectively. It was reported that the diameter of the BAEC is ~ 10-15 µm (Kyle et al., 1998). The cells do not maintain their circular shape and they became more flat when they spread on the surface (King et al., 2005). Therefore it is expected to obtain a lower thickness value at the end of the experiment.

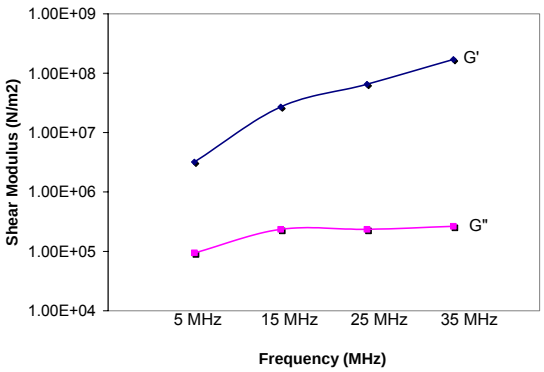

Figure 9-8 Loss and storage modulus of interfacial layer at 5 MHz, 15 MHz, 25 MHz, and 35 MHz

Secondly cell attachment on the MTSM sensor was modeled as two-layer system (fig 9.9. According to surface plasmon resonance microscopy (SPRM) studies (Giebel et al., 1999), the gap in focal contact area is only a few nanometers, while cell membrane is separated from the substrate about 30 nm in close contact area and about 100–150 nm in the rest part of cells, respectively. Based on these considerations, it is reasonable to include two layers on the MTSM sensor surface: a finite interfacial gap and a semi-infinite cell layer. In addition, for simplicity, all the three layers are assumed uniform in the cell-covered area.

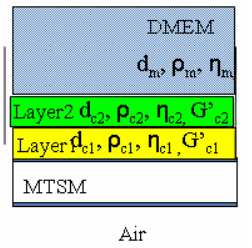

Figure 9-9 Two-layer model of the cell attachment on the MTSM sensor

In figure 9.10, the properties of two-layer viscoelastic layer determined by the MTSM/GA technique are presented. It was assumed that the displacement of the acoustic wave is continuous throughout the layers. It was observed that the storage modulus of the second layer is frequency dependent while loss modulus is frequency independent at higher level (at 15 MHz, 25 MHz and 35 MHz). The second layer shows more like soft rubber (at 5 MHz) and hard rubber at 15 MHz, 25 MHz and 35 MHz. The first layer shows a lossy system behavior. The storage and loss modulus is almost equal to each other. It was reported that the diameter of the BAEC is ~ 10-15 μm.

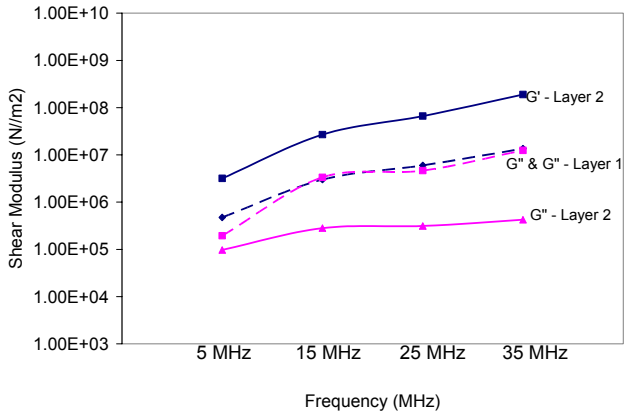

Figure 9-10 Loss and storage modulus of first and second layer at 5 MHz, 15 MHz, 25 MHz, and 35 MHz

9.2.6 Discussions

The MTSM/GA technique has been applied to determine the mechanical and structural properties of the interfacial biological processes. For case studies, properties of monolayer of an antibody and BAECs on the MTSM sensor were investigated because of their importance in science and engineering fields such biosensing and tissue engineering.

Monolayer of antibody was formed on the MTSM sensor by passive adsorption. The MTSM/GA technique was calibrated by loading the MTSM sensor with DI water at time 0. Properties of semi-infinite DI water were determined and they were in good agreement with literature values. After calibration measurements, final maximum magnitude and the resonance frequency values observed at the end of the antibody experiment were plugged into the MTSM/GA technique. The changes in the resonance frequency were observed to be ~150 Hz, 250 Hz and 350 Hz at 15 MHz, 25 MHz and 35 MHz respectively. The changes in the maximum magnitude were around -0.03 dB, -0.015 dB and -0.05 at 15 MHz, 25 MHz and 35 MHz respectively. The kinetics of antibody adsorption showed a typical protein binding kinetics. It was shown that the antibody layer thickness determined by the MTSM/GA technique was ~10.3 nm to 11 nm. These values were in good agreement with the literature

values which were found to be around 10 nm. The density values of the antibody layer were calculated to be around 1050 kg/m_3. Furthermore it was shown that the protein layer shows like a Newtonian medium with relatively low storage modulus (~$5x10^4$ N/m^2) and higher loss modulus which is in the range of ~10^5 N/m^2 to 10^6 N/m^2 depending on the harmonic. Storage modulus showed a frequency – independent behavior while the loss modulus changed with the frequency.

The BAEC adhesion on the gelatin coated MTSM sensor has been monitored. For calibration measurements, the mechanical properties of DMEM solution have been determined first at 37 ^{0}C. As discussed in the experimental method section, the cells were suspended in the DMEM solution. It was shown that DMEM solution is a Newtonian medium with zero stiffness. The viscosity and density values were determined to be ~$1.1x10^{-3}$ kg/m.s and ~1020 kg/m^3.

The mechanical and structural properties of the gelatin layer were not able to be determined by the MTSM/GA technique. The frequency data had a high noise level (~100 Hz) because no curve fitting technique was applied. In addition no change was observed in the magnitude data (fig. 9.6b). The thickness of the layer was determined to be ~10 nm by AFM measurements. Initially, the cell-surface interactions were modeled as one-layer viscoelastic system. As seen in fig. 9.8, the storage modulus increases with the frequency while the loss modulus stay relatively stable at 15 MHz, 25 MHz and 35 MHz. The system behaves like a soft rubber at 5 MHz but reflects hard rubber properties at higher frequencies. It was shown that the thickness of the viscoelastic layer was around 5 μm. The density value was determined to be ~1070 kg/m^3. It was shown that density of several cell types vary between 1000 kg/m^3 to 1100 kg/m^3 (Wegener et al., 1998). It was shown that the cell-surface interactions can be modeled as two-layer viscoelastic system. The first layer was considered as a 100 nm thick viscoelastic layer which represents the interfacial gap between the cell and the sensor's

surface, gelatin layer, cell binding and cell wall. This layer's properties showed like a lossy system. The ratio between G' to G" is equal to ~1 while the second layer had more like hard rubber properties.

9.3 Summary and Conclusions

The MTSM/GA technique has been applied to determine the mechanical and structural properties of antibody and cell monolayers attached on the MTSM sensor. The values determined by the MTSM/GA technique were compared to the literature values when it is available.

It was shown that the results obtained by the MTSM/GA technique are in very good agreement with available literature information. Furthermore, for the first time, the MTSM/GA technique provided the mechanical properties of layered structure of the cell-extracellular matrix interactions. In addition, monitoring the kinetics of interfacial phenomena and layer forming processes in real time and interpreting those undergoing processes by analyzing an evolution of the material parameters such as density, elasticity, viscosity and the thickness provides a very unique tool for in-depth interpretation of complex biological processes. More comprehensive studies will be the focus of the future work.

In conclusion, the MTSM/GA technique provides an exciting quantitative tool which enables obtaining the mechanical and structural properties of single and multi-layer biological interfaces.

10 CONCLUSIONS AND FUTURE WORK

10.1 Conclusions

A novel technique merging the multi-resonance thickness shear mode (MTSM) measurement technique and the genetic-algorithm (GA) based data analysis method has been developed and validated theoretically and experimentally.

It was shown that the MTSM/GA technique, which consists of four fundamental components; MTSM sensor as an interfacial sensor, multi-resonance operation of the MTSM sensor, real-time kinetics monitoring and GA-based data analysis method, is capable of:

- Quantitative characterization of single and multi-layer (two-layer) viscoelastic biological interfacial processes.
- Determining all mechanical (density, viscosity and stiffness) and geometrical properties (thickness) of the viscoelastic biological interfaces

For the first time, it was proven theoretically and experimentally that the MTSM/GA measurement technique enables full quantification of the complex biological interfacial processes. It was shown that the MTSM/GA technique is capable of solving under-determined problem, thus enabling a powerful tool to determine mechanical and structural properties of the biological interfacial processes in real time.

Furthermore, for the first time, comprehensive theoretical and experimental study on the multi-layer biological interfacial processes has been performed. The MTSM/GA technique was theoretically and experimentally tested with judiciously chosen control experiments, and then successfully applied to determine the mechanical properties of very important, from practical point of view, biological interface formed of cells and extracellular matrix.

Finally, the proposed MTSM/GA approach opens a new and very exciting opportunity for quantitative characterization of complex biological, chemical, and physical multilayer systems, which are very important in emerging fields such as nanotechnology, medical diagnosis, , drug discovery and personalized medicine

10.2 Future work

The future work will include four proposed studies;

1. The theoretical and experimental foundation of the MTSM/GA technique will be extended to study the heterogeneous media.

2. Application of the advanced MTSM/GA technique for quantitative characterization important biological processes and phenomena such as:

- cell adhesion process in real time.
- blood platelet adhesion and aggregation on extra-cellular matrix such as collagen.

4. The MTSM/GA technique will be extended for applications to quantitatively characterize multiple-layer biological process consisting more than two-layers.

11 REFERENCES

Alig et al, 1996. “Ultrasonic shear wave reflection method for measurements of the viscoelastic properties of polymer films”. Rev. Sci. Instrumen. 68. 1536-1542

An Y.H. and K.L. Martin, 2003 ‘Handbook of histology methods for bone and cartilage’, Human Press, pp. Ch. 4.

Anishetty A., E. Ergezen, A. Mehta, B. Onaral, K. Pourrezaei, Q. Zhang, R. Lec., 2008. “High Frequency TSM Sensors for Hepatitis-B Surface Antigen (HBsAg) Detection”. International Acoustic Devices Conference, December 10-11, Orlando, FL.

Arwin, 2000. “Ellipsometry on thin organic layers of biological interest: characterization and applications”. Thin Solid Films, v. 377, pp. 48-56.

Ayad M., Nagy L. Torad. 2009. “Alcohol vapors sensor based on thin polyaniline salt film and quartz crystal microbalance”. Talanta. V. 78. pp. 1280-1285

Back T., U. Hammel and H. P. Schwefel. 1997. "Evolutionary Computation: Comments on the History and Current State," IEEE Transactions on Evolutionary Computation, vol. 1, pp. 3.

Balakrishnan P. and V. S. Jacob. 1996."Genetic Algorithms for Product Design," Management Science, vol. 42, pp. 1105-1117

Bandey H L., Stephen J. Martin, and Richard W. CernosekA. Robert Hillman. 1999. “Modeling the Responses of Thickness-Shear Mode Resonators under Various Loading Conditions”. Anal. Chem., v. 71, pp. 2205-2214

Behling C, Ralf Lucklum and Peter Hauptmann. 1997. “Possibilities and limitations in quantitative determination of polymer shear parameters by TSM resonators” Sensors and Actuators A: Physical V. 61, pp. 260-266

Black, J., Mattson, R.U., 1982. “Relationship between porosity and mineralization in the Haversian osteon”. Calcified Tissue International v. 34, pp. 332–336.

Boschetti, F. Dentith, M. List, R. 1995. “Genetic algorithms incorporating a pseudo-subspace method”. Evolutionary Computation, 1995, IEEE International Conference on .v. 2, pp. 557-560.

Cannizzaro et al, 2000. “A novel biotinylated degradable polymer for cell-interactive applications”. Biotechnology and Bioengineering, v. 58, pp. 529-535.

Chen Meng-Yi, Yu-Long Sun, Chunfeng Zhao, Mark E. Zobitz, Kai-Nan An, Steven L. Moran, Peter C. Amadio. 2007. “Substrate adhesion affects contraction and mechanical

properties of fibroblast populated collagen lattices" Journal of Biomedical Materials Research Part B: Applied Biomaterials. Volume 84B Issue 1, Pages 218 – 223

Chen X., Martyn C. Davies, Clive J. Roberts, Kevin M. Shakesheff, Saul J. B. Tendler, and Philip M. Williams. 1996 "Dynamic Surface Events Measured by Simultaneous Probe Microscopy and Surface Plasmon Detection" Anal. Chem., v. 68 , pp 1451–1455

Cho Nam-Joon, J. Nelson D'Amour, Johan Stalgren, Wolfgang Knoll, Kay Kanazawa, Curtis W. Frank. 2007. "Quartz resonator signatures under Newtonian liquid loading for initial instrument check". Journal of colloid and Interface Science. v. 315. pp. 248-254

Cho Nam-Joon, Kay K. Kanazawa, Jeffrey S. Glenn, and Curtis W. Frank. 2007. "Employing Two Different Quartz Crystal Microbalance Models To Study Changes in Viscoelastic Behavior upon Transformation of Lipid Vesicles to a Bilayer on a Gold Surface". Anal. Chem. V. 79. pp. 7027-7035.

Choi D., Yoon Ki-Chan. 2001. "A design method of an automotive wheel-bearing unit with discrete design variables using genetic algorithms". Journal of tribology vol. 123, no1, pp. 181-187

Cote G. L., R. M. Lec and M. Pishko. 2003. "Emerging biomedical sensing technologies and their applications". *IEEE Sensors Journal*. v. 3. pp.251-266.

Cynthia A. Reinhart-King, Micah Dembo, and Daniel A. Hammer. 2005. "The Dynamics and Mechanics of Endothelial Cell Spreading" Biophysical Journal V. 89 pp 676–689

Daikhin L and Michael Urbakh. 1996 "Effect of Surface Film Structure on the Quartz Crystal Microbalance Response in Liquids". Langmuir, 12, 6354-6360

Davies PF, Robotewskyj A, Griem ML. 1993. "Endothelial cell adhesion in real time. Measurements in vitro by tandem scanning confocal image analysis". J Clin Invest v. 91 pp. 2640–52.

Davies MC, Roberts CJ, Tendler SJB, Williams PM, 1997. "The surface analysis of polymeric biomaterials". In: Braybrook J, editor. Biocompatibility: assessment of materials and devices for medical applications. Chichester: Wiley. p. 65-100.

Dewar R J., Dean C. Ash, Matthew J. German, Malcolm J. Joyce. 2006. "Practical considerations of the QCM as a viscometer within the food industry: Performance deterioration with repeated use and surface roughness". Journal of Food Engineering. V.75 pp. 461–468

Dong Y. and Curtis Shannon. 2000. "Heterogeneous Immunosensing Using Antigen and Antibody Monolayers on Gold Surfaces with Electrochemical and Scanning Probe Detection" Anal. Chem., 2000, 72 (11), pp 2371–2376

Du B., Ilchat Goubaidoulline, and Diethelm Johannsmann. 2004 "Effects of Laterally Heterogeneous Slip on the Resonance Properties of Quartz Crystals Immersed in Liquids". Langmuir. V. 20 pp. 10617-10624

Dylkov M.S., Sanzharovskii A.T., Zubov P.I. 1966. “The effect of thickness on the strength of polymer films”. Mekhanika Polimerov. 2. 940-942

Edvardsson M, Michael Rodahl, Bengt Kasemo, and Fredrik Ho1o1k. 2005. “A Dual-Frequency QCM-D Setup Operating at Elevated Oscillation Amplitudes”. Anal. Chem. V. 77. pp. 4918-4926.

E. Ergezen, M. Appel, P. Shah, J.Y. Kresh R.M. Lec and D.M. Wootton, 2007 “Real-time monitoring of adhesion and aggregation of platelets using thickness shear mode (TSM) sensor” Biosensors and Bioelectronics .V. 23, Issue 4, Pages 575-582

Ergezen E., Hart R. W., Philip R., Lec, R. M.; 2008 "A high frequency thickness shear mode (TSM) sensor for detection of biomarkers for prostate cancer." Proceedings of IEEE International Frequency Control Symposium, 19-21 May 2008 Page(s):341 - 345

E Ergezen, S Hong, K A Barbee, R Lec. 2007. “Real time monitoring of the effects of Heparan Sulfate Proteoglycan (HSPG) and surface charge on the cell adhesion process using thickness shear mode (TSM) sensor”. v. 22 pp. 2256-60

Elliott, J.T., Tona, A., Woodward, J., Jones, P., Plant, A., 2003a “Thin films of collagen affect smooth muscle cell morphology”. Langmuir. V. 19, pp. 1506–1514.

Elliott J T., John T. Woodward, Kurt J. Langenbach, Alex Tona, Peter L. Jones, Anne L. Plant. 2005 “Vascular smooth muscle cell response on thin films of collagen”. Matrix Biology. V. 24, pp.489 – 502

Evans C.R., G. McHale, N.J. Shirtcliffe, S.M. Stanley, M.I. Newton. 2005. “The effect of SU-8 patterned surfaces on the response of the quartz crystal microbalance” Sensors and Actuators A. v.123–124, pp. 73–76

Fan W., Edward A. Fox. 2004 “The Effects of Fitness Functions on Genetic Programming-Based Ranking Discovery For WebSearch” Journal of the American Society for Information Science and Technology” V55 , pp. 628 - 636

Féréol S., R. Fodil, V.M. Laurent, E. Planus, B. Louis, G. Pelle, D. Isabey. 2008. “ Mechanical and structural assessment of cortical and deep cytoskeleton reveals substrate-dependent alveolar macrophage remodeling” Bio-Medical Materials and Engineering. Volume 18, Pages105-118

Francois M. 2008 “Development of an Acousto-Electric Biochemical Sensor (AEBS) For Monitoring Biological and Chemical Processes”, Drexel University

Fredriksson, C., S. Kihlman, M. Rodahl, and B. Kasemo. 1998. “The piezoelectric quartz Crystal mass and dissipation sensor: a means of studying cell adhesion”. *Langmuir,* v.14, pp.248-251.

Galipeau D.W., Vetelino J.V., Lec R. M. and Freger C.1991. “The Study of Polyimide Film properties and Adhesion Using a Surface Acoustic Wave Sensors", ANTEC ’91, *Conference Proceedings, Society of Plastic Engineers and Plastic Engineering*, Montreal, pp. 1679-1984

Garaia G, B.B. Chaudhurib. 2007. ‘Adistributed hierarchical genetic algorithm for efficient optimization and pattern matching’ Pattern Recognition. V. 40. pp. 212 – 228

Garcia AJ, Ducheyne P, Boettiger D. 1997 “Quantification of cell adhesion using a spinning disc device and application to surface-reactive materials”. Biomaterials. V.18 pp. 1091–8.

Giebel, K., Bechinger, C., Herminghaus, S., Riedel, M., Leiderer, P., Weiland, U., Bastmeyer, M., 1999. Biophys. J. 76, 509–516.

Godefroid P. and Sarfraz Khurshid. 2002 “Exploring Very Large State Spaces Using Genetic Algorithms”. TACAS 2002, LNCS 2280, pp. 266–280.

Gollas B, Joanne M. Elliott and Philip N. Bartlett. 2000. “Electrodeposition and properties of nanostructured platinum films studied by quartz crystal impedance measurements at 10 MHz” Electrochimica Acta Volume 45, Issues 22-23, Pages 3711-3724

Granstaff V.D. and Stephen J. Martin J.. 1994. “Characterization of a thickness-shear mode quartz resonator with multiple nonpiezoelectric layers”. Appl. Phys. 75 (3), pp. 1

Grant et al., 2001. Layer by layer assembly of collagen Thin Films: Controlled Thickness and Biocompatibility”. Biomedical Microdevices, v.3, pp. 301-306

Greczyło T. and Ewa Debowska. 2005 “Finding viscosity of liquids from Brownian motion at students’ laboratory” Eur. J. Phys. V. 26 827–833

Greisler H.P., S. Johnson, K. Joyce, S. Henderson, N.M. Patel and T. Alkhamis, 1990. “The effects of shear stress on endothelial cell retention and function on expanded polytetrafluoroethylene”. *Arch. Surg*. v. 125, pp. 1622–1625.

Gryte DM, Ward MD, Hu WS. Real-time measurement of anchorage-dependent cell adhesion using a quartz crystal microbalance. Biotechnol Prog 1993;9(1):105–8.

Han W. and S.M. Lindsay, "Probing molecular ordering at a liquid-solid interface with a magnetically oscillated atomic force microscope," Applied Physics Letters, vol. 72, pp. 1656-165

Harmanjatinder S. Sekhon, Jennifer A. Keller, Neal L. Benowitz and Eliot R. Spindel. 2001 “Prenatal Nicotine Exposure Alters Pulmonary Function in Newborn Rhesus Monkeys” American Journal of Respiratory and Critical Care Medicine. V. 164

Hook F., Larsson C., Fant C., 2002. “Biofunctional Surfaces Studied by Quartz Crystal Microbalance with Dissipation Monitoring”. Encyclopedia of Surface and Colloid Science. 774-790.

Hong S., Ertan Ergezen, Ryszard Lec, Kenneth A. Barbee. 2006 “Real-time analysis of cell–surface adhesive interactions using thickness shear mode resonator”. *Biomaterials.* V.27 pp. 5813–5820

S Hong, E Ergezen, K Barbee, R Lec. 2005 “BAEC adhesion analysis using Thickness Shear Mode sensor.” Annual International Conference of the IEEE Engineering in Medicine and Biology Society. IEEE Engineering in Medicine and Biology Society. Conference. pp:1047-1050

Hovgaard M B, Mingdong Dong, Daniel Erik Otzen, and Flemming Besenbacher. 2007. “Quartz Crystal Microbalance Studies of Multilayer Glucagon Fibrillation at the Solid-Liquid Interface” Biophysical Journal. v. 93. pp. 2162-2169

Hubbell, J.A., and R. Langer. 1995. “Tissue engineering”. *Chem. Eng*. News, pp. 42-54.

Hulmes D J S, Miller A, White S and Doyle B B J 1977. J. Molec. Biol. V.110 pp. 643

Janshoff A, Wegener J, Sieber M, Galla HJ. Double-mode impedance analysis of epithelial cell monolayers cultured on shear wave resonators. Eur Biophys J 1996;25(2):93–103.

Jiang L, Jeanne Hossenlopp, Richard Cernosek, and Fabien Josse. 2003. “Characterization of Epoxy Resin SU-8 Film Using Thickness-Shear Mode (TSM) Resonator”. Proceedings of the 2003 IEEE International Frequency Control Symposium and PDA Exhibition. Issue 4-8, pp.986 – 992

Johannsmann D., Ilya Reviakine, Elena Rojas, and Marta Gallego. 2008. “Effect of Sample Heterogeneity on the Interpretation of QCM(-D) Data: Comparison of Combined Quartz Crystal Microbalance/Atomic Force Microscopy Measurements with Finite Element Method Modeling”. Anal. Chem. V. 80. pp. 8891-8899.

Johne B. 2008 “Epitope Mapping by Surface Plasmon Resonance in the BIAcore” Methods in Molecular Biology. V.66 pp. 1940-6029

Kaba M., H-W. Li, A.S. Daryoush, J-P. Vilcot, D. Decoster, J. Chazelas, G. Bouwmans, Y. Quiquempois, and F. Deborgies, 2006 “Improving Thermal Stability of Opto-Electronic Oscillators”, IEEE Microwave Magazine, August 2006, pp. 38-47.

Kanazawa K. and Nam-Joon Cho. 2009. “Quartz Crystal Microbalance as a Sensor to Characterize Macromolecular Assembly Dynamics”. Journal of Sensors. doi:10.1155/2009/824947

Katz A. and Ward M. D. 1996. “Probing solvent dynamics in concentrated polymer films with a high frequency shear mode quartz resonator. J. Applied Physics. V. 80. pp. 4153

Klinth et al, 2006. “A novel application of multi-wavelength TIRF spectroscopy for real time monitoring of antithrombin interactions with immobilized heparin”. Biosensors and Bioelectronics v. 21, pp. 1973-1980.

Kim J. R. and M. Gen, "Genetic algorithm for solving bicriteria network topology designproblem," Evolutionary Computation, 1999.CEC 99.Proceedings of the 1999 Congress on, vol. 3, 1999.

Kino S. G., 1987. “Acoustic waves; devices, imaging, analog and signal processing”. Prentice-hall signal processing series. pp.30

Kopecki Z, Adams D & Cowin AJ. 2008. “c-myb proto-oncogene is up-regulated in hypertrophic scars and correlates with increased collagen I” Wound Practice and Research. Vol. 16. No. 3

Krebs P. W. 1995. “Genetic algorithms in molecular recognition and design”. Trens in Biotechnology. V.13. pp. 516-521

Kunze M., Kenneth R. Shull, and Diethelm Johannsmann. 2006. “Quartz Crystal Microbalance Studies of the Contact between Soft, Viscoelastic Solids”. Langmuir. V. 22. pp. 169-173

Kylie A. Hotchkiss, Lisa J. Matthias, Philip J. Hogg. 1998 “Exposure of the cryptic Arg-Gly-Asp sequence in thrombospondin-1 by protein disul¢de isomerase” Biochimica et Biophysica Acta 1388 478-488

Kwon Y.D, Soon-Bum Kwon, Seung-Bo Jin, Jae-Yong Kim. 2003. “Convergence enhanced genetic algorithm with successive zooming method for solving continuous optimization problems”. Computers and Structures v. 81 pp. 1715–1725

Kwoun S.., R. M. Lec, Cairncross R. A., Shah P., Brinker C. J. 2006. “Characterization of Superhydrophobic Materials Using Multiresonance Acoustic Shear Wave Sensors”. *IEEE Transactions on Ultrasonics Ferroelectrics and Frequency Control*. v.53. pp.1400- 1403

Langevin M.H, Donna M Rizzo, James R Fox, Gary J Badger, Junru Wu, Elisa E Konofagou, Debbie Stevens-Tuttle, Nicole A Bouffard, and Martin H Krag. 2007 “Dynamic morphometric characterization of local connective tissue network structure in humans using ultrasound” BMC Systems Biology. V. 1 pp. 25

Lee A, M. Ahmadi, G. Jullien, W. Miller and R. Lashkari, "Digital filter design using genetic algorithm," Advances in Digital Filtering and Signal Processing, 1998 IEEE Symposium on, pp. 34-38,

Lee D, Kyungsook Han. 2002. “Prediction of RNA Pseudoknots Comparative Study of Genetic Algorithms’. Genome Informatics. V. 13. pp. 414-415

Li F., James H.-C. Wang, Qing-Ming Wang. 2007. “Monitoring cell adhesion by using thickness shear mode acoustic wave sensors”. *Biosensors and Bioelectronics*, v. 23, pp. 42–50

Li J, Thielemann C, Reuning U, Johannsmann D. 2004 “Monitoring of integrin-mediated adhesion of human ovarian cancer cells to model protein surfaces by quartz crystal

resonators: evaluation in the impedance analysis mode". Biosens Bioelectron. V. 20 pp.1333–7.

Liao W., Wei F., Qian X. M., Zhao S. X. 2004. "Characterization of protein immobilization on alkyl monolayer modified silicaon (111) surface". Sensors and Actuators B. 101. 361-367

Lin Z, Christopher M. Yip, I. Scott Joseph, Michael D. Ward. 1993. "Operation of an ultrasensitive 30-MHz quartz crystal microbalance in liquids". Anal. Chem., 1993, 65 (11), pp 1546–1551

Lin Z., Yip M. C., Joseph S. I., Ward D. M. 1993. "Operation of an ultrasensitive 30 MHz quartz crystal microbalance in liquids". Anal. Chem. V. 65. pp.1546-1551.

Liou A, Tzong-Heng Chi, I-Jun Yu. 2007 "Improving Genetic Algorithms with Solution Space Partitioning and Evolution Refinements" Third International Conference on Natural Computation (ICNC 2007)

Liu Y., Xiao Yu, Rui Zhao, Di-Hua Shangguan, Zuyi Bo, Guoquan Liu. 2003." Quartz crystal biosensor for real-time monitoring of molecular recognition between protein and small molecular medicinal agents". Biosensors and Bioelectronics. V 19, Pp 9-19

Liu M., Sun J., Bock C., Chen Q. 2009. "Thickness dependent mechanical properties of Polydimethylsiloxane". J. Micromech. Microeng. 19. 1-4

Lucklum R. and Hauptman P. 1997. "Determination of polymer shear modulus with quartz crystal resonators". *Faraday Discuss*. v. 107. pp.123-140.

Lucklum R. and P. Hauptman. 2000 "The Df-DR QCM technique: an approach to an advanced sensor signal interpretation," Electrochimica Acta, vol. 45, pp. 3907.

Lucklum R., Peter Hauptmann. 2000. "The quartz crystal microbalance: mass sensitivity, viscoelasticity and acoustic amplification". Sensors and Actuators B 70 _2000. 30–36

Lucklum R., C. Behling, and P. Hauptmann. 1999. "Signal amplification with multilayer arrangements on chemical quartz crystal resonator sensors'. 1999 Joint Meeting EFTF - IEEE IFCS

Luo C., Schneider T., White R., Currie J., Paranjape M. 2003 A simple deflection testing method to determine Poission's ratio for MEMs applications. J. Micromech. Microeng. 13. 129-133

Macakova L., Eva Blomberg, and Per M. Claesson. 2007 "Effect of Adsorbed Layer Surface Roughness on the QCM-D Response: Focus on Trapped Water" Langmuir., v.23, pp. 12436-12444

Maeda M., Shunsuke Tani, Akihiko Sano, Keiji Fujioka. 1999. "Microstructure and release characteristics of the minipellet, a collagen-based drug delivery system for controlled release of protein drugs'. Journal of Controlled Release 62 (1999) 313–324

Martin S., Gregory C. Frye, and Antonio J. Ricco. 1995. “Effect of Surface Roughness on the Response of Thickness-Shear Mode Resonators in Liquids” Anal. Chem. pp. 2910-2922

Martin S.J and G.C. Frye, 1991 "Polymer film characterization using quartz resonators," IEEE Ultrasonics Symposium, pp. 393-398,

Martin, S. J.; Frye, G. C.; Senturia, S. D. 1994 “Dynamics and Response of Polymer-Coated Surface Acoustic Wave Devices: Effect of Viscoelastic Properties and Film Resonance” Anal. Chem. V.66, pp. 2201-2219.

Martin S.J, Helen L. Bandey, and Richard W. Cernosek. 2000. “Equivalent-Circuit Model for the Thickness-Shear Mode Resonator with a Viscoelastic Film Near Film Resonance’. Anal. Chem., v. 72 pp 141–149

Martin B., Harold Hager. 1989. “Flow profile above a quartz crystal vibrating in liquid”. J Appl. Phys. V. 65 (7)

Mathur et al, 2000. “Atomic Force and Total Internal Reflection Fluorescence Microscopy for the Study of Force Transmission in Endothelial Cells”. Biophysical Journal, v. 78, p. 1725-1735.

Matthew P. Goertz, J. E. Houston, and X.-Y. Zhu. 2007 “Hydrophilicity and the Viscosity of Interfacial Water. Langmuir. V. 23. pp. 5491–5497

Marx KA, Zhou T, Montrone A, Shultze H, Braunhut SJ. A quartz crystal microbalance cell biosensor: detection of microtubule alterations in living cells at nM nocodazole concentrations. Biosens Bioelectron 2001;16:773–82.

Merve PA and Barclay AN, 1996. “Analysis of cell adhesion molecule interactions using surface plasmon resonance”. Curr. Opinion Immunol. v.8, pp. 257-262

McHale G., M. I. Newton, M. K. Banerjee and J. A. Cowen. 2000. “Acoustic wave–liquid interactions”. Material Science and Engineering: C. V.12, pp. 17-22

Milani G., F. Milani. 2007. “Genetic Algorithm for the Determination of Binodal Curves in Ternary Systems Polymer–Liquid(1)–Liquid(2) and Polymer(1)–Polymer(2)–Solvent” J Comput Chem. V. 28. pp. 2203–2215

Min Lo et al, 2000. “Cell Movement Is Guided by the Rigidity of the Substrate”. Biophysical Journal. v. 79, pp. 144-152.

Morray Boima, Suiqiong Li, Jeanne Hossenlopp, Richard Cernosek, and Fabien Josse. 2002 “PMMA Polymer film characterization using thickness-shear mode quartz resonator’. IEEE International Frequency Control Symposium and PDA Exhibition. pp.294-300

Munson B.R., D.F. Young and T.H. Okiishi, 1998 “Fundamentals of fluid mechanics”, New York: John Wiley, pp. 877.

Myhra, 2004. “A review of enabling technologies based on scanning probe microscopy relevant to bioanalysis”. Biosensors and Bioelectronics, v.19, pp. 1345-1354

Nair et al, 2005. “Preliminary study of viscoelastic bulk properties for cell-substrate interaction in scaffold guided tissue engineering”. Proceedings of the IEEE 31st Annual Northeast Bioengineering Conference. pp. 184 – 186

Ndiritu J. G., T. M. Daniell. 2001. ‘An Improved Genetic Algorithm for Rainfall-Runoff Model Calibration and Function Optimization” Mathematical and Computer Modeling. V.33 pp. 696-706

Neyfakh Jr. AA, Tint IS, Svitkina TM, Bershadsky AD, Gelfand VI. Visualization of cellular focal contacts using a monoclonal antibody to 80kD serum protein adsorbed on the substratum. Exp Cell Res1983;149(2):387–96.

Newton M. I., Evans, C.R Simons, Hughes DC. 2007. “Semen quality detection using time of flight and acoustic wave sensors”. Applied Physics Letters. v. 90 (15) 154103

Nunalee F. Nelson, Kenneth R. Shull, Bruce P. Lee, Phillip B. Messersmith. 2006. “Quartz Crystal Microbalance Studies of Polymer Gels and Solutions in Liquid Environments”. Anal. Chem. V. 78. pp. 1158-1166.

Pardo Loreto Rodríguez-, José Fariña Rodríguez, Claude Gabrielli, Hubert Perrot, and Remi Brendel. 1995 “Sensitivity, Noise, and Resolution in QCM Sensors in Liquid Media”. IEEE SENSORS JOURNAL, V. 5, N. 6, pp.1251

Paulinas M., Andrius Ušinskas. 2007. “A Survey of genetic algorithms applications for image enhancement and segmentation”. Information technology and control.
V. 36, No.3

Povinelli R. and Xin Feng. 1999 “Improving genetic algorithms with hashing fitness values” Proc. Artificial Neural Networks in Eng. Conf., pp. 399-404

Raines, E.W., Koyama, H., Carragher, N.O., 2000. ‘The extracellular matrix dynamically regulates smooth muscle cell responsiveness to PDGF’. Ann. N. Y. Acad. Sci. 902, 39– 51

Raum et al, 2003. “Multilayer Analysis: Quantitative Scanning Acoustic Microscopy for Tissue Characterization at a Microscopic Scale”. IEEE Transductions on Ultrasonics, Ferroelectronics, and Frequency Control, v. 50, pp. 507-515.

Redepenning J, Schlesinger TK, Mechalke EJ, Puleo DA, Bizios R. Osteoblast attachment monitored with a quartz crystal microbalance. Anal Chem 1993;65(23):3378–81.

Roach, P; McHale, G; Evans, CR, Shirtcliffe NJ, Newton MI. 2007. “Decoupling of the liquid response of a superhydrophobic quartz crystal microbalance”. *Langmuir*, v.23, pp.9823-9830

Rosenbaum J.F. 1998. “Bulk acoustic Wave Theory and Devices”. Boston, MA: Artech House Publishers

Rosenson RS, A McCormick and EF Uretz. “Distribution of blood viscosity values and biochemical correlates in healthy adults” Clinical Chemistry, V. 42, pp. 1189-1195,

Saluja A., Kalonia S. D. 2005. “Application of Ultrasonic Shear Rheometer to Characterize Rheological Properties of High Protein Concentration Solutions at Microliter Volume”. Journal of Pharmoceutical Sciences. V. 94. pp. 1161-1168

Sapper A., Wegener J., Janshoff A., 2006. “Cell Motility Probed by Noise Analysis of Thickness Shear Mode Resonators”. Anal. Chem. v.78, pp.5184-5191.

Schulz et al, 2004. “Spectroscopic ellipsometry on biological materials – investigation of hydration dynamics and structural properties”. Thin Solid Films, v. 455, pp. 731.

Schwartz et al., 2003. “Development and Use of Fluorescent Protein Markers in Living Cells”. Science, v.300, pp. 87-91.

Silke J D, Dannöhl Wolfgang, J. Parak, Otto Müller ,Wilhelm K. Aicher and Manfred Radmacher. 2000. “Colloids Substrate dependent differences in morphology and elasticity of living osteoblasts investigated by atomic force microscopy” Surfaces B: Biointerfaces Volume 19, Issue 4, Pages 367-379

Sendner C , Dominik Horine, Lyderic Bocquet, and Roland R. Netz. 2009. “Interfacial Water at Hydrophobic and Hydrophilic Surfaces: Slip, Viscosity, and Diffusion”. Langmuir, v.25 pp. 10768–10781

Shire S J., Zahra Shahrokh, Jun Liu. 2004. “Challenges in the development of high protein concentration formulations” Journal of Pharmaceutical Sciences. Volume 93 Issue 6, Pages 1390 - 1402

Sivanandam S. N. and Deepa S. N. 2008. Introduction to Genetic Algorithms. Springer Berlin Heidelberg. New York. 34-35

Sorial J. 2000. “A piezoelectric interfacial phenomena biosensor” masters thesis. Drexel University

Stathakis D. and I. Kanellopoulos. 2008. “Global Optimization versus Deterministic Pruning for the Classification of Remotely Sensed Imagery”. Photogrammetric Engineering & Remote Sensing. Vol. 74, pp. 1259–1265.

Striebel C., A. Brecht and G. Gauglitz, 1994. “Characterization of biomembranes by spectral ellipsometry, surface plasmon resonance and interferometry with regard to biosensor application”, Biosens. Bioelectron. v. 9, pp. 139–146.

Su H and Thompson M. 1996. “Rheological and interfacial properties of nucleic acid films studied by thickness – shear mode sensor and network analysis”. Can. J. Chem., v.74, pp.344-358

Szabad, Z.; Sangolola, B.; McAvoy. 2000. “Genetic optimisation of manipulation forces for co-operating robots”, Systems, Man, and Cybernetics, 2000 IEEE International Conference on. V. 5, pp. :3336 - 3341

Thaler D- BJ, Giannone G, Dobereiner HG, Sheetz MP. 2004 “Nanometer analysis of cell spreading on matrix-coated surfaces reveals two distinct cell states and STEPs”. Biophys J 86(3):1794–806.

Tsutsui S, Yoshiji Fujimoto, Ashish Ghosh. “Forking GAs: GAs with Search Space Division Schemes” Evolutionary Computation, MIT Press, Vol. 5, pp. 61-80

Unger R. and J. Moult, "Genetic algorithms for protein folding simulations," J. Mol. Biol., vol. 231, pp. 75-81, May 5. 1993.

Urbakh M and Leonid Daikhin. 2007. “Surface morphology and the quartz crystal microbalance response in liquids”. Colloids and Surfaces A. Physicochemical and Engineering Aspects. V. 134. pp.75-84

Vives A A., Antonio Arnau. ‘Piezoelectric transducers and applications’. pp 92 Springer 2004

Voinova M.V., M. Jonson and B. Kasemo. 2002. “Missing mass effect in biosensors QCM applications”. Biosensors & Bioelectronics. V. 17, pp. 835-841

Voros J. 2004. “The Density and Refractive Index of Adsorbing Protein Layers”. Biophysical Journal. 87. 553-561

Yang N., Kenneth Kar HoWong, John R de Bruyn and Jeffrey L Hutter. 2009 “Frequency-dependent viscoelasticity measurement by atomic force microscopy” Meas. Sci. Technol. V. 20. 025703 (9pp)

Yang D., Huang C., Lin Y., Tsaid D., Kao L., Chi C. Lin C., 2003 “Tracking of secretory vesicles of PC12 cells by total internal reflection fluorescence microscopy”. Journal of Microscopy, v. 209, pp. 223-227

Yang et al., 1993. “Interfacial Properties and the Response of the Thickness-Shear-Mode Acoustic Wave Sensor in Liquids”. Langmuir, v. 9, pp. 802-811.

Ying P, Gang Jin and Zulai Tao. 2004. “Competitive adsorption of collagen and bovine serum albumin—effect of the surface wettability”. Colloids and Surfaces B: Biointerfaces Volume 33, Issues 3-4, 15 February 2004, Pages 259-263

Wang S and Atam P. Dhawan. 2008. “Shape-based multi-spectral optical image reconstruction through genetic algorithm based optimization”. Computerized Medical Imaging and Graphics. V. 32, pp. 429-441

Wegener, J., Seebach, J., Janshoff, A., Galla, H.-J., 2000. Biophys. J. 78, 2821–2833.

Wegener J, Janshoff A, Galla HJ. 1998. Cell adhesion monitoring using a quartz crystal microbalance: comparative analysis of different mammalian cell lines. Eur Biophys J v. 28 pp. 26–37.

Wendt S, Gernot A. Fink, Franz Kummert. 2002. “Dynamic Search space pruning for time constrained speech recognition”. In International Conference on Spoken Language Processing, v. 1, pp. 377-380

Westphal S. and Bornmann A. 2002. “Bimolecular detection by surface plasmon enhanced Ellipsometry”. Sensors and Actuators B. 84. 278-282

Wong et al, 2004. “Balance of chemistry, topography, and mechanics at the cell–biomaterial interface: Issues and challenges for assessing the role of substrate mechanics on cell response”. Surface Science, v.570, pp. 119-133.

Wood R. L. 2006. Proceedings of the Institution of Mechanical Engineers. Part B. Journal of engineering manufacture. vol. 220, pp. 715-728

Zhang Q. 2006 “Characterization of the interfacial interactions between microparticles and surfaces using piezoelectric sensors” PhD Dissertation. Drexel University.

Zhuang H, Pin Lu, Siak Piang Lim, and Heow Pueh Lee. 2008. “Effects of Interface Slip and Viscoelasticity on the Dynamic Response of Droplet Quartz Crystal Microbalances”. Anal. Chem. V. 80. pp. 7347-7353

Ziblat et al., 2006. “Infrared Surface Plasmon Resonance: A Novel Tool for Real Time Sensing of Variations in Living Cells”. Biophysical Journal, v. 90, pp. 2592-2599

Zimmermann B, Ralf Lucklum, Peter Hauptmann, Jens Rabe and Stephanus Büttgenbach. 2001 “Electrical characterisation of high-frequency thickness-shear-mode resonators by impedance analysis”Sensors and Actuators B: Chemical. V. 76, Issues 1-3, 1 Pp 47-57

Appendix 1. Genetic Algorithms

A1.1 Genetic Algorithms

A1.1.1 Basic definitions of terms

A solution to the problem is called an individual; the total number of solution is called population. Each individual has a number of chromosomes that represent each parameter of the problem, e.g. the following is simple system that can be modeled using genetic algorithm.

$y(t+1) = y*a+b*y*x+c*x$

$x(t+1) = x*d+a*x*y+f*y$

In this case a, b, c, d and e are each represented by an individual's chromosome (i.e. the individual will have six chromosomes). Each chromosomes contains a fixed number of genes, the number of genes per chromosome determine the resolution of the total solution. In a genetic algorithm the solution is codified as a binary number, this occurs in most of the cases however there are algorithms that work with floating point numbers. However, the binary number codification simplifies the algorithm understanding. It is not the scope of this evolution application to deal with floating point genetic algorithms and it will not be mentioned. The bitstring codification of the genetic algorithm is known as the genotype and using a conversion function the genotype can be transformed into phenotype which is the physical expression of the individual itself.

An individual representing a solution to the problem above would have six chromosomes with a certain number of genes. As mentioned above the number of genes per chromosome is mostly determined by the broadness of the range in which each chromosome lies. If a is been looked between $a1 < a < a2$ and $\Delta a = a1-a2$ is relatively small (narrow range) and the required resolution is not that high a small number of genes can be selected. Since the

solution is coded in a binary form the total number of solution is a power of two (8 genes per chromosome yield 256 different solutions). When the number of genes is chosen big the solution has more resolution, however the computation time increases exponentially.

Every individual has to be weighed according to its *fitness*. The individual fitness value determines its survival and breeding probability. A higher fitness individual has higher probability of survival. An individual will have low fitness function in case it fails to act when it encounters an obstacle, e.g. it fails to escape from a predator. However, it is important to underline that no matter how low is the fitness every individual has a probability to survive from one generation to the other and to generate offspring.

Sometimes the fitness function is one of the algorithm biggest constraints. In many real world examples the solution is not trivial and to some extent fitness evaluation becomes so complicated that the use of computational approximations techniques is required. Hence, computation time increases since it is required a large number of fitness evaluations in order to find a satisfactory solution.

The population represents all the solutions for the problem. The size of the population is the number of individuals. Ideally, having a large population would help finding a better solution however in reality the population can be increase up to certain extent. The computational cost of a genetic algorithm is relatively high. Therefore a large number of individuals increase the time it takes the algorithm to find a solution.

Number of Generations

The generation value keeps track of the number of times the algorithm is executed. The GA programmer can establish beforehand the maximum number of generations the algorithm has to run before breaking the loop and showing a solution. Basically, the Generation value represents the total number of iterations it were needed to estimate the best solution for a given problem.

Population Initialization

The population represents the whole set of solutions. The algorithm starts with a population generated using a random number generator to generate a zeros and ones matrix. In the population each row is a vector that represents a particular individual or a solution for the modeled problem. The size of the population is a very important factor for the correct functioning of the algorithm. When the population size is too big (>100) the algorithm becomes very slow, however it is more likely that it will need a smaller number of generations since a bigger solution space exits. A typical size of a population is around one hundred individuals.

Each individual is modeled as a sequence of bits (or bitstring). The length of the sequence varies according to the number of chromosomes or parameters the algorithm is searching and the numbers of genes per chromosome. For example, for an individual with six chromosomes and 5 genes per chromosomes the length of the vector would be 30 and for a population of 100 individuals it would be necessary to create a matrix of 30 columns by 100 rows. It is possible to show the power of a genetic algorithm used to search for a solution that represents six parameters (chromosomes) and each chromosome contains five genes (bits). There is going to be a total of 32 possible different values for each parameter. Now since the solutions comprise six different parameters with 32 different values.

The total number of possible solutions will be $32^6 = 1{,}073{,}741{,}824$, therefore to find the optimal solution it is necessary to evaluate all these solutions one by one. A typically implemented genetic algorithm with a population size of one hundred takes approximately between one and two hundred generations to find the fittest (optimal) solution, this is for two hundred generations it is necessary to evaluate only 20,000 solutions. The later number is several orders of magnitude smaller than the needed to find the solutions one by one.

Generally, the number of genes per chromosome is at least twelve, therefore, the computation cost is several orders of magnitude smaller when a genetic algorithm is implemented.

A1.1.2. Population Evaluation

The population is evaluated by the fitness function. The fitness function is defined by the programmer and it contains the objectives of a given population. The fitness function must reflect the relevant measures to be optimized. This function evaluates the function being searched for the set of parameters of each member of the population. The output of the fitness function is a vector that contains the fitness for each member of the population. This vector helps in the selection of individual for generating new offspring or individuals that will be included in the new generated population.

The fitness function is unique to each genetic algorithm implementation. This is the part of the algorithm that requires the most knowledge about the problem the user wants to model. In many occasions the fitness function becomes so complicated that an approximation of it is necessary in order to evaluate a certain population. By only changing the fitness function an implemented genetic algorithm can solve a completely different model.

A1.1.3 *Termination Condition*

The termination condition is determined in the beginning of the algorithm by the user. Typically, there are two termination conditions, the first one is when the algorithm finds a solution with a given fitness value. The second one is when the algorithm reaches a certain number of generations. The user chooses to implement either one condition or the other, or the two conditions together. For example, the algorithm has to end when it finds a solution

with a fitness value of ten or when the total number of generation is higher than one hundred. This guarantees that the algorithm will not iterate indefinably.

A1.1.4 Selection of Individual

While the fitness function evaluates whether a solution is good or bad, selection mechanisms underline better solution inside a population by taking into account the corresponding fitness value of each solution. This operator does not create a new solution. It only helps the genetic algorithm to determine which individuals will pass from one generation to the other and to select the individuals that will be reproduced, in other words the individuals that will generate new offspring.

There are several selection mechanisms that can be implemented in a genetic algorithm. The most frequent selection methods are *roulette wheel*, *tournament selection* and *ranking selection*. The following paragraphs describe the basics of each of these selection mechanisms.

- *Roulette wheel*

This mechanism assigns an individual a portion of the roulette wheel which is proportionate to the solution fitness. Thus, an individual with twice the fitness doubles the chances of being selected. A limitation of this method takes place when a solution fitness is much higher than the rest of the solutions (supersolution), this is, the supersolution will occupy most of the wheel area and the probability of this solution to be selected will be extremely high, therefore the algorithm might converge to this solution even if this solution is not the optimum one.

Another problem associated with roulette wheel mechanism is when most of the population members have more or less the same fitness. In this case, the roulette wheel is

distributed equally among all the solutions and every solution is equally likely to be selected. These two problems can be avoided by scaling the roulette wheel between a maximum and a minimum fitness value. This is especially useful once the algorithm is near the convergence point.

- *Tournament Selection*

In tournament selection a group of n (when only two individuals are selected, n =2, it is called binary selection) individuals is randomly selected from the entire population. This group takes part in a tournament where the individual of the group with the highest fitness value is the winner. Hence, this individual is the one that gets selected from the population. When only two individuals are selected it is called binary selection. Tournament selection can easily implement and there is no need to sort the entire population. Even though tournament selection deterministically selects the higher fitness individual from the group, the individuals of the group are still selected at random; this is, it is possible to select a group of poor solutions (low fitness) and have a poor solution selected for the new population. It is necessary to consider the fact that sometimes two good solutions generate a low fitness offspring while two bad solutions generate a high fitness one.

- *Ranking Selection*

Ranking selection is similar to roulette wheel selection except that the solutions are ranked according to their fitness in an ascending or descending order. This is, the lowest ranking individual is ranked in the 1st place the following is in the 2nd and this continues until the nth place which corresponds to the highest ranked individual. Once all the individuals are ranked a probability distribution is generated for the population. This probability distribution can be linear or non linear. Finally, samples are drawn from the population using the probability distribution. Contrary to what would happens in the roulette

wheel mechanism in ranking selection having an individual whose fitness value would occupy ninety percent of the roulette wheel would not diminish the probability of lower individuals to be selected

In addition to the selection mechanism it is worth mention two concepts associated with selection the first one is the concept of elitism and second one is the theory of selective pressure:

• An elitist strategy assures that the best individual of a generation survives to the next generation. This ensures that the algorithm keeps the best solution until a better one is found.

• The theory of selective pressure is related to the takeover time of the selection operator. The takeover time is the speed at which the best solution in the initial population would occupy the complete population by only applying the selective mechanism. If the selection mechanism takes a large number of iterations for a determined solution to take over the entire population the selective pressure is the selection mechanism is small, and vice versa. When selective pressure is high, the population looses diversity relatively quickly. Therefore, there is a risk of premature convergence to a non desired solution. This can be avoided with a higher mutation rate or a larger population.

Now that selection mechanism have been covered it is possible to discuss the two genetic operators that produce the variations that generate a new population from the selected individuals of the previous one. These two operators are *mutations* and *crossovers*. The mechanism will be explained in the following sections.

A1.1.5 Mutation

Mutation is the best known genetic operator for producing variations in a given population. In mutation one allele of a gene is replaced by a different one. When a bitstring

representation is used for a given solution a mutation is a random change in one or more of the bits. For example: an individual with the following genotype 110011 mutates the third position therefore the resulting genotype for the individual would be 111011. A commonly rate for mutation is one mutation per individual. This is, only one bit is mutated in the entire bitstring that represents the solution. For example, if the bitstring has a length of 100 the mutation rate should be 1/100 or one percent.

Even though mutations are most of the times combined with crossover (see below), some genetic algorithm have shown that mutation without crossover can be extremely efficient for finding an optimal solution. However, the use of both operators provides added benefits. Finally, mutations can be seen as an operator that assures population diversity. In addition, mutations reduce the selective pressure of the selective mechanism.

A1.1.6 Crossover

Ideally the concept of crossover is the following: given two high fitness individuals what is intended is to create a new individual that combines the best features from each of them. Since the best features of an individual are unknown the best way to go is to recombine features at random. Crossover works in the following way: the bitstring representation of a solution of length L of each individual is divided into two or three segments. The point in which the bitstring is separated is selected at random and is denominated crossover point.

When the sequence is separated into two segments is known as single crossover, otherwise is known as multiple crossover. Once the crossover point is determined the first segment of the first individual is recombined with the second segment of the second individual, generating an offspring that contains information from both individuals. A second offspring is generated combining the second segment of the first individual with the first segment of the second. When two points crossover is selected two points are selected at

random, instead of one, and the generated segments from the two parents are swapped in order to generate offspring. In spite of the fact that multiple crossovers points can generate more than two offspring, typically only two offspring are considered for the next generation.

There are many alternatives to single and multiple point crossover methods. A frequent alternative is known as uniform crossover. Uniform crossover randomly swaps individual bits between the two parents. In this method, a mask is generated randomly. The mask is also a bitstring. The way the mask works is the following, for the first offspring the algorithm contrast the first parent with the mask bit by bit, for example if the first bit of the mask is a one the algorithm transfer the bit value of the first parent to the offspring and if it is a zero it copies the first bit of the second parent to the offspring. The second offspring is generated in the same way, however the when the first bit is a one the first bit of the second parent is transferred to the offspring.

Appendix 2. Calculation of the Quality Factor

Two methods have been utilized to calculate the quality factor. The first method was implemented by using the magnitude response of the MTSM sensor. As seen in fig. A2.1, the frequency values (f_2 and f_1) at 3dB bandwidth of magnitude response were determined. The ratio between the resonance frequency to the difference between f_2 and f_1 was defined as quality factor.

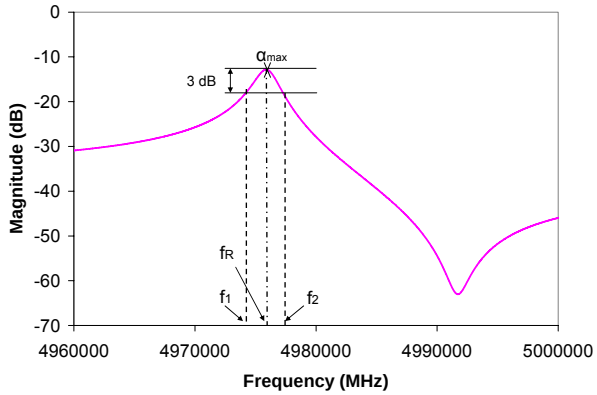

Figure A2.1 Quality factor calculation by using 3dB bandwidth in S21 response of MTSM sensor

In the second method, quality factor was determined by using the phase response of the MTSM sensor (fig. A2.2). It was suggested that another way to calculate the Q-factor is to use the phase data.

$$\left|S_{21}\right| = e^{-\frac{\omega\tau}{2Q}} \qquad \text{(A2.1)}$$

$$\left|S_{21}\right|_{dB} = 20\log_{10}\left|S_{21}\right| \qquad \text{(A2.2)}$$

Replacing $\left|S_{21}\right|$ by its value and ω by 2πf, it was obtained that;

$$Q = \frac{-27.3 f_0 \tau}{\left|S_{21}\right|_{dB}} \qquad \text{(A2.3)}$$

This equation takes into account the group delay time of the system. Group delay time is negative slope of the transmission phase angle with respect to the frequency. τ is equal to (Kaba et al., 2006);

$$\tau = -\frac{\Delta\phi}{\Delta\omega} = -\frac{1}{360^0}\frac{\Delta\phi}{\Delta f} \qquad \text{(A2.4)}$$

The two parameters ΔΦ and Δf are obtained from the graph

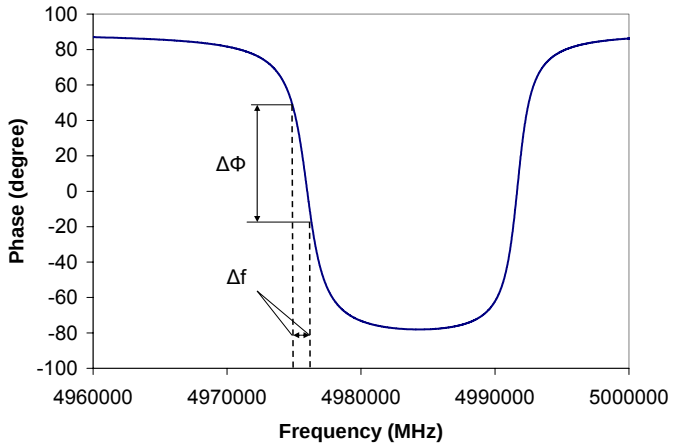

Figure A2.2. Quality factor calculation by using phase data of the MTSM sensor

Appendix.3 Acoustic shear wave in a MTSM sensor and transmission line model

Acoustic waves can be generated in a MTSM sensor utilizing the piezoelectric effect. A schematic diagram of a MTSM sensor with generated shear acoustic waves is shown in figure A3.1.

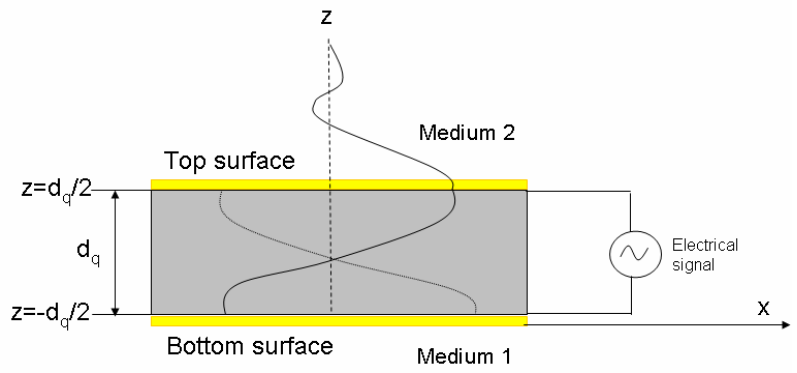

Figure A3.1 Side cross-sectional view of MTSM sensor, showing shear displacement profiles for the fundamental frequency

Two gold electrodes are normally coated on the top and bottom surfaces of the quartz plate. When an electric signal is applied between the two electrodes, acoustic waves are generated through the piezoelectric effect. The quartz plate exhibits a mechanical shear motion in x direction. To predict the behaviors of a MTSM sensor, it is essential to create the wave equations in the sensor.

A3.1 Equation of motion and constitutive equations

Quartz plate has a thickness of d_q and a cross-section area of A_q and the stress applied to the plate is T_q. For a small value of d_q, the net translational force, F_{trans}, applied to the quartz plate is (Kino, 1987)

$$F_{trans} = \frac{\partial T_q}{\partial z} d_q A_q \qquad \text{(A3.1)}$$

According to Newton's second law,

$$F_{trans} = m_q a_q = (\rho_q d_q A_q) \frac{\partial^2 u_q(z)}{\partial t^2} \qquad \text{(A3.2)}$$

where, m_q, ρ_q is mass and of the quartz plate respectively. $u_q(z)$ is the displacement of a mass point within the plate.

Velocity of the mass point is first derivation of the displacement, $v_q(z) = \frac{\partial u_q(z)}{\partial t}$, and the acceleration of the mass point is second derivation of the displacement; $a_q(z) = \frac{\partial^2 u_q(z)}{\partial t^2}$.

Then,

$$\frac{\partial T_q}{\partial z} d_q A_q = \rho_q d_q A_q \frac{\partial^2 u_q(z)}{\partial t^2} \qquad \text{(A3.3)}$$

The equation of motion of the shear acoustic wave inside the quartz plate can be given as;

$$\rho_q \frac{\partial^2 u_q(z)}{\partial t^2} = \frac{\partial T_q}{\partial z} \qquad \text{(A3.4)}$$

Relationship between strain (S) and stress (T) for an elastic media is given as;

$$T = cS = G \frac{\partial u}{\partial z} \qquad \text{(A3.5)}$$

where G is the elastic constant. When Eq. A3.5 is combined with Eq. A3.4, the wave equation of the shear wave is found as

$$\frac{\partial^2 u_q}{\partial z^2} = \frac{\rho_q \partial^2 u_q}{G_q \partial t^2} = \frac{\partial^2 u_q}{v_q^2 \partial t^2} \qquad \text{(A3.6)}$$

where, v_q is the velocity of the acoustic wave propagation in the quartz plate

$$v_q = \sqrt{\frac{G_q}{\rho_q}} \tag{A3.7}$$

By applying the partial derivative, $\partial / \partial z$, to eq. A3.4 and combining it with the equation of conversation of mass $\frac{\partial S_q}{\partial t} = \frac{\partial v_q}{\partial z}$ we may have

$$\frac{\partial}{\partial z}(\frac{\partial T_q}{\partial z}) = \frac{\partial}{\partial z}(\rho_q \frac{\partial^2 u_q(z)}{\partial t^2}) \tag{A3.8}$$

$$\frac{\partial^2 T_q}{\partial z^2} = \rho_q \frac{\partial}{\partial z}\frac{\partial v_q(z)}{\partial t} = \rho_q \frac{\partial}{\partial t}\frac{\partial v_q(z)}{\partial z} \tag{A3.9}$$

$$\frac{\partial^2 T_q}{\partial z^2} = \rho_q \frac{\partial}{\partial t}\frac{\partial S_q}{\partial t} = \rho_q \frac{\partial^2}{\partial t}\frac{S_q}{\partial t} \tag{A3.10}$$

By considering the constitutive equation Eq. A3.5, the wave equation in the form of stress, T_q, is obtained as

$$\frac{\partial^2 T_q}{\partial z^2} = \frac{\rho_q}{G_q}\frac{\partial^2 T_q}{\partial t^2} = \frac{1}{v_q^2}\frac{\partial^2 T_q}{\partial t^2} \tag{A3.11}$$

The solutions of the displacement and the stress to Eq. A3.5 and Eq. A3.8 can be easily found in the form of

$$\begin{aligned} u_q &= (u_{qF}e^{-jk_q z} + u_{qB}e^{jk_q z})e^{j\omega t} \\ T_q &= (T_{qF}e^{-jk_q z} + T_{qB}e^{jk_q z})e^{j\omega t} \end{aligned} \tag{A3.12}$$

where, u_{qF} and u_{qB} are the magnitudes of the displacement of the forward and backward propagating waves, respectively. T_{qF} and T_{qB} are the magnitudes of the stress of the forward and backward propagating waves, respectively. The wave number, k_q, is determined by

$$k_q = \frac{\omega}{v_q} = \frac{\omega}{\sqrt{\frac{G_q}{\rho_q}}} = \omega\sqrt{\frac{\rho_q}{G_q}} \tag{A3.13}$$

where, ω is the frequency of the acoustic wave and v_q is the velocity of the acoustic wave. The magnitudes of the displacement, u_{qF} and u_{qB}, in Eq. A4.9 and the magnitudes of the stress, T_{qF} and T_{qB}, in Eq. A4.10 can be determined by applying the boundary conditions of the acoustic waves inside and outside the TSM sensor.

A3.2 Boundary Conditions

There are two boundary conditions to be satisfied. One is the continuity of the transverse displacement of the acoustic wave and the other is the continuity of the shear stress.

Continuity of the transverse displacement

This requires that the transverse displacement (perpendicular to the Z axis) of the acoustic waves in the quartz plate and in the media must be equal at the two boundaries.

At the bottom boundary: $z=-d_q/2$

$$u_q\Big|_{z=-\frac{d_q}{2}} = u_{m1}\Big|_{z=-\frac{d_q}{2}} \qquad \text{(A3.14)}$$

At the top boundary: $z=d_q/2$

$$u_q\Big|_{z=\frac{d_q}{2}} = u_{m2}\Big|_{z=\frac{d_q}{2}} \qquad \text{(A3.15)}$$

where, u_q is the displacement of the acoustic wave in the quartz plate, u_{m1} and u_{m2} are the displacements of the acoustic wave in the medium 1 and medium 2, respectively.

Continuity of the shear stress

The continuity of the shear stress requires that the shear component of the stress at the two boundaries to be equal.

At the bottom boundary: $z=-d_q/2$

$$T_q\Big|_{z=-\frac{d_q}{2}} = T_{m1}\Big|_{z=-\frac{d_q}{2}} \qquad \text{(A3.16)}$$

At the top boundary: $z=d_q/2$

$$T_q\Big|_{z=\frac{d_q}{2}} = T_m\Big|_{z=\frac{d_q}{2}} \qquad \text{(A3.17)}$$

where, T_q is the stress in the quartz plate, T_{m1} and T_{m2} are the stress in the medium 1 and medium 2, respectively. By applying the boundary conditions to the solution to the wave equation in Eq. A3.12, the magnitudes of the displacement or stress can be determined.

A3.3 Derivation of transmission line model

A3.3.1 MTSM sensor as a three-port network

A MTSM sensor with a physical model described in fig. A3.1 can be considered as a three-port network with two acoustic ports and one electrical port, as shown in fig. A3.2. The forces and particle velocities at the two acoustic ports are defined as F_1, F_2 and v_1, v_2, respectively. The forces and velocities at the two surfaces of the MTSM sensor, z = -dq/2 and z = dq/2, can be defined as (Kino, 1987)

$$F_1 = -A.T_q\Big|_{z=-\frac{d_q}{2}} \qquad \text{(A3.18)}$$

$$F_2 = -A.T_q\Big|_{z=\frac{d_q}{2}} \qquad \text{(A3.19)}$$

$$v_1 = v_q\Big|_{z=-\frac{d_q}{2}} \qquad \text{(A3.20)}$$

$$v_2 = v_q\Big|_{z=\frac{d_q}{2}} \qquad \text{(A3.21)}$$

where, d_q is the thickness of the MTSM sensor and A is the area covered by the electrodes on each surface of the quartz plate.

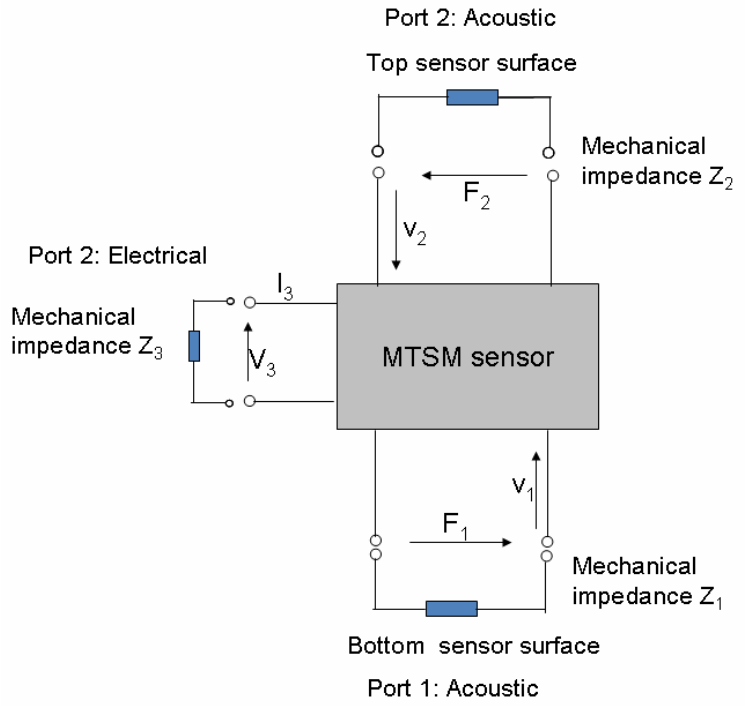

Figure A3.2. A MTSM sensor modeled as three-port model

According to Gauss's law, the current at the electrical port, I_3, is

$$I_3 = j\omega * A * D_q \tag{A3.22}$$

Therefore, the mechanical impedance at port 1 and port 2 can be defined as

$$Z_1 = -\frac{F_1}{v_1} = \frac{AT_q\Big|_{z=-\frac{dq}{2}}}{v_q\Big|_{z=-\frac{dq}{2}}} \tag{A3.23}$$

$$Z_2 = -\frac{F_2}{v_2} = \frac{A.T_q\Big|_{z=\frac{dq}{2}}}{v_q\Big|_{z=\frac{dq}{2}}} \tag{A3.24}$$

And the electrical impedance at port 3 can be defined as

$$Z_3 = -\frac{V_3}{I_3} \tag{A3.25}$$

The characteristic of the three-port network are determined by the interactions between the parameters at the three ports, such as the force and velocity at port 1 and port 2, and the current and voltage at port 3. Then, a matrix relating these parameters can represent the characteristic of the three-port network. To get this matrix, we start with the constitutive equation of piezoelectric materials has different forms that can be converted to each other, one of them is used here as

$$T = c^D.S - h.D \qquad \text{(A3.26)}$$

$$E = -h..S + \frac{1}{\varepsilon^S}.D \qquad \text{(A3.27)}$$

Where, h is the transmitting constant, $h=e/\varepsilon^S$; c^D is the elastic constant when D is zero or constant, $c^D = c^E.(1+e^2/(c^E.\varepsilon^S))=c^E.(1+K^2)$; c^E is the elastic constant when E is zero or constant; K^2 is the coupling constant, $K^2 = e^2/(c^E+\varepsilon^S)$; e is the piezoelectric stress constant; ε^S is the permittivity when S is zero or constant.

The displacement of the shear wave inside the quartz plate is given in Eq. A3.12. Similarly, the expression of the particle velocity is found as

$$v_q=(v_{qF}.e^{-jk_q z}+ v_{qF}.e^{-jk_q z}).e^{j\omega t} \qquad \text{(A3.28)}$$

When an electric flux density, D_q, is present, the form of the stress changes to

$$T_q=(T_{qF}.e^{-jk_q z}+ T_{qB}.e^{-jk_q z}-h.D_q).e^{j\omega t} \qquad \text{(A3.29)}$$

Substitute the velocity in Eq. A3.28 and the stress in Eq. A3.29 into the equation of motion as in Eq. A4.3. The magnitudes of the stress, T_{qF} and T_{qB}, can be related to those of the velocity, v_{qF} and v_{qB},

$$\frac{\partial T_q}{\partial z} = \rho_q.\frac{\partial^2 u_q(z)}{\partial t^2} = \rho_q.\frac{\partial v_q(z)}{\partial t} \qquad \text{(A3.30)}$$

$$T_{qF}.e^{-jk_q z}.(-j.k_q) + T_{qB}.e^{jk_q z}.(j.k_q) = \rho_q.(v_{qF}.e^{-jk_q z} + v_{qB}.e^{jk_q z}).j\omega \qquad \text{(A3.31)}$$

$$T_{qF} = -\frac{\rho_q.\omega}{k_q}.v_{qF} = \frac{\rho_q.\omega}{\omega/\sqrt{c_q^D/\rho_q}}.v_{qF} = -\sqrt{c_q^D.\rho_q}.v_{qF} = -Z_0.v_{qF} \quad \text{(A3.32)}$$

$$T_{qB} = -\frac{\rho_q.\omega}{k_q}.v_{qB} = \frac{\rho_q.\omega}{\omega/\sqrt{c_q^D/\rho_q}}.v_{qB} = -\sqrt{c_q^D.\rho_q}.v_{qF} = -Z_0.v_{qB} \quad \text{(A3.33)}$$

where, $Z_0 = \sqrt{c_q^D.\rho_q}$

Using the boundary conditions in Eqs. A3.20. and A3.21, the velocity in Eq. A3.28 becomes

$$v_1 = v_q\Big|_{z=-\frac{dq}{2}} = v_{qF}.e^{-jk_q(-\frac{dq}{2})} + v_{qB}.e^{jk_q(-\frac{dq}{2})} \quad \text{(A3.34)}$$

$$v_2 = v_q\Big|_{z=\frac{dq}{2}} = -v_{qF}.e^{-jk_q(\frac{dq}{2})} - v_{qB}.e^{jk_q(\frac{dq}{2})} \quad \text{(A3.35)}$$

Solve the above equations for v_{qF} and v_{qB} and obtain

$$v_{qF} = \frac{v_1.e^{jk_q\frac{d_q}{2}} + v_2.e^{-jk_q\frac{d_q}{2}}}{e^{jk_qd_q} - e^{-jk_qd_q}} = \frac{v_1.e^{jk_q\frac{d_q}{2}} + v_2.e^{-j\beta_q\frac{d_q}{2}}}{2j.\sin(k_q.d_q)} \quad \text{(A3.36)}$$

$$v_{qB} = \frac{v_1.e^{-jk_q\frac{d_q}{2}} + v_2.e^{jk_q\frac{d_q}{2}}}{e^{-jk_qd_q} - e^{jk_qd_q}} = \frac{v_1.e^{-jk_q\frac{d_q}{2}} + v_2.e^{jk_q\frac{d_q}{2}}}{-2j.\sin(k_q.d_q)} \quad \text{(A3.37)}$$

Substitute the above expressions of v_{qF} and v_{qB} into eq. A3.28 and we get the velocity of particle vibration inside the quartz plate

$$v_q = \frac{-v_1\sin\left[k_q(z-\frac{d_q}{2})\right] - v_2\sin\sin\left[k_q(z+\frac{d_q}{2})\right]}{\sin(k_q.d_q)} \quad \text{(A3.38)}$$

Next, we want to find the relations of F_1, F_2 and V_3 with v_1, v_2 and I_3. First, substitute the general form of the stress in Eq. A3.25 into the boundary condition in Eq. A3.18 and consider the relations in Eq. A3.32 and 33, Eq. A3.36 and 37 and Eq. A3.22 (Zhang, 2006)

$$
\begin{aligned}
F_1 &= -A(T_{qF}.e^{-jk_q z} + T_{qB}.e^{jk_q z} - h.D_q)\Big|_{z=-\frac{dq}{2}} \\
&= -A.[(-Z_0.v_{qF}).e^{-jk_q(-\frac{d_q}{2})} + (-Z_0.v_{qB}).e^{jk_q(-\frac{d_q}{2})} - hD_q] \\
&= -A.[(-Z_0\frac{v_1 e^{jkq\frac{dq}{2}} + v_2 e^{-jkq\frac{dq}{2}}}{2j.\sin(k_q d_q)}).e^{-jkq(-\frac{dq}{2})} + (Z_0\frac{v_1 e^{-jkq\frac{dq}{2}} + v_2 e^{jkq\frac{dq}{2}}}{-2j.\sin(k_q d_q)}).e^{-jkq(-\frac{dq}{2})} - h.D_q] \\
&= A.[Z_0.\frac{v_1.e^{jk_q t_q} + v_2}{2j\sin(k_q d_q)} + Z_0\frac{v_1.e^{-jk_q d_q} + v_2}{2j\sin(k_q d_q)} + h\frac{I_3}{j\omega A}] \\
&= -j.[A.Z_0.\cot(k_q d_q).v_1 + A.Z_0.\csc(k_q d_q).v_2 + \frac{hI_3}{\omega}]
\end{aligned}
\tag{A3.39}
$$

Second, by following the similar procedures, the expression of F_2 can be found as

$$
\begin{aligned}
F_2 &= -A(T_{qF}.e^{-jk_q z} + T_{qB}.e^{jk_q z} - h.D_q)\Big|_{z=\frac{dq}{2}} \\
&= -A.[(-Z_0.v_{qF}).e^{-jk_q(\frac{d_q}{2})} + (Z_0.v_{qB}).e^{jk_q(\frac{d_q}{2})} - hD_q] \\
&= -A.[(-Z_0\frac{v_1 e^{jk_q\frac{d_q}{2}} + v_2 e^{-jk_q\frac{d_q}{2}}}{2j.\sin(k_q d_q)}).e^{-jk_q(-\frac{d_q}{2})} + (Z_0\frac{v_1 e^{-jk_q\frac{d_q}{2}} + v_2 e^{jk_q\frac{d_q}{2}}}{-2j.\sin(k_q d_q)}).e^{jk_q(\frac{d_q}{2})} - h.D_q] \\
&= A.[Z_0.\frac{v_1 + v_2.e^{-jk_q d_q}}{2j\sin(k_q d_q)} + Z_0\frac{v_1.e^{jk_q d_q} + v_2}{2j\sin(k_q d_q)} + h\frac{I_3}{j\omega A}]
\end{aligned}
\tag{A3.40}
$$

Third, we need to find and expression of the voltage at port 3, V_3, in terms of v_1, v_2, and I_3. By extracting the electric field, E from Eq. A3.22. and using A3.29 we get

$$
\begin{aligned}
V_3 &= \int_{-\frac{dq}{2}}^{\frac{dq}{2}} E_3.dz = \int_{-\frac{dq}{2}}^{\frac{dq}{2}}(-h.S + \frac{D_q}{\varepsilon^S}).dz = \int_{-\frac{dq}{2}}^{\frac{dq}{2}}(-h\frac{T + h.D}{c^D} + \frac{D_q}{\varepsilon^S}).dz \\
&= \frac{-h}{c^D}.\int_{-\frac{dq}{2}}^{\frac{dq}{2}}(T_{qF}.e^{-jk_q z} + T_{qB}.e^{jk_q z})dz + \int_{-\frac{dq}{2}}^{\frac{dq}{2}}\frac{D_q}{\varepsilon^S}dz \\
&= \frac{-h}{c^D}.\left(\frac{T_{qF}}{-jk_q}.e^{-jk_q z}\Big|_{-dq/2}^{dq/2} + \frac{T_{qB}}{jk_q}.e^{jk_q z}\Big|_{-dq/2}^{dq/2}\right) + \frac{D_q}{\varepsilon^S}(\frac{d_q}{2} - (-\frac{d_q}{2})) \\
&= \frac{-h}{c^D}\frac{2\sin(k_q\frac{d_q}{2})}{\beta_q}(T_{qF} + T_{qB}) + \frac{d_q D_q}{\varepsilon^S}
\end{aligned}
\tag{A3.41}
$$

Then, by using the relations in Eqs. A3.32 and 33, A3.36 and 37, and A3.22, the above equations becomes

$$V_3 = \frac{-h}{c^D}\frac{2\sin(k_q\frac{d_q}{2})}{k_q}(-Z_0.v_{qF} + Z_0 v_{qB}) + \frac{d_q}{\varepsilon^S}.\frac{I_3}{j.\omega.A}$$
$$= -j\frac{h.Z_0}{c^D.k_q}(v_1 + v_2) + \frac{I_3}{j.\omega.C_0} \quad \text{(A3.42)}$$
$$= -j\frac{h}{\omega}(v_1 + v_2) + -j\frac{I_3}{\omega.C_0}$$

Combining Eqs. A3.39 and A3.40with Eq. A3.42 gives the relations

$$\begin{bmatrix} F_1 \\ F_2 \\ V_3 \end{bmatrix} = -j\begin{bmatrix} Z_q\cot(\beta_q d_q) & Z_q\csc(\beta_q d_q) & \frac{h}{\omega} \\ Z_q\csc(\beta_q d_q) & Z_q\cot(\beta_q d_q) & \frac{h}{\omega} \\ \frac{h}{\omega} & \frac{h}{\omega} & \frac{1}{\omega C_0} \end{bmatrix}\begin{bmatrix} v_1 \\ v_2 \\ I_3 \end{bmatrix} \quad \text{(A3.42)}$$

where, $C_0=\varepsilon^S.A/d_q$; $Z_q=A.Z_0 = A(c_q^D\rho_q)^{1/2}$ is the acoustic impedance of the quartz plate; $h = e/\varepsilon^S$ is the transmitting constant.

To obtain the expression of the electrical impedance, Z_3, in terms of the properties of the quartz plate and the acoustic impedance of the loadings at port 1 and port 2, we need to retrieve the relations of v_1 and v_2 with I_3 from Eq. A3.42, which can be expanded as following.

$$F_1 = -Z_1.v_1 = -j\left[Z_q\cot(k_q d_q).v_1 + Z_q\csc(k_q d_q)v_2 + \frac{h}{\omega}I_3\right] \quad \text{(A3.43)}$$

$$F_1 = -Z_2.v_2 = -j\left[Z_q\csc(k_q d_q).v_1 + Z_q\cot(k_q d_q)v_2 + \frac{h}{\omega}I_3\right] \quad \text{(A3.44)}$$

$$V_3 = Z_3.I_3 = -j\left[\frac{h}{\omega}v_1 + \frac{h}{\omega}v_2 + \frac{1}{\omega C_0}I_3\right] \quad \text{(A3.45)}$$

Then, the relation between v_1 and v_2 can be found from Eqs. A3.43 and A3.44 by eliminating I_3 from these two equations.

$$v_2 = v_1 \frac{Z_q[\cot(k_q d_q) - \csc(k_q d_q)] + jZ_1}{Z_q[\cot(k_q d_q) - \csc(k_q d_q)] + jZ_2} \tag{A3.46}$$

Next, substitute Eq. A3.46 into Eq. A3.43 to get the relation between v_1 and I_3 as

$$v_1 = \frac{\frac{h}{\omega} I_3}{-Z_q \cot(k_q d_q) - jZ_1 - Z_q \csc(k_q d_q) \frac{Z_q[\cot(k_q d_q) - \csc(k_q d_q)] + jZ_1}{Z_q[\cot(k_q d_q) - \csc(k_q d_q)] + jZ_2}} \tag{A3.47}$$

Then, substitute Eqs. A3.47 and A3.46 into Eq. A3.45 and obtain the expression of Z_3,

$$\begin{aligned} Z_3 &= \frac{V_3}{I_3} = \frac{h}{j\omega}\frac{v_1}{I_3} + \frac{h}{\omega}\frac{v_2}{I_3} + \frac{1}{j\omega C_o} \\ &= \frac{h}{j\omega}\frac{v_1}{I_3}.(1 + \frac{Z_q[\cot(k_q d_q) - \csc(k_q d_q)] + jZ_1}{Z_q[\cot(k_q d_q) - \csc(k_q d_q)] + jZ_2}) + \frac{1}{j\omega C_o} \\ &= \frac{h^2}{j\omega}\frac{2.Z_q[\cos(k_q d_q) - 1] + j.(Z_1 + Z_2).\sin(k_q d_q)}{(Z_q{}^2 + Z_1.Z_2).\sin(k_q d_q) - jZ_q(Z_1 + Z_2)\cos(k_q d_q)} + \frac{1}{j\omega C_o} \end{aligned} \tag{A3.48}$$

Finally, we obtain the electrical impedance of the TSM sensor with any media applied to the two surfaces of the sensor as;

$$Z_3 = \frac{1}{j\omega C_0}[1 + \frac{K'^2}{k_q d_q}\frac{2Z_q^2[\cos(k_q d_q) - 1] + jZ_q(Z_1 + Z_2)\sin(k_q d_q)}{(Z_q^2 + Z_1.Z_2)\sin(k_q d_q) - jZ_q(Z_1 + Z_2)\cos(k_q d_q)}] \tag{A3.49}$$

Where, $K'^2 = K^2/(1+K^2)$ and $K^2 = e^2/(c^E.\varepsilon^S)$) is the piezoelectric coupling constant; $Z_q = A(c_q^D \rho_q)$ is the acoustic impedance of the quartz plate; Z_1 is the acoustic impedance at port 1; Z_2 is the acoustic impedance at port 2; k_q is the wave number; d_q is the thickness of the MTSM sensor.

Based on the three-port network model of a MTSM sensor discussed above, the Transmission Line Model can be derived from Eq. A3.42.

First, four parameters in an impedance matrix are defined in Eq. A3.50;

$$Z_{11} = Z_{22} = -jZ_q \cot(k_q d_q)$$
$$Z_{12} = Z_{21} = -jZ_q \csc(k_q d_q) \qquad \text{(A3.50)}$$

Then, Eqs. A3.43, A3.44, A3.45,

$$F_1 = (Z_{11} - Z_{12}).v_1 + Z_{12}(v_1 + v_2) + \frac{h}{\omega} I_3$$
$$F_2 = (Z_{22} - Z_{12}).v_2 + Z_{21}(v_1 + v_2) + \frac{h}{\omega} I_3 \qquad \text{(A3.51)}$$
$$V_3 = \frac{h}{j\omega}(v_1 + v_2) + \frac{h}{j\omega C_o} I_3$$

The first term on the right hand side of Eq. A3.51 can be seen as a voltage generated by a current, v_1, through the impedance, $Z_{11} - Z_{22}$. Similarly, the second term can be seen as a voltage generated by a current, $v_1 + v_2$, through the impedance, Z_{12}. The third term can be seen as a voltage proportional to the current, I_3, seen at port 3. Therefore, a TLM model named Mason series equivalent circuit can be constructed as in Figure A3.3.

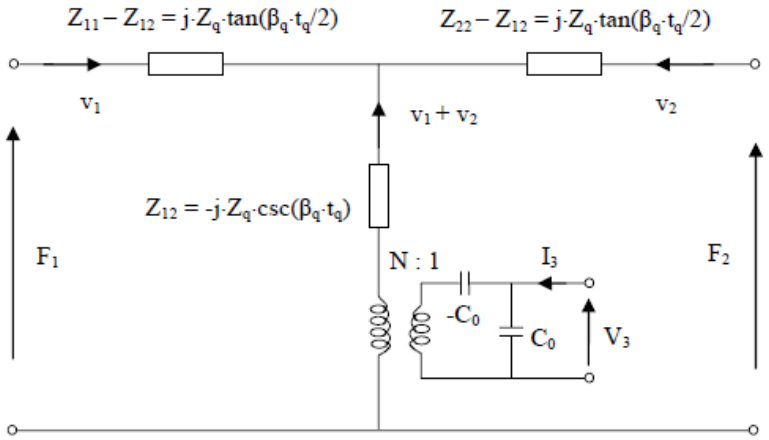

Figure A3.3 Three port Mason model of piezoelectric quartz (Kino, 1987)

In Figure A3.3, the turn ratio of the transformer is $N = hC_0 = (e/\varepsilon^S)(\varepsilon^S A/d_q)$. When port 3 is open circuit or $I_3 = 0$, the third term in first two terms in Eqs. A3.51 equals to zero and this Mason equivalent circuit changes to a T network equivalent of a coaxial transmission line with impedance of Z_q.

A3.3.2 Mason transmission line model (Two-port model)

Three-port model can be simplified to a two-port model by connecting appropriate impedance across the acoustical port representing the side of the quartz having the uncoated electrode (Fig. A3.4).

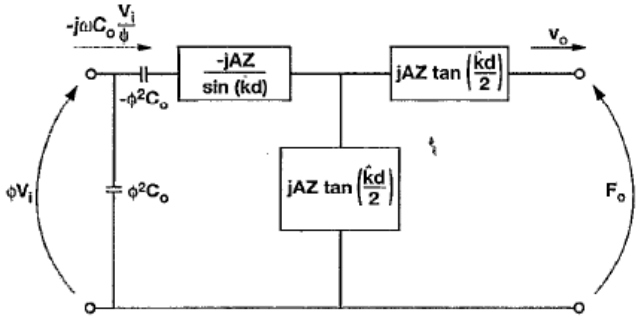

Figure A3.4 Two port Mason model of piezoelectric quartz with one stress-free interface (Rosenbaum, 1988, pp.218)

If the bottom electrode has a significant area1 mass density, its impedance is $j\omega p_s$,, where p_s is the areal mass density of the electrode (kg/m^2). For simplicity, it is assumed that the bottom electrode is thin enough to model its impedance as a short (zero impedance), corresponding to a stress-free interface. The transformer in Fig. A3.2 is then eliminated by standard circuit methods [ref] to yield the two-port equivalent-circuit model of the quartz with one stress-free interface. This circuit model has one acoustical port and one electrical port.

A simple implementation of the two-port Mason model, as detailed in (Martin et al.,1994) is to write a matrix equation to express the output current and voltage as a linear function of the input current and voltage and the acoustic parameters of the layer,

$$\begin{bmatrix} V_i \\ I_i \end{bmatrix} = \begin{bmatrix} A & B \\ C & D \end{bmatrix} \begin{bmatrix} V_0 \\ I_0 \end{bmatrix} \tag{A3.52}$$

where the voltages V and the currents I may be either electrical or acoustical variables. Note that if the output variables are known, the input variables are calculated by multiplying both sides of Eq. A3.52 by the inverse of the ABCD transformation matrix.

The transformation matrix entries in Eq.3.52, for a nonpiezoelectric layer, are as follows:

$$\begin{aligned} A &= \cos(\hat{k}d) \\ B &= jZ\sin(\hat{k}d) \\ C &= j\frac{\sin(\hat{k}d)}{Z} \\ B &= \cos(\hat{k}d) \end{aligned} \tag{A3.53}$$

where $\hat{k}$ and d are the complex propagation constant and the layer thickness, respectively. 2 is the characteristic impedance of the layer material,

$$Z=(\rho G)^{1/2} \tag{A3.54}$$

where G is the complex shear modulus and ρ is the mass density. The complex propagation constant, $\hat{k}$, is defined such that

$$\gamma = j\hat{k} = j\omega\sqrt{\rho / G}, \tag{A3.55}$$

where k is the wave propagation constant and w is the angular frequency of oscillation.

For a piezoelectric layer, the matrix entries relating the electrical voltage and current to the acoustical voltage (stress) and current (particle velocity) are as follows:

$$
\begin{aligned}
A_q &= \left[\frac{j\phi^2}{\omega C_0} + A(a+b) \right] / \phi a, \\
B_q &= \left[\frac{2j\phi^2 a}{\omega C_0} + A(a^2+2ab) \right] / \phi a, \\
C_q &= \left[\frac{j\omega C_0 A(a+b)}{\phi a} \right] \\
D_q &= \left[\frac{j\omega C_0 A(a^2+2ab)}{\phi a} \right]
\end{aligned}
\tag{A3.56}
$$

where

$$
\begin{aligned}
a &= jZ_q \tan\left(\frac{\hat{k}_q d_q}{2}\right) \\
b &= \frac{-jZ_q}{\sin(\hat{k}_q d_q)}
\end{aligned}
\tag{A3.57}
$$

$\hat{k}_q$ is the complex wave propagation constant for quartz, and d_q is the quartz thickness. Co, the capacitance of the AT-cut quartz, is

$$C_0 = \frac{\varepsilon_{22} A}{d_q} \tag{A3.58}$$

where ε_{22} is the quartz permittivity, and A is the active electrode area. Z_q, the characteristic impedance of the quartz, is analogous to Eq. A3.54

$$Z_q = \sqrt{\rho_q \bar{c}_{66}} \tag{A3.59}$$

where $\bar{c}_{66}$ is the piezoelectrically stiffened complex shear modulus of the lossy quartz.

The turns ratio of the transformer $\phi = hC_0 = (e_{26} / \varepsilon_{22})C_0$ (A3.60)

e_{26} is the piezoelectric stress constant.

The procedure for modeling a quartz resonator with multiple layers is to stack the layers (represented by concatenating the 2x2 matrices for each layer), starting with the knowledge that the top of the composite resonator is stress free, and working toward calculating the variables at the electrical port.

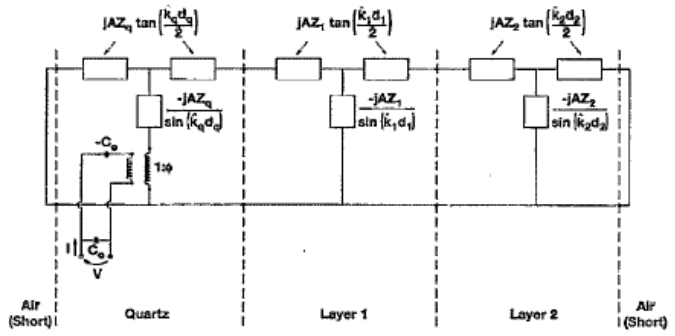

Figure A3.5 Mason model of composite resonator having a stress free interface on one side and two arbitrary films on the other side (Martin et al., 1994)

Figure A3.5 is an example of a Mason model of a composite system having two nonpiezoelectric layers on a quartz resonator. Applying the matrix multiplication principle embodied in Eqs. A3.52;

$$\begin{bmatrix} V \\ I \end{bmatrix} = \begin{bmatrix} A_q & B_q \\ C_q & D_q \end{bmatrix} \begin{bmatrix} A_1 & B_1 \\ C_1 & D_1 \end{bmatrix} \begin{bmatrix} A_2 & B_2 \\ C_2 & D_2 \end{bmatrix} \begin{bmatrix} V_2 \\ I_2 \end{bmatrix}$$
$$= \begin{bmatrix} A_q(A_1B_2I_2 + D_2B_1I_2) + B_q(C_1B_2I_2 + D_1D_2I_2) \\ C_q(A_1B_2I_2 + D_2B_1I_2) + D_q(C_1B_2I_2 + D_1D_2I_2) \end{bmatrix} \quad \text{(A3.61)}$$

with V,=0 for the stress-free interface on top of layer 2. The impedance at the electrical port can then be calculated from V/I, noting that the unknown I_2 cancels out. The impedance is, therefore,

$$Z = \frac{A_qV_q + B_qI_q}{C_qV_q + D_qI_q} \quad \text{(A3.62)}$$

where, for two layers

$$V_q = A_1 B_2 + B_1 D_2 = jZ_1[(\frac{Z_2}{Z_1})\cos(\hat{k}_1 d_1)\sin(\hat{k}_2 d_2) + \sin(\hat{k}_1 d_1)\cos(\hat{k}_2 d_2)] \quad \text{(A3.63)}$$

and

$$I_q = C_1 B_2 + D_1 D_2 = -(\frac{Z_2}{Z_1})\sin(\hat{k}_1 d_1)\sin(\hat{k}_2 d_2) + \cos(\hat{k}_1 d_1)\cos(\hat{k}_2 d_2)] \quad \text{(A3.64)}$$

Note that, for any number of layers, V_q/I_q, is the acoustic impedance, Z_s, seen at the quartz surface because V_q/I_q is the impedance calculated by multiplying the transformation matrices for the nonpiezoelectric layers only.

Under certain conditions, it is valid to use an element proportional to this surface impedance, Z, in the motional arm of MTSM equivalent circuit. The electrical admittance is rewritten as

$$Y = \frac{C_q V_q + D_q I_q}{A_q V_q + B_q I_q} = \frac{C_q Z_s + D_q}{A_q Z_s + B_q} = j\omega C_0 (1 + \frac{Y_m}{j\omega C_0}) \quad \text{(A3.65)}$$

A3.3.4 Lumped Element Model

The Transmission Line Model (TLM) gives an accurate representation of the interactions between the impedance of the acoustic loadings at port 1, 2 of a MTSM sensor and the electrical impedance at port 3. However, the TLM is complex and the simulation of the TLM within a large frequency spectrum is difficult. Since MTSM sensors are usually used as a resonator in various applications, the modeling of a MTSM sensor is mostly interested in its operation at its resonance frequency or a small vicinity of its resonance frequency. Therefore, a simplified model of the TLM is required for easy simulation and data retrieving at the frequencies close to the resonance frequency of a TSM. The Lumped Element Model (LEM) is the one that satisfied these requirements.

The LEM can be created by analyzing the impedance of a MTSM sensor given in Eq.

A3.49. For an unloaded MTSM sensor, both sensor surfaces are stress free, $T_{m1} = T_{m2} = 0$. According to Eqs. A3.23 and A3.24, the acoustic impedance at port 1 and port 2 equal to zero, $Z_1 = Z_2 = 0$. Then the electrical impedance at port 3, Z_3, for an unloaded TSM sensor becomes

$$Z_3 = \frac{1}{j\omega C_0}[1 - K^2 \frac{\tan(\frac{k_q d_q}{2})}{\frac{k_q d_q}{2}}] = \frac{Z_{C_0} Z_m}{Z_{C_0} + Z_m} \tag{A3.66}$$

where

$$Z_{Co} = \frac{1}{j\omega C_0} \tag{A3.67}$$

$$Z_m = \frac{1}{j\omega C_0}[\frac{1}{K^2} \frac{\frac{k_q d_q}{2}}{\tan(\frac{k_q d_q}{2})} - 1] \tag{A3.68}$$

Eq. A3.66 shows that the electrical impedance of an unloaded MTSM sensor, Z_3, is equivalent to two impedances, Z_{C0} and Z_m, in parallel. Z_{C0} is the impedance of a capacitor C_0, which is the static capacitance of the quartz plate. Since a MTSM sensor is used as a resonator, it is understandable to represent Z_m as the impedance of an electrical resonator, which consists of an inductor L_1, a capacitor C_1 and a resistor R_1 in series. Figure A3.6 shows this lumped element model of an unloaded TSM sensor, also called Butterworth-Van Dyke (BVD) model.

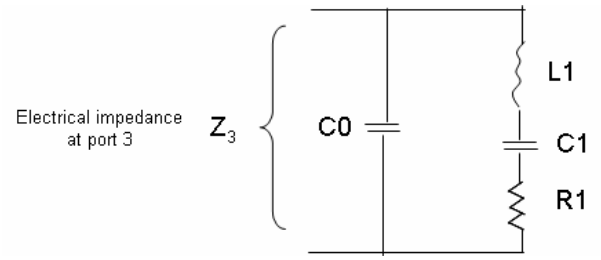

Figure A3.6 A lumped element model of an unloaded MTSM sensor

Next, we need to find the expression of each component in this LCR resonator. The impedance of this LCR resonator, Z_{LCR}, is

$$Z_{LCR} = j\omega L_1 + \frac{1}{j\omega C_1} + R_1 \tag{A3.69}$$

By equalizing this Z_{LCR} to the impedance of the electrical resonator given in Eq.A3.68, we should be able to get the expressions of L1, C1 and R1. With the assumption that the operating frequency of a MTSM sensor is in the vicinity of its resonance frequency, some important properties can be derived.

$$\begin{aligned} \tan(\frac{k_q d_q}{2}) &= \sum_{N=1,3,\ldots} \frac{k_q d_q}{(\frac{N\pi}{2})^2 - (\frac{k_q d_q}{2})^2} \approx \frac{4k_q d_q}{(N\pi)^2 - (k_q d_q)^2} \\ (k_q d_q)^2 &= \frac{(N\pi)^2 - 8K'^2}{1 + j\frac{\omega\mu_q}{c_q}} \end{aligned} \tag{A3.70}$$

Assuming that $(N\cdot\pi)^2 >> 8\cdot K'^2$ and using the properties in Eq.A3.70, the impedance in Eq. A3.68 becomes

$$
\begin{aligned}
Z_m &\approx \frac{1}{j\omega C_0}\left[\frac{1}{K'^2}\frac{\frac{\beta_q d_q}{2}}{\frac{4\beta_q d_q}{(N\pi)^2-(\beta_q d_q)^2}}-1\right] \\
&\approx \frac{1}{j\omega C_0}\left[\frac{1}{K'^2}\frac{(N\pi)^2-(\beta_q d_q)^2}{8}-1\right] \\
&\approx \frac{1}{j\omega C_0}\left[\frac{(N\pi)^2-\frac{(N\pi)^2-8K'^2}{1+j\frac{\omega\mu_q}{c_q}}}{8}-1\right] \\
&\approx \frac{1}{j\omega C_0}\left[\frac{(N\pi)^2(1+j\frac{\omega\mu_q}{c_q})-(N\pi)^2+8K'^2}{8K'^2(1+j\frac{\omega\mu_q}{c_q})}-1\right] \\
&\approx \frac{1}{j\omega C_0}\left[\frac{(N\pi)^2}{8K'^2}-\frac{(N\pi)^2}{8K'^2(1+j\frac{\omega\mu_q}{c_q})}+\frac{1}{8K'^2(1+j\frac{\omega\mu_q}{c_q})}-1\right] \\
&\approx \frac{1}{j\omega C_0}\left[\frac{(N\pi)^2}{8K'^2}-\frac{(N\pi)^2}{8K'^2}(1-j\frac{\omega\mu_q}{c_q})+(1-j\frac{\omega\mu_q}{c_q})-1\right] \\
&\approx \frac{1}{j\omega C_0}\left[(\frac{(N\pi)^2}{8K'^2}j\frac{\omega\mu_q}{c_q})-j\frac{\omega\mu_q}{c_q}\right]
\end{aligned}
\qquad \text{(A3.71)}
$$

Finally, the expressions of the values of the lumped elements in Figure A3.6, L1, C1 and R1, can be found as

$$C_0=\frac{\varepsilon^S A}{d_q} \qquad C_1=\frac{8K'^2}{(N\pi)^2}C_0 \qquad L_1=\frac{1}{\omega_n{}^2 C_1} \qquad R_1=\frac{\mu_q}{c_q C_1}$$

where, ε^S is the permittivity when S is zero or constant; A is the cross-section area of electrodes; d_q is thickness of quartz plate; h is the transmitting constant; $K'^2 = K^2/(1+K^2)$ and $K'^2 = e^2/(c^E.\varepsilon^S)$ piezoelectric coupling constant; e is the piezoelectric stress constant; c^E is the elastic constant when E is zero or constant; N is the order of harmonic frequency, N = 1, 3, 5… ; ωN is the Nth harmonic frequency; μ_q is viscosity of quartz plate.

Appendix 4. MatLab program codes for the simulations

The MTSM/GA technique was implemented in the MATLAB software. Four MatLab programs were developed: 1. The MTSM/GA technique for single-layer viscoelastic systems 2. The MTSM/GA technique for single-layer viscoelastic systems, 3.Transmission line model for multi-layer viscoelastic systems, and 4. For the simulation of the MTSM sensor with a viscoelastic film, the m-file format of MatLab software was used to generate 3-D type surface mesh graphs.

A4.1 M-file of the MTSM/GA technique for single-layer viscoelastic systems

The matlab program consists of seven functions, namely; Main.m, calculate.m, evalpob1.m, IniPobl.m, Ran_no_repo.m, Rep1.m and Show_Plots

A4.1.1 Main.m

This function is the main function which calls the other sub-functions.

```
%% General Information
%Genetic Algorithm Main Program
%Matias Hochman - Ertan Ergezen
%% Clear all the variables and the Screen.
%Clear screen
clc
close all;
clear all;
format long
%% Initial Values
```

```
% Number of individuals
 indiv_numb = 50;
%Number of chromosomes
chromo_numb=4;
%Need to find four variables, each variable is a chromosome.
%Genes / Chromosome
 genesperchromosome=16;
%Mutation Pobability (%)
 mut_prob=.5;
% Required Fitness
% fitness = 99;
% Elitism
elit = 1; %1 elitism, 0 non elitism
global dlayer rholayer viscoslayer c66layer expo weight  f_exp att_exp  f_exp3 f_exp4
att_exp3 att_exp4 att_exp5 att_exp6 att_exp7 att_exp8
%Input Data
 f_exp3 = 24921680;
att_exp3 =-1.3788;
att_exp4 =-23.4898;%before
f_exp4 =  24995450;
 f_exp =14952560;%640
 att_exp = -2.1811;%-0.0477
att_exp5 = -17.7562;
att_exp7 = -22.8594;
att_exp8 = -31.6534;
```

```
att_exp6 = -32.1680;
%Parameters to transform from Binary to Integer
expo = [genesperchromosome-1:-1:0];
weight = 2.^expo;
%% Initialize Population
c66layer11=[0 1e7];
c66layer22= [0 0];
viscoslayer11=[.001:0.001:.01];
viscoslayer22=[0.001 0.001];
dlayer11=[200e-9 500e-9];
dlayer22=[10000e-9 10000e-9];
for baba=1:length(viscoslayer22)-1;
for app=1:length(viscoslayer11)-1;
for pp=1:length(c66layer22)-1;
for mut=1:length(c66layer11)-1;
for xxx=1:length(dlayer22)-1;
c66layer = [[c66layer11(mut) c66layer11(mut+1)];[c66layer22(pp) c66layer22(pp+1)];[0
000000]];
AB=[300 1000 500 500 300 300];
fitnesss=[99.99999 99 99 99.9 99.9 99.9];
for loopo=1:1;
   ab=AB(loopo);
   dlayer = [[dlayer11(xxxx) dlayer11(xxxx+1)];[dlayer22(xxx) dlayer22(xxx+1)];[10000e-9
10000e-9]];
rholayer = [[1000 1400];[1000 1000];[1000 1000]];          %Density of layers
```

```
viscoslayer=[[viscoslayer11(app)viscoslayer11(app+1)];[viscoslayer22(baba)
viscoslayer22(baba+1)];[0.001 0.001]];
 fitness=fitnesss(loopo);
for loop=1:2;
clear Population
Population=IniPobl(indiv_numb,chromo_numb,genesperchromosome,0); %10
%% Genetic Algo5rithmP
% Evaluate the initial population
[f,fittest,masapto,Genotipo,DA,DF,DK,DL,DM]=evalpob1(Population,genesperchromosome,
indiv_numb,chromo_numb);
% Starts a loop to look for the fittest solution.
% While the best fittest solution is below the required fitness the loop
% will continue, another while loop is used in order to restart the random
% generator.
I=1;
Generation = 1;
tic
max_fit = 0;
    while ((fittest < fitness))&((Generation < ab))
     % Reproduction and Mutation
Population=Rep1(f,Population,mut_prob,indiv_numb,genesperchromosome,chromo_numb,el
it);
     % Evaluate
[f,fittest,Phenotype_fittest,Genotype,DA,DF,DK,DL,DM]=evalpob1(Population,genesperchr
omosome,indiv_numb,chromo_numb);
```

```
clc
disp(fittest);
disp(DA);
disp(DF);
disp(DK);
disp(DL);
disp(DM);
fit(Generation)=fittest;
if fittest > max_fit
   max_fit = fittest;
   indiv = Phenotype_fittest;
end;
disp(Generation);
loops=[ loop baba mut app]
disp('dlayer');
 disp(dlayer(1,1) + (dlayer(1,2)-dlayer(1,1))/(2^genesperchromosome-1)*indiv(1));
 disp('rholayer');
 disp(rholayer(1,1) + (rholayer(1,2)-rholayer(1,1))/(2^genesperchromosome-1)*indiv(2))
disp('viscoslayer');
disp(viscoslayer(1,1)    +    (viscoslayer(1,2)-viscoslayer(1,1))/(2^genesperchromosome-
1)*indiv(3));
disp('c66layer')
disp(c66layer(1,1) +(c66layer(1,2)-c66layer(1,1))/(2^genesperchromosome-1)*indiv(4));
Generation = Generation + 1;
%disp(Generation)
```

```
        mut_prob = rand*20;
     fprintf('%f\n',mut_prob)
    end;
a(loop)=c66layer(1,1)+(c66layer(1,2)-c66layer(1,1))/(2^genesperchromosome-1)*indiv(4);
b(loop)=rholayer(1,1)+(rholayer(1,2)-rholayer(1,1))/(2^genesperchromosome-1)*indiv(2);
c(loop)= viscoslayer(1,1) + (viscoslayer(1,2)-viscoslayer(1,1))/(2^genesperchromosome-
1)*indiv(3);
d(loop)= dlayer(1,1) + (dlayer(1,2)-dlayer(1,1))/(2^genesperchromosome-1)*indiv(1);
 M=[DA DF DK DL DM dlayer(1,1)*1e9 dlayer(1,2)*1e9 viscoslayer(1,1) viscoslayer(1,2)
c66layer(1,1) c66layer(1,2) loopo loop fittest Generation a(loop) b(loop) c(loop)
d(loop)*1e9];
dlmwrite('results.txt',M,'precision','%.6f','delimiter','\t','newline','pc','-append');
end
end
end
   end
end
end
    end
end
%Elapsed Time
Elapsed_Time=toc;
disp('Time Elapsed:  ');
disp(Elapsed_Time);
```

A4.1. 2 Calculate.m

Calculate.m consists of the fitness function. It evaluates the performance of individual solutions.

```
//////////////////
function [frequency1, attenuation1, phase3, fitness, frequency33, attenuation333] = calculate(dlayer_ii,rholayer_ii,viscoslayer_ii,c66layer_ii,w,f_exp,att_exp,f_exp3,att_exp3,f_exp4,att_exp4,att_exp5,att_exp6,att_exp7,att_exp8);
%QUARTZ CONSTANTS
e_f= 14961735;
dq = (14998450/e_f)*(1e-3/3);
r = 3.5e-3;                         %Radius of active electrode area (m)
Area = pi*r*r;                      %Active electrode area (m^2)
E22 = 3.982e-11;                    %Permittivity of quartz (A^2 s^4 Kg^-1 m^-3)
E26 = 9.53e-2;                      %Piezoelectric constant of quartz (A s m^-2)
C0 = E22 * Area / dq;               %Static capacitance of quartz (F)
C66 = 2.947e+10;                    %Stiffness constant of quartz (N/m^2)
viscosityq = 3.5e-4;                %Viscosity of quartz (Kg m^-1 s^-1)
rhoq = 2.651e+3;                    %Density of quartz (Kg/m^3)
phi = E26/E22*C0;                   %Transformer Ratio
f =14952540:20:14952580;
%Frequency (Hz)
w = 2*pi*f;



layer = 1;
```

```
%To find Loaded Resonance Frequency
for i=1:1:length(w)
MatrixMultiplication = [1 0; 0 1];
for n = 1:layer
Glayer(n) = c66layer_ii(n) + (j.*w(i)*viscoslayer_ii(n)); %Complex shear modulus of load
Zz(n) = (rholayer_ii(n)* Glayer(n))^0.5;   %Characteristic impedance of load  (ohms)
klayer(n) = w(i) *((rholayer_ii(n)/Glayer(n))^0.5);  %Wave propagation constant for load
A(n) = cos(klayer(n)*dlayer_ii(n));
B(n) = j*Zz(n)*sin(klayer(n)*dlayer_ii(n));
C(n) = j*sin(klayer(n)*dlayer_ii(n))/Zz(n);
D(n) = cos(klayer(n)*dlayer_ii(n));
LayerMatrix = [A(n) B(n); C(n) D(n)];
MatrixMultiplication = MatrixMultiplication*LayerMatrix;
end;
MatrixMultiplication1 = MatrixMultiplication*[0;1];
Vq = MatrixMultiplication1(1);
Iq = MatrixMultiplication1(2);
Zs(i) = Vq/Iq;
Z0(i) = 1/(j*w(i)*C0);              %Impedance of static branch
Gq = C66 + (j*w(i)*viscosityq);     %Complex shear modulus of quartz
kq = w(i) * ((rhoq/Gq)^0.5);        %Wave number for Quartz
Zq = (rhoq * Gq)^0.5;               %Characteristic impedance of quartz (ohms)
a = j * Zq * tan(kq*dq/2);          %impedance involved in Aq-Dq
b = -j * Zq / (sin(kq*dq));         %impedance involved in Aq-Dq
Aq = (((j*phi*phi)/(w(i)*C0))+(Area*(a+b)))/(phi*a);
```

```
Bq = (((2*j*phi*phi*a)/(w(i)*C0))+(Area*(a*a+2*a*b)))/(phi*a);

Cq = (j*w(i)*C0*Area*(a+b))/(phi*a);

Dq = (1i*w(i)*C0*Area*(a*a+2*a*b))/(phi*a);

Zm(i) = (Aq*Zs(i)+Bq)/(Dq-j*w(i)*C0*Bq+Zs(i)*(Cq-j*w(i)*C0*Aq)); %Motional impedance of loaded quartz

Zt1(i) = (Aq*Zs(i)+Bq)/(Cq*Zs(i)+Dq);

S1(i)=100./(100+Zt1(i));

end;

M1=sqrt((real(S1)).^2+(imag(S1)).^2);

dB1=20*log10(M1);

[attenuation1,Indexs1] = max(dB1');

frequency1=f(Indexs1);

phaseloaded = angle(S1)*180/pi;

phase3=phaseloaded(Indexs1);

df=abs(f_exp-frequency1);

da=abs(attenuation1*1-att_exp*1);

da3 = sqrt((att_exp4*1-phase3*1)^2);

  r2 = 3.5e-3;                    %Radius of active electrode area (m)

  Area2 = pi*r2*r2;                %Active electrode area (m^2)

  E222 = 3.982e-11;                %Permittivity of quartz (A^2 s^4 Kg^-1 m^-3)

  E262 = 9.53e-2;                  %Piezoelectric constant of quartz (A s m^-2)

  C02 = E222 * Area2 / dq2;              %Static capacitance of quartz (F)

  C662 = 2.947e+10;                %Stiffness constant of quartz (N/m^2)

  viscosityq2 = 3.5e-4;            %Viscosity of quartz (Kg m^-1 s^-1)

rhoq2 = 2.651e+3;                  %Density of quartz (Kg/m^3)
```

```
phi2 = E262/E222*C02;                    %Transformer Ratio
f2= 24921680;
w2 = 2*pi*f2;
%To find Loaded Resonance Frequency
for i=1:1:length(w2)
MatrixMultiplication2 = [1 0; 0 1];
for n = 1:layer
Glayer2(n) = c66layer_ii(n) + (j.*w2(i)*viscoslayer_ii(n)); %Complex shear modulus of load
Zz2(n) = (rholayer_ii(n)* Glayer2(n))^0.5;    %Characteristic impedance of load  (ohms)
klayer2(n) = w2(i) *((rholayer_ii(n)/Glayer2(n))^0.5);        %Wave propagation constant for
load
A2(n) = cos(klayer2(n)*dlayer_ii(n));
B2(n) = j*Zz2(n)*sin(klayer2(n)*dlayer_ii(n));
C2(n) = j*sin(klayer2(n)*dlayer_ii(n))/Zz2(n);
D2(n) = cos(klayer2(n)*dlayer_ii(n));
LayerMatrix2 = [A2(n) B2(n); C2(n) D2(n)];
MatrixMultiplication2 = MatrixMultiplication2*LayerMatrix2;
end;
MatrixMultiplication12 = MatrixMultiplication2*[0;1];
Vq2 = MatrixMultiplication12(1);
Iq2 = MatrixMultiplication12(2);
Zs2(i) = Vq2/Iq2;
Z02(i) = 1/(j*w2(i)*C02);            %Impedance of static branch

   Gq2 = C662 + (j*w2(i)*viscosityq2);     %Complex shear modulus of quartz
```

```
   kq2 = w2(i) * ((rhoq2/Gq2)^0.5);       %Wave number for Quartz
   Zq2 = (rhoq2 * Gq2)^0.5;              %Characteristic impedance of quartz (ohms)
   a2 = j * Zq2 * tan(kq2*dq2/2);         %impedance involved in Aq-Dq
   b2 = -j * Zq2 / (sin(kq2*dq2));        %impedance involved in Aq-Dq
   Aq2 = (((j*phi2*phi2)/(w2(i)*C02))+(Area2*(a2+b2)))/(phi2*a2);
   Bq2 = (((2*j*phi2*phi2*a2)/(w2(i)*C02))+(Area2*(a2*a2+2*a2*b2)))/(phi2*a2);
   Cq2 = (j*w2(i)*C02*Area2*(a2+b2))/(phi2*a2);
   Dq2 = (j*w2(i)*C02*Area2*(a2*a2+2*a2*b2))/(phi2*a2);
Zm2(i)    =    (Aq2*Zs2(i)+Bq2)/(Dq2-j*w2(i)*C02*Bq2+Zs2(i)*(Cq2-j*w2(i)*C02*Aq2));
%Motional impedance of loaded quartz
Zt2(i) = (Aq2*Zs2(i)+Bq2)/(Cq2*Zs2(i)+Dq2);
S122(i)=100./(100+Zt2(i));
end;
phaseloaded22 = angle(S122)*180/pi;
M22=sqrt((real(S122)).^2+(imag(S122)).^2);
dB22=20*log10(M22);
 [attenuation333,Indexs333] = max(dB22');
frequency33=f2(Indexs333);
da2 = abs(attenuation333*1-att_exp3*1);
df2 = abs(f_exp3-frequency33);
fa=df+da;
%   end
fitness = 100/(1+fa);
```

A4.1.3 EvalPobl.m

This function is used for the evolution of the individuals.

```
%evalpob.m function
[f,fmax,fittest_ind,Genotipo,DA,DF,DK,DL,DM] =
evalpob1(Population,genesporcromosoma,nroindiv,nrocromosomas);
global dlayer rholayer viscoslayer c66layer expo w f_exp att_exp f_exp3 f_exp4 att_exp3
att_exp4 att_exp5 att_exp6 att_exp7 att_exp8
expo = [genesporcromosoma-1:-1:0];
weight = 2.^expo;
layer=1;
%Transforming the Genotype into phenotype
for r=1:nroindiv
  for t=1:nrocromosomas
     for s=1:genesporcromosoma
       chromosome_aux(s)=Population(r,s+(t-1)*genesporcromosoma);
    end;
    Genotipo(r,t)=dot(chromosome_aux,weight);
  end;
end;
%Phenotype for each individual.
f = zeros(1,nroindiv);
for r=1:nroindiv
%Phenotype for each individual
for k = 1:layer
dlayer_i(k)=dlayer(k,1)+(dlayer(k,2)-dlayer(k,1))/(2^genesporcromosoma-
1)*Genotipo(r,1+(4*(k-1)));
```

```
rholayer_i(k) = rholayer(k,1) + (rholayer(k,2)-rholayer(k,1))/(2^genesporcromosoma-
1)*Genotipo(r,2+(4*(k-1)));
viscoslayer_i(k) = viscoslayer(k,1) + (viscoslayer(k,2)-
viscoslayer(k,1))/(2^genesporcromosoma-1)*Genotipo(r,3+(4*(k-1)));
c66layer_i(k) = c66layer(k,1) + (c66layer(k,2)-c66layer(k,1))/(2^genesporcromosoma-
1)*Genotipo(r,4+(4*(k-1)));
end;
 [frequency1(r),attenuation1(r),phase3(r), f(r),frequency33(r),attenuation333(r)] =
calculate(dlayer_i,rholayer_i,
viscoslayer_i,c66layer_i,w,f_exp,att_exp,f_exp3,att_exp3,f_exp4,att_exp4,att_exp5,att_exp6,
att_exp7,att_exp8);
end;
 [fmax,order] = max(f);
  DA=frequency1(order);
  DF=attenuation1(order);
  DK=phase3(order);
  DL=frequency33(order);
  DM=attenuation333(order);
for j=1:4
   fittest_ind(j)=Genotipo(order,j);
end;
```

A4.1.5 IniPop.m

This function initializes the population.

```
%IniPop.m % creation of many different combination for each genes. For
%example if number of individual is 100, and number of chromosemes is 4,
```

```
%genes per chromosomes is 16, then for each gene you have 100 different configuration.
function [population] = IniPobl(nroindiv,nrocromosomas,genesporcromosoma,seed_);
if seed_ ~= 0
   disp('seeded')
   rand('seed',seed_);
   population = round(rand(nroindiv,nrocromosomas*genesporcromosoma)); %Everytime
you start with the same rand numbers, so u stay in the loop.
else
   disp('not seeded')
   population = round(rand(nroindiv,nrocromosomas*genesporcromosoma));
end
end
```

A4.1.6 Ran_no_rep.m

This function generates random number without repetition.

```
% Generates Random numbers without repetition
%Ran_no_rep(value, number of elements to select);
function [Ran] = Ran_no_rep(number, num);
Ran=zeros(1,num);
Ran(1)=1+round((number-1)*rand(1));
for i = 2:num
   n=0;
   while n == 0
      a = 1+round((number-1)*rand);
      n=0;
```

```
        for j = 1:(i-1)
            if a == Ran(j)
                n=0;
                break;
            else
                n=1;
            end
        end
    end
    Ran(i)=a;
    n=0;
end;
```

A4.1.7. Rep1.m

This function performs elitism and crossover.

```
%Rep1.m
function [Population] = rep1(f,Pop,probmut, num_indiv ,genesXchromo,chromo_num,elit);
%% Look for the fittest Solution
%Find the descending order of the fitness of the population
[c,order]=max(f);
%Adds Elitism, the best solution survives
clear Population
if elit == 0
    Population=Pop(1+round(rand*(num_indiv-1)),:);
else
```

```
    Population=Pop(order,:);
end
%% New Aproach!
Pick = Ran_no_rep(num_indiv,num_indiv);
for i = 1:5:num_indiv
    for j = 1:5
        fit_data(j) = f(Pick((i-1)+j));
        Group(j,:) = Pop(Pick((i-1)+j),:);
    end
    [a,b] = sort(fit_data,'descend');
    cp=2+(round(rand*(genesXchromo*chromo_num - 4)));
    parent1=Group(b(1),:);
    ddd = 1+Ran_no_rep(4,1);
    parent2=Group(b(ddd),:);
    son1=[parent1(1:cp),parent2(cp+1:genesXchromo*chromo_num)];
    son2=[parent2(1:cp),parent1(cp+1:genesXchromo*chromo_num)];
    Population = [Population; parent1; parent2; son1; son2];
    Population = [Population; Group(b(round(rand*2)+3),:)];
end
Population = Population(1:num_indiv,:);
%% Mutation
for i = 2:num_indiv
    for j = 1 : (genesXchromo * chromo_num)
        if (probmut * 10) >= round(rand*1000)
            Population(i,j) = not(Population(i,j));
```

```
      end;
    end;
end;
```

A4.1.8 Show_Plots.m

This function plots the graphs.

```
%Graficar.m
load 'a.txt';
load 'p.txt';
load 'l.txt';
larvaexp=l';
pupaexp=p';
adultoexp=a';
fb=6553.6;
ful=65536;
fua=ful;
fcel=655360;
fcea=fcel;
fcpa=fua;
b=Phenotype_fittest(1)/fb
ul=Phenotype_fittest(2)/ful
ua=Phenotype_fittest(3)/fua
cel=Phenotype_fittest(4)/fcel
cea=Phenotype_fittest(5)/fcea
cpa=Phenotype_fittest(6)/fcpa
```

```
larvamod(1)=larvaexp(1);
pupamod(1)=pupaexp(1);
adultomod(1)=adultoexp(1);
for k=2:40,
  larvamod(k)=b*adultomod(k-1) * exp(-cel*larvamod(k-1)-cea*adultomod(k-1));
  pupamod(k)=(1-ul)*larvamod(k-1);
  adultomod(k)=pupamod(k-1)*exp(-cpa*adultomod(k-1))+(1-ua)*adultomod(k-1);
end;
 rango=(0:2:79);
figure(1);
%subplot(2,1,1); stem(rango,larvamod); title('Larvae Model'); xlabel('Weeks');
%subplot(2,1,2); stem(rango,larvaexp); title('Larvae Experimental'); xlabel('Weeks');
subplot(3,1,1);
a=plot(rango,larvamod,'g-o',rango,larvaexp,'r-x');
title('Larvae');
legend('Model', 'Experimental');
xlabel('Weeks');
ylabel('Number');
%figure;
%subplot(2,1,1); stem(rango,pupamod); title('Pupas Modelo'); xlabel('Semanas');
%subplot(2,1,2); stem(rango,pupaexp); title('Pupas Experimental'); xlabel('Semanas');
subplot(3,1,2);
a=plot(rango,pupamod,'g-o',rango,pupaexp,'r-x');
title('Pupae');
legend('Model', 'Experimental');
```

```
xlabel('Weeks');
ylabel('Number');
%figure;
%subplot(2,1,1); stem(rango,adultomod); title('Adultos Modelo'); xlabel('Semanas');
%subplot(2,1,2); stem(rango,adultoexp); title('Adultos Experimental'); xlabel('Semanas');
subplot(3,1,3);
a=plot(rango,adultomod,'g-o',rango,adultoexp,'r-x');
title('Adults');
legend('Model', 'Experimental');
xlabel('Weeks');
ylabel('Number');
Nrango=(1:1:length(fit));
createfigure_fitness(Nrango,fit)
%plot(Nrango,fit); title('Max fitness of each generation'); xlabel('Generations');
```

A4.2 M-file of the MTSM/GA technique for two-layer viscoelastic systems

The matlab program of the MTSM/GA technique for two-layer viscoelastic systems consists of seven functions, namely; Main.m, calculate.m, evalpob1.m, IniPobl.m, Ran_no_repo.m, Rep1.m and Show_Plots

A4.2.1. Main.m

This function is the main function which calls the other sub-functions.

```
%% General Information
%Genetic Algorithm Main Program
%Matias Hochman - Ertan Ergezen
%% Clear all the variables and the Screen.
%Clear screen
```

```
clc
close all;
clear all;
format long
%% Initial Values
% Number of individuals
indiv_numb = 50;
%Number of chromosomes
chromo_numb=12;
%Need 6to find four variables, each variable is a chromosome.
%Genes / Chromosome
genesperchromosome=16;
%Mutation Pobability (%)
 mut_prob=.5;
% Required Fitness
% fitness = 99;
% Elitism
elit = 1; %1 elitism, 0 non elitism
% w -> Angular Frequency
% freq_range =4.984e6:5:4.985e6;
% w = pi*2*freq_range;
 global dlayer rholayer viscoslayer c66layer expo weight w f_exp att_exp  f_exp3 f_exp4
att_exp3 att_exp4 att_exp5 att_exp6 att_exp7 att_exp8
 %% Input Data
f_exp3 = 14967800;
```

```
att_exp3 =-6.1513;

att_exp4 =2.1886;

f_exp4 =  4979300;

f_exp =4976090;

att_exp = -.8100;

att_exp5 = -17.7562;

att_exp6 = -32.1680;

att_exp7 = -22.8594;

att_exp8 = -31.6534;

%% Parameters to transform from Binary to Integer

 expo = [genesperchromosome-1:-1:0];

weight = 2.^expo;

%% Initialize Population

% If the last parameter is different than 0 the Random generator number is

 seeded with the number.

dlayer11=[1000e-9 1000e-9];

dlayer22=[300e-9 300e-9];

 c66layer11=[1e6 1e7];

c66layer22=[1e6 1e7];

viscoslayer11=[.001 .01];

viscoslayer22=[.01 .1];

for baba=1:length(viscoslayer22);

for app=1:length(viscoslayer11)-1;

for ppp=1:length(dlayer22)-1;

for mutt=1:length(dlayer11)-1;
```

```
for mut=1:length(c66layer11)-1;
for pp=1:length(c66layer22)-1;
dlayer = [[dlayer11(mutt) dlayer11(mutt+1)];[dlayer22(ppp) dlayer22(ppp+1)];[10000e-9
10000e-9]];
rholayer = [[1200  1200];[1100 1100];[1000 1000]];            %Density of layers
viscoslayer=[[viscoslayer11(app) viscoslayer11(app+1)];[viscoslayer22(baba)
viscoslayer22(baba+1)];[0.001 0.001]];
c66layer = [[c66layer11(mut) c66layer11(mut+1)];[c66layer22(pp) c66layer22(pp+1)];[0
000000]];
AB=[50 1000 500 500 300 300];
fitnesss=[99.999999 99 99 99.9 99.9 99.9];
for loopo=1:1;
   ab=AB(loopo);
   fitness=fitnesss(loopo);
for loop=1:25;
clear Population

Population=IniPobl(indiv_numb,chromo_numb,genesperchromosome,0); %10
 %% Genetic Algo5rithmP
% Evaluate the initial population
[f,fittest,masapto,Genotipo,DA,DF,DK,DL,DM]=evalpob1(Population,genesperchromosome,
indiv_numb,chromo_numb);
 % Starts a loop to look for the fittest solution.
% While the best fittest solution is below the required fitness the loop
% will continue, another while loop is used in order to restart the random
```

```
% generator.
I=1;
Generation = 1;
tic
max_fit = 0;
    while ((fittest < fitness))&&((Generation < ab))
     % Reproduction and Mutation
Population=Rep1(f,Population,mut_prob,indiv_numb,genesperchromosome,chromo_numb,el
it);
%       imshow(Population)
%       pause(.5)
      % Evaluate
[f,fittest,Phenotype_fittest,Genotype,DA,DF,DK,DL,DM]=evalpob1(Population,genesperchr
omosome,indiv_numb,chromo_numb);
      clc
      disp(fittest);
       disp(DA);
          disp(DF);
     fit(Generation)=fittest;
      if fittest > max_fit
         max_fit = fittest;
         indiv = Phenotype_fittest;
      end;
      disp(Generation);
      loops=[ loop baba mut app]
```

```
        disp('dlayer');
         disp(dlayer(1,1) + (dlayer(1,2)-dlayer(1,1))/(2^genesperchromosome-1)*indiv(1));
       disp('viscoslayer');
       disp(viscoslayer(1,1) + (viscoslayer(1,2)-viscoslayer(1,1))/(2^genesperchromosome-
1)*indiv(3));
       disp('c66layer')
       disp(c66layer(1,1) +(c66layer(1,2)-c66layer(1,1))/(2^genesperchromosome-1)*indiv(4));
            disp('dlayer 2');
            disp(dlayer(2,1) + (dlayer(2,2)-dlayer(2,1))/(2^genesperchromosome-1)*indiv(5));
           disp('viscoslayer 2');
           disp(viscoslayer(2,1) + (viscoslayer(2,2)-viscoslayer(2,1))/(2^genesperchromosome-
1)*indiv(7));
           disp('c66layer 2')
           disp(c66layer(2,1) +(c66layer(2,2)-c66layer(2,1))/(2^genesperchromosome-
1)*indiv(8));
Generation = Generation + 1;
mut_prob = rand*20;
fprintf('%f\n',mut_prob)
   end;
    a(loop)= c66layer(1,1) +(c66layer(1,2)-c66layer(1,1))/(2^genesperchromosome-
1)*indiv(4);
    b(loop)= rholayer(1,1) + (rholayer(1,2)-rholayer(1,1))/(2^genesperchromosome-
1)*indiv(2);
    c(loop)= viscoslayer(1,1) + (viscoslayer(1,2)-viscoslayer(1,1))/(2^genesperchromosome-
1)*indiv(3);
```

```
    d(loop)= dlayer(1,1) + (dlayer(1,2)-dlayer(1,1))/(2^genesperchromosome-1)*indiv(1);
      e(loop)= rholayer(2,1) + (rholayer(2,2)-rholayer(2,1))/(2^genesperchromosome-
1)*indiv(6);
      g(loop)= c66layer(2,1) +(c66layer(2,2)-c66layer(2,1))/(2^genesperchromosome-
1)*indiv(8);
      h(loop) = dlayer(2,1) + (dlayer(2,2)-dlayer(2,1))/(2^genesperchromosome-1)*indiv(5);
     ff(loop)= viscoslayer(2,1) + (viscoslayer(2,2)-
viscoslayer(2,1))/(2^genesperchromosome-1)*indiv(7);
% % %
      M=[DA DF DK DL DM c66layer(1,1) c66layer(1,2) c66layer(2,1) c66layer(2,2)
viscoslayer(1,1) viscoslayer(1,2) viscoslayer(2,1) viscoslayer(2,2) dlayer(1,1)*1e9
dlayer(1,2)*1e9 dlayer(2,1)*1e9 dlayer(2,2)*1e9 fittest Generation a(loop) b(loop) c(loop)
d(loop)*1e9 e(loop) ff(loop) g(loop) h(loop)*1e9];
dlmwrite('antibody1.txt',M,'precision','%.6f','delimiter','\t','newline','pc','-append');
end
end
end
end
end
end
end
end
%Elapsed Time
Elapsed_Time=toc;
disp('Time Elapsed:  ');
```

```
disp(Elapsed_Time);
```

A4.2.2 Calculate.m

This function performs the fitness calculations based on the fitness function.

```
function [fitness,attenuation1,frequency1,phase3,frequency4,phase22] =
calculate(dlayer_ii,rholayer_ii,
viscoslayer_ii,c66layer_ii,w,f_exp,att_exp,f_exp3,att_exp3,f_exp4,att_exp4,att_exp5,att_exp
6,att_exp7,att_exp8);
dq = 1e-3/3;                    %Quartz Thickness (m)
r = 3.5e-3;                     %Radius of active electrode area (m)
Area = pi*r*r;                  %Active electrode area (m^2)
E22 = 3.982e-11;                %Permittivity of quartz (A^2 s^4 Kg^-1 m^-3)
E26 = 9.53e-2;                  %Piezoelectric constant of quartz (A s m^-2)
C0 = E22 * Area / dq;           %Static capacitance of quartz (F)
C66 = 2.947e+10;                %Stiffness constant of quartz (N/m^2)
viscosityq = 3.5e-4;            %Viscosity of quartz (Kg m^-1 s^-1)
rhoq = 2.651e+3;                %Density of quartz (Kg/m^3)
phi = E26/E22*C0;               %Transformer Ratio
 f =4976080:10:4976100;
%Frequency (Hz)
w = 2*pi*f;
layer = 2;
%To find Loaded Resonance Frequency
for i=1:1:length(w)
    MatrixMultiplication = [1 0; 0 1];
      for n = 1:layer
```

```
 Glayer(n) = c66layer_ii(n) + (j.*w(i)*viscoslayer_ii(n)); %Complex shear modulus of load
 Zz(n) = (rholayer_ii(n)* Glayer(n))^0.5;  %Characteristic impedance of load -Lead alloy
(ohms)
klayer(n) = w(i) *((rholayer_ii(n)/Glayer(n))^0.5);   %Wave propagation constant for load
        A(n) = cos(klayer(n)*dlayer_ii(n));
        B(n) = j*Zz(n)*sin(klayer(n)*dlayer_ii(n));
        C(n) = j*sin(klayer(n)*dlayer_ii(n))/Zz(n);
        D(n) = cos(klayer(n)*dlayer_ii(n));
        LayerMatrix = [A(n) B(n); C(n) D(n)];
        MatrixMultiplication = MatrixMultiplication*LayerMatrix;
end;
   MatrixMultiplication1 = MatrixMultiplication*[0;1];
  Vq = MatrixMultiplication1(1);
   Iq = MatrixMultiplication1(2);
Zs(i) = Vq/Iq;
   Z0(i) = 1/(j*w(i)*C0);            %Impedance of static branch
Gq = C66 + (j*w(i)*viscosityq);    %Complex shear modulus of quartz
   kq = w(i) * ((rhoq/Gq)^0.5);       %Wave number for Quartz
   Zq = (rhoq * Gq)^0.5;             %Characteristic impedance of quartz (ohms)
a = j * Zq * tan(kq*dq/2);         %impedance involved in Aq-Dq
b = -j * Zq / (sin(kq*dq));        %impedance involved in Aq-Dq

   Aq = (((j*phi*phi)/(w(i)*C0))+(Area*(a+b)))/(phi*a);
   Bq = (((2*j*phi*phi*a)/(w(i)*C0))+(Area*(a*a+2*a*b)))/(phi*a);
   Cq = (j*w(i)*C0*Area*(a+b))/(phi*a);
```

```
    Dq = (j*w(i)*C0*Area*(a*a+2*a*b))/(phi*a);
Zm(i) = (Aq*Zs(i)+Bq)/(Dq-j*w(i)*C0*Bq+Zs(i)*(Cq-j*w(i)*C0*Aq));  %Motional
impedance of loaded quartz
     Zt1(i) = (Aq*Zs(i)+Bq)/(Cq*Zs(i)+Dq);
    S1(i)=100./(100+Zt1(i));
 end;
M1=sqrt((real(S1)).^2+(imag(S1)).^2);
dB1=20*log10(M1);
[attenuation1,Indexs1] = max(dB1');
frequency1=f(Indexs1);
 [attenuation33,Indexs33] = min(dB1');
 frequency4=f(Indexs33);
phaseloaded = angle(S1)*180/pi;
 phase3=phaseloaded(Indexs1);
 phase22=phaseloaded(Indexs33);
df=abs(f_exp-frequency1);
da=abs(attenuation1*1-att_exp*1);
fa=df+da;
%   end
fitness = 100/(1+fa);
```

A4.2.3 evalpob1.m

This function evaluates the individuals

```
%evalpob.m
function [f,fmax,fittest_ind,Genotipo,DA,DF,DK,DL,DM] =
evalpob1(Population,genesporcromosoma,nroindiv,nrocromosomas);
```

```
global dlayer rholayer viscoslayer c66layer expo w DA DF f_exp att_exp f_exp3 f_exp4
att_exp3 att_exp4 att_exp5 att_exp6 att_exp7 att_exp8
expo = [genesporcromosoma-1:-1:0];
weight = 2.^expo;
  layer=2;
%Transforming the Genotype into phenotype
for r=1:nroindiv
   for t=1:nrocromosomas
       for s=1:genesporcromosoma
         chromosome_aux(s)=Population(r,s+(t-1)*genesporcromosoma);
      end;
      Genotipo(r,t)=dot(chromosome_aux,weight);
   end;
end;
%Phenotype for each individual.
f = zeros(1,nroindiv);
for r=1:nroindiv
  %Phenotype for each individual
for k = 1:layer
dlayer_i(k) = dlayer(k,1) + (dlayer(k,2)-dlayer(k,1))/(2^genesporcromosoma-
1)*Genotipo(r,1+(4*(k-1)));
rholayer_i(k) = rholayer(k,1) + (rholayer(k,2)-rholayer(k,1))/(2^genesporcromosoma-
1)*Genotipo(r,2+(4*(k-1)));
viscoslayer_i(k) = viscoslayer(k,1) + (viscoslayer(k,2)-
viscoslayer(k,1))/(2^genesporcromosoma-1)*Genotipo(r,3+(4*(k-1)));
```

```
c66layer_i(k) = c66layer(k,1) + (c66layer(k,2)-c66layer(k,1))/(2^genesporcromosoma-
1)*Genotipo(r,4+(4*(k-1)));
end;
 [f(r),attenuation1(r),frequency1(r),phase3(r),frequency4(r),phase22(r)] =
calculate(dlayer_i,rholayer_i,
viscoslayer_i,c66layer_i,w,f_exp,att_exp,f_exp3,att_exp3,f_exp4,att_exp4,att_exp5,att_exp6,
att_exp7,att_exp8);
end;
[fmax,order] = max(f);
  DA=frequency1(order);
  DF=attenuation1(order);
  DK=phase3(order);
  DL=frequency4(order);
  DM=phase22(order);
for j=1:8
   fittest_ind(j)=Genotipo(order,j);
end;
```

A4.2.4 InilPop.m

This function initializes the population

```
%IniPop.m % creation of many different combination for each genes. For
%example if number of individual is 100, and number of chromosemes is 4,
%genes per chromosomes is 16, then for each gene you have 100 different configuration.
function [population] = IniPobl(nroindiv,nrocromosomas,genesporcromosoma,seed_);
if seed_ ~= 0
    disp('seeded')
```

```
    rand('seed',seed_);
    population = round(rand(nroindiv,nrocromosomas*genesporcromosoma)); %Everytime
you start with the same rand numbers, so u stay in the loop.
else
    disp('not seeded')
    population = round(rand(nroindiv,nrocromosomas*genesporcromosoma));
end
end
```

A4.2.5 Ran_no_rep.m

This functions generates random numbers without repetition.

```
% Generates Random numbers without repetition
%Ran_no_rep(value, number of elements to select);
function [Ran] = Ran_no_rep(number, num);
Ran=zeros(1,num);
Ran(1)=1+round((number-1)*rand(1));
for i = 2:num
    n=0;
    while n == 0
        a = 1+round((number-1)*rand);
        n=0;
        for j = 1:(i-1)
            if a == Ran(j)
                n=0;
                break;
            else
```

```
            n=1;
          end
        end
    end
    Ran(i)=a;
    n=0;
end;
```

A4.2.6 Rep1.m

It performs elitism and crossover

```
function [Population] = Rep1(f,Pop,probmut, num_indiv ,genesXchromo,chromo_num,elit)
%% Look for the fittest Solution
%Find the descending order of the fitness of the population
[c,order]=max(f);
%Adds Elitism, the best solution survives
clear Population
if elit == 0
    Population=Pop(1+round(rand*(num_indiv-1)),:);
else
    Population=Pop(order,:);
end
%% New Aproach!
Pick = Ran_no_rep(num_indiv,num_indiv);
for i = 1:5:num_indiv
    for j = 1:5
        fit_data(j) = f(Pick((i-1)+j));
```

```
        Group(j,:) = Pop(Pick((i-1)+j),:);
    end
    [a,b] = sort(fit_data,'descend');
    cp=2+(round(rand*(genesXchromo*chromo_num - 4)));
    parent1=Group(b(1),:);
    ddd = 1+Ran_no_rep(4,1);
    parent2=Group(b(ddd),:);
    son1=[parent1(1:cp),parent2(cp+1:genesXchromo*chromo_num)];
    son2=[parent2(1:cp),parent1(cp+1:genesXchromo*chromo_num)];
    Population = [Population; parent1; parent2; son1; son2];
    Population = [Population; Group(b(round(rand*2)+3),:)];
end
Population = Population(1:num_indiv,:);
%% Mutation
for i = 2:num_indiv
    for j = 1 : (genesXchromo * chromo_num)
        if (probmut * 10) >= round(rand*1000)
            Population(i,j) = not(Population(i,j));
        end;
    end;
end;
```

A4.3. Matlab program code for transmission line model of the MTSM sensor

```
clear
%QUARTZ CONSTANTS
dq = 1e-3/3;
```

```
r = 3.5e-3;                    %Radius of active electrode area (m)
Area = pi*r*r;                 %Active electrode area (m^2)
E22 = 3.982e-11;               %Permittivity of quartz (A^2 s^4 Kg^-1 m^-3)
E26 = 9.53e-2;                 %Piezoelectric constant of quartz (A s m^-2)
C0 = E22 * Area / dq;          %Static capacitance of quartz (F)
C66 = 2.947e+10;               %Stiffness constant of quartz (N/m^2)
viscosityq = 3.5e-4;           %Viscosity of quartz (Kg m^-1 s^-1)
rhoq = 2.651e+3;               %Density of quartz (Kg/m^3)
phi = E26/E22*C0;              %Transformer Ratio
f =24.8e+6:100:25.1e+6;
w = 2*pi*f;                    %Angular frequency (rad/sec)
% Please enter the layer values
layer=2;                       % Number of layers
dlayer = [1000e-9 300e-9 10000e-9];   %Thickness of layers
rholayer = [1200 1150 1000];   %Density of layers
viscoslayer=[0.006 0.05 0.001];
C66layer=[4e7 8e6 0];
%To find Loaded Resonance Frequency
for i=1:1:length(w)
MatrixMultiplication = [1 0; 0 1];
for n = 1:layer
Glayer(n) = C66layer(n) + (j*w(i)*viscoslayer(n)); %Complex shear modulus of load
Zz(n) = (rholayer(n)* Glayer(n))^0.5; %Characteristic impedance of load -Lead alloy (ohms)
klayer(n) = w(i) *((rholayer(n)/Glayer(n))^0.5);    %Wave propagation constant for load
A(n) = cos(klayer(n)*dlayer(n));
```

```
B(n) = j*Zz(n)*sin(klayer(n)*dlayer(n));

C(n) = j*sin(klayer(n)*dlayer(n))/Zz(n);

D(n) = cos(klayer(n)*dlayer(n));

LayerMatrix = [A(n) B(n); C(n) D(n)];

MatrixMultiplication = MatrixMultiplication*LayerMatrix;

end;

MatrixMultiplication1 = MatrixMultiplication*[0;1];

Vq = MatrixMultiplication1(1);

Iq = MatrixMultiplication1(2);

Zs(i) = Vq/Iq;

Z0(i) = 1/(j*w(i)*C0);              %Impedance of static branch

Gq = C66 + (j*w(i)*viscosityq);     %Complex shear modulus of quartz

kq = w(i) * ((rhoq/Gq)^0.5);        %Wave number for Quartz

Zq = (rhoq * Gq)^0.5;               %Characteristic impedance of quartz (ohms)

a = j * Zq * tan(kq*dq/2);          %impedance involved in Aq-Dq

b = -j * Zq / (sin(kq*dq));         %impedance involved in Aq-Dq

Aq = (((j*phi*phi)/(w(i)*C0))+(Area*(a+b)))/(phi*a);

Bq = (((2*j*phi*phi*a)/(w(i)*C0))+(Area*(a*a+2*a*b)))/(phi*a);

Cq = (j*w(i)*C0*Area*(a+b))/(phi*a);

Dq = (j*w(i)*C0*Area*(a*a+2*a*b))/(phi*a);

Zm(i) = (Aq*Zs(i)+Bq)/(Dq-j*w(i)*C0*Bq+Zs(i)*(Cq-j*w(i)*C0*Aq));  %Motional
impedance of loaded quartz

Zt1(i) = (Aq*Zs(i)+Bq)/(Cq*Zs(i)+Dq);

S212(i)=100./(100+Zt1(i));

end;
```

```
w2=2*3.14*25e6;
dop = 1/((-
1*w2)*(((rholayer(1)*rholayer(1))/((C66layer(1)*C66layer(1))+(w2*viscoslayer(1)*w2*visc
oslayer(1))))^0.25)*sin(-0.5*(atan(w2*viscoslayer(1)/C66layer(1)))));
phaseloaded = angle(S212)*180/pi;
[attenuationi1,Indexsi1] = min(phaseloaded');
M2=sqrt((real(S212)).^2+(imag(S212)).^2);
dB1loaded=20*log10(M2);
%amplitude and frequency at max point
[attenuation22,Indexs22] = max(dB1loaded');
frequency2=f(Indexs22);
%amplitude and frequency at min point
[attenuation33,Indexs33] = min(dB1loaded');
frequency3=f(Indexs33);
%phase at max and min point
phase3=phaseloaded(Indexs22);
phase4=phaseloaded(Indexs33);
%min phase and frequency at min phase
[phase22,Indexs222] = min(phaseloaded');
frequency4=f(Indexs222);
M=[frequency2 attenuation22 phase3 attenuation33 frequency3 phase4 phase22 frequency4
];
N = [f' phaseloaded' dB1loaded'];
dlmwrite('sim.txt',M,'precision','%.6f','delimiter','\t','newline','pc','-append');
dlmwrite('phase.txt',N,'precision','%.6f','delimiter','\t','newline','pc','-append');
```

```
figure (1)
pp=plot(f,dB1loaded);
set(pp,'LineWidth',3);
set(gca,'fontsize',20);
xlabel('Frequency (Hz)','fontsize',20)
ylabel('S21 (dB)','fontsize',20)
hold on
figure (2)
ppp=plot(f,phaseloaded);
set(ppp,'LineWidth',3);
set(gca,'fontsize',20);
xlabel('Frequency (Hz)','fontsize',20)
ylabel('Phase (degree)','fontsize',20)
hold on
```

A4.5. Matlab program codes for creating 3-D surface mesh graphs

```
clear;
%QUARTZ CONSTANTS
dq = 1e-3/3;                    %Quartz Thickness (m)
r = 3.5e-3;                     %Radius of active electrode area (m)
Area = pi*r*r;                  %Active electrode area (m^2)
E22 = 3.982e-11;                %Permittivity of quartz (A^2 s^4 Kg^-1 m^-3)
E26 = 9.53e-2;                  %Piezoelectric constant of quartz (A s m^-2)
C0 = E22 * Area / dq;           %Static capacitance of quartz (F)
C66 = 2.947e+10;                %Stiffness constant of quartz (N/m^2)
viscosityq = 3.5e-4;            %Viscosity of quartz (Kg m^-1 s^-1)
```

```
rhoq = 2.651e+3;                    %Density of quartz (Kg/m^3)
phi = E26/E22*C0;                    %Transformer Ratio
f =4.90e+6:1000:5.03e+6;
w = 2*pi*f;                          %Angular frequency (rad/sec)
% Please enter the layer values
layer=2;                                    % Number of layers
C66layer11=[0 1e3 1e4 1e5 2e5 3e5 4e5 5e5 6e5 7e5 8e5 9e5 1e6 2e6 3e6 4e6 5e6 6e6 7e6
8e6 9e6 1e7 2e7 3e7 4e7 5e7 6e7 7e7 8e7 9e7 10e7 1e9];
C66layer22 = 8e6;
viscoslayer2=0.05;
viscoslayer1 = 0.001:((0.1-0.001)/(length(C66layer11)-1)):0.1;
  dlayer11=1000e-9;
       dlayer22=300e-9;
   for l = 1:length(C66layer11)
C66layer = [C66layer11(l) C66layer22 0 0 0 0 0 0 0 0];
for row = 1:length(viscoslayer1)
layerviscosity = [viscoslayer1(row) viscoslayer2 0.001  0.001 0.001 0.001 0.001 0.001 0.001
0.001 0.001];
for irow = 1:length(dlayer11)
dlayer=[dlayer11(irow) dlayer22 10e-6 1e-6 10e-6 10e-6 10e-6 10e-6 10e-6 10e-6];
for i=1:1:length(w)


    MatrixMultiplication = [1 0; 0 1];
    for n = 1:layer
```

```
Glayer(n) = C66layer(n) + (j*w(i)*layerviscosity(n)); %Complex shear modulus of load
Zz(n)= (rholayer(n)* Glayer(n))^0.5;   %Characteristic impedance of load -Lead alloy (ohms)
  klayer(n) = w(i) *((rholayer(n)/Glayer(n))^0.5);          %Wave propagation constant for load
          A(n) = cos(klayer(n)*dlayer(n));
          B(n) = j*Zz(n)*sin(klayer(n)*dlayer(n));
          C(n) = j*sin(klayer(n)*dlayer(n))/Zz(n);
          D(n) = cos(klayer(n)*dlayer(n));
          LayerMatrix = [A(n) B(n); C(n) D(n)];
          MatrixMultiplication = MatrixMultiplication*LayerMatrix;
  end
MatrixMultiplication1 = MatrixMultiplication*[0;1];
Vq = MatrixMultiplication1(1);
Iq = MatrixMultiplication1(2);
Zs(i)= Vq/Iq;
Z0 = 1/(j*w(i)*C0);              %Impedance of static branch
    Gq = C66 + (j*w(i)*viscosityq);     %Complex shear modulus of quartz
    kq = w(i) * ((rhoq/Gq)^0.5);        %Wave number for Quartz
    Zq = (rhoq * Gq)^0.5;               %Characteristic impedance of quartz (ohms)
    a = j * Zq * tan(kq*dq/2);          %impedance involved in Aq-Dq
    b = -j * Zq / (sin(kq*dq));         %impedance involved in Aq-Dq
    Aq(i)= (((j*phi*phi)/(w(i)*C0))+(Area*(a+b)))/(phi*a);
    Bq (i)= (((2*j*phi*phi*a)/(w(i)*C0))+(Area*(a*a+2*a*b)))/(phi*a);
    Cq(i) = (j*w(i)*C0*Area*(a+b))/(phi*a);
    Dq (i)= (j*w(i)*C0*Area*(a*a+2*a*b))/(phi*a);
```

```
   Zm(i) = (Aq*Zs(i)+Bq)/(Dq-j*w(i)*C0*Bq+Zs(i)*(Cq-j*w(i)*C0*Aq));  %Motional
impedance of loaded quartz
Zt1(i) = (Aq(i)*Zs(i)+Bq(i))/(Cq(i)*Zs(i)+Dq(i));
S212(i)=100./(100+Zt1(i));
end
M2=sqrt((real(S212)).^2+(imag(S212)).^2);
dB1loaded=20*log10(M2);
      [attenuation22,Indexs22] = max(dB1loaded');
   frequency2=f(Indexs22);
   max_point(row,l)=attenuation22;
   max_pointf(row,l)=frequency2;
   w2=2*pi*frequency2;
   dop(row,l) = 1/((-
*w2)*(((rholayer(1)*rholayer(1))/((C66layer(1)*C66layer(1))+(w2*layerviscosity(1)
*w2*layerviscosity(1))))^0.25)*sin(-0.5*(atan(w2*layerviscosity(1)/C66layer(1)))));
end
  end
end
figure(1)
surf(C66layer11,viscoslayer1,max_point)
colorbar('fontsize',22)
 shading interp
 set(gca,'fontsize',22);
 xlabel('Stiffness (N/m^2)','fontsize',22)
 ylabel('Viscosity (kg/m.s)','fontsize',22)
```

```
 zlabel('Max. Mag. (dB)','fontsize',22)
  set(gca, 'xscale', 'log')
 set(gca, 'yscale', 'log')
figure(2)
surf(C66layer11,viscoslayer1,(max_pointf-max_pointf(1,1)))
colorbar('fontsize',22)
 shading interp
 set(gca,'fontsize',22);
 xlabel('Stiffness (N/m^2)','fontsize',22)
 ylabel('Viscosity (kg/m.s)','fontsize',22)
 zlabel('Relative Change in Res. Freq. (Hz)','fontsize',22)
 set(gca, 'xscale', 'log')
 set(gca, 'yscale', 'log')
 bobo=1;
if bobo==2;
   figure(1)
plot(dlayer11,(max_point-max_point(1)))
set(gca,'fontsize',22);
 xlabel('Thickness (nm)','fontsize',22)
 ylabel('Change in Magnitude (dB)','fontsize',22)
 zlabel('S21(dB)','fontsize',22)
figure(2)
plot(dlayer11,(max_pointf-max_pointf(1)))
set(gca,'fontsize',22);
 xlabel('Thickness (nm)','fontsize',22)
```

```
 ylabel('Change in Res. Freq. (Hz)','fontsize',22)
 zlabel('S21(dB)','fontsize',22)
figure (1)
plot (dlayer11,max_pointf-max_pointf(1))
 set(gca,'fontsize',22);
 xlabel('Thickness (um)','fontsize',22)
 ylabel('Relative Change in Res. Freq. (Hz)','fontsize',22)
 hold on
 figure (2)
plot (dlayer11,max_point)
 set(gca,'fontsize',22);
 xlabel('Thickness (um)','fontsize',22)
 ylabel('S21 (dB)','fontsize',22)
 hold on
% slope calculation
    for ii=1:length(C66layer11);
        for bbbb=1:length(viscoslayer1)-1;
  slope_ampv(bbbb,ii)=(max_point(bbbb+1,ii)-max_point(bbbb,ii))/(viscoslayer1(bbbb+1)-
viscoslayer1(bbbb));
  slope_freqv(bbbb,ii)=(max_pointf(bbbb+1,ii)-max_pointf(bbbb,ii))/(viscoslayer1(bbbb+1)-
viscoslayer1(bbbb));
end
end
for i=1:length(viscoslayer1);
        for bbb=1:length(C66layer11)-1;
```

```
  slope_amps(i,bbb)=(max_point(i,bbb+1)-max_point(i,bbb))/(C66layer11(bbb+1)-
C66layer11(bbb));
  slope_freqs(i,bbb)=(max_pointf(i,bbb+1)-max_pointf(i,bbb))/(C66layer11(bbb+1)-
C66layer11(bbb));
end
end
vis_value=0;
 for bbbb2=2:length(viscoslayer1);
vis_value(bbbb2)=vis_value(bbbb2-1)+(viscoslayer1(bbbb2)-viscoslayer1(bbbb2-1));
 end
C66_value=0;
 for bbbbb=2:length(C66layer11);
 C66_value(bbbbb)=C66_value(bbbbb-1)+(C66layer11(bbbbb)-C66layer11(bbbbb-1));
 end
figure(3)
surf(C66layer11,vis_value(2:27),slope_ampv)
colorbar('fontsize',20)
 shading interp
 set(gca,'fontsize',20);
 xlabel('Stiffness (N/m^2)','fontsize',20)
 ylabel('Viscosity (kg/m.s)','fontsize',20)
 zlabel('Amplitude Sensitivity (for viscosity)','fontsize',20)
 set(gca, 'xscale', 'log')
 set(gca, 'yscale', 'log')
figure(4)
```

```
surf(C66_value(2:22),viscoslayer1,slope_amps)
colorbar('fontsize',20)
shading interp
 set(gca,'fontsize',20);
 xlabel('Stiffness (N/m^2)','fontsize',20)
 ylabel('Viscosity (kg/m.s)','fontsize',20)
 zlabel('Amplitude Sensitivity','fontsize',20)
 set(gca, 'xscale', 'log')
 set(gca, 'yscale', 'log')
end
%Calculating Depth Of Penetration
dop(i) = 1/((-
1*w(i))*(((rho1*rho1)/((C66load1*C66load1)+(w(i)*viscosity1*w(i)*viscosity1)))^0.25)*si
n(-0.5*(atan(w(i)*viscosity1/C66load1))));
```

Appendix 5. List of Symbols

F = force (Newton)
δ = penetration depth (m)
ρ = density (kg/m^3)
ρ_1 = density of the first layer of the multi-layer viscoelastic system (kg/m^3)
ρ_2 = density of the second layer of the multi-layer viscoelastic system (kg/m^3)
ρ_3 = density of the third layer of the multi-layer viscoelastic system (kg/m^3)
η = viscosity (kg/m.s)
η_1 = viscosity of the first layer of the multi-layer viscoelastic system (kg/m.s)
η_2 = viscosity of the second layer of the multi-layer viscoelastic system (kg/m.s)
η_3 = viscosity of the third layer of the multi-layer viscoelastic system (kg/m.s)
ω = angular frequency (s^{-1})
C = stiffness (N/m^2)
C_1 = stiffness of the first layer of the multi-layer viscoelastic system (N/m^2)
C_2 = stiffness of the second layer of the multi-layer viscoelastic system (N/m^2)
C_3 = stiffness of the third layer of the multi-layer viscoelastic system (N/m^2)
A = area of active electrode of MTSM (m^2)
c = stiffness constant (N/m^2)
S = strain
u = displacement (m)
h = turn ratio of transformer
n = harmonic number
k = propagation constant (m^{-1})
v = particle velocity (m/s)
d = thickness of the viscoelastic layer loaded on the MTSM sensor (m)
d_1 = thickness of the first layer of multi-layer viscoelastic system (m)
d_2 = thickness of the second layer of multi-layer viscoelastic system (m)
d_3 = thickness of the third layer of multi-layer viscoelastic system (m)
Z = acoustic impedance (ohm)
c^D = stiffness constant (N/m^2)
e = piezoelectric stress constant ($9.53x10^3$ A s m^{-2})
D = electrical displacement ($coulomb/m^2$)
ε^S = quartz permittivity (3.982x10-11 A^2 s^4 kg^{-1} m^{-3})
I = current (coulomb)
C_0 = static capacitance of MTSM (farad)
I_i = input current (ampere)
I_o = output current (ampere)
V_i = input voltage (volt)
V_o = output voltage (volt)
G = complex shear modulus (N/m^2)
G' = storage modulus (N/m^2)
G" = loss modulus ($j\omega\eta$) (N/m^2)
z_1 and z_2 = left and right boundary planes of non-piezoelectric acoustic medium (m)
Z_t=total electromechanical impedance of the MTSM sensor (Ω)
R = 50 Ω matching impedance
Z_0^{film} = characteristic impedance of the viscoelastic coating, given by $(\rho_f G)^{1/2}$ (Ω)

ρ_f = density of viscoelastic film (kg/m^3)
d_f = thickness of viscoelastic film (m)
L1 = equivalent inductance of the unloaded MTSM sensor (H)
C1 = equivalent capacitance of the unloaded MTSM sensor (F)
R1 = equivalent resistance of the unloaded MTSM sensor (Ω)
L2 = inductance caused by the perturbation of the MTSM sensor (H)
R2 = resistance caused by the perturbation of the MTSM sensor (H)
C_0 = intrinsic capacitance of the MTSM sensor (F)
N = harmonic number
K^2 is the square of the quartz electromechanical coupling
ω_s is the angular frequency for the unperturbed MTSM sensors (radian)
Z_e = complex electrical load (Ω)
$Z_q=(\rho_q\mu_q)^{0.5}$ is the quartz shear wave characteristics impedance (Ω)
ρ_q = mass density of the quartz (kg/m^3)
μ_q = shear stiffness of the quartz (N/m^2)
Z_s = shear mechanical impedance at the device surface (Ω)
f_s = resonance frequency (Hz)
f_0 = resonance frequency of MTSM sensor (Hz)
ω_0 = angular frequency
d_q = thickness of the MTSM sensor (m)
η_q = viscosity of quartz (kg/ms)
C_q = stiffness of quartz (N/m^2)
d_p = thickness of the polymer layer (m)
η_p = viscosity of polymer layer (kg/ms)
C_p = stiffness of polymer layer (N/m^2)
rand = command to create random numbers in MatLab
Q factor = quality factor of the MTSM sensor
Q_{max} = maximum quality factor of the MTSM sensor that can be achieved
d_c = thickness of the Newtonian medium (m)
ρ_c = density of the Newtonian medium (kg/m^3)
η_c = viscosity of the Newtonian medium (kg/ms)
ρ_l = density of liquid (kg/m^3)
η_l = viscosity of liquid (kg/ms)
$Z_1 = (\rho_1 G_1)^{1/2}$ acoustic impedance of the first layer adjacent to the MTSM sensor (Ω)
ρ_1 = density of the first viscoelastic layer (kg/m^3)
G_1 = complex shear modulus of first viscoelastic layer (N/m^2)
Z_2 = acoustic load acting on the top of the first coating (Ω)
L2 = inductance of first viscoelastic layer
R2 = resistance of second viscoelastic layer
L3 = inductance of second viscoelastic layer
R3 = resistance of the second layer's properties.
d_{p2} = thickness of the second polymer layer (m)
η_{p2} = viscosity of second polymer layer (kg/ms)
C_{p2} = stiffness of second polymer layer (N/m^2)
T_q = stress applied to the quartz plate (
F_{trans} = translational force applied to the quartz plate (Newton)
u_q = displacement of a mass point within the plate (m)
v_q = velocity of the mass point (m/s)
a_q = acceleration of the mass point (m/s^2)

u_{qF} = magnitudes of the displacement of the forward (m)
u_{qB} = magnitude of the displacement backward (m)
T_{qF} = magnitudes of the stress of the forward propagating wave
T_{qB} = magnitudes of the stress of the backward propagating wave
k_q = wave number
u_{m1} = displacements of the acoustic wave in the medium 1 (m)
u_{m2} = displacements of the acoustic wave in the medium 2 (m)
T_{m1} = stress of the acoustic wave in the medium 1
T_{m2} = stress of the acoustic wave in the medium 2
Z_1 = mechanical impedance at port 1 (Ω)
Z_2 = mechanical impedance at port 2 (Ω)
Z_3 = electrical impedance at port 3 (Ω)
F_1 = force at port 1 (Newton)
F_2 = force at port 2 (Newton)
v_1 = particle velocity at port 1 (m/s)
v_2 = particle velocity at port 2 (m/s)
V_3 = voltage at seen at port 3 (volt)
I_3 = current seen at port 3 (ampere)
h = transmitting constant
c^D = the elastic constant when D is zero
D = flux density
c^E = the elastic constant when E is zero
ε^S = the permittivity when S is zero or constant